

DESIGN OF A PROTOTYPE BUILDING PANEL FOR RAINWATER STORAGE AND ENERGY GENERATION

BY

KEAMOGETSE BRIDGET MOKOMELE

A thesis submitted to the Faculty of Engineering and the Built Environment
Department of Civil Engineering and Geomatics
in fulfilment of the requirements for the degree of
Master of Engineering: Civil Engineering
at

Cape Peninsula University of Technology

Supervisor: Prof Kumar Pallav

Co-supervisor: Prof Atanda Raji

Cape Town
15 December 2023

CPUT copyright information

The thesis may not be published either in part (in scholarly, scientific or technical journals), or as a whole (as a monograph), unless permission has been obtained from the University

Declaration

I declare that this research dissertation is my own unaided work. It is being submitted for the Master of Engineering Degree at Cape Peninsula University of Technology, Cape Town. It has not been submitted before for any degree or examination in any other University.



(Signature)

Signed in Cape Town this 15 day of December 2023

Abstract

The functionality of buildings, such as walls carrying loads and transferring such loads to the foundation, needs to be modernized by adding value, where walls can, through load-bearing or non-load-bearing walls, harvest and store rainwater and generate energy as an alternative to conventional electricity. The need for alternative water supply for secondary use and alternative energy is gradually gaining momentum in South Africa (SA). SA encounters a challenge in addressing the demand for essential energy and water services in rural communities. The imperative for decentralised, sustainable, cost-effective clean energy and water solutions is important in rural areas.

This research aims to design a prototype building panel for rainwater storage and renewable energy generation. The objective is to determine the rainwater volume in cubic meters (m^3) to be harvested on a 10-Watt peak (Wp) panel, which forms a building panel with dimensions of 345mm \times 60mm \times 200mm referred to as *mBP* and a rainwater harvesting (RWH) tank with dimensions of 314mm \times 50mm \times 195 referred to as *iBP*, embedded in the building panel, the power output of a 10Wp polycrystalline flexible solar cell (FSC) on a vertical surface, and technology-related costs.

Existing experimental rainfall data was used to analyse rainfall intensities. Theoretical research strategies are applied, consisting of mathematical calculations for the design of; a non-load-bearing (NLB) building panel, bolt, rainwater storage (RWS) and photovoltaic (PV) systems, using Computer-Aided Drawings and modelling a building panel incorporating RWS and PV and simulating rainwater. Modelling of the RWS tank included using polylactic acid (PLA) as a construction material, moulded into an *mBP* and *iBP* for a RWH tank. PLA is a filament used in 3D printing, a low-density polyethylene (LDPE) chosen as construction material derived from corn-starch or sugarcane.

All electrical components were connected. The building panel was assembled using a Sika 219i marine adhesive sealant to join the FSC to one side of the building panel (345mm \times 200mm), and placed on pegboards (800mm \times 200mm \times 2) which acted as a vertical wall. All testing components were placed on this vertical panel, including the prototype, the MPPT, the battery, and a 5mm perforated recycled polyethylene terephthalate (rPET) 2ℓ bottle. The tests were conducted on both the RWH and the PV systems. For the RWH system, the collected data was the depth of the rain every 15-minute intervals. For PV, the collected data was Wattage(W), Voltage(V) and Amperes(A). While PVsyst was used as a simulation tool for grid-tied and standalone systems.

Mathematical computations were employed to assess the structural integrity of the proto-type building panel and bolt design, evaluating their capacity to withstand the Rainwater (RW) harvesting system when the associated tank reaches 100% capacity. Results indicated that the building panel, coupled with the bolt design, demonstrated resilience against the weight imposed by the RW harvesting system at full capacity. The accumulated rainwater ranged from 37mm to 126mm, while the generated energy varied between 7W and 15W.

Furthermore, the prototype underwent evaluation under 0% and 100% full capacity scenarios, yielding cumulative energy outputs of 7W and 15W, respectively. In a simulated standalone system, the performance ratio (PR) exhibited a modest rate of 0.56, while the solar fraction (SF) demonstrated a high rate of 0.956. Conversely, the grid-tied system achieved a PR of 80.2% under normal Standard Test Conditions (STC) efficiency.

The prototype's total cost, including value-added tax (VAT), amounted to R11203. Estimated financial figures included revenue of R77935, expenses totalling R38700, and a resultant profit of R50438.

Acknowledgements

I wish to thank:

- The Devine Creator and all my guardian angels, wholeheartedly, for giving me the strength to pursue my studies successfully and for overcoming all the challenges I was faced with during this crucial period; thank you for always being by my side.

To my most prestigious and respected supervisors:

- Prof Kumar Pallav cannot express my gratitude for morphing this challenging and interesting path with me. I can write a thesis expressing my gratitude for your endless assistance, continuous motivation and unwavering support. I was scared to research this project, but your calm and stern voice gave me assurance that we could do it as a team. You helped me through and through till I got it right. Thank you so much for everything; you are the best supervisor, advisor and leader. Sir, you ROCK!
- Prof Raji, your expertise, knowledge and information sharing elevated my drive to the next level. Thank you for always being there to support, motivate, encourage and challenge me to do better. Thank you for always sharing the motivating messages; they were impactful.
- Dr Khahledi, this journey started with you. You were my motivation to further my studies. Thank you from the bottom of my heart for constantly giving me the support I needed, the listening ear and the constructive advice. You are and have always been my inspiration.
- Mr. J Pieterse of Primwood, thank you for being industrious with me and giving me various material options to consider. You opened my eyes to the plastic recycling industry and showed me there is no limit to recycled plastics.
- Prof Jordaan, thank you for being more than a facilitator; attending your workshops helped me unpack my methodology, which I struggled to express in writing.
- Mr AD Williams and Ms A Mhlanga, thank you from the bottom of my heart for assisting with SolidWorks and Invertor when I needed help the most. I'm forever grateful.
- Solomon and Desere of D & S Solutions, thank you so much for assisting speedily in importing some of the research materials. Your assistance is highly appreciated.
- Mr Jason Rassouw of ACDC Hermanus, thank you for donating some PV cables towards this research project.
- Mr Ernst Olivier of AgriMark Hermanus, thank you so much for the price reduction for the board and other necessary materials.
- Mr TK of Netram Technologies, Century City, your assistance in printing the model came at the right time. Thank you for your patience and for not getting tired of my constant questions.
- Curtis and Dr Zama Katamzi-Joseph, thank you for assisting with the PV connection and modelling information.
- I am grateful to Prof V Fester and your team for your continuous support, encouragement, and information sharing. Your efforts never go unnoticed. Keep up with your excellent work.
- I do not know how to thank you to Ms T Mohajane and Ms M Loke, my sisters, to peers, advisors, and shoulder to cry on. I appreciate every bit of help and for always jumping to my rescue. Thank you from the bottom of my heart for your never-ending support, your time and words of encouragement. You were never too busy for me. Continue to support other research students in need. God bless you both in your doctoral journey.
- My family, thank you from the bottom of my heart for every kind of support you could offer, you always jumped to help whenever I needed any form of assistance. I am forever grateful.

The financial assistance of the Technology Transfer Office towards this research is highly acknowledged, as well as the full bursary offerings from the CPUT Centre for Postgraduate Studies. Opinions expressed in this thesis and the conclusions arrived at, are those of the author and are not necessarily to be attributed to the Technology Transfer Office and CPUT Centre for Postgraduate Studies.

Patent

Patent filling is in Process (Design of a building panel for rainwater storage and energy generation).

DEDICATION

I dedicate this work to my late grandparents Mr Semelo Seranyana Mokomele and Mrs MmaThabo Rosinah Mokomele, my late uncles Thabo, Kagiso, and Tebogo Mokomele; my late uncle and late brother, who passed away as I was in the process of submitting this research thesis, Lesotho and Thuso Mokomele. The four pillars of the Mokomele family are my four mothers, Motlalepula, Khutshalo, Regomodicwe and Mpho Mokomele. My sisters Mrs Kehilwe Ngqulana, Palesa and MmaBoitumelo Mokomele, my brothers Zakhele, Tsepiso, Thapelo and Thabiso Mokomele. My number one, my cheerleader, motivator, best friend and daughter, Tebogo Tino Love Mokomele, thank you for taking all the photos to compile this thesis. You were there with me from the beginning and encouraged me to stay on course till the end. You longed to come to my graduation, and I knew I had to give you this experience. Hence, I had to complete my research project. To all Mokomele grandchildren and greatgrandchildren; pursue what our late grandparents bestowed in us, get educated and smell of Masters and PhDs wherever you go, and rub it onto the next generation. Our parents laid the foundation, and we, raise the bar higher with every generation.

Mokomele, we got this, Aluta!

Table of Contents

Page

Declaration.....	ii
Abstract.....	iii
Acknowledgements	iv
Patent.....	vi
Table of Contents	ix
List of Figures.....	xii
List of Tables.....	xv
Nomenclature.....	xvi
Terms and concepts	xviii
Chapter 1 Introduction	1
1.1 Background and Motivation	1
1.2 Research problem.....	2
1.3 Identified Gap	2
1.4 Objectives and outcomes	2
1.5 Significance	3
1.6 Delineation	3
1.7 Methodology	3
1.8 Thesis Overview.....	3
Chapter 2 Literature review and theory	5
2.1 Introduction	5
2.2 Load-bearing building panel	5
2.2.1. Background	5
2.2.2. Materials	6
2.2.3. Insulation.....	9
2.2.4. Material characteristics.....	9
2.2.5. Structural characteristics	10
2.3 Non-load-bearing building panel.....	13
2.3.1. Background	13
2.3.2. Materials	14
2.3.3. Insulation.....	15
2.3.4. Material characteristics.....	15
2.3.5. Structural characteristics	16
2.4 Rainwater Harvesting	18
2.5 Historical data on rainfall in the Western Cape (WC).....	19
2.5.1. Rainfall and Climate in Cape Town	20
2.5.2. Rainwater Harvesting Methods	22
2.5.3. Rainwater Harvesting Process.....	23
2.5.4. Rainwater Harvesting Components	23
2.5.5. Materials	25
2.5.6. Risks.....	26
2.5.7. By-laws	27
2.6 Photovoltaic (PV)	27

2.6.1.	Historical energy use in South Africa	29
2.6.2.	Solar panel types.....	30
2.6.3.	Solar irradiation.....	33
2.6.4.	Solar cell power-output	34
2.6.5.	Performance of a PV cell	34
2.6.6.	Photovoltaic Efficiencies	35
2.6.7.	PV Materials	36
2.6.8.	Solar cell characteristics.....	41
2.6.9.	Types of PV systems and components.....	42
2.6.10.	By-laws	43
2.7	Energy utilisation in buildings.....	44
2.8	Biodegradable polymer for reuse	45
2.9	Summary.....	46
2.10	Conclusion	47
Chapter 3	Concept Development & Research Methodology	48
3.1	Introduction	48
3.2	Concept development	48
3.3	Research design	52
3.4	Study Setting.....	52
3.5	Research Methodology.....	53
3.3.1.	Data	56
3.3.2.	Research equipment	58
3.3.3.	Data collection and analysis.....	59
3.4	Conclusion	60
Chapter 4	Model and Design	61
4.1	Introduction	61
4.2	Modelling.....	61
4.3	Simulation.....	61
4.4	Model.....	86
4.5	Building panel design.....	91
4.6	Design Calculations.....	91
4.7	Materials.....	95
4.8	Prototype costs.....	96
4.9	Conclusion	98
Chapter 5	Construction System and Validation	100
5.1	Prototype Construction and Assembly	100
5.2	Validation.....	103
5.5.1.	Rainwater harvesting data	104
5.5.2.	PV data	106
5.3	Conclusion	110
Chapter 6	Results and Discussion	111
6.1	RWH and PV results	111
6.2	Discussions.....	124
6.2.1.	Simulation	124
6.2.2.	Calculations	128

6.2.3. Systems Validation	130
6.2.4. Costs	131
6.3 Conclusion	131
Chapter 7 Conclusions and recommendations	133
7.1 Conclusions	133
7.2 Recommendations	135
References.....	136
Appendix A – Standalone output data	143
Appendix B – Grid-tied system output data	144
Appendix C – System Validation	146
Appendix D – Model development.....	149
Appendix E – Graphs from system validation	153

List of Figures

Figure 2.1	An illustration of a typical construction of a building panel (Kim et al., 2020).....	5
Figure 2.2	An illustration of a precast concrete double wall (Kim et al., 2020).....	7
Figure 2.3	An illustration of 720a four-point bending test with dimensions in (mm) and measurement (a) and test rig image (b) (Hänig and Weller, 2021).....	8
Figure 2.4	An example of a load-bearing wall (a) and an infill wall (b) (Schmitt, 2018; Schmitt, 2020).....	11
Figure 2.5	Geometric relationships between vertical deformation (x) and bridged lengths (y) for fully supported slabs (Schmitt, 2018)	11
Figure 2.6	P1-F-A and P2-FA force-deflection diagrams compared to analytical calculations (monolithic glass as reference) Hänig and Weller, 2019.....	12
Figure 2.7	An illustration of a non-load bearing panel (Miccolli et.al. 2016).....	14
Figure 2.8	Hydrological Cycle indicating natural requirements to sustain water availability, a natural water recycling method (Betasolo & Smith, 2020)	19
Figure 2.9	Historic data on rainfall in the Western Cape (WC) - The Day Zero CT drought are the poleward migration of moisture (Sousa et. al., 2018)	20
Figure 2.10	Illustrates Surface runoff Harvesting technique (Anchan & Prasad 2021)	22
Figure 2.11	Illustrates Groundwater recharge, where a well is artificially recharged employing a recharge technology as a rainwater harvesting method (Veerana and Jeet, 2020).....	22
Figure 2.12	A process flow diagram illustration of rainwater harvesting, Maity et al., (2018)	23
Figure 2.13	Illustrates rainwater harvesting components and how they inter-connect (Novak et al., 2014).	23
Figure 2.14	Illustration of a basic solar cell diagram (Sainthiya,2017)	28
Figure 2.15	Schematic of a solar PV array (Sreega et al., 2017).....	29
Figure 2.16	SA primary energy supply (DoE,2022).....	30
Figure 2.17	A schematic illustration of a typical monocrystalline solar cell (Al Mansur et al., 2022) .	31
Figure 2.18	A visual difference between a monocrystalline (a) and a polycrystalline (b) solar panel (Ayadi et al., 2022)	32
Figure 2.19	An image of a typical thin film solar cell (Ayadi et al., 2022)	32
Figure 2.20	Schematic illustration of a flexible solar cell (Li et al., 2021).	32
Figure 2.21	'Optimum angle for an equator-facing plane ensuring maximum annual plane solar irradiance for South African area', (Huld, 2017).	33
Figure 2.22	Illustration of an equivalent circuit for PV panels (Ramos et al., 2010).....	41
Figure 2.23	PV module I-V curve with three distinct points (Ma et al., 2014).....	42
Figure 2.24	Optimal Solar PV Tilt Angle for Maximum Annual Irradiance (Jurasz et al., 2020).....	43
Figure 2.25	Illustration of an integrated sustainable roof design incorporating BIPV, green roof and RWH (Sheng et al., 2011)	44
Figure 2.25	An illustration of green building scoring, weight system in table 1 is compared to table 2 (Sheng et al., 2011)	45
Figure 2.26	Illustration of properties for various plastic materials exposed to varying temperatures for each material type (Andoh et al., 2016).....	46
Figure 3.1	Freehand prototype concept drawing	49
Figure 3.2 a)	AutoCad generated concept, b) concept showing how rainfall will be simulated	49
Figure 3.3	Initial mould design before dimensions were altered	50

Figure 3.4	Altered drawing dimensions and revised design	50
Figure 3.5	Animated illustration.....	51
Figure 3.6	Study area, Civil Engineering and Geomatics Department locality map at CPUT Bellville Campus, South Africa (Google Maps, 2015).	53
Figure 3.7	Flow chart diagram for the model.	54
Figure 3.8	Represents a graphical illustration of the annual average rainfall over the 10-years, giving rainfall depth measured in millimetres per month.....	57
Figure 3.9	Illustrates the all the testing equipment used.	59
Figure 4.1	Sun paths.....	63
Figure 4.2	PV orientation and tilt angle	65
Figure 4.3	Hourly distribution and hourly consumption graph.	65
Figure 4.4	Preliminary design results	66
Figure 4.5	Flow chart diagram illustrating a typical PVSyst simulation process flow	67
Figure 4.6	Illustration of required PLOL	68
Figure 4.7	Standalone PV input data.....	69
Figure 4.8	Depicts the I_{sc} , M_{pp} , V_{oc} relationship.....	70
Figure 4.9	I/V curve irradiance relationship.....	71
Figure 4.10	Efficiency vs irradiance relationship.....	71
Figure 4.11	Graphical presentation of the systems efficiency profile	72
Figure 4.12	Storage design information.....	73
Figure 4.13	Solar performance ratio and solar Fraction	74
Figure 4.14	Normalised production and loss factor.....	75
Figure 4.15	Typical layout of a standalone PV system.	76
Figure 4.16	Detailed ohmic loss diagram.	76
Figure 4.17	Energy loss diagram	77
Figure 4.18 a)	Typical layout of a grid-tied system b) Grid-tied system configuration.....	78
Figure 4.19	Graphical annual energy output	79
Figure 4.20	Grid tied system input data.....	80
Figure 4.21	I/V curve illustration for a 250Wp Grid tied system	81
Figure 4.22	Illustrates the efficiency curve	82
Figure 4.23	Inverter output parameters	83
Figure 4.24	Normalized productions per installed 250Wp	84
Figure 4.25	Normalized production and loss factors: N_p 80Wp.....	84
Figure 4.26	Performance ratio	85
Figure 4.27	Losses in group of parallel strings	85
Figure 4.28	Energy loss diagram	86
Figure 4.29	Freehand drawing for the revised concept.....	87
Figure 4.30	Prototype CAD drawing with dimensions.	87
Figure 4.31	Pre-model, illustrating how the final should look like when completed	88
Figure 4.32	Prototype building panel isometric view.	89
Figure 4.33	Prototype building panel with PV isometric view	90
Figure 5.1	Flow chart diagram for construction and assembling of the prototype, including design and procurement phases.	100
Figure 5.2	An illustration of a flow chart diagram with project images on the sequence for system construction and assembly.	102

Figure 5.3	(a) illustrates the finished building panel, placed horizontally on a flat surface, presenting the bottom part of the building panel, whereas, (b) illustrates the back of the building panel and its opening to the RWS tank.....	103
Figure 5.4	(c) Presents one of the connecting sides with the opening to the RWS and, and (d) illustrates the alternating side of the building panel with the PV panel's junction box.....	103
Figure 5.5	Assembled prototype building panel being validated	104
Figure 6.1	Recorded rainfall depths (mm) over a total duration of ten days of practical experiment	112
Figure 6.2	Graphical illustration of rainfall depth (mm) and energy generated (W) on the first day of the experimental work, resuming from 08:00 up to 17:00.....	113
Figure 6.3	Graphical illustration of rainfall depth (mm) and energy generated (W) during third hour of experimental, resuming from 10:00 up to 11:00	114
Figure 6.4	A bar graph presentation of rainfall depth (mm) and power generated (W) during eight hour of the experimental work, which took place between 15:00-16:00.....	115
Figure 6.5	Energy generated presented graphically for the total duration of the experiment between 08:00 and 17:00.....	116
Figure 6.6	Graphical illustration of cumulative energy generated (W) during the 10 day period of study, depicting the total hourly energy generated	117
Figure 6.7	A clear graphical presentation of energy generated in Watts when the rainwater storage is both 0% and 100% full. With experiments conducted from 08:00 – 12:00 when water storage was 0% and from 12:00 - 17:00 when water storage was 100% full.	118
Figure 6.8	Graphical illustration of rainfall depth (mm) and energy generated (W) on the first day of the experimental work, resuming from 08:00 up to 17:00.....	119
Figure 6.9	Graphical illustration of rainfall depth (mm) and energy generated (W) on the first day of the experimental work, resuming from 08:00 up to 17:00.....	120
Figure 6.10	Graphical illustration of rainfall depth (mm) and energy generated (W) on the first day of the experimental work, resuming from 08:00 up to 17:00.....	121

List of Tables

Table 2.1	Minimum and maximum rainfall calculations for Cape Town	21
Table 2.2	Provides a descriptive function for each component.	24
Table 2.3	Provides material type and characteristics related to the types of materials used.	25
Table 2.4	Solar modules are made up of different types of solar cells with varying efficiencies, namely (Jon Franke, 2021).....	35
Table 2.5	Types of solar cells, their classification, and an illustration of their structural layers.	36
Table 4.1	Incident data by Meteo database	62
Table 4.2	Global Horizontal Irradiation table	62
Table 4.3	Optimised yield results.....	64
Table 4.4	End-user load definition.....	64
Table 4.5	Meteo data for Bellville South indicating the typical meteorological year (TMY) for plane tilt=90°, azimuth=0°, Albedo=0.2	78
Table 4.6	Graphs comparing curve types to curve parameters and both parameters were plotted.81	
Table 4.7	Details mensuration for building panel components.....	92
Table 4.8	Design table for non-load bearing building panel, RWH and PV system	92
Table 4.9	PLA material elements	96
Table 4.10	Prototype building costs	97
Table 4.11	Revenue table	97
Table 4.12	Expenses table.....	98
Table 4.13	Profit and loses table.....	98
Table 5.1	RWH data set.....	105
Table 5.2	PV data set	106
Table 5.3	Rainfall & PV data set when storage is 0% & 100% respectively	107
Table 5.4	Combined cumulative data for Rainwater collection, energy generation, and when the storage is 0% & 100% respectively at 15 minutes intervals.....	108
Table 6.1	Statistical analysis for rainfall during the 10 days of study.....	122
Table 6.2	Statistical analysis for energy generated from PV during the ten days of study.	123
Table C.1	Combined data for Rainwater collection, energy generation, and when the storage is 0% & 100%, respectively, with cumulative data at hourly intervals	146

Nomenclature

Constants

A	Area (m ²)
a	End distance from centre of hole (mm)
\tilde{a}	Number of vertical connections of bolts (dimensionless)
A _b	Cross sectional area of a bolt based on its nominal diameter (m ²)
Ah	Ampere-hours
B _r	Factored bearing resistance (N)
C	Coefficient of runoff by rational method (dimensionless)
d	Diameter of pipe (mm)
DOD	Depth of discharge (%)
e	Eccentricity of applied load (mm)
E	Youngs Modulus of Elasticity (MPa)
F	Applied load (N)
f_u	Minimum tensile strength of a bolt (MPa)
F _v	Vertical force (N)
g	Gravitational acceleration (m/s ²)
G	Solar irradiance (W/m ²)
H	Height (mm)
hrs	Hours
Hz	Hertz
I	Current (A)
<i>i</i>	Rainfall intensity (mm/hr)
I _{mpp}	Current at maximum power point
I _{rms}	Root mean square value of current (A)
I _{sc}	Short circuit current (A)
L	Length (mm)
LiFePO4	Lithium-Ion Phosphate
ℓ	Litres (mm)
n	Dimensionless Number of bolts (dimensionless)
nr	Total number of years of record (dimensionless)
N	Newtons (N)
P	Applied load (N)
Pr	Power (W)
P _u	Ultimate load (MPa)
r _{max}	Distance from centroid to extreme bolt (mm)

R_s	Serie Resistance (Ω)
R_{sh}	Shunt Resistance (Ω)
R_{serie}	Serie Resistance (Ω)
R_{shunt}	Shunt Resistance (Ω)
T_r	Factored tensile resistance (N)
T_{max}	Maximum cell temperature ($^{\circ}C$)
T_{min}	Minimum cell temperature ($^{\circ}C$)
T_u	Maximum tension of bolt (N)
t	Thickness of thinner place (mm)
u	Velocity (m/s)
V	Voltage (V)
v	Volume (m^3)
V_{oc}	Open circuit voltage (V)
V_{mpp}	Voltage at maximum power point (V)
V_r	Shear resistance of bolts (N)
V_{rms}	Root square mean value of voltage (V)
V_u	Maximum shear of a bolt which is also a resultant of tangential force and the Vertical force for each bolt designed (N)
W	Width (mm)
W_p	Watt peak (W)

Greek letters

Ω	Ohm
γ	Density (kg/m^3)
ϵ_{trans}	Transverse strain (-)
ϵ_{strain}	Axial strain (-)
η	Efficiency of the panel (%)
ν	Poisson ratio (-)
π	3.141592
ϕ	Diameter of bolt (mm)
φ_{br}	Bolt resistance factor = 0.67
$^{\circ}C$	Degree Celcius

Terms and concepts

BIPV	Building Integrated Photovoltaic
CBRI	The Central Building Research Institute
CDW	Construction Demolition Waste
CoCT	City of Cape Town
CT	Cape Town
DC	Direct Current
DHI	Diffuse Horizontal Irradiance
EPS	Expanded Polystyrene
FE	Fine Element
FSC	Flexible Solar Cell
FT	Transposition factor
FTE	Flexible Transparent Electrode
GB	Green Buildings
GHI	Global Horizontal Irradiance
GPCP	Glass Plastic Composite Panels
GSI	Global Solar Irradiance
GTP	Glass Timber Panel
HFM	Heat Flow Meter
IAM	Incident Angle Modifier
IGPCP	Innovative Glass Plastic Composite Panels
LB	Load-bearing
LSF	Lightweight Steel Frame
MPPT	Maximum Power Point Tracking
MSERC	The Mandas Structural Engineers Research Centre
NLB	Non-Load Bearing
NOCT	Nominal Operating Cell Temperature
OSC	Organic Solar Cell
PCE	Power Conversion Efficiency
PE	Polyethylene
PET	Polyethylene terephthalate
PLA	Polyactic acid
PPMA	Polymer polymethyl-methacrylate
PV	Photovoltaic
rPET	Recycled Polyethylene terephthalate
RE	Renewable Energy
r.u.t	Round up to
RWH	Rainwater Harvesting

RWS	Rainwater Storage
SANS	South African National Standards
SAWS	South African Weather Services
STC	Standard Test Conditions
TB	Thermal Break Strips
TGE	Timber Glass Element
TGWE	Timber Glass Wall Element
UV	Ultraviolet
WC	Western Cape

Chapter 1 Introduction

South Africa (SA) faces a challenge in meeting the demand for energy and water supply to rural communities. In the 21st Century, water shortage is one of the biggest challenges (Gohel et al.,2020), resulting in drought due to climate change.

As a result, the environmental impact stemming from climate change, characterised by heightened occurrences of drought, coupled with the escalating expenses associated with fossil fuel-dependent energy sources, has adversely impacted the well-being of the local people. Clean, decentralised, sustainable, and economically viable electricity and water solutions are essential to uplift rural communities. This necessity is further underscored by the concurrent rise in population, directly correlating with an increasing demand for these essential resources.

1.1 Background and Motivation

Approximately 31% of the South African (SA) population live in rural communities, and over 60% of rural homes lack access to electricity, whereas 19% have no adequate water access. About 20% of water is available for non-potable use. On average, SA consumes 237 litres(*l*) per capita per day (Savelli *et al.*, 2021).

For the past two decades, the government, non-government organisations and businesses have sought innovative measures to avert climate change, improve inhabitants' livelihoods, and preserve the resources for future generations. Available sustainable technologies are relatively costly for the public where SA experiences economic disparities in wealth and income.

The dependency on municipal water and energy generated from fossil fuels has worsened the challenges relating to climate change (Gibberd, 2020). This dependency is slowly sprawling into the rural parts of the country. SA rural areas have more significant opportunities to omit the reliance on municipal water as well as the use of conventional fossil fuel-based energy and hedge into sustainable resources that offer durability and independence, such as rainwater harvesting (RWH) and alternative green energy in the form of photovoltaic (PV). This omission will simultaneously assist with the reduction of atmospheric emissions. A similar opportunity exists by giving significance and functionality to a non-load-bearing (NLB) building panel.

Researchers affirmed that the unsustainable water use in the middle- and upper-income classes worsened the hydrological drought (Savelli *et al.*, 2021). Also, the sharp reduction of available water in the Cape Town (CT) area, Western Cape (WC) Province, results from a precipitation deficit. Six significant dams had reached a storage capacity of 28,3%, with only 12,3% of useable water at the end of the meteorological drought.

The need for the supply of clean, sustainable and affordable energy is pivotal for developing and developed countries across the board. With the population increase, the demand for adequate buildings, water, and energy supply equally increases. Thus, implementing energy and water efficiency is necessary to develop green buildings.

1.2 Research problem

SA faces a challenge to meet the demand with the supply of energy and water to rural communities. This research project designed a triple-purpose prototype panel that links two existing green technologies into a single component used for rainwater storage and energy generation whilst providing the functionality of a building panel.

1.3 Identified Gap

Much research has been done autonomously on PV and RWH systems. The collected literature has no suggestion or work to integrate a prototype building panel used simultaneously for rainwater storage and energy generation. The latter is the gap this research proposes to accomplish; (Gobin et al., 2019) approve by asserting that the connection between water scarcity and fossil fuel sources has growing implications and is critically vital for the planning of future water and energy blends. Attoye et al., (2017) reviewed and identified the customisation of Building Integrated Photovoltaic (BIPV) strategies and how these can be adopted. The availability of both technologies designed and modelled to cater for financially struggling communities, especially in the rural areas of SA or informal settlements. This technology is viewed as an integrated system, and collaborative research is now based on an integrated system which opens an opportunity for researchers to focus on one sustainable solution (Wang *et al.*, 2017)

1.4 Objectives and outcomes

This research aimed to design a prototype building panel for rainwater storage and renewable energy generation.

The following were the objectives of the research work:

- i) To determine the volume of rainwater harvested in a rainwater storage tank with inside dimensions of $314 \times 50 \times 195$ mm embedded in a building panel referred to as *iBP*
- ii) To determine the power output of a 10W solar cell placed on a vertical surface of a building panel with $345 \times 60 \times 200$ mm outside dimensions referred to as *mBP*
- iii) To determine the related costs for this technology.

Even though individual sustainable technologies are readily available, these technologies ease the pressure on the supply and improve on challenges SA faces, such as water scarcity and power outages. The expected outcomes of this research identify knowledge and theoretical gap types in this study. The following are the expected outcomes of this research:

- i) To successfully develop a triple-purpose prototype building panel retrofitting rainwater storage/harvesting to a 10W renewable energy (RE) generating photovoltaic panel. This harvested water can be intended for secondary water use, and this integrated system is designed as a building panel.
- ii) To develop a turnkey solution that introduces functionality to a building panel and solves on-site water-related and energy supply problems.
- iii) To determine the effectiveness and understand the adequacy of an RWS tank made from recycled plastics functioning as a building panel generating 10Watt-peak (Wp) and costs.
- iv) To establish the efficiency of energy generated from photovoltaic panels when a polycrystalline flexible solar cell (FSC) is used instead of a conventional solar panel.

The model reduces the need for the supply of water and the supply of energy from the grid.

1.5 Significance

Water scarcity and power outages are real-time problems that will last for generations. Rainwater has been devised as an engineering solution to water problems that conserve water resources measured as small-scale technology (Chandramouli, 2015). Gobin et al. (2019) approve by asserting that the connection between water scarcity and fossil fuel energy sources has growing implications and is critically vital for the future planning for the blend of both water and electricity. The design of a prototype building panel storing rainwater and generating energy is a solution for rural communities. SA rural areas and informal settlements have greater opportunities to omit the dependency on municipal water and the use of conventional fossil fuel-based energy and hedge into sustainable resources that offer durability and independence, such as RWH and RE in the form of PV. This research contributes to the Engineering body of knowledge and abides by the CPUT ethics guidelines.

1.6 Delineation

This research focused on designing a triple-purpose panel, a non-load-bearing building panel that harvests water and generates energy. It incorporated water demand (non-potable) and energy demand for households in rural areas. Because the research only focused on direct household use, it excluded the design and use of water treatment plants, overhead powerlines and transformers.

1.7 Methodology

To fulfil the objectives of this study, the project is developed in different stages, consequently requiring assembling. The developmental stages included PV material procurement, building panel design, manufacturing and assembly. PV materials and some components were sourced from China. The *mBP* designs were conducted autonomously, incorporating preliminary freehand drawings and model buildings, design calculations for the building panel, RWH system, and PV, 2D CAD, and 3D drawings. PV simulation on PVSyst for a standalone and grid-tied system. The *mBP* manufacturing phase required the conversion of drawings to a printable lithograph format known as an STL file and choosing a clear-coloured filament for the final product. The model was printed from a Creality Ender – 3Neo 3D printing machine. The prototype assembly process took place, starting with the wiring of the PV components, the connection of the peg boards, and the adjoining PV and *mBP* using a Sika 219i marine adhesive sealant. All components were connected, and the prototype was ready for verification.

1.8 Thesis Overview

Chapter 2: Literature Review: provides a concise overview of previous research and advancements related to the project. This section explores the existing knowledge and developments in building panel technologies, highlighting their characteristics, advantages, and limitations. The chapter begins by reviewing autonomously conducted work on different types of building panels and materials.

Furthermore, the chapter delves into the rainwater harvesting methods, processes, and components. It encompasses a comprehensive review of the collecting and storing rainwater techniques, including different storage systems, filtration methods, and distribution mechanisms. The various components

involved in rainwater harvesting systems are also discussed, shedding light on their functionality and importance. The next section focuses on solar cell types, efficiencies, and PV materials. It examines the different types of solar cells available in the market, such as monocrystalline, polycrystalline, and thin-film cells, emphasizing their respective efficiencies and performance characteristics. Additionally, the review encompasses an analysis of the materials used in photovoltaic technology, discussing their properties and suitability for solar cell fabrication.

Chapter 3: Research Methodology: provides a detailed account of the research methodology employed in the project. It elucidates the data collection process, including the relevant information sources. The chapter outlines the research design, highlighting the methodologies utilized to investigate the study's objectives.

Furthermore, this chapter presents the analysis and presentation of the collected data. It describes the analytical techniques to interpret the gathered information and draw meaningful conclusions. The results obtained from the data analysis are then presented using appropriate visual aids and statistical representations.

Chapter 4 Model and Design: Provides details and procedure on model execution and design calculations; the software employed for PV simulation integrates standalone and grid-tied systems, and PVsyst software is used for the simulation and outcomes presentation. The simulation began with the preliminary design for off-grid and grid-tied systems. The design calculations entailed building panel design for NLB building panel, bolt design calculations, RWH system design and PV system design.

Furthermore, this chapter provides sufficient information on the prototype material chosen, such as material characteristics and elements. The method used to combine all three technologies. The design calculations were conducted autonomously for each technology design and the cost breakdown for the prototype. The design calculations were in accordance with the SANS codes of practice. The cost breakdown for the project was also conducted in this chapter.

Chapter 5 Construction and Validation: provides details of the construction of the building panel, the assembly of the building panel, and the validation process. The systematic details include the location where the prototype was developed, what instrument was used, how long it took to finalise the prototype, the material used, the chosen colour, and the motivation for the material choice.

Meanwhile, the validation process provides details on all the experiments that were conducted, the data collected during the experiment period, the equipment used, the time taken, and the method of conducting tests.

Chapter 6 Results and Discussions: draw results and discuss in detail the outcomes of experimental results obtained during the validation process and some of the pertinent design aspects conducted during the design phase, not reported on under construction and validation. The outcomes from the experimental examinations were verified if they aligned with the aims and objectives of this study.

Chapter 7, Conclusions and Recommendations, summarises the research study and findings. Conclusions are drawn from the research project's findings, and recommendations are suggested for future work relating to the design of prototype building panels and rainwater storage for energy generation.

Chapter 2 Literature review and theory

Literature and theory of research work that has been conducted scholarly to the engineering body of knowledge has been reviewed and analysed to show the gap of this study.

2.1 Introduction

This section focuses on a building panel and the protective material joined to the outside of a wall of a house, a large commercial building or a high-rise building. A building panel consists of two types, namely, load-bearing building panels and NLB building panels. A load-bearing panel (LB) supports the weight of a floor or a roof structure, whereas an NLB panel carries its weight. The building panel designed in this research study comprises a rainwater collecting system capable of generating energy through solar power. Previously, most buildings are viewed for their aesthetic value; implementing sustainability implies considering each building structure's functionality. The functionality of buildings, such as walls carrying loads and transferring such loads to the foundation, needs to be modernised by adding value, where walls can, through load-bearing or non-load-bearing walls, harvest and store rainwater and generate energy as an alternative to conventional electricity.



Figure 2.1 An illustration of a typical construction of a building panel (Kim et al., 2020)

2.2 Load-bearing building panel

2.2.1. Background

The building's load-bearing components include examining structures for the building's bases, parapets and pillars, slabs, and roofs. The review focuses on how the cellular structure is presented. Space-forming and load-carrying building materials and structures provide unique shapes of geometric structures (Lámer, 2021). (Premrov et al., 2021) Numerous studies in the body of existing literature demonstrate that window and door apertures can, to some extent, increase the stiffness and horizontal load-bearing capacity of such wall features. As a result, timber-glass elements (TGE) that use insulation-glazed sheathing instead of traditional sheathing can support some degree of horizontal loads. Naturally, it is necessary to provide horizontal force transfer across the fictitious glass panel's tensile diagonal and over the connection glass-timber plane (GTP) through the proper aided epoxy resin. In addition, it should be stressed that the timber-glass wall element (TGWE)'s load-bearing should be used in models of timber-glass prefabricated objects that were experimentally constructed as simplified box-house models and integrated into prefabricated frame-panel macro-wall systems with load-bearing walls.

(Motteu,1977) A more thorough analysis of structures and safety inspection of the load-bearing wall was required due to the rapid industrialization of housing development, especially in concrete systems with large panels, during the 1960s, which explains why much commission work was previously focused on this area. The following categories were used to group the various developments in the work:

-Wall construction resistance and the reaction of structures with specific attention to massive structures of panels.

-Structural defects call for renovating old buildings (Motteu,1977). During the 1990s, the full wall systems were produced in one piece, measuring 1250mm in length. Most window and door openings were built due to technological requirements after speedier fabrication (Premrov et al.,2021).

Different types of materials for load-bearing panels that are under research and in the market are briefly discussed to give an overview of available and explorable resources where this research can employ what is identified as gaps.

2.2.2. Materials

Building-integrated photovoltaic (BIPV) is a modern material - available to architects that performs double duty as an energy source and an element of the building envelope (Attoye et al., 2017). One of the most severe issues developing countries encounter is deplorable housing conditions and severe housing shortages in cities and the countryside. The disparity between housing supply and demand is rapidly expanding. One of the most significant barriers to solving the problem is the lack of exuberant costs for building materials (Premrov et al., 2021).

Even though building materials costs are high (Premrov et al., 2021), (Mathur,1984), research has illustrated the progress and changes in load-bearing brickwork design and construction. The Central Building Research Institute (CBRI), Roorkee, researched better-valued bricks with low production costs (which offset the escalating building costs) and created and designed semi-mechanised brick equipment. CBRI proposed innovative methods of producing high-quality bricks made from soils that would otherwise be unsuitable for such purposes as black cotton soils. CBRI has also proposed the design of load-bearing brick construction for multi-story buildings.

The Madras Structural Engineering Research Centre (MSERC) has provided information on masonry's compressive strength. It developed prism examinations for masonry work to compare the relationship between the strength of a masonry unit and that of an actual wall strength (Mathur,1984).

In determining masonry uniaxial load-bearing capacity subjected to bending while considering the membrane effects due to information technology (I.T) based travel-controlled design procedure, and used iterative calculations. The analytical calculation process was validated using the outcomes of fine element (FE) simulations and test results from the literature. The resulting membrane compressive force and the horizontal capacity load with the corresponding horizontal deformation of the wall were compared for all three models. It was demonstrated that the evaluation of the individual results exhibited good agreement and was accurate enough to design the wall's structural layout (Schmitt, 2018).

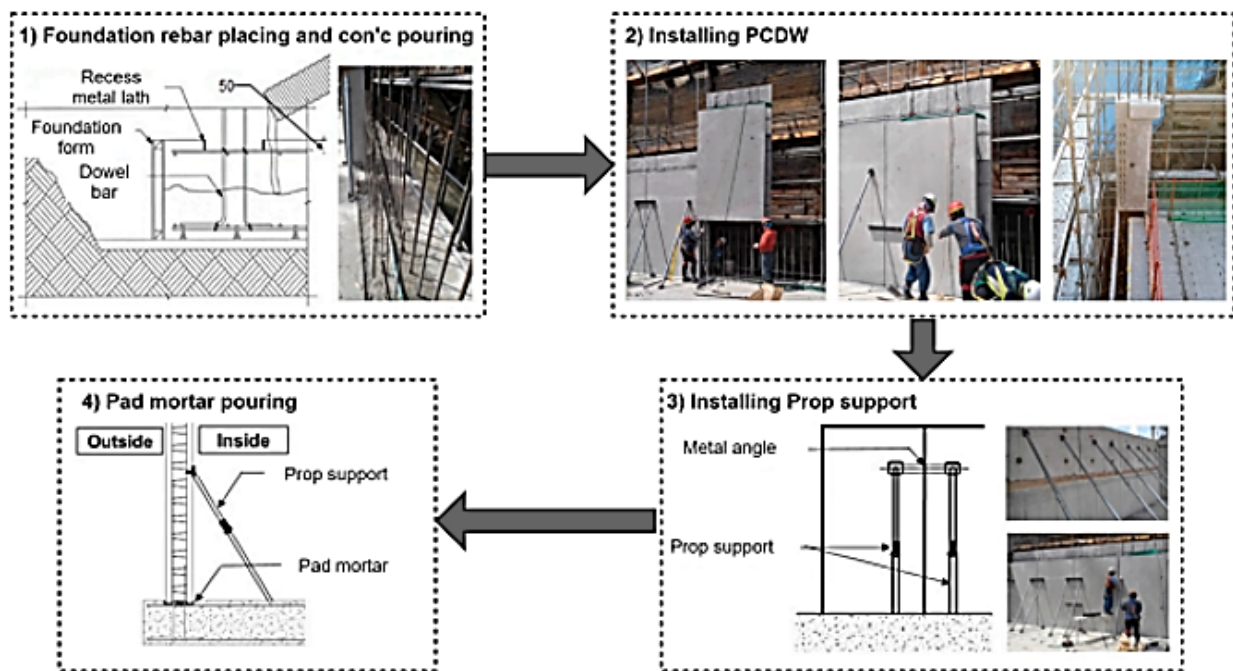


Figure 2.2 An illustration of a precast concrete double wall (Kim et al., 2020)

Depending on the functions of the building panel, they are widely known for aesthetics and insulation, and they serve as infill walls.

Masonry walls are conventional materials used in the building industry; research considers innovative materials, such as composite materials, qualified as load-bearing building panels. (Hänig and Weller, 2021) Innovative glass plastic composite panels (IGPCP) are strong, have low self-weight, and possess high structural load-bearing capability. These characteristics make the composite panel appropriate for thin, light glass production and give the building sector new design options. However, the material characteristics of the improved polymethylmethacrylate (PPMA) polymer interlayer core are adequate for the same design considerations. The material behaviour of thermoplastics polymer also varies with temperature and age over time due to environmental factors.

This considerably impacts the load-bearing behaviour of composite panels and determines the application limits for composite panels in the building sector.

IGPCP is an improved material developed after Neeroglass; both are glass plastic composite panels (GPCP). (Hänig and Weller, 2019) NEEROGLOSS is a brand-new GPCP made of cover layers of slim glass and acrylic glass, acting as the polymer interlayer core. Without additional epoxy resins or interlayer films, the glass cover layers are joined to the polymer interlayer core while manufacturing the chemical process created and carried out by KRD Coatings GmbH.

Glass is an isotropic, linear-elastic construction material that permits rapid design to internal forces and tensions during the design phase. The material characteristics of each layer have a significant impact on the load-bearing behaviour of composites (Hänig and Weller, 2019). The stiffness, strength, and creep behaviour of thermoplastic interlayers, which are used in the construction industry, vary depending on the duration of load and temperature range of -20 to +60 degrees Celsius (°C). As a result, the viscoelastic characteristics of the interlayer material and the bond between the two components significantly impact the GPCP's load-bearing behaviour.

The composite load-bearing behaviour is highly influenced by the time-and-temperature-dependant hardness of the polymer interlayer material, as with the shear connection between glass cover layers (Hänig and Weller, 2021). There has to be more research and development into high-performance transparent and lightweight structures because of the trend towards huge glass façades and the desire to conserve materials (Hänig and Weller, 2019). To lower self-weight while exploiting the excellent durability of glass, a combination of polymeric interlayer cores chemically linked to cover layers of thin glass approximately 3mm in thickness is being developed. The IGPCPs work as a single unit to provide sufficient high-performance load-bearing behaviour.

The load-bearing behaviour is examined in four-point bending tests in accordance with DIN EN 1288-3:2000-09 2000, which also determines the linear composite stiffness and glass stress response (Hänig and Weller, 2021). At least five test samples per series were loaded at 400 Newtons per minute (N/min) at +23 °C, up to a force of 400 Newtons (N). The strain in the x direction and the deflections in the z direction were measured using axial strain gauges on the glass surfaces (centre top and bottom) and vertical displacement sensors in the centre edge. Figure 2.2 is one bending roller. A thorough explanation and assessment of composite load-bearing tests are provided (Hana and Weller 2019b).

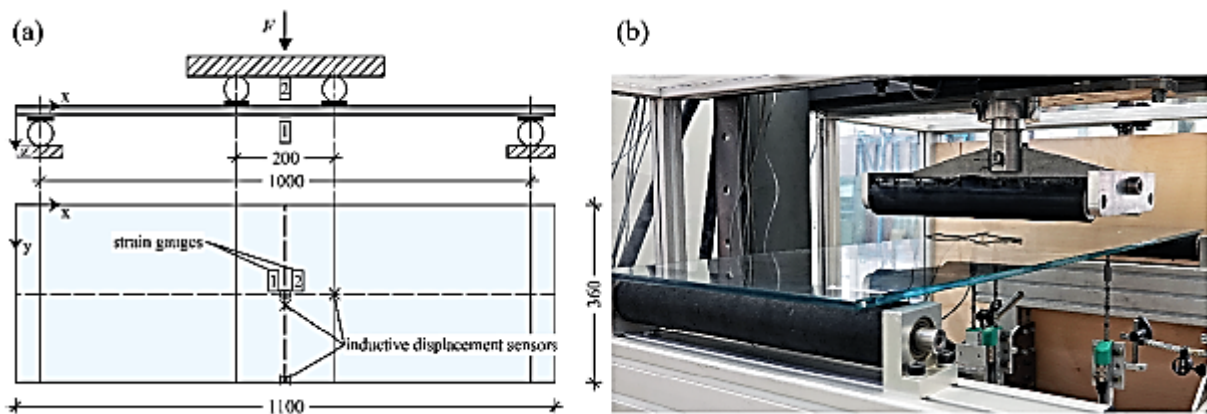


Figure 2.3 An illustration of 720a four-point bending test with dimensions in (mm) and measurement (a) and test rig image (b) (Hänig and Weller, 2021)

Different materials provide different functionality, purpose and characteristics. Some materials differ, and some are similar. Research has not shown similarities or differences between various explored materials; however, lightweight steel frame (LSF) materials that were primarily explored deal with thermal conductivity in building structures.

Thermal conductivity in steel frame materials has the potential to produce thermal bridge effects that are significant but unwanted and present special challenges for LSF for building elements. Accurate thermal characterisation of the envelop elements has been required to provide a consistent assessment for elements has been required to provide a consistent assessment of the heat behaviour and energy effectiveness in building structures. Measurements are the most dependable methods for this thermal characterisation under controlled laboratory conditions. Research has indicated thermal break (TB) strips as a popular method for preventing thermal bridges. The thermal performance of 20 LB and NLB LSF wall formations is assessed using a heat flow meter (HFM) under controlled laboratory conditions (Santos and Mateus,2020).

Methods of construction and site elements geared toward economy enhancement and productivity improvements are important, as are design considerations for load-bearing and non-load-bearing walls (Hendry, 2001).

The functionality of building panels includes aesthetics and insulation, and they also serve as infill walls. An overview of insulation and its role on the load-bearing panel is briefly illustrated in section 2.2.3. Insulation is also explored to identify the gap in this research.

2.2.3. Insulation

The research examines waste materials, specifically rPET bottles, as an alternative building resource (Semenov et al., 2021) (Mousakhani et al., 2022). Various research was conducted investigating the use of rPET materials in brick production, where it was found that rPET has excellent potential to be used structurally and thermally in building elements (Mousakhani et al., 2022). At the same time, other research observed an increase of 57% in compressive strength where concrete blocks were packed with void PET bottles. The research concluded that using waste PET bottles potentially contributes to an increased insulation R-value for external building walls, offsetting environmental pollution and construction cost savings (Semenov et al., 2021) (Mousakhani et al., 2022).

Other research illustrated timber frames comprised of studs, longitudinal posts, and sheathing boards are used to construct prefabricated framed-panel wall elements such as fibre-plaster or OSB that are unilateral or bilateral and attached to the timber frame with nails or staples. The exterior wall elements are frequently thermally insulated by installing soft thermal insulation that is positioned between the frame and the outer stiff thermal insulation. Due to technological limitations, these prefabricated pieces were initially only produced as single-panel components with a standard length of 1250mm. In the 1990s, the full wall system was constructed in one piece, measuring 1250mm. Most window and door openings were constructed due to technological requirements after speedier fabrication (Premrov et al, 2021) (Schmitt, 2020).

Various measures are implemented to enhance efficiency in construction materials, where expanded polystyrene (EPS) is utilised for various purposes. Sandwiched concrete panels made from EPS are an affordable, lightweight building material that serves as both a load-bearing and an insulating component. Sandwiched concrete panels made from EPS help construct homes quickly and conserve resources. This experimental study tries to evaluate the performance of EPS-sandwiched concrete panels exposed to changing corrosion levels using the impressive current corrosion technique (Garhwal et al., 2022).

2.2.4. Material characteristics

This research briefly discusses various construction materials and their characteristics, where it was found that building envelope components must be accurately thermally characterised for a meaningful evaluation of thermal behaviour and energy efficiency. The measurements under lab-controlled settings are one of the most reliable approaches for this thermal characterization. The evaluation of the thermal performance of LSF building elements poses specific issues due to the significant heat conductivity differences between steel frame materials and cavity insulation, which can cause undesirable considerable thermal bridge effects. TB strips are one of the most common strategies for preventing thermal bridges. Research has used an HFM to verify the thermal performance of 20 LB and NLB LSF wall designs under controlled laboratory settings (Santos and Mateus,2020).

Thermal performance is also researched on lightweight permeable foam ceramics. Depending on the application, lightweight permeable ceramic offers a variety of benefits over densely sintered ceramic. Foam ceramic possesses a low thermal conductivity and is a good noise barrier when used as a building material with insulation properties. Foam ceramic is considered a suitable material for decorative and non-structural construction elements, and it is also apt for the production of thermal and sound insulation for any suitable construction (Mutafchieva et al, 2022). Research also examined the marl clay characteristics found near the village of Lovets near Shumen, with foaming additives made of coal, and the technology for manufacturing regulations for foam ceramic. It was found that foam ceramic thermal insulation improves physical-mechanical and tribological pointers where the heat conductor coefficient is low (Mutafchieva et al, 2022), (Kinnane et al.,2022).

Research studies make an effort to evaluate the thermally conductive and non-conductive shear connectors and how they interact with the wythes and insulation to provide load resistance to both flexural and direct shear loading. Lateral and direct shear loads on precast concrete sandwich panels depend on the panel's capacity to take on composite action. To determine the load capacity and failure modes, key aspects are the span and thickness of the wythe, the mechanisms and concrete strength, the insulation, and the shear design connectors. To design an adequate and successful system, it is especially important to understand the post-cracking behaviour that occurs before pull-out, shear, or buckling failure. This behaviour is significantly pragmatic and requires understanding (Kinnane et al., 2022), (Lámer. G, 2021).

2.2.5. Structural characteristics

This research looks at various structural characteristics of different building materials and how these respond to load-bearing building panels. Each characteristic for the corresponding varying material is individually briefly discussed.

A novel method for looking at a building's supporting structures and spatial boundary systems uses cells. Two scales of cell modelling are suggested for describing a building's auxiliary systems. A building's supporting structures and space delimitation systems are described using cell modelling on two scales. One scale represents the entire structure, and in that paradigm, the two-dimensional cell defined by the walls and slabs serves as the fundamental unit walls and pillars (Lámer. G, 2021).

Instead of being an imposed load in the conventional sense, the resulting normal force is a vertical reaction force that comes from constraints. However, the wall must first deform horizontally and then move vertically for this force to occur. It should be noted that, in this case, the horizontal loading results in an additional normal force acting through the vertical direction on a wall subject to lateral bending (Schmitt, 2018).

A load-bearing capacity of infill masonry walls considering the deformation-based membrane effect as indicated in Figure 2.4.

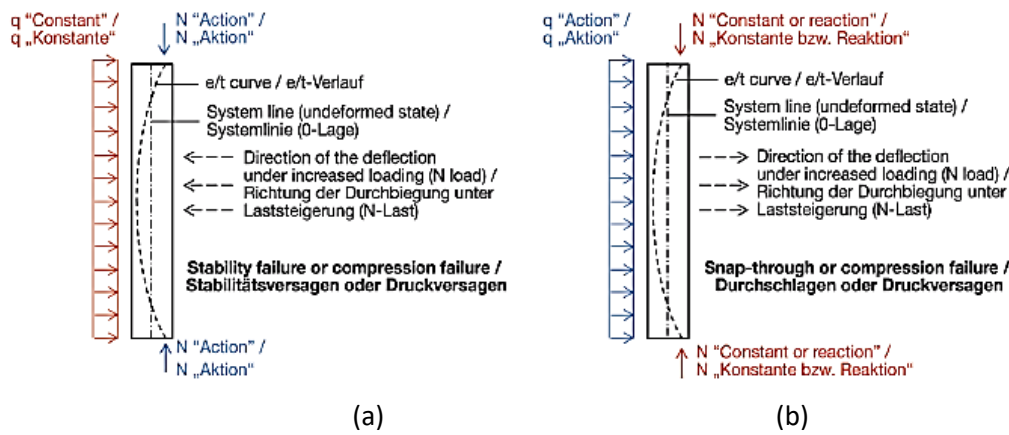


Figure 2.4 An example of a load-bearing wall (a) and an infill wall (b) (Schmitt, 2018; Schmitt, 2020)

The load-bearing capacity of the system is determined by using general formulas initially supplied for calculating the deformation-based membrane compressive force (Schmitt, 2018).

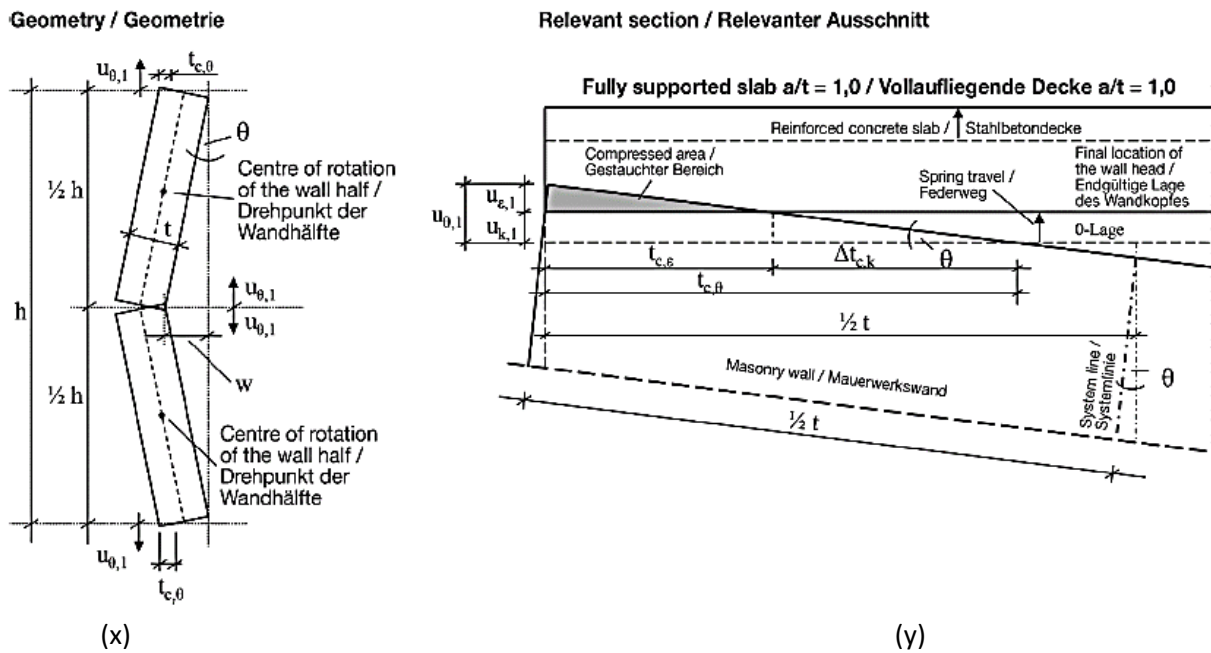


Figure 2.5 Geometric relationships between vertical deformation (x) and bridged lengths (y) for fully supported slabs (Schmitt, 2018)

This research looks at moment-curvature and gives a brief overview, subsequently determining load-deformation behaviour load-bearing building panels are capable of undergoing, where Schmitt, (2018), Dem'yanov et al (2019) illustrate a group of individual moment-curvature curves are used to determine the moment-curvature relationship. As curvature increases, so do the acting normal forces, so each curvature of an individual section has a moment-curvature curve.

(Gunkler. E, 2014) Point loads result from columns and beams perpendicular to horizontal joints causing concentrated loads in masonry walls. Theoretically, compressive strength is caused by multi-axial stress situations that occur locally beneath the load area with numerical values bigger than the mono-axial

compressive strength of the masonry wall. About 30 years ago, standard testing specimens were last used in Germany, increasing the load factors without using the walls.

The examined masonry types, at the time, were composed of common masonry unit sizes and types as well as joint and mortar formations; even though this no longer appears to be the case. This opens an opportunity to examine the application of precast concrete sandwich panels.

Upon applications of lateral and direct shear loads to precast concrete sandwich panels, the structural response is determined by the ability of the panel to develop composite action. To determine the capacity of load and modes of failure, the wythes' thickness, the composition and strength of the concrete mix, the insulation, and the nature of shear connectors all have a role. A discussion has been conducted on thermally conducive and non-conductive shear connectors and the interaction with wythes and insulation to provide load resistance to direct shear loading. The post-cracking behaviour before pull-out, shear, or buckling failure has been observed to vary significantly. It must be understood to design systems that successfully fit the purpose (Kinnane et al., 2022).

(Hänig and Weller, 2019) Analysed calculations with short-term experiment results were compared with experimental short-term results in a force-deflection diagram to validate the model for the new glass-plastic composite panels, as shown in figure 2.6. The PMMA interlayer core's Young's modulus was set to 3300N/mm² with a Poisson ratio of 0.37. Young Modulus and Poissons ratio were employed.

The analytical calculations (dot-dashed lines) roughly agree with the experimental results, according to the charts in figure 2.6 (mean values - dashed lines). The calculations are conservative and result in higher deflections.

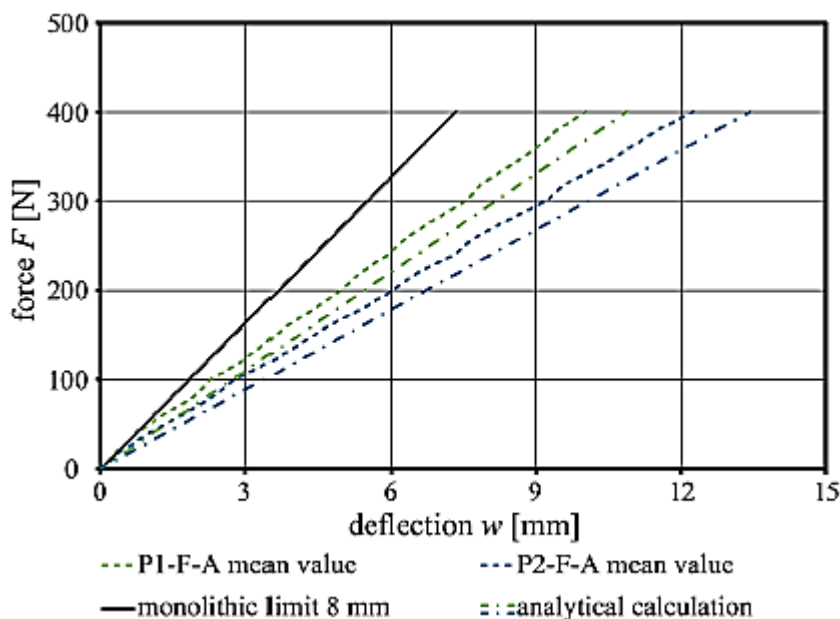


Figure 2.6 P1-F-A and P2-FA force-deflection diagrams compared to analytical calculations (monolithic glass as reference) Hänig and Weller, 2019

(Schmitt, 2018) To accurately determine the load capacity applied horizontally on masonry infill walls that are not reinforced, spanning in the same direction where the creation of non-linear calculation is modelled. Vertical forces, also known as membrane compressive forces, occur in this model under specific support conditions. The presented non-linear calculation procedure has led to the developing a practically

useful design model. Still, it only deals with the membrane effect in a crude and insufficiently precise manner. This has successfully bridged the gap between the systems used in practice and the current calculation procedures by formally incorporating real support conditions. In the future, designing masonry walls with area loading-wind loads and expansion loads is possible while considering support conditions, thereby realistically considering the membrane compressive force based on deformation.

(Schmitt, 2018) Verifying the load-bearing capacity of load-bearing masonry walls under a small vertically imposed load is an intriguing application. It has been demonstrated that, in typical practical situations, the associated structural model design and the development of the calculation process can be used to verify the required minimum imposed load. Veracity for all wind zones is possible depending on the support stiffness caused by the wall and slab thickness.

(Schmitt, 2018) Iterative calculations are used to verify the uniaxial load-bearing capacity of masonry that is primarily due to bending while considering membrane effects because an IT-based travel-controlled procedure to calculate is used to determine the load-bearing capacity of the system. The analytical calculation process was validated using the outcomes of (fine element) FE simulations and test results from the literature. The resulting membrane compressive force, the horizontal load capacity, and the horizontal deformation associated with all three wall models were compared. It could be demonstrated that the evaluation of the individual results exhibits good agreement and is accurate enough to design the structural wall.

2.3 Non-load-bearing building panel

2.3.1. Background

As: LB (previously discussed) and NLB are discussed in this section. NLB panel carries its weight in any structure. Different materials used in the construction industry and those currently under are highlighted and briefly discussed, considering their structural and material characteristics.

Non-load-bearing walls are essential to any building (Pitroda et al., 2016). The structural design, hauling distance, self-weight, and construction influence this type of wall construction. The physical characteristics of a non-load-bearing wall are determined by the materials used and their specifications, so research or determination of various suitable materials for NLB wall construction is required. (Al-Shaleh, and Attiogbe, 1997) The lateral resistance to wind load factor controls the designs used in Kuwait, such as non-load-bearing masonry walls.

The key indicators for NLB walls have been researched, including economic indicators, flexibility, availability, strength, cost, weight, soundproofing, life span, and thermal conductivity. The analytic research was to investigate the adequacy and benefits of NLB walls made of various materials such as Polymer Precast Panel, Fly Ash Brick, Autoclaved Aerated Concrete (AAC)Block, Acotec Panel, Traditional Stone, Paper Fiber Reinforced Foam Concrete (PFRFC) Material, Clay Bricks, Glass Fiber Reinforced Gypsum (GFRG) Panel (Pitroda et al., 2016)

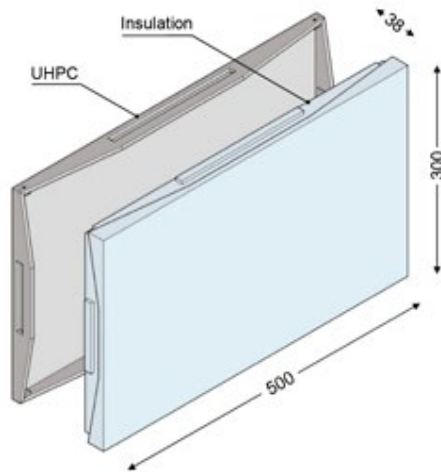


Figure 2.7 An illustration of a non-load bearing panel (Miccolli et.al. 2016)

2.3.2. Materials

Research has provided a layout for constructing a contemporary masonry wall, which commences with a brief application description and related benefits (Hendry, 2001). Manufacturing masonry materials, such as clay, concrete, and calcium silicate, comes in a wide variety of unit sizes, shapes, and colours. For improved workability, research recommends the addition of lime as a plasticizer to cement/sand mixture, typically mortar. New advancements in mortar formulations have emerged, including thin-bed mortars for precise unit measurements and mortars exhibiting enhanced heat-related properties. Comprehensive overviews of design considerations for both load-bearing (LB) and non-load-bearing (NLB) walls are presented, along with construction methods and site particle recommendations to optimise economic efficiency and productivity (Hendry, 2001).

The precast sandwich panel review was initiated to evaluate the body of research conducted, examine projected design solutions, and verify the outcomes to find future research focuses. The latter identifies specific advances in high-strength concrete without steel but with high strength (O’Hegarty and Kinnane, 2020).

Improvements from the commencement of research and material efficiencies to component levels demonstrate ventilated façade panels that possibly produce modular envelop systems from construction and demolition waste (CDW), meeting specific performance requirements for a certain type of construction product. Furthermore, the results for hygrothermal and the monitoring of field energy consumption in buildings indicate that the panel developed is appropriate for use as a high-performing building envelope in practical environmental conditions. Field monitoring at the entire building level indicates that the development panel suits a high-performance building envelope in real-world environmental conditions (Pečur et al., 2020).

Some of the development panels include concrete wythes that are lighter and thinner; these lighter and thinner concrete wythes are now possible, thanks to high-performance concrete and normal reinforcement methods. Numerous new fibre-reinforced polymer connectors facilitate shear loads that could minimise localised heat loss transferred across layers and have been developed and tested. Modern low-conductivity insulation technologies enable astonishing low U-values for building thinner walls. All

these advancements broaden the applicability of sandwich panels to a broader range of building typologies while enhancing the inherent benefit of precast cladding (O'Hegarty and Kinnane, 2020).

2.3.3. Insulation

This research considers insulation and briefly provides an overview of some NLB materials and their performance. Depending on the performance of the material used in constructing NLB, such material can be considered for insulation owing to its insulation value. This research also considers materials for insulation mechanisms attached to NLB walls. Research considers insulation. Briefly, it provides an overview of some materials and their performances.

(Ariyanayagam, and Mahendran, 2018) The fire design of NLB LSF walls, which behave differently than LB walls, is governed by insulation and integrity failures. Numerous in-depth studies have been carried out to examine the heat-related and structural performance of LB LSF walls that have been exposed to fire and lined with gypsum plasterboard. However, these studies are only applicable to LSFs that are not load-bearing. Small-scale NLB wall fire tests compare the outcomes of tests carried out under the same circumstances rather than simulating actual fire behaviour.

But concrete wythes' performance differs from that of NLB walls lined with gypsum plasterboards, and because of high-performance concrete and conventional reinforcement technologies, lighter and thinner concrete wythes are now conceivable. Fibre-reinforced polymer connectors from various innovations have been developed and verified, enabling shear load transfer across layers where thermal loss has been minimised. Modernised insulation technologies with low conductivity permit the construction of low U-values for thin walls. The appropriate expansion for the sandwich panel developments boosts the value of building classifications and appreciates developed and verified precast cladding (O'Hegarty and Kinnane, 2020).

Developing composite action for the structural response for precast concrete sandwich panels due to lateral and direct shear loads depends on the panel's capacity. The capacity and failure modes affect the length, width elements, and strength of a concrete mix with insulation combined with the type of shear connectors. Discuss thermally conductive and non-conductive shear connectors and how they interact with wythes and insulation to provide resistance to flexural and direct shear loading. The successful system design fit before pull-out, shear, or buckling failure for the post-cracking behaviour has differed significantly and must be understood (Kinnane et al., 2022).

Precast concrete cladding is regaining popularity as a building cladding material. A level precast concrete sandwich panel is distinguished by thermal resistance with an insulation layer between two concrete wythes and secured with mechanical connectors. It also provides cladding solutions for new buildings and efficient thermal cladding and cladding replacement for renovations (O'Hegarty and Kinnane, 2020).

2.3.4. Material characteristics

The evolution in the construction industry leads to the improved development of building materials, with trends leaning towards sustainable construction materials and enhanced material characteristics, where research briefly reviewed some improved characteristics for some construction materials.

In the construction industry, the employment of sustainable materials is gaining popularity and importance. Because of their lightweight, improved insulation properties, and quick installation, EPS in

precast concrete sandwich systems is slowly replacing traditional blockwork systems. System design optimisation and manufacturing are required to produce quality products that provide superior insulation, durability, and rapid installation while ensuring adequate bonding, strength, and mechanical properties to suit their purpose. According to research, the technical properties of the sustainable lightweight precast concrete sandwich panel for NLB partition wall system depend on the mix design and durable production. An experimental program was created to determine the best mixture proportions for the EPS concrete core. To determine the physical and mechanical properties of the researched EPS concrete system, experimental testing and calculations were used to achieve practical system production and installation procedures that were researched. Before concrete testing, quality control assurance establishes a relationship between the density of EPS concrete and its compressive strength. The results revealed a high correlation coefficient between the core density and compressive strength (Moutassem and Al Mara, 2021).

Al-Shaleh and Attiogbe (1997) state that lateral resistance to the design of wind loads is a controlling factor for NLB masonry walls, such as those in Kuwait. Walls built with locally available materials require data on flexural strength characteristics to ensure the safety of the walls. Small-scale wallets are used to verify the flexure of masonry walls built with an aerated concrete block that was autoclaved, sand-cement, concrete blocks or calcium silicate bricks. The epoxy glue mortar was used to construct the aerated block of concrete wallets that were aerated. In contrast, the sand-cement mortar was used to build the block of concrete and brick wallets to form calcium silicate. The tests for unreinforced masonry were carried out following the British Standard.

Ariyanayagam, and Mahendran, (2018) For the thermal and structural behaviour of fire-exposed gypsum and plasterboards lined LB LSF walls, more detailed research has been conducted and is limited to NLB LSF walls. LB walls and NLB LSF walls differ in characteristics governed by insulation or integrity failure for fire design. Comparative results are provided under identical conditions, where small-scale NLB wall fire tests do not simulate the actual fire behaviour.

2.3.5. Structural characteristics

A dependable analysis of buildings' thermal behaviour and energy efficiency requires precise thermal characterisation of the envelop elements. The measurements under laboratory-controlled conditions are more precise practises for performing thermal characterisation of this nature. Assessment of the thermal performance of LSF elements of the building presents unique challenges owing to the high thermal conductivity contrast between cavity insulation and steel frame materials, which can result in thermal bridge effects that are not required. The other common thermal bridge mitigation approach uses thermal break (TB) strips. Research has shown the measurement of 20LB and NLB LSF under test lab conditions using HFM, indicating the heat performance of LB and NLB LSF (Santos and Mateus, 2020).

To obtain a vertical mechanism of models with discreet connections by reducing vertical to horizontal flexural capacity ratio and improving on varying lateral connections, decreasing the horizontal span between connections. For the development of the vertical plastic mechanism, the flexural ratio capacity of 0.5 is required for sheets with a ratio of 1.0. In contrast, for sheets with a span larger than 1.5, a ratio capacity of 10 was needed (Alawad et al., 2020).

Using sustainable construction materials is growing in popularity and becoming increasingly important. Owing to their lightweight, improved insulation properties and quick installation, precast concrete sandwich systems containing EPS gradually replace traditional blockwork systems. As a result, there is a need for design optimisation and manufacturing of such systems. To provide more insulation, durability, and rapid installation while also ensuring adequate bonding, strength, and mechanical properties suitable for the purpose, design optimisation and manufacturing of this system are required. Research shows that the system's technical properties depend highly on the mix design and sustainable lightweight precast concrete sandwich panel for the NLB partition wall system. An experimental program was created to verify the best mixture proportions for the EPS concrete core. Practical system production and installation procedures were researched. Experimental testing and calculation were applied to determine an EPS concrete system's physical and mechanical properties. A relationship between the plastic density of EPS concrete and its compressive strength was established to assure quality control before concrete casting (Moutassem and Al Mara, 2021).

Using EPS concrete in the built environment is progressing as a sustainable construction material. Even though one of the largest energy consumers has been identified as the construction sector, it necessitates effective measures and solutions to address sustainability. Exclusive research confirms the possibility of replacing natural aggregate with recycled CDW in concrete production, where hygrothermal properties and mechanical durability are improved (Pečur et al., 2020).

Research on TB strip materials has been conducted, and steel stud flanges have been evaluated. Similar thermal performances have been found in inner and outer TB strips, and an increase in the latter has been observed. However, the performing TB material was Aerogel, which outperformed recycled rubber and cork/rubber composite TB strips. Furthermore, it was also observed that the performance of the TB strips was identical for the examined structural LB and non-structural NLB LSF walls (Santos and Mateus, 2020).

The structural response, upon applying lateral and direct shear load to precast concrete sandwich panel, determines the panel's ability to develop composite action. Load capacity and failure modes are determined by the role of the span thickness constituents and strength of the concrete mix, the insulant, and the natural part shear connectors. Research on the interaction of thermally conductive and non-conductive shear connectors with wythes and insulation on how load resistance to flexure and direct shear loading has been applied. Outcomes for successful systems designs, adequate for post-cracking behaviour, prior to pull-out, or buckling failure, vary significantly and must be understood have been observed (Kinnane et al., 2022).

The difference between NLB precast concrete cladding panel's boundary conditions and monolithic cast-in-place walls is that they rely on discreet connections for attachment to the main structural system, typically at the floor diaphragm. When panels are designed to withstand far-field blast loading, discreet diaphragm connections are commonly idealised as horizontal curves of continuous support, with cladding panel edges assuming vertical (primary) one-way flexural behaviour (Alaward et al., 2020).

The present work aims to develop a building panel incorporating water storage and solar energy. According to the collected literature, the engineering body of knowledge has not illustrated a building panel capable of storing water whilst generating energy.

2.4 Rainwater Harvesting

RWH is a small-scale solution to intermittent water for domestic water use and to prevent RW runoff into sewer or storm drains (Jay Gohel, Hina Bhatu, 2020). RWH system performance reduces stormwater runoff due to green-roof installation as it modifies runoff variability. Potential water savings are decreased, and the volume of retained water increases when the catchment area covers the green roof extensively (Almeida et al., 2021). Drawing on alternative supplies, such as onsite RWH systems, effectively boosts the resilience and reliability of water resources that are for potable and non-potable water usage (Gibberd, 2020). An emphasis on optimal management of available water supplies has increased due to the widening gap between water demand and supply (Chandramouli, 2015). A method utilised to supplement surface and groundwater in areas where the water supply system was inadequate to meet demand, and also a strategy for reducing the effects of climate change on water supplies (Aladenola and Adiboye, 2010).

(Campisano et al., 2017) Rainwater harvesting (RWH) is the world's oldest system for meeting water supply requirements, and (Helmreich and Horn, 2009) is mainly regarded as a suitable source of potable water; this scenario depends on the precipitation intensity.

Where Homer's formula calculates the rainfall intensity as follows

$$i = \frac{A}{(t+b)^n} \quad (2.1)$$

$$i = \frac{A_1(1+C \log P)}{(t+b)^n} \quad (2.2)$$

$i = \text{intensity}$

$t = \text{rainfall duration}$

$A, A_1, C, b, n = \text{local parameters}$

With appropriate management of the water table, it can decrease water and flood disasters in areas of developing countries. RWH is a tool employed during the rainy season, where runoff can be harnessed and used for households or agroecosystems (Helmreich and Horn, 2009). A strategy to improve water consumption efficiency in buildings is non-potable water usage (Santos et al., 2020). Rainwater was devised as an engineering solution to water problems that conserve water resources and is measured as small-scale technology (Chandramouli, 2015).

Research revealed RWH is progressively building momentum as a source of water supply. In urban environments, the primary use for rainwater collection is for non-potable needs. In contrast, in rural and informal communities with minimal municipal water supply, RWH is vital since it is used for potable water (Vuong, Ichikawa and Ishidaira, 2016).

Furthermore, it has been mentioned that RWH is generally considered an annual source of drinking water, compared to groundwater, which may effectively have a high concentration of fatal contaminants.

Climate change affects variables such as rainfall, temperature, frost, chill units and carbon dioxide. Rapid population, economy, and industry growth drive climate and gas emissions (Du Plessis, 2017). The RWH system has aided in tackling water shortages. As part of the Sustainable Development Goals (SDGs) of achieving global water security, RWH has been promoted as the core strategy for sustaining water

resources (Kanno *et al.*, 2021). RWH harbours other potential benefits that are generally ignored due to focusing on water conservation (Campisano *et al.*, 2017).

One study investigated the ability of the RWH system to offset a portion of daily non-potable water demand in university buildings, where the findings showed that using accurate daily water consumption data rather than average values improves the outcomes, particularly in buildings with variable water consumption patterns over time, by up to 11%. In terms of the runoff coefficient, it was determined that variable values are preferable to average values. Runoff variability associated with green roof installation was found to lower RWH system performance due to reduced stormwater runoff (Almeida *et al.*, 2021).

It was found that economic constraints and local regulations influence the degree to which RWH systems are implemented and how RWH technology can be selected (Campisano *et al.*, 2017).

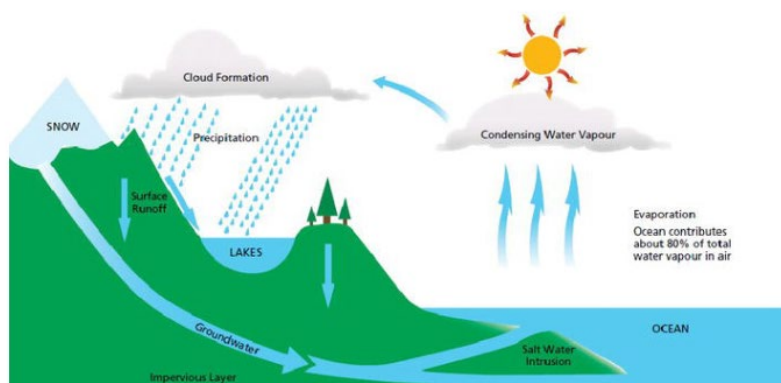


Figure 2.8 Hydrological Cycle indicating natural requirements to sustain water availability, a natural water recycling method (Betasolo & Smith, 2020)

2.5 Historical data on rainfall in the Western Cape (WC)

Cape Town's recorded water history begins in 1834, with the first reservoirs built in 1850, using spring and surface water. Due to an overabundance of supply, storage capacity is increasing. Smaller dams were erected as a solution but were unable to meet demand, giving birth to six larger dams to supply water to the Western Cape Water Supply System (WCWSS) built between 1920 (Steenbras) and 2006 (Berg River Dam), with 900MCM/year total yield and reliant on winter rainfall, averaging $600\text{mm}\cdot\text{yr}^{-1}$ (Roffe, *et al.*, 2021). CT and its surroundings have relied on surface water as a supply for about 170 years, with annual rainfall fluctuation spanning from Voëlvlei Dam (North) to Theewaterskloof (East). The largest catchment dam, Theewaterskloof, takes two years to fill with average rainfall, whereas the rest fill in a single season (Kaiser and Macleod, 2018).

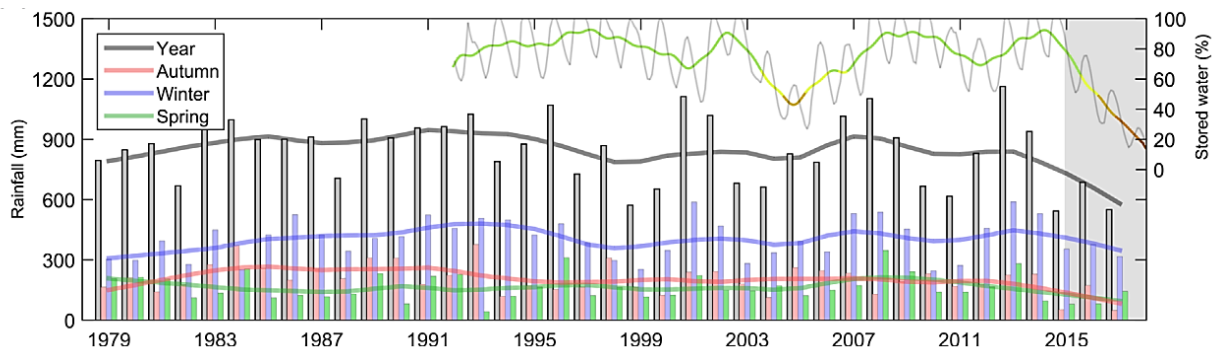


Figure 2.9 Historic data on rainfall in the Western Cape (WC) - The Day Zero CT drought are the poleward migration of moisture (Sousa et. al., 2018)

Water comprises two chemical elements: oxygen (O_2), hydrogen (H), and energy. Water represents life, and this is one element that is irreplaceable by anything. Water, a classic element of the Earth, is life's matter and matrix, mother, and medium whose utilization rate constantly increases. Without water, there is no life—a crucial element in sustaining livelihoods and agroecosystems (van Eekelen *et al.*, 2015). In the 21st Century, water shortage has been one of the biggest challenges. On average, SA consumes 237 litres (l) per capita per day. About 20% of available water is used for non-potable use (Jay Gohel, Hina Bhatu, 2020).

Most developing countries experience water scarcity, as reported by different researchers worldwide (Helmreich and Horn, 2009). In recent times, SA has experienced challenges relating to climate change. This is also a global phenomenon where water resources are being depleted rapidly, and drought has increased (Du Plessis, 2017).

2.5.1. Rainfall and Climate in Cape Town

In the 21st Century, water shortage has been one of the biggest challenges (Jay Gohel, Hina Bhatu, 2020). Remember that, on average, SA consumes 237 litres (l) per capita per day. About 20% of available water is used for non-potable use (Jay Gohel, Hina Bhatu, 2020). Most developing countries experience water scarcity, as reported by different researchers worldwide (Helmreich and Horn, 2009). In recent times, SA has experienced challenges relating to climate change. This is also a global phenomenon where water resources are being depleted rapidly, and drought has increased (Du Plessis, 2017).

As a result, following the driest three consecutive wet seasons (April 1-October 31) in 2015-2017, Cape Town was named a disaster area following the worst drought in nearly a century. Cape Town's drought was severe, with "zero-day" water storage months away, resulting in rough water rationing for the city's 3.8 million residents (Richman and Leslie, 2018). Data sets and lengths have shown a consistent drying trend where land surface temperatures have demonstrated an increase in temperature of $0.1^{\circ}C\text{-yr}^{-1}$ between the year 2000-2017 (Jury, 2020) where, (Richman and Leslie, 2018) the Intergovernmental Panel on Climate Change (IPCC), issued a warning more than a decade ago on global climate change trends to Cape Town and other major cities around the world.

SA is classified as a semi-arid country due to differences in topography, where climate changes from dry to semi-dry conditions along north-western regions to semi-humid and wet along coastal areas (Du Plessis, 2017). Climate change is a known global phenomenon where water resources are depleted and drought increases. It affects natural variables such as rainfall, temperature, humidity, frost, chill units and carbon

dioxide. Rapid population growth, the economy, and industry drive climate change and greenhouse gas emissions (du Plessis and Schloms, 2017).

When discussing events like droughts and floods, water and climate experts frequently use the term "return period" or "recurrence interval" to indicate the rarity (or not) of a specific event and calculated according to the Weibull formula.

The years 2015-2017 were the driest since 1933. This merely means that the drought will occur once every 84 years. However, if we could go back further, the 2017 drought might be considered even more uncommon (Wolski, 2018). The rainfall experienced between 1841 and 2020 indicated a decline of 10%, enforcing stringent water restrictions from 200L per person per day to 50L per person per day (Roffe, et al., 2021).

With these stringent rules on water restriction, it is pragmatic to know the minimum and maximum rainfall that can be collected to facilitate future infrastructure planning for municipalities. Cape Town experienced an average minimum of 5mm of rainfall and an average maximum of 150mm of rainfall during 2022 (SAWS, 2023). This calculated rainfall can be adapted into the Municipal Adaptation Plan (MAP).

Table 2.1 Minimum and maximum rainfall calculations for Cape Town

Location		Top Surface Area	Volume	Weight
	Cape Town	South Africa		
Dimensions	Length	314 mm		
	Breadth	50 mm		
	Depth	195 mm		
Rain Water Harvesting			0.0188m ²	3.062x10 ⁻³ m ³
Minimum Rainfall (5mm)				3.06kg
Maximum rainfall (150mm)			0.0942m ³	
			2.826m ³	

These experiences have led researchers to examine an overall framework for facilitating MAP development. Climate change and rainfall variability have increased the need to adapt city-level operations for resource management and infrastructure planning, focusing mainly on the national level, leaving municipal-scale adaptation unaddressed (Mukheibir and Ziervogel, 2007). Also, the National Adaptation Programmes of Action for Least Prepared Countries (NAPALPC) was developed under the United Nations Framework Convention on Climate Change (UNFCCC). As a result, the primary challenge for planners and policymakers was to guarantee that climate change consequences were recognized and adequately incorporated into urban planning to avoid or mitigate residual effects ((Mukheibir and Ziervogel, 2007).

2.5.2. Rainwater Harvesting Methods

Rainwater collection has been practised for decades. It is a method of collecting and storing rainwater from rooftops, land surfaces, or rock catchments through the use of basic techniques such as natural and/or manmade ponds and reservoirs (Helmreich and Horn, 2009), (Adham et al., 2011), (Kahinda and Taigbenu 2011). Figures 2.12 and 2.13 illustrate the two methods for collecting rainwater.

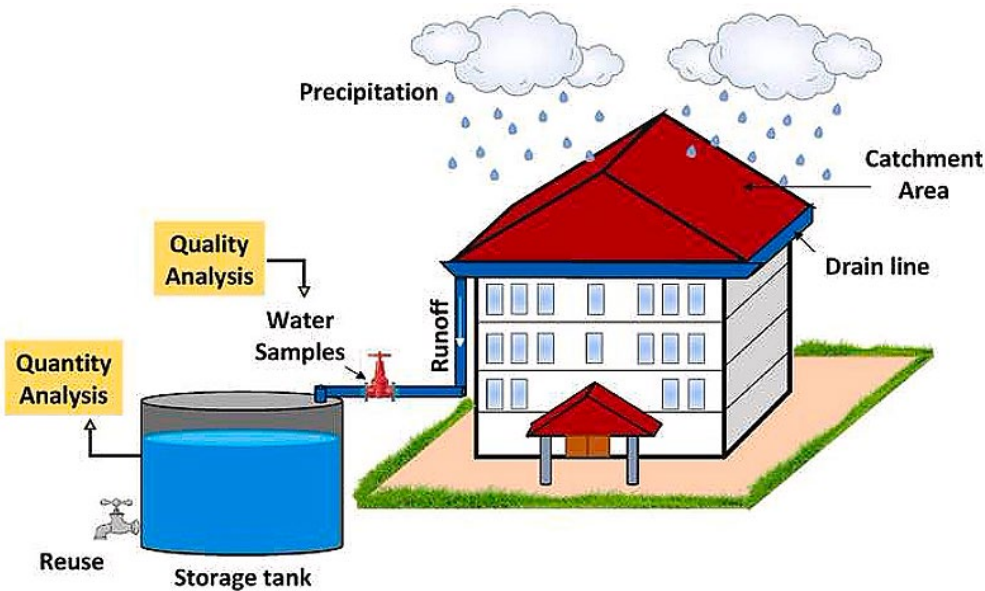


Figure 2.10 Illustrates Surface runoff Harvesting technique (Anchan & Prasad 2021)

To determine rainwater harvesting, the area of catchment (m^2) x amount of rainfall (mm) x runoff coefficient is calculated using the Rational method for predicting peak runoff.

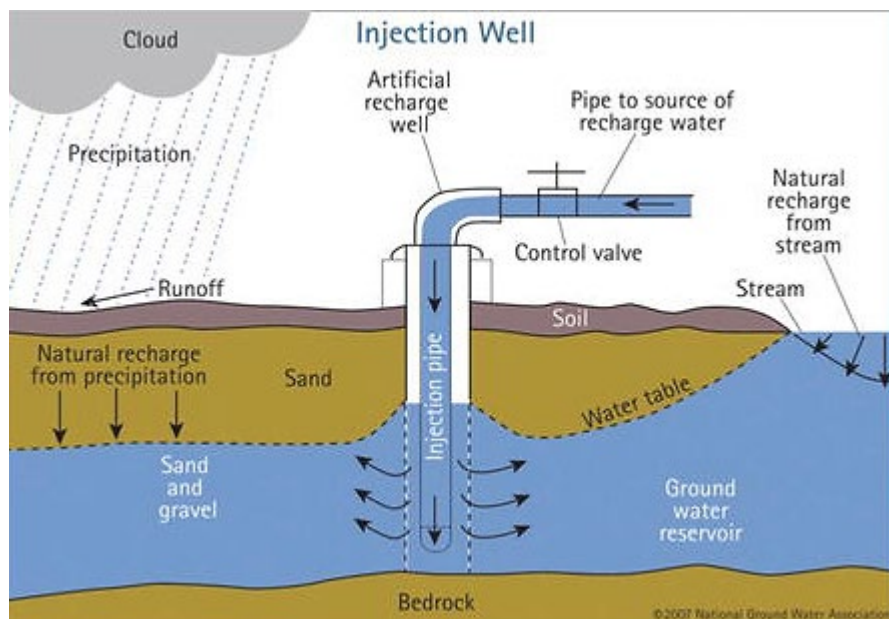


Figure 2.11 Illustrates Groundwater recharge, where a well is artificially recharged employing a recharge technology as a rainwater harvesting method (Veerana and Jeet, 2020).

2.5.3. Rainwater Harvesting Process

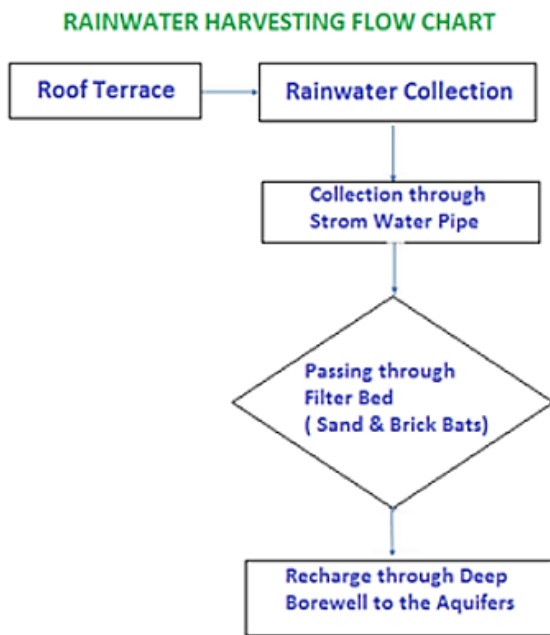


Figure 2.12 A process flow diagram illustration of rainwater harvesting, Maity et al., (2018)

2.5.4. Rainwater Harvesting Components

Water demand and RWH are increasingly becoming a directly proportional phenomenon. Factors to consider for the determination of rainwater storage design are as follows; the determination of catchment area, harvested water valuation, water outflow calculation, estimation of water demand, selection of catchment area based on demand, calculation of rainwater pipe diameter, and outflow pipes as well as the design of a recharged well (Mishra et al., 2020). Figure 2.13 illustrates the RWH components, and the table gives the functions of each component.

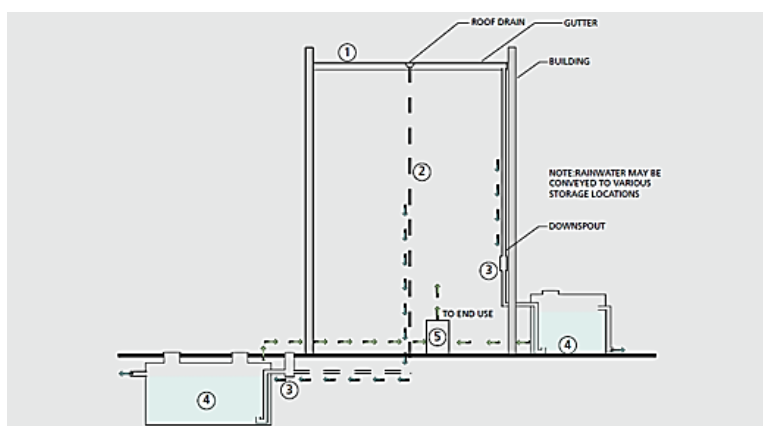


Figure 2.13 Illustrates rainwater harvesting components and how they inter-connect (Novak et al., 2014).

Table 2.2 Provides a descriptive function for each component.

Component	Function
Catchment / Collection surface	It protects persons and materials from the elements, acts as a surface for collecting rainwater (Novak et al.,2014), and supplies high-quality drinking water while supporting livelihoods. Beneficial to ecosystems, allowing living creatures that rely on clean water to grow and flourish (Leutnat et al., 2018), Le Flock et al., 2022)
Conveyance (conduit & gutters)	Gutters main responsibility is to manage the water flow. Rainwater is often transmitted from the point of collection (roof) to a storage tank. Water flow is channelled from roofs, and over downspouts and directed to designated areas outside the property during rainy days (Novak et al., 2014). The roof can collect a lot of leaves and other debris with or without a gutter system, causing water to stagnate and overflow (Gui & Zhang, 2020), (Santos & Rahmawati, 2022)
Filter / Prefiltration	Pre-storage filtration, also known as input percolation, where the elimination of a variety of contaminants occurs from rainfall. Some in the industry believe this is the system's most significant component (Anchan & Prasad 2021). The significance of decreasing organic and inorganic waste in rainfall cannot be emphasized. The following are examples of common pollutants that create problems: <ul style="list-style-type: none"> • Organic matter from trees and plants • Droppings from fowl • Animal, fowl, rodent, and bug carcasses • Trash • Dirt and pollen • Pollution particulates, with the following commonly used filters, downspout filters, basket-type filters, centrifugal-type filters, and cascading-type filters. A greater degree of water quality in the storage tank can be attained by lowering pollutant loads with good prefiltration. Tank, equipment, and other component maintenance costs can also be minimal (Novak et al., 2014).
Storage Facility	The most apparent or noticeable component of a RWH system is the storage container (cistern, tank). It is where collected rainwater is diverted and stored for later use. The storage tank's primary purpose is safety (Anchan & Prasad 2021), (Santos & Rahmawati, 2022). Rainwater is collected and prefiltered before being transported and stored, where it is distributed on demand (Novak et al.,2014).
Recharge Structure / Distribution	The element in charge of distribution is supplying water of sufficient quality as well as pressure (Novak et al., 2014)

Calculating the number of rainwater pipes

$$Q = n \frac{\pi}{4} d^2 v \quad (2.8)$$

Q = Discharge

n = Minimum number of pipes

d = Diameter of rainwater pipe

v = Velocity of water on the roof, entering the pipe.

To design the diameter of a discharge pipe, considering the catchment area. The water velocity is calculated first (Mishra et al., 2020)

$$V^2 = U^2 + 2aS \quad (2.9)$$

v = Velocity of water entering the Discharge pipe

U = Velocity of rainwater entering rainwater pipe

S = Height of building

a = Acceleration due to gravity (g)

where

$g = 9.81 \text{ m/s}$

2.5.5. Materials

Material design and consideration are critical aspects researched during prototype development. Some of the considered and important factors, such as sustainability, availability, durability, and affordability, make the product attractive, effective (functional, durable and robust) and compliant with governing laws. Governed by the SANS 1731:2017, which specifies the criteria for the source of raw material ultraviolet (UV) protection, mass, wall thickness, diffusion, resistance to stress crack and strength for various sizes. Other important factors or aspects to consider are the choices of materials and how these materials will impact the environment. Research indicated that various materials, such as synthetic materials, which include glass, plastics and metals, are used as storage vessels for rainwater collection (Majesty, et al., 2013)

Table 2.3 Provides material type and characteristics related to the types of materials used.

Material Type	Characteristics
Plastic	Various forms of plastics have been utilised in industry to produce rainwater storage systems. The standard plastic storage tank is typically used for the storage of RW. (Andoh et al., 2021), Commonly used polyethylene materials are low-density polyethylene (LDPE) ranging between 910kg/m^3 - 925kg/m^3 produced at high pressure. High-density polyethylene (HDPE) has densities ranging between 940kg/m^3 - 965kg/m^3 produced in low-pressure processes. A waxy feel, and stiffness with no hardness or brittleness characterise LDPE. Nonbiodegradable materials disposed of in landfills threaten the environment. The decomposition of plastic waste in landfill sites takes a long time. However, recycled products have an estimated 50 – 60% capital saving on manufacturing (Tawiah P. O. , Andoh P. Y., 2016).

Metal	Elevated water tanks made of containment vessels combining conical tanks are popularly used. These water structures are composed of welded curved metal plates along their circumference and in the longitudinal direction, forming an upper tubular cone. These types of tanks comprise steel vessels and reinforced concrete, a roof providing resistance to lateral movements, and wired fine mesh located at the bottom, where high compressive stress and bending moment occur. The composition of their material properties are as follows: Modulus of Elasticity = 2×10^5 MPa, Yield stress = 300MPa and Poisson ratio = 0.3 (El Ansary et al., 2009)
Concrete	Concrete water towers are some of the world's recognised water distribution facilities and water network systems. Globally, the latter plays a crucial role in supplying municipal water and firefighting systems, especially where the concrete water tower becomes a lifeline in serving potable water and firefighting operations (Gurkalo et al., 2016).

Recycling existing materials has been at the forefront, where such materials are considered sustainable and cutting-edge in developing novel products.

2.5.6. Risks

Water scarcity has been a major issue in many developing countries. Water demands for agricultural and urban growth are putting further strain on water supplies in an ever-changing climate. Rainwater is a potentially useful alternate water supply for potable and non-potable needs. Water and food crises in some locations could be alleviated with good management. Rainwater may be contaminated with microorganisms and harmful substances, necessitating treatment before use. Specialized chemical, physical, and biological approaches are applied to prevent contamination and increase the quality of captured rainwater (Singh et al., 2022).

For storage tank foundations, designers should adhere to manufacturer-recommended specifications and designs. Using opaque materials, gaskets, and/or caulking should help prevent light from entering the tank, as light stimulates algae advancement. Positioning tanks away from direct sunlight whenever feasible helps achieve cooled water temperatures. Furthermore, other components may be more vulnerable to UV damage caused by sunlight, rain, and temperature. A proper plan is required to position the storage tank on the property (Novak et al., 2014).

It is advised to safeguard the storage and conveyancing pipework from pollution and overflow during construction and follow a strict maintenance plan after installation has been completed (Novak et al., 2014).

The primary sources of pollution in rainwater storage are wind-blown trash, organic matter from trees, droppings from birds and animals, and consumption of contaminated harvested rainwater, leading to health risks. Storage tanks can augment breeding sites for mosquitoes, including species that transmit the dengue virus, triggering health concerns. Microbial contamination of collected rainwater indicated by E.

coli (or thermotolerant coliforms) is fairly common. Rainwater has also been found to contain Pseudomonas, Cryptosporidium, Giardia, Campylobacter, Vibrio, Salmonella, Shigella, and other pathogens (Maity & Das, 2018), (Novak et al., 2014).

2.5.7. By-laws

The City of Cape Town (COCT) encourages using alternative water sources to help reduce the dependency on municipal drinking water from our dams, creating long-term customer savings and enhancing water sustainability. This is COCT's effort to strengthen water resilience; unexpected rainfall has become the "new normal." Nonetheless, health and environmental risks associated with developing and using alternative water systems must be properly supervised and regulated (City of Cape Town, 2016).

The Bill of Rights in the Constitution of the Republic of South Africa (1996) assured all South Africans the right to adequate water. Water is a limited resource essential to all parts of existence; thus, it must be carefully managed for the benefit of everybody (SA constitution, 1994), (UNSDG,1997).

The water resource is strictly regulated. The government manages water on behalf of all citizens under two key laws. The National Water Act (1998) and the Water Services Act (1998) followed the Constitution (1997, (DWS, 2022)). However, by law, COCT has been obligated to provide Cape Town with treated water that meets the SANS 241 quality requirement for 'potable' drinking water (City of Cape Town, 2016).

COCT highly advises following the DWS 1996 Water Quality Guidelines as best practice, as they were created to reduce health hazards (City of Cape Town, 2016).

Following those recommendations, the SANS 241 national standard for water quality was produced. It establishes the required standard for drinking quality water given to consumers by Water Service institutions such as the City, as well as other uses involving close human contact and potential ingestion (including water features and swimming pools – detailed in the South African Bureau of Standards (SABS) www.sabs.co.za), (City of Cape Town,2016).

According to the COCT's Water By-law, no alternative water, whether treated or untreated (even if it meets SANS 241 requirements), may be used for drinking, cooking (including food preparation), or body washing (ablution), (City of Cape Town, 2016).

According to the collected literature, the engineering body of knowledge has not illustrated a building panel capable of storing water whilst generating energy from solar energy.

2.6 Photovoltaic (PV)

A photovoltaic cell is a technology that is used to collect solar energy and convert it into electric energy. A typical solar panel comprises 60,72, and 90 different solar cells connected in a series configuration. With layers of boron, phosphorus and silicon, these layers individually provide the following: i) boron – positive charge; ii) phosphorus - negative charge and silicon – acts as a semiconductor (Mutombo and Numbi, 2019).

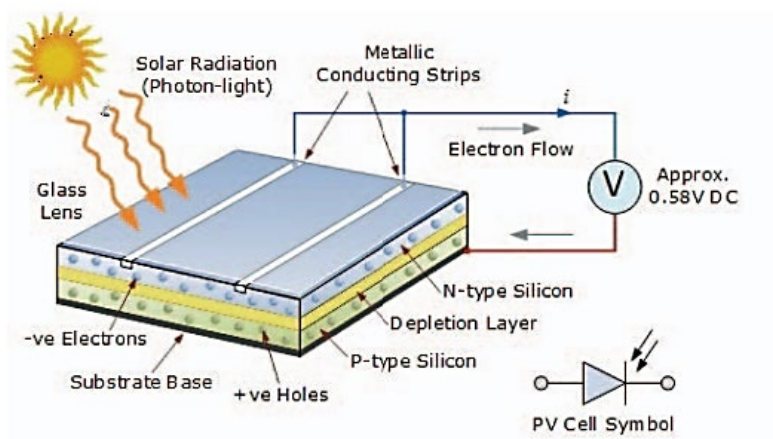


Figure 2.14 Illustration of a basic solar cell diagram (Sainthiya,2017)

In technical terms, photovoltaic directly converts solar insolation into electricity; photovoltaic is known as PV, a process of converting light (photons) into electricity (voltage). PV system is a tool used to generate sustainable renewable energy, Mutombo and Numbi (Mutombo and Numbi, 2019), (Ramos Hernanz et al., 2010) that PV system, an environmentally friendly technology for producing electricity with the best performance obtained when high insolation incident with solar cells. Carbon dioxide emission reduction requires revising policies to increase the global use of renewable energies, such as Solar PV. Implementing alternative energy, ecosystem protection through certified emission reduction (CER), and encouraging the use of alternative energy through incentive programs were devised as strategies for these policy changes (Ramos Hernanz et al., 2010).

Solar cell power output is given by:

$$Pr = G \times A \times \eta \quad (2.10)$$

Moreover, Efficiency conversion is given by the following:

$$\eta = \frac{P_{out}}{P_{in}} \times 100 \quad (2.11)$$

Where;

P_r = Electricity power output (W)

G = Solar irradiance (W/m^2)

A = Area (m^2)

η = Efficiency

P_{out} = Power output (W)

P_{in} = Incident solar (W)

(Kumar et al., 2019), Access to energy is a continuous accomplishment. Solar energy, a readily available energy resource for electricity generation in South Africa, is abundant. Solar energy and access to energy as an alternative energy source work intermittently. Thus, solar cannot replace conventional energy but reduce GHG emissions and supply sustainable energy when power outages kick in. Hence, (Ramos Hernanz et al., 2010) reiterated the policy revision for the application of RE to curb CO₂ emissions.



Figure 2.15 Schematic of a solar PV array (Sreega et al., 2017)

2.6.1. Historical energy use in South Africa

In SA, coal contributed to 69% of 83% of the main energy supply in 2017 due to the ample coal supply. Post 1994, electricity demand increased by 4% per annum (p.a); however, by 2007, electricity reserves dropped, negatively impacting SAs' economic growth of 6%.

Coal, with less energy cost, is considered an essential primary source and is likely to remain for the next 25 years, with SA as one of the highest electricity users in Africa, owing to mining industries. Existing coal plants encourage electricity generation by using coal because SA's electricity cost is the lowest in the world (Mutombo and Numbi, 2019), (Attoye and Hassan, 2017).

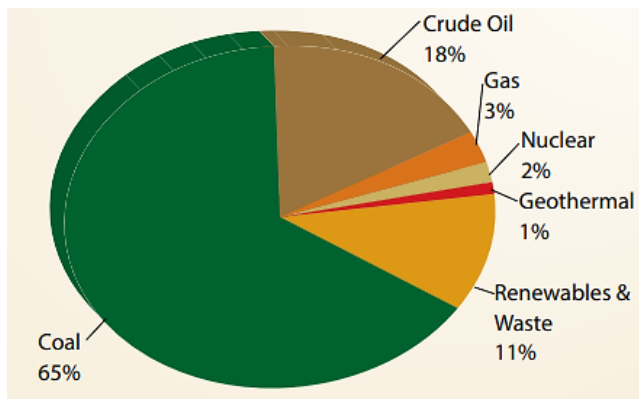


Figure 2.16 SA primary energy supply (DoE,2022)

Energy made from coal dominates the energy landscape in SA, even though various RE options are available to supplement demand and reduce loading on the grid (Mutombo and Numbi, 2019).

Energy is the ability to work and exists in different forms, such as electricity, thermal, mechanical, nuclear, and chemical, which can be transformed from one form to another. In modern life, one of the basic needs is electricity. Energy is dynamic and can be formulated in different ways to generate power. Energy is needed to sustain and simplify human life. With technological advancement, energy generation has been evolving and shifting in alignment with the United Nations Sustainable Development Goals (UNSDGs), which state the availability of clean and affordable energy for all. Access to adequate electricity makes living difficult (Johnson and Ogunseye, 2017).

In SA, the national daily average electricity consumption is 30KWatt hours (kWh) generated from coal-sourced electricity, with the ailing power plants, constant power outages, and the ever-increasing cost of energy. Eskom, the sole coal-sourced-energy producer in SA, ensures that supply meets the demand, even if, at times, load shedding is the optimal solution. According to Eskom, cost recovery for capital and operation expenditure may be impossible to recuperate from tariffs alone due to low consumption levels in rural communities. Eskom, a parastatal operating on 230Volts (V) and 50Hertz (Hz) supplies SA's electricity. With a total of 37 745 Megawatts (MW) of power supply, Eskom generates electricity from various technologies, namely: 13 Coal-fired power stations with a capacity of 37 745 MW; 1 Nuclear station with a capacity of 1910MW; two Hydroelectric stations with a capacity of 600MW; 2 Pumped storage with the capacity of 1400MW; 4 Open Cycle Gas Turbine Stations (OCGTs) with the capacity of 2426MW and 1 Windfarm with the capacity of 3MW (Noor Jamal, 2015), (Mutombo and Numbi, 2019).

With the current state of energy generation in SA, which places the country in a compromised position with Greenhouse Gas (GHG) emissions, the implementation process for alternative energy usage is slowly gaining momentum. The latter is preceded by Eskom's 49M Energy Efficiency (EE) program, where incandescent bulbs were changed to fluorescent bulbs throughout the country when the population was still 49 million. The Kyoto Protocol of 1997 and the Paris Agreement of 2015 were guidelines for mitigating environmental pollution (Attoye and Hassan, 2017). South Africa entered into these agreements to show its commitment to addressing GHG mitigation and how it will manage climate change and its effects.

2.6.2. Solar panel types

The classification of solar modules is in accordance to i) first generation, made up of polysilicon and monocrystalline silicon materials; ii) second generation, which consists of thin film solar cells; and iii) third

generation, described as emerging PVs, which are researched and developed for commercial use, which are also a composition of varying organic materials, understood to be produced at low cost, and improved solar cell efficiency (Bagher et al., 2015), (Jon Franke, 2021). Silicon material is mostly prevalent in solar cell manufacturing due to its availability, durability, and microelectronics industry experience (Nogueira et al., 2015). Most solar modules circulating on the market have an efficiency ranging between 15% to 20%, and the efficiency of silicon solar cells hovers between 13-18%. Output power generated may vary due to differences in temperature and atmospheric factors such as solar irradiance and ambient temperature (Supian, Ekaputri & Priharti, 2020).

According to (Jon Franke, 2021), Monocrystalline Panels(MCPs), Polycrystalline Panels(PCPs), Thin Film Panels(TF), and Passivated Emitter Rear Cell Panels (PERCs) are different types of solar cells which possess varying efficiencies.

i) Monocrystalline Panels (MCPs)

Monocrystalline is a commonly used silicon cell. These are produced by cutting cylindrical bars into thin pellet shapes (Nogueira, et al., 2015 and Taşçioğlu, et al.,2016); the silicon is divided into slices, cut into rectangular blocks, separated to form a panel with a thickness of 0.5 mm and a dark blue colour weighing less than 10 grams. Besides high production costs, their ability to convert solar irradiance into electric energy hovers around 15%. Cutting thinner wafers increases the efficiency and cost reduction of crystalline solar cells and better utilisation (Nogueira *et al.*, 2015; Taşçioğlu, Taşkın and Vardar, 2016).



Figure 2.17 A schematic illustration of a typical monocrystalline solar cell (Al Mansur et al., 2022)

ii) Polycrystalline Panels (PCPs)

Polycrystalline cells fall under first-generation cells (Bagher et al., 2021). PCPs are one of the widely used silicon cells. They are produced from silicon blocks due to the melting of pure silicon in special moulds (Nogueira *et al.*, 2015). This type of solar cell is used in the PV and electronics industry in its raw format (Bagher et al., 2015). They have an efficiency of about 13% in converting sunlight into electricity. Module efficiency falls when the rise in temperature is influenced by cell insulation (Nogueira *et al.*, 2015).



(a)**(b)**

Figure 2.18 A visual difference between a monocrystalline (a) and a polycrystalline (b) solar panel (Ayadi et al., 2022)

iii) Thin Film Solar Cells (TFSCs)

Thin-film cells are considered second-generation solar cells (Bagher et al., 2015) and have consistent efficiency (Xing *et al.*, 2021). They consist of three commercialised technologies, namely: Amorphous Silicon (α -Si), Copper Indium Gallium Selenine (CIGS) and Cadmium Telluride (CdTe) (Nogueira et al., 2015; Taşçioğlu, Taşkın and Vardar, 2016, Bagher et al., 2015). TFSCs are made by depositing thin PV materials on glass, plastic, or metal substrates with less thickness variation of nanometres (nm) to micrometres (μ m). TFPs efficiency is lower compared to other types, and to generate equal power, they need a larger surface area (Bagher et al., 2015). The use of affordable and minimum material with increased capacity production is lightweight, and their use in BIPV increases their choice of preference for commercialisation, rendering TFSCs as being less expensive to produce.



Figure 2.19 An image of a typical thin film solar cell (Ayadi et al., 2022)

iv) Flexible solar cells

Attention has been drawn to flexible, stretchable organic solar cells (OSC), owing to their possible application of being worn, bendable and stretchable as well as weighing less, their cost is low, procedures on low temperature, flexible, and partially transparent production (Qin et al., 2020). OSC has achieved more than 17% on power conversion efficiency (PCE) required by the market (Qin et al., 2020). A flexible transparent electrode (FTE), a photoactive layer, and a top electrode are all components of a flexible device. The photoactive layer produces excitons after light absorption, which are a formation of donor and acceptor blend. Freed electrons and holes are separated from the diffusion of excitons to the donor-acceptor boundary (Qin et al., 2020 Bagher et al., 2015), conveyed to applicable electrodes, and collected.

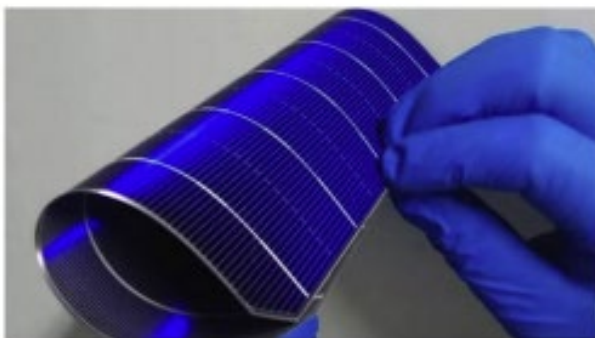


Figure 2.20 Schematic illustration of a flexible solar cell (Li et al., 2021).

2.6.3. Solar irradiation

Solar irradiation is generally known or referred to as sunlight, a term used when the sun emits electromagnetic radiation (Huld, 2017). According to (Huld, 2017) and (Kumar, et al., 2019), Solar irradiation is made up of three types, namely;

Direct Normal Irradiance (DNI) – when the earth’s surface directly receives solar irradiation with no obstruction, measured in watts per square meter (W/m^2), and highly relevant for concentrated solar power (CSP) systems.

Diffuse Horizontal Irradiance (DHI) – when molecules, clouds and other atmospheric particles scatter the sunlight reaching the Earth’s surface in multi-directions, measured in W/m^2 relevant for both PV and CSP. Global Horizontal Irradiance (GHI) – when the horizontal surface receives a total of DNI and DHI sunlight, measured in W/m^2 , mostly for use in the applications of solar energy and solar energy systems.

Global Solar Irradiation (GSI) varies between a minimum and a maximum of $1.63 \text{ MWh}/m^2/\text{year}$ and $2.56 \text{ MWh}/m^2/\text{year}$, respectively, with sunshine duration between 7.4 hours and 9.4 hours. London has an annual solar radiation of $108 \text{ kWh}/m^2/\text{year} = 2.79 \text{ kWh}/m^2/\text{d} \times 365 \text{ days}$ (energy department, n.d.).

SA averages more than 2500 hours of sunshine for most areas per annum, with the highest 24-hour global radiation average of $220 \text{ W}/m^2$, compared to the USA and Europe, with 24-hour global standards of $150 \text{ W}/m^2$ and $100 \text{ W}/m^2$, respectively. SA has a readily accessible resource for solar energy generation that is exploited to its maximum capacity (Rehman, Bader and Al-Moallem, 2007; Kumar *et al.*, 2019).

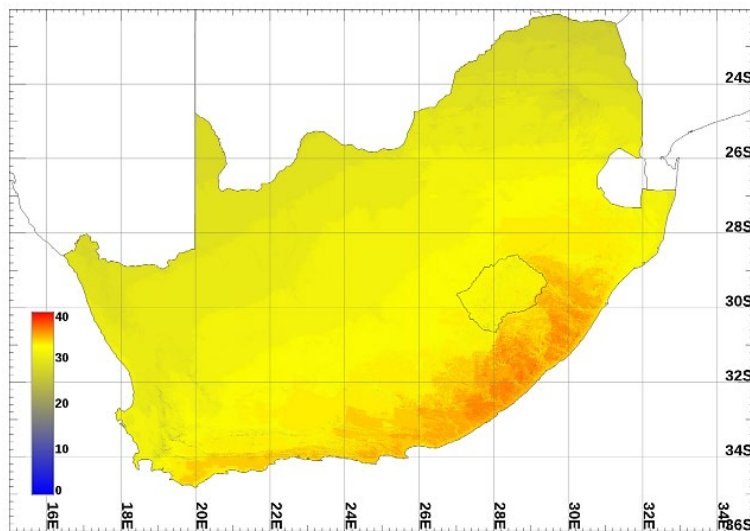


Figure 2.21 ‘Optimum angle for an equator-facing plane ensuring maximum annual plane solar irradiance for South African area’, (Huld, 2017).

Solar irradiance is given by

$$G = \frac{Pr}{A} \quad (2.12)$$

$G = \text{Solar irradiation } (W/m^2)$

$Pr = \text{Power } (W/kW)$

$A = \text{Area } (m^2)$

2.6.4. Solar cell power-output

Single crystalline construction for monocrystals allows high output ratings to generate maximum power capacity. Therefore, with technological advancements, polycrystalline has bridged the gap, meaning a 60-cell polycrystalline solar cell can produce 240 – 300W. However, monocrystalline solar cells have more power capacity per cell than polycrystalline. The power output for conventional crystalline panels is more than that of thin film. Uniformity in size does not guarantee a standard measure of power capacity; additionally, thin film panels vary due to their physical size (Zhang *et al.*, 2021, Gaungul and Chala, (2019). Solar cell power output is given by calculated as follows:

$$Pr = V \times I \quad (2.13)$$

$$Pr = V_{rms} \times I_{rms} \times \cos \phi \quad (2.14)$$

And the PV power output is given by:

$$Pr = A \times \eta \times G \quad (2.15)$$

Where:

Pr = Power output

V = Voltage generated by the solar cell

I = Current produced by the solar cell

V_{rms} = Root Mean Square value of voltage

I_{rms} = Root Mean Square value of current

$\cos \phi$ = Phase angle between current and voltage waveforms

A = Total surface area of panels

η = Efficiency of PV panels

G = Solar irradiance

2.6.5. Performance of a PV cell

Ensuring optimal solar cell performance requires meticulous consideration of various factors during the design stage. Jon Franke (2021) explains that these factors encompass temperature, fire rating, hail rating, and classifications such as Class A, Class B, and Class C, alongside Hurricane and Light-Induced Degradation (LID) considerations.

Temperature stands as an important factor influencing a solar cell's energy generation. The temperature coefficient, indicating power output reduction per degree Celsius rise above 25°C, diverges between solar cell types. Monocrystalline and polycrystalline cells exhibit coefficients between -0.3% to 5% per °C, while thin-film panels, with a coefficient near -2% per °C, emerge as a prudent choice for hotter environments (Gaungul and Chala, 2019).

The fire rating of solar panels is imperative for safety compliance, with the International Building Code of 2016 mandating alignment with roof fire ratings. In some US states, like California, solar modules are required to share the same fire classification as the roofs they are installed upon (Kumar *et al.*, 2019).

Hail rating, evaluated through safety standards such as UL 1703 and UL 61703, gauges a solar module's resilience against hail impacts. Crystalline modules can withstand impacts up to 50 mph, showcasing their durability under adverse weather conditions (Rehman, Bader, Al-Moallem, 2007; Kumar et al., 2019).

Classifications A, B, and C delineate the efficacy of solar panels against fire exposure, with specific criteria for flame spread distances. These classifications are crucial for installations in areas prone to high fire risk and increased wildfire occurrences (Rehman, Bader, Al-Moallem, 2007; Kumar et al., 2019).

Hurricane rating specifications recommended by the US Department of Energy include criteria such as ASTM E1830-15 ratings, locking capabilities based on DIN 65151 standards, through-bolting with fasteners, a 3-frame rail system, and tubular frames to enhance rigidity and resist twisting. Additionally, boundary fencing around modules is advised to mitigate wind forces (Rehman, Bader, Al-Moallem, 2007).

Light-induced degradation (LID) is identified as a performance loss in crystalline modules during initial sun exposure hours. This phenomenon may impact actual performance compared to factory flash test data provided by PV module providers (Zhang et al., 2021; Jon Franke, 2021).

2.6.6. Photovoltaic Efficiencies

Explain the definition of panel efficiency here and how it applies or should be understood.

Table 2.4 Solar modules are made up of different types of solar cells with varying efficiencies, namely (Jon Franke, 2021)

Type of solar cell	Efficiency (%)
i) Monocrystalline	20%
ii) Polycrystalline	15 -17%
iii) Thin film	9-15%
iv) Passivated Emitter Rear Cell panels	20-25%

Solar panel design will incorporate the following parameters that affect the efficient output of solar PV (Zhang *et al.*, 2021). These parameters are the intensity of solar radiation, surface temperature, temperature coefficient, parallel resistance, and ideality factor. Further, Johnson and Ogunseye added shading, a factor of 0.1%, cable sizing, battery storage, components ratings, Battery system, inverter and charge controller (Johnson and Ogunseye, 2017).

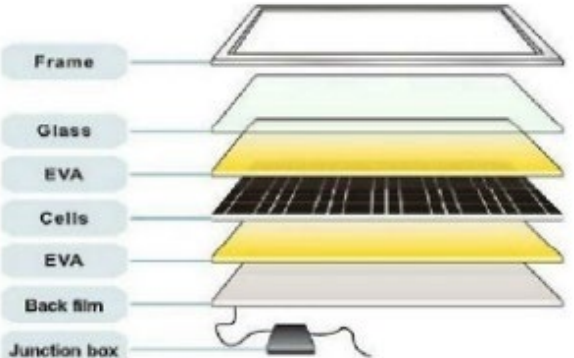
2.6.7. PV Materials

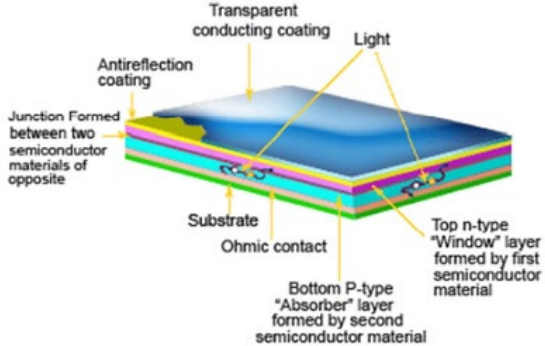
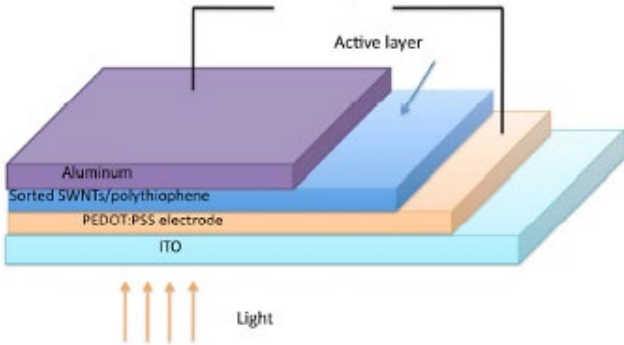
Table 2.25 describes different PV materials, their types, structural layer composition, and classification, and also use different illustrations to show the different materials in each solar cell.

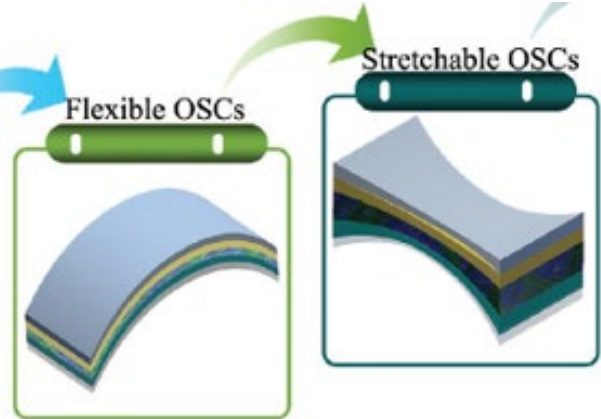
Table 2.5 Types of solar cells, their classification, and an illustration of their structural layers.

Type	Classification	Description	Structural Layer Illustration
Amorphous		A 1-micro meter (μm) thin layered silicon depositing vapour at a low temperature of 75°C on a glass or metal substrate forming amorphous silicon panels. Amorphous silicon cells have a more competitive edge due to low production costs (Bagher et al., 2015). A cell structure with a single sequence consisting of a layer of p-i-n, due to sun exposure, later experiences massive power output degradation. A triple-layer method was employed, optimising the solar spectrum, with 1μ solar cell yielding 7% due to the Staebler-Wronski degradation effect.	
CIGS		CIGS, as it is known, holds controversy in PV materials. A thin film solar cell is used to convert sunlight into electric energy. Its manufacturing process involves the thin layers of Copper (Cu), Indium (I), Gallium (G) and Selenide (S), deposited on different substrate materials such as glass or plastic backing for the collection of current electrodes are placed at the front and back (Bagher et al., 2015). A thinner film is needed because the absorption coefficient is high and the absorption is strong for sunlight. Flexibility in CIGS results from layer thinness,	

		<p>permitting pliable substrate to be deposited (Bhager et al., 2015).</p>	<p>Copper Indium Gallium Selenide (CIGS)</p> <ul style="list-style-type: none"> ZnO, ITO - 2500Å CdS - 700Å CIGS - 1-2.5µm Mo - 0.5-1µm Glass, Metal Foil, Plastics
CdTe		<p>They are designed to absorb and convert sunlight to energy by using cadmium telluride as a thin, thin-layered semiconductor. CdTe possesses a small carbon footprint, uses less water and has the shortest payback period compared to other solar technologies. The recycling of CdTe panels mitigates the impact of environmental toxicity. However, public scepticism and uncertainties have been a concern. It is understood that pollutants are not produced during the operation of these modules and pose minimum environmental problems (Bagher et al., 2015).</p> <p>The use of CdTe in the European Union has posed safety concerns; however, regulations in China permit the exporting of cadmium and its compounds.</p>	<p>Cadmium Telluride (CdTe)</p> <ul style="list-style-type: none"> Glass SnO₂, Cd₂SnO₄ - 0.2-0.5µm CdS - 600-2000Å CdTe - 2-8µm C-Paste with Cu or Metals
Monocrystalline		<p>They are known as monocrystalline silicon or single-crystal Si. Electronic equipment uses single-crystal silicone / monocrystalline material based. Mono-Si, whose crystal lattice is solid, with solid edges and grain-free edges, are light-absorbing materials used in PV solar cell manufacturing.</p>	

		<p>Monocrystalline are different from other allotropies, such as amorphous and polycrystalline silicon. They contain pure silicon; however, small amounts of other elements are added to change their semiconductor properties. The Czochralski process is used, where cylinders are sliced into thinner wafers. The most crucial is the single crystal silicon due to its affordability and availability in electronic devices (Bhager et al., 2015).</p>	 <p>The diagram illustrates the layered structure of a monocrystalline solar panel. From top to bottom, the layers are: a silver Frame, a clear Glass layer, a yellow EVA (Ethylene Vinyl Acetate) layer, a grid of black solar Cells, another yellow EVA layer, a grey Back film, and a Junction box at the bottom right corner with two electrical leads.</p>
--	--	--	--

<p>Thin Film Solar Cell</p>		<p>TFSC typically include CdTe, CIGS and α-Si. They are made by depositing thin PV material layers on glass, plastic and metal substrate with thickness variation from nanometer (nm) to micrometer (μm). TFSC with wafer to a maximum of $200\mu\text{m}$, are flexible with less weight and drag, use BIPV and can be laminated onto windows (Bhager et al., 2015).</p>	
<p>Polycrystalline</p>		<p>They are known as poly-Si / polysilicon and are used in their raw format in industries of PV and electronics. To manufacture polysilicon, metallurgical silicon is used through a purification process where volatile compounds are distilled and decomposed at high temperatures into silicon. Polycrystalline for solar silicon is less pure, whereas, for the electronic industry, polysilicon impurity levels are less than one part per billion (ppb). The metal flake effect is given by the crystallites that are small crystals from polysilicon, also known as multisilicon. Its input material is rods smashed into precise-sized portions, then cast into ingots to recrystallise single crystals. These are thinly sliced Si wafers to produce solar cells (Bhager et al., 2015).</p>	
<p>OSC</p>		<p>Compared to what the market requires in efficiency, OSC has achieved above 17% on PCE. THE FTE photoactive layer and a top electrode are components of a flexible device (Bhager et al., 2015). (Qin et al., 2020) Their high performance is associated with:</p>	

		<ul style="list-style-type: none">-superior transparency, where photons and active layer pass through and are observed respectively.-high conductivity, where the series resistance of the devices is reduced-excellent mechanical flexibility for the performance upkeep after bending-low surface roughness that helps circumvent seepages-suitable work function aids in charge extraction efficiency.	 <p>The diagram illustrates the transition from Flexible OSCs to Stretchable OSCs. On the left, a blue arrow points to a curved, multi-layered structure labeled 'Flexible OSCs'. A green arrow points from this structure to a similar multi-layered structure on the right labeled 'Stretchable OSCs', which is shown being stretched.</p>
--	--	---	---

2.6.8. Solar cell characteristics

The sun cell and diode exhibit notable similarities in cellular composition, sharing attributes akin to exponential semiconductors, as Ramos et al. (2010) documented. A photovoltaic (PV) module comprises traditional solar cells, represented as a current source with an incorporated diode, as illustrated in Figure 2.25. The model introduces series resistance (R_s) and parallel resistance (R_{sh}) to account for losses incurred during actual operation.

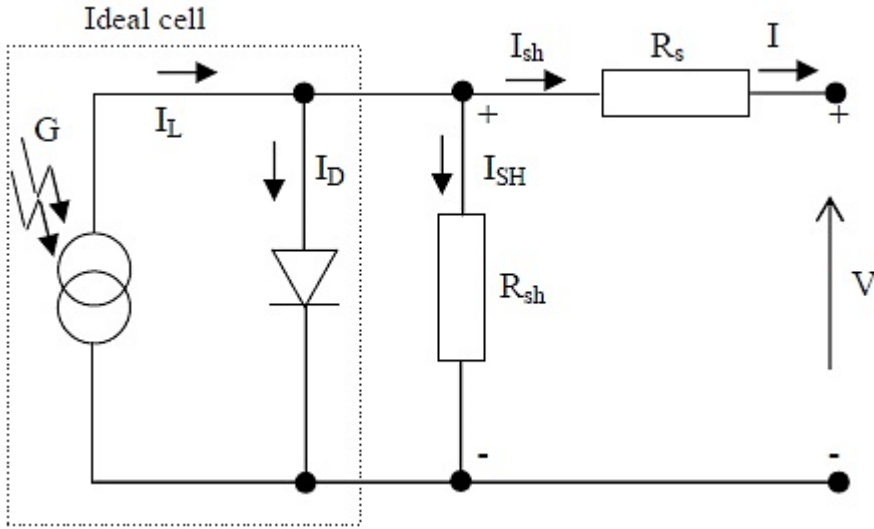


Figure 2.22 Illustration of an equivalent circuit for PV panels (Ramos et al., 2010)

A difference in Incident light gives the equivalent circuit for the PV module. I_L and I_D a normal diode, illustrated in fig 2.25, is given by

$$I = I_L - I_D \tag{2.16}$$

Gow and Manning simplified the work model as

$$I = I_L - I_0 \cdot \left(e^{\frac{(V+IR_s)q}{akT_cK}} - 1 \right) \tag{2.17}$$

However, the inclusion of additional parameters is required to observe PV terminal characteristics, which are given by

$$I = I_L - I_0 \cdot \left(e^{\frac{(V+IR_s)q}{akT_cK}} - 1 \right) - \frac{(V+IR_s)}{R_{sh}} \tag{2.18}$$

The dependency on the PV module, voltage, solar irradiance on the PV module, windspeed and ambient temperature is presented by the output current produced in equation 2.18

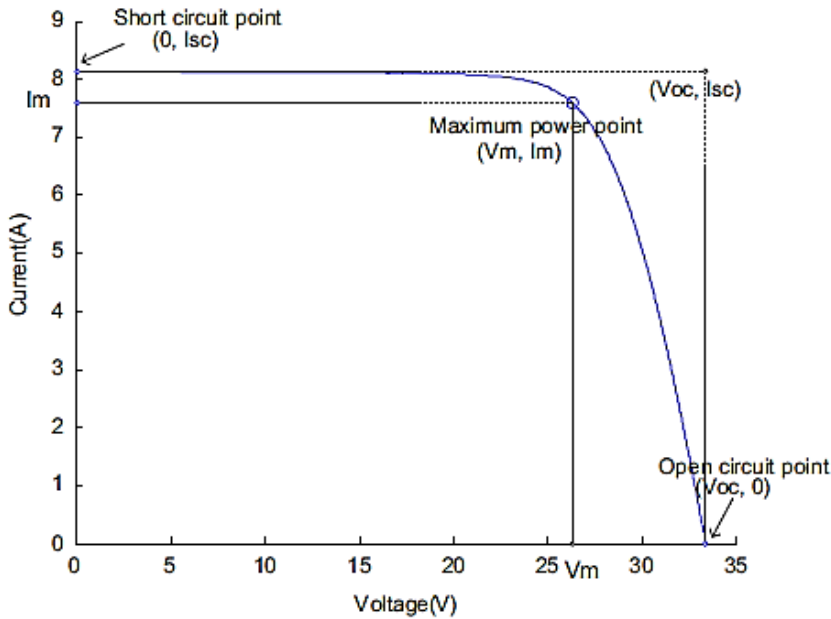


Figure 2.23 PV module I-V curve with three distinct points (Ma et al., 2014)

This research uses models to generate data points for current and voltage, which are then connected to form an I-V curve. The main goal is to match predicted I-V curves to the experimental curves of a practical photovoltaic (PV) system at three key points. These points are short-circuit (0, I_{sc}), maximum power point (V_m , I_m), and open circuit (V_{oc} , 0). Previous studies on PV mathematical and simulation models have been reviewed, and the commonly used 5-parameter model involved in this study was discussed (Ma et al., 2014).

I_L = Current generated by incident light (A)

I_D = Diode current (A)

I = Net current of a cell (A)

V_c = Voltage of cell (V)

I_0 = Saturation current of a diode

q = Charge of an electron, equal to 1.6×10^{-19} (Coul)

a = diode ideality constant

k = Boltzman's constant, 1.38×10^{-23} J/K

T_{cK} = Cell temperature

V = Voltage (V)

R_s = Resistance in series

2.6.9. Types of PV systems and components

Decentralised PV systems are encouraged for most energy-destitute rural communities in Sub-Saharan Africa (Opoku et al., 2023). However, a standalone energy system comprising a solar panel, battery system, charge controller and some loads transmits electricity to rural homes in off-grid areas (Chowdhury and Mourshed, 2016) is shown in the figure 2.24.

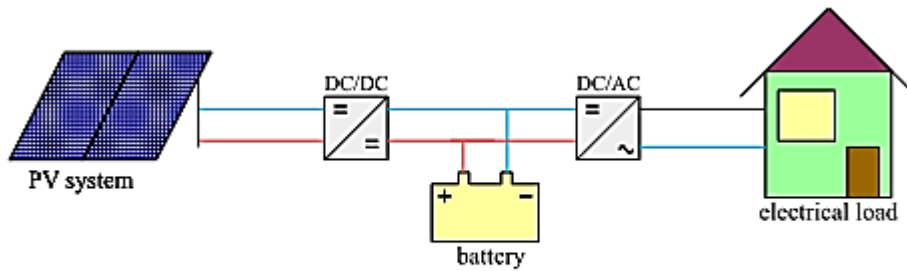


Figure 2.24 Optimal Solar PV Tilt Angle for Maximum Annual Irradiance (Jurasz et al., 2020)

Off-grid components

The photovoltaic system is a crucial component that converts sun rays into electric power through the photo-voltaic effect (Ramos et al., 2010). The solar charger located in the system controls the flow of current to and from the batteries, ensuring that they are not subjected to overcharging, which could cause damage to the batteries and the system (Opoku et al., 2023). Load refers to the energy-consuming devices connected to the PV system, such as lighting, refrigeration, and air conditioners (Jurasz et al., 2020). The amount of load connected to the system determines the size of the PV system.

In summary, the PV system comprises the PV, solar charger, battery and load. Understanding the functions of these components is crucial to maximising the system's efficiency and ensuring that households have a reliable and uninterrupted power supply.

2.6.10. By-laws

COCT developed bylaws for small-scale embedded generation (SSEG) of not more than 1000kVa, where a different document, Standard for Interconnection of Embedded Generation (EEB 705), is applicable for the generation of more than 1000kVa interconnection, which is in line with the Electricity Regulation Act 4 of 2006 (ERA) and associated Regulations, South African Grid Codes and Occupational Health and Safety Act 85 of 1993 (OHS) (City of Cape Town, 2021)

A written consent shall be provided to the Director of Electricity Generation and Distribution Department (EGD) of the City of Cape Town (CoCT), for consumers wishing to lawfully install and connect for consumer operational requirements of alternative electricity generation, will follow the applicable procedure provided as per regulatory compliance (with process ERA, OHS, South African Grid Codes, etc.), ethics (e.g. SANS 10142-1) and stipulations (e.g. NRS) (City of Cape Town, 2021).

Schedule 2 of ERA specifies registration and licensing requirements SSEG need to comply with, provided by the Licensing Exemption and Regulation Notice under section 36(4) of the ERA (2006) published by the Department of Mineral Resources and Energy (DMRE) and National Energy Regulator of South Africa (NERSA), (City of Cape Town, 2021), (DMRE, 2022), (NERSA, 2020)

Inverters with a South African Bureau of Standards (SABS) mark, with test certificates clarifying compliance by the National Regulatory Services (NRS) 097-2-1 edition, will be required as proof of compliance by CoCT (City of Cape Town, 2021).

Installed grid-tied SSEG shall be certified in agreement with CoCT's requirements, professionally registered with the Engineering Council of South Africa (ECSA), and liable for compliance with design, protection, and relevant standards.

- A professional (engineer, engineering technologist) or certified engineer may signoff commercial, industrial and residential SSEG installations, whereas
- A professional technician only certifies SSEG installation for residential use (City of Cape Town, 2021).

The objective of the present work is to develop a building panel that incorporates water storage and solar energy, according to the collected literature, the engineering body of knowledge has not illustrated a building panel capable of storing water whilst generating energy.

2.7 Energy utilisation in buildings

The effects of climate change caused policymakers, governments, engineers, architects, and builders to make necessary adjustments regarding various approaches to sustainable green building designs and sustainable construction materials. The latter includes using sustainable materials, insulation, energy efficiency technologies, heating, ventilation, air-conditioning (HVAC) systems and sustainable designs.

Buildings absorbing thermal irradiance from the outward environment call for renewed consideration of the discomfort in buildings caused by global warming, an environmental temperature issue. Research estimates that 70 % of energy demand can be saved, provided energy efficiency and building components are properly implemented and designed while incorporating sustainability (Bida et al., 2021).

From the produced energy, buildings consume 75% of the network energy supply, while in the modern day, sustainable and green buildings receive world attention (Bida et al., 2021; Sheng et al., 2011). BIPV replaces conventional building materials and is considered a prevailing and adaptable tool performing a dual purpose to meet zero-energy building requirements. Its applications include roofs, facades, and glazing, and it is reasonably priced and has improved efficiency (Lamnini and Kadar, 2017).

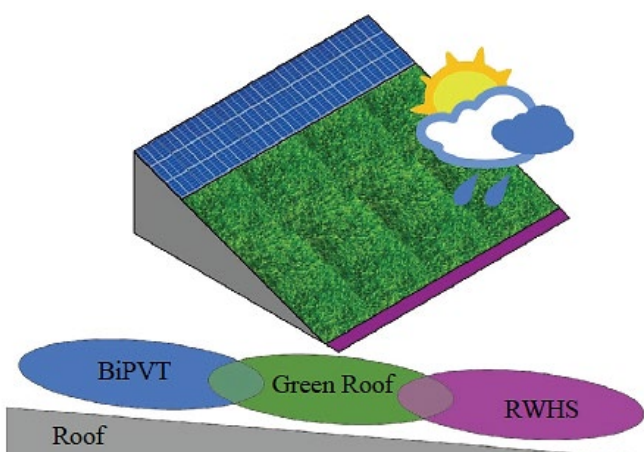


Figure 2.25 Illustration of an integrated sustainable roof design incorporating BIPV, green roof and RWH (Sheng et al., 2011)

The combined technologies explore the potential benefits of green roof building, where some of the benefits include Economic benefits - the monetary accrual as a result of BIPV application; design benefits – BIPV integration and function of building component; environmental benefits – improvements on the environment as a result of BIPV application; an increase in roof ambient temperature from installed PV, the generated energy and used to irrigate the green roof, and the harvested RW can be used during drier months (Sheng et al., 2011 and Attoye et al., 2017).

LEED 2009 (New Construction And Major Renovations) Criteria	Maximum Score	Scoring Weight
<u>EA Credit 2: On-site Renewable Energy</u>		
Assess the project for non-polluting and renewable energy potential including solar energy	7	7 / 110
<u>SS Credit 7.2: Heat Island Effect—Roof</u>		
Install a vegetated roof that covers at least 50% of the roof area.	1	1 / 110

Figure 2.26 Illustration of a scoring criteria used by LEED (Sheng et al., 2011)

Green Building Index Version 1.0 (Non-Residential New Construction)	Maximum Score	Scoring Weight
<u>EE 4 Renewable Energy</u>		
Assess the project for renewable energy potential including solar energy	5	5 / 100
<u>SM 12 Greenery & Roof</u>		
Install a vegetated roof for at least 50% of the roof area.	1	1 / 100

Figure 2.27 An illustration of the green building scoring weight system (Sheng et al., 2011)

Figures 2.26 illustrates the criteria used by Leadership in Energy and Environmental Design (LEED) in grading for new construction and major renovations whereas figure 2.27 illustrates the weight scoring system used by the green buildings index for new construction and major renovations. (Sheng et al., 2011)

The GB rating system is a tool used to measure green buildings. Figure 2.26 shows that RE projects used for solar energy supply have higher than green roof space used for vegetation. Two different bodies, LEED and Green Building Index Version, give these scoring systems, measuring new construction and major renovations and Non-residential new construction, respectively. Both scoring systems prefer energy generation technologies, with roof installations compared to vegetation green roofs. This is indicated by the high-scoring RE projects received against green roof projects (Sheng et al.,2011)

2.8 Biodegradable polymer for reuse

Polymer Materials recycling

(Andoh et al., 2016), iterated that polyethylene terephthalate (PET) is an easily recyclable polymer affecting its properties. Using sustainable materials is at the forefront when considering reducing GHG emissions and disposing of waste from landfills. Research conducted between LDPE, HDPE and PET is tested for Youngs Modulus (E), toughness, stiffness, tensile strength, and hardness, where collected polymer samples chopped, heated at 180°C, and compressed, is melted into strips that are cut into pellets. It is found that reused plastic materials decrease in tensile strength, and the temperature from the extrusion process causes E. Thermoplastics to also degrade when heated and cooled down. Also, the

elongation percentage of PET and HDPE was within the virgin plastic material range, whereas LDPE fell outside this range. The recycled plastics exposed to the environmental conditions and contamination levels may have reduced the mechanical properties of a plastic polymer.

Material	Young's Modulus (GPa)	Ultimate Strength (MPa)	Elongation (%)	Glass	Composition
				Transition Temperature (°C)	
High density polyethylene	0.8	26-33	150	130	(C ₂ H ₄) _n
Polyethylene terephthalate	0.11-0.45	25-May	500	80	(C ₂ H ₄) _n
Low density polyethylene	2-2.7	55	125	250	(C ₁₀ H ₈ O ₄) _n

Figure 2.28 Illustration of properties for various plastic materials exposed to varying temperatures for each material type (Andoh et al., 2016)

2.9 Summary

This study comprehensively examines three interconnected technologies: building panels integrated with a rainwater (RW) collection system capable of generating photovoltaic (PV) energy. Each technology is individually assessed, and an autonomous review of related research is conducted to identify gaps.

Significant advancements in building panels for both load-bearing and non-load-bearing structures are explored, emphasising sustainability, low-energy materials, compliance with green building standards, and using carbon-neutral materials. These innovations are thoroughly investigated in response to the evolving demand for eco-friendly construction materials.

The research also explores the development of rainwater harvesting, prompted by recent municipal water scarcity concerns. While this technology proves viable and efficient, its successful implementation requires careful consideration of various variables to ensure optimal outcomes.

On another front, photovoltaic (PV) technology has experienced substantial growth in both domestic and industrial applications. Continuous improvement in PV technology is evident, with a notable focus on organic and transparent solar cells. This advancement enables solar energy harvesting on various planes, including vertical and horizontal orientations and West and East-facing structures. The evolution of PV technology opens up new possibilities for energy generation from sunrise to sunset, contributing to a more sustainable and comprehensive energy landscape.

2.10 Conclusion

The existing literature underscores the depth of research on building panels, rainwater harvesting, and solar photovoltaic systems. Our focus is creating a building panel that seamlessly integrates water storage and solar energy generation. Despite the comprehensive literature review, the engineering knowledge base lacks documentation of a building panel capable of storing water and generating energy concurrently.

Various materials have been explored in building panel innovation, emphasising sustainability and novelty. Research efforts span both load-bearing and non-load-bearing panels, with a constant drive to enhance them by exploring new materials or novel combinations of existing ones.

Rainwater harvesting, a critical facet of sustainable practices, has undergone extensive investigation, encompassing diverse methodologies. The need for novel approaches is evident, and the literature reflects a spectrum of researched rainwater harvesting methods.

While photovoltaics have experienced widespread adoption, extensive research endeavours have focused on developing PV panels. This includes expanding module sizes and enhancing panel efficiencies across different types.

Building Integrated Photovoltaics (BIPV) has emerged as a popular area of investigation, aiming to integrate green technology into buildings seamlessly. This integration aligns to achieve net-zero energy buildings, serving as a strategy for mitigating greenhouse gas emissions and offering a solution for offsetting carbon emissions in the building sector.

Despite this extensive research, a notable gap exists in the absence of literature detailing the design of a prototype building panel capable of rainwater storage and energy generation.

Chapter 3 Concept Development & Research Methodology

3.1 Introduction

The enhancement of building functionalities, specifically in load-bearing and load-transfer capacities of walls, necessitating a modernised approach that adds value. This involved the integration of rainwater harvesting and energy generation capabilities within walls, whether load-bearing or non-load-bearing, as an alternative to traditional electricity sources. The growing demand for alternative water sources for secondary use and renewable energy in South Africa is gaining traction, driven by the increasing challenges and costs associated with conventional resource supply.

To address these challenges sustainably, there is a need for a comprehensive turnkey solution that caters to the needs of rural communities while prioritizing environmental considerations. This research endeavours to fill this gap by conceptualizing and designing a prototype building panel that serves the triple purpose of rainwater storage and energy generation as a unified technology.

The study quantified the rainwater harvesting capacity in cubic meters (m³) achievable on a 10-Watt peak (Wp) panel. The designed building panel *mBP*, incorporated an *iBP*. Additionally, the research explored the power output of a 10Wp flexible solar cell when mounted on a vertical surface and analysed technology-related costs. This holistic approach aimed to provide a sustainable and economically viable solution for addressing rural communities' water and energy needs.

This chapter details the conceptual development and methodology in designing a prototype building panel for rainwater storage and energy generation. It provides theoretical research methods and compares them to practical methods to test the integrity of the prototype building panel. Historical rainfall patterns for Cape Town in the Western Cape have been used as a tool in the commencement of the design. The prototype is designed for conditions at the CPUT campus, Belville.

3.2 Concept development

The concept was initiated by Prof Pallav after experiencing water and electricity outages while relocating to Cape Town, South Africa, in 2018. This ignited a concept that would add value to the built environment for high-rise buildings through RWH methods and electricity generation from renewable sources such as PV. This concept was meant to add value and functionality to the high-rise buildings. The pertinent question was: how can these technologies be integrated into a building panel without compromising the functionality of each component?

The initial project was supposed to be a building panel with capillary tubes to collect rainwater for storage and generate energy for high-rise buildings. The scope changed as the need for water leaned towards rural communities and energy needs, imposing design changes to the building panel.

Initially, these research requirements were not easily understood, but enthusiasm, curiosity, and interest in integrating sustainability into the built environment were enough motivation to pursue this research. The first conceptual model was constructed from a Weetbix box, with an added concept made from cardboard. Solar PV was made from foil with solar cells printed on tracing paper covered in clear plastic,

emulating a real PV panel. A shower head was also made from the cardboard box. This was motivation to build confidence in this research work and pave the way to understanding the preliminary concept.

After some discussions with the team, the advice was to build the model to scale.

This is when the free hand concept was initiated. It was during the workshop conducted by Prof Jordaan that the concept was sketched in the notebook, and later a freehand concept, as shown in Figure 3.1

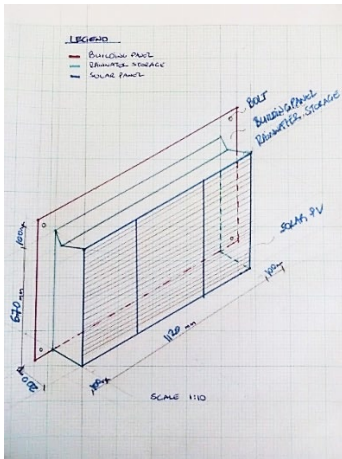


Figure 3.1 Freehand prototype concept drawing

The next phase was to produce the drawing on AutoCAD, and it was done. As shown, the dimensions of a typical building panel were selected; 1120mm × 670mm × 200mm, which would have made it difficult to carry the prototype.

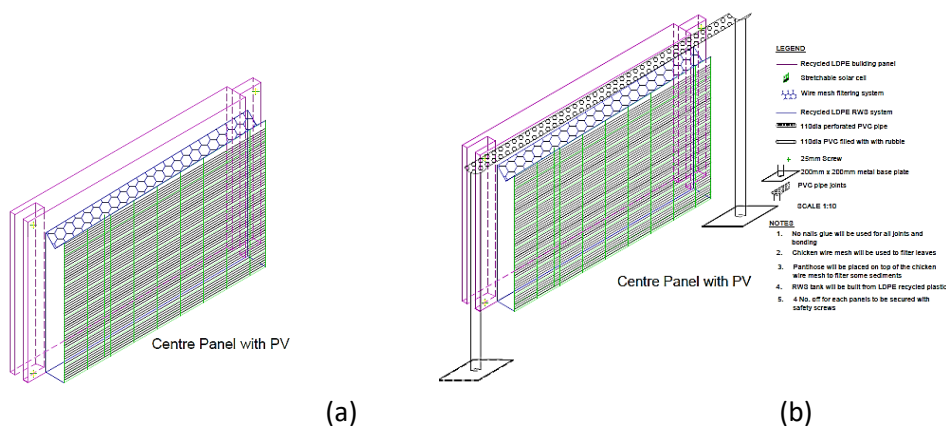


Figure 3.2 a) AutoCad generated concept, b) concept showing how rainfall will be simulated

The initial dimensions of a building panel, as shown in Figure 3.1 and Figure 3.2, were reduced because of size. Also, the concept had a protruding RWS and energy generation system.

The design dimensions were altered from 1120 × 670 × 200mm to 550 × 335 × 100mm, and the design was revised where the building panel, the rainwater harvesting system and the PV panel were now a panel with three functions as shown in Figure 3.3 and Figure 3.4. Also, during this time, a 3D model for moulding was required so research could commence with printing. One of the aspiring researchers from the mechanical engineering department volunteered and assisted with the mould drawing, as shown in Figure 3.3

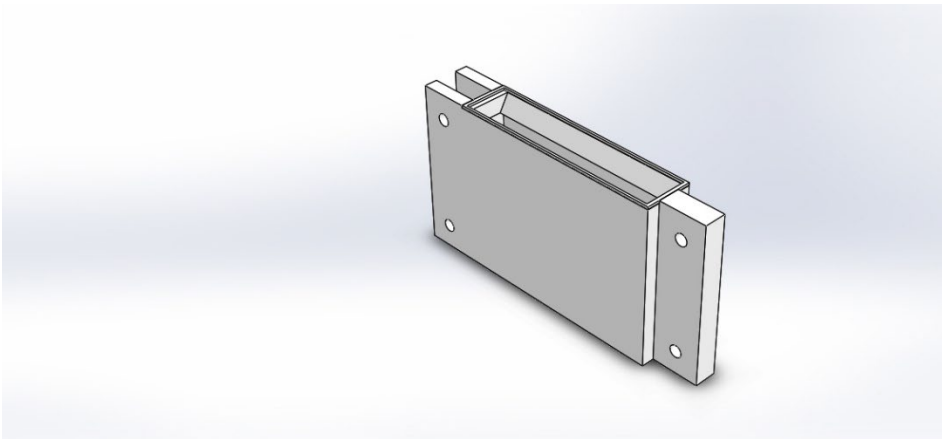


Figure 3.3 Initial mould design before dimensions were altered

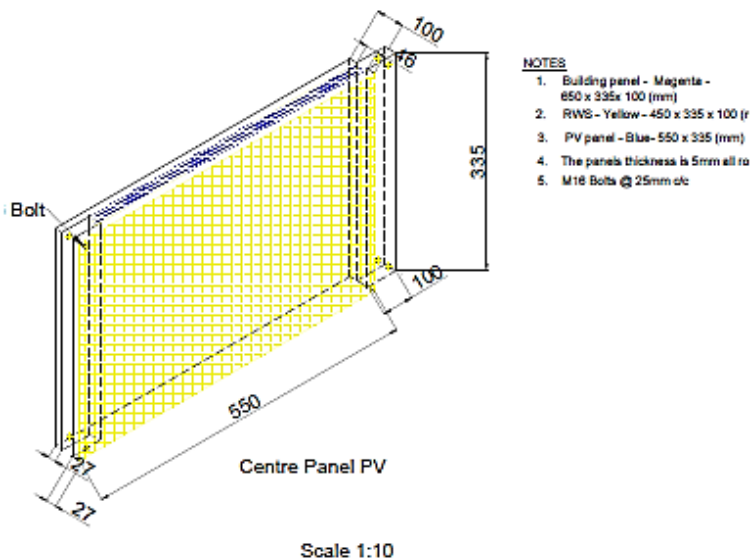


Figure 3.4 Altered drawing dimensions and revised design

After much deliberation with the team, it was suggested that the building panel dimensions were big and needed to be revised again. Thus, the new panel dimensions were revised to an *mBP* and an *iBP*. This meant the prototype could be easily placed on a desk while presenting.

This research aimed to incorporate material recycling into the concept, using a local company that recycles plastics to assist with developing this prototype. This aligned with the SA 2030 vision of creating sustainable green jobs. Following the CPUT ethics code of conduct, the necessary paperwork was signed as per agreement between the researcher and the company. However, the facility's owner could not assist further because of technological challenges.

AutoCAD 2D was the initial drawing program utilised in developing the prototype, AutoCAD 3D was also used, and SolidWorks was the inventor. These changes were due to improvements instituted in the prototype development.

Attempting to illustrate the graphical kinetic of the prototype, 3D animation was a solution, and this research managed to find an animator. However, only part of the animation was fulfilled, as shown in Figure 3.5. The animator was no longer available to assist with the animation.



Figure 3.5 Animated illustration

While busy with animation, this research needed to make progress and started searching for printing the model. The initial plan was to build it at one of the CPUT design facilities. When that did not materialise, researchers had to search for another option, which took almost 3 months to figure out and find a reputable company that could assist. This required out-of-the-box thinking, and the search for an alternative recycling company was needed. With the research team's effort, it was suggested that CPUT facilities be used. With no traction, ideas emerged to utilise private 3D printing companies, and most were printing smaller models compared to the project's requirements. Only after March 2023 did the project team come across the printing facility in Claremont, which referred this research to Netram Technologies in Milnerton, which is capable of printing up to 1m x 1m prototype models. Funds were a stumbling block, but did not stop the project from progressing.

The utilisation of a PV panel depended on the availability of the choice of material, either a flexible solar cell or a stretchable solar cell. Local distribution companies did not carry either of the two materials. Still, they managed to source it through a CPUT-registered vendor, D&S Technology Solutions, who imported PV materials and procured a thin-film flexible solar cell with its components.

PV simulation was required as part of the design process. Various PV simulation programs were suggested to be best suited for research work. These were PVSyst, Homer, RETScreen, SolarPro ESPr, NRELSAMAN and Matlab. After methodically going through each program, PVSyst was a preferred choice. The first PVSyst downloaded was version 6, which has a different interface than version 7. Version 6 options are on the screen, whereas with version 7, one can easily miss the pull-down menus if attention is not paid to them correctly. And that is what occurred with this research. However, research work reached a dead end with PVSyst. The program seemed simple, but the input data challenges were beyond recognition. According to research, the simulation was supposed to be aligned with the real prototype, but PVSyst had other plans. All the consumption data was changed because there was no compatibility between components. The first simulation was on a 30W system, then increased to 50W, then reduced to 10W, which is not featured in the PVSyst program. After attempting a 10W, an 80W system was trialed, then a 300W. After a 300W, something clicked and defined research is about investigating, so it was realised that the preliminary design, one of the options, was not done. And now the PVSyst has been downloaded and

deleted 3 to 4 times. The fifth time PVSyst was installed, a decision was made to purchase a student version to make all options available and work swiftly.

There was also an option to simulate rainfall, and finding a computerised rainwater simulation program was challenging. There were two that were referred, but there was no time to read about them, learn to simulate on time, or be able to integrate the results into this research work.

The final journey, as a big part of the research, is about learning, investigating, asking questions, and trying it out, and that is what this research did in the end: learned how to simulate PV system design, learn how to produce 3D drawing and prepare it for 3D printing, learn, learn, learn repeatedly keep on learning and never stop.

3.3 Research design

Theoretical research strategies are applied. These strategies include mathematical calculations for designing the building panel, bolt, RWH, and PV systems. Also included in the theoretical strategy is the application of 3D Computer-Aided Drawings (CAD), real-time rainwater and energy simulation, the PV simulation using PVSyst, and the modelling of a building panel with an RWS system, including a PV system.

To recap, the *i*BP with a 5mm wall thickness is embedded in an *m*BP. The bolt size is M12, and the nominal diameter (DN) is 13mm. The building panel has an interlocking finish and a female and male connector. The building panel design follows the SANS 10162, the rainwater harvesting design is in accordance with SANS1739-2017, and the photovoltaic design is in accordance with SANS 10142-1 and SANS 101066. The PLA χ is 1250kg/m³. The bolt class is given a 4.8 following the SANS 10162.

3.4 Study Setting

The study area selected for this research is the CPUT Bellville campus, Cape Town, in the Western Cape Province in South Africa. CT has been applauded as one of the best conducive locations in the country to research, as shown in Figure 3.1. Accessibility to resources as well as the broad scope the area offers. CPUT is the only University of Technology in the Western Cape province



Figure 3.6 Study area, Civil Engineering and Geomatics Department locality map at CPUT Bellville Campus, South Africa (Google Maps, 2015).

3.5 Research Methodology

This research encompassed the design of two existing technologies, RWS and solar panels, modelled into a non-load-bearing (NLB) building panel. Existing rainfall data was used to help analyse the rainfall intensities over ten years. The data provided a guide in the design of these technologies.

Theoretical research strategies were applied. The strategies included mathematical calculations for designing the building panel, RWH and PV systems, applying Computer-Aided Drawings (CAD), PV simulation, and modelling a building panel with RWS and PV systems.

This research encompassed the simulation and modelling of a building panel with a RWS and a PV system. A 10-year rainfall data set was collected from the South African Weather Services (SAWS) to determine rainwater storage capacity and for determining the amount of RWH (m^3), the area of catchment (m^2) \times amount of rainfall (mm) \times runoff coefficient. Calculations are used to determine the amount of energy that could be harvested and how long the solar energy could be harvested over time or the time of the technology.

Modelling of the RWS tank included using polylactic acid (PLA), moulded into an *mBP*. PLA is a filament used in 3D printing. Low-density polyethylene (LDPE) is derived from cornstarch or sugar cane, making it renewable.

The prototype was designed on an Autocad 3D program and exported to a Lithograph file known as an STL file. The printer used a communicable language it recognised to print the model: Geometric code, also called G-code. The G-code is comprised of coordinates used for positioning and giving printing directions. The G-code also instructed the printer how much filament to extrude or squeeze.

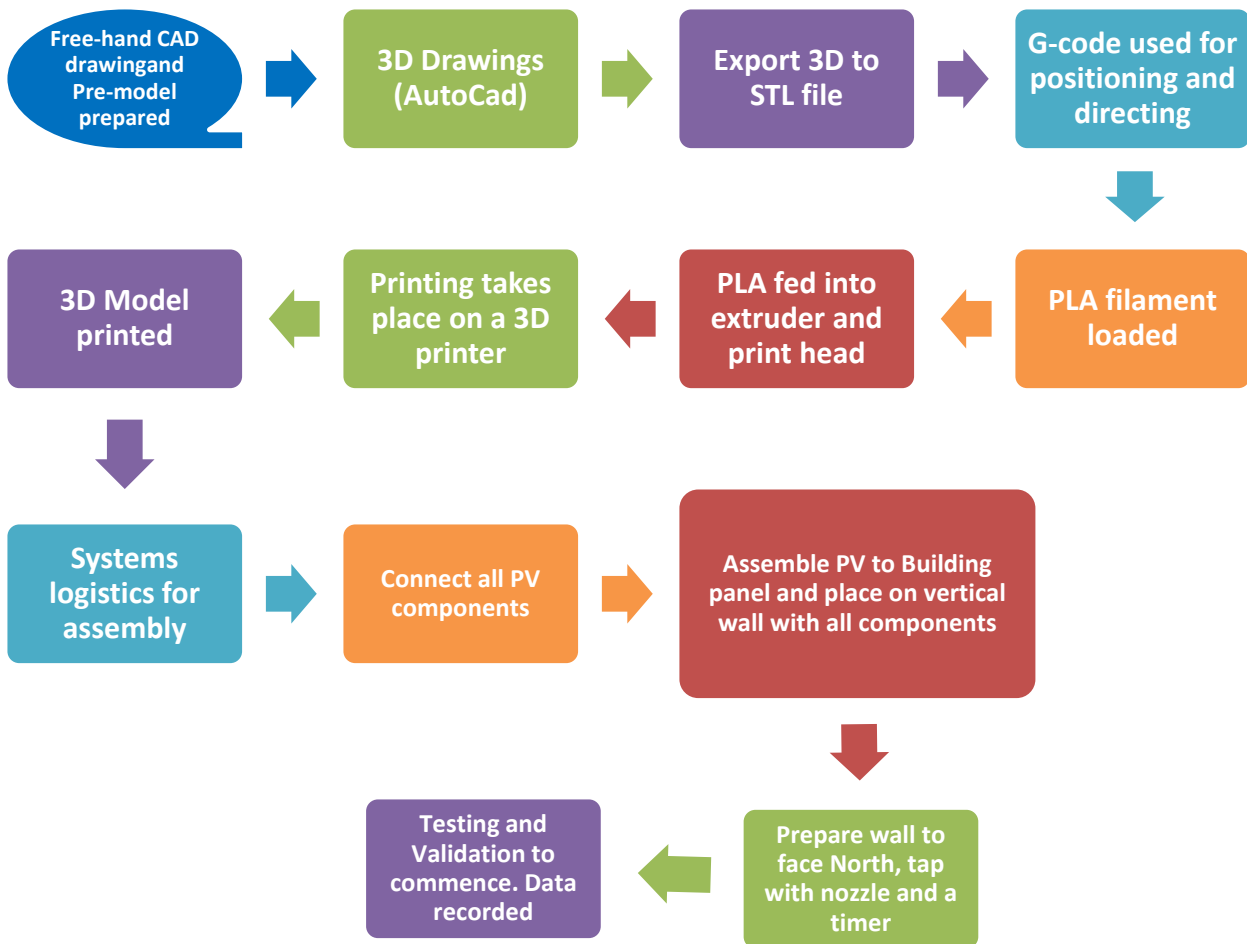


Figure 3.7 Flow chart diagram for the model.

i. The process

The clear filament s was loaded onto the printer, where the filament was fed into the extruder, and it poured itself up to the printing head. The 3D file exported to an STL file is saved on an external drive and loaded to print. The printer starts heating up, and the first layer is printed. This layer ensures the surface is flat and produces good-quality printing. Each printed layer is 1mm thick. The printer was set up for varying layer thicknesses between 5mm, and the solid outer thicknesses varied between 14mm and 13mm.

ii. Rainfall simulation

Upon completion of the panel, the polyepthalene (PET) bottle was recycled to simulate rain. The recycled polyepthalene (rPET) bottle was cut in half along its length, leaving the cap on. A screwdriver punched holes through the remaining half as a medium to pass water through. The hosepipe transported water from the tap to the rPET bottle, emulating clouds. The released water passed through the hosepipe, with the nose sprinkler attached to the hosepipe.

To determine the amount of RWH (m^3), the area of the catchment (m^2) \times amount of rainfall (mm) \times runoff coefficient

iii. Photovoltaic

A 10W polycrystalline flexible solar cell (polycrystalline FSC) was imported from China with the following solar PV components: Modular MPPT Solar Charge Controller in accordance with ISO9001:2015 and ISO14001:2015, a 5V Remote Meter for solar charge controller in accordance with ISO9001:2015 and ISO14001:2015, a 12V 7Ah Lithium ion Phosphate (LiFePO₄) battery, the connecting wire between the battery and the MPPT solar charge controller, the RS485 communication bus cable and the locally sourced 6mm solar PV to the MPPT charge control cable. The PV connection and wiring were executed with the assistance of a qualified PV technician. The 6mm cable was measured and cut to size with a wire stripper. The direct current (DC) output cable is connected to the 6mm cable, joining the two wires with a TE 2way barrier strip connector. The cable connected the MPPT solar charger with the polycrystalline FSC. The LiFePO₄ battery wire was connected to the MPPT solar charger, where the positive and negative points were unscrewed, the positive and negative wires were connected, respectively, and the screw was tightened. The negative and positive terminals were black and red, respectively. A load of not more than 12V was connected to the MPPT solar charger to test if the PV, MPPT solar charger and Battery were working.

To measure the power output of the solar panel, multiply solar panels watt (W) \times average sun hours \times 75%.

Two peg boards with the following dimensions, 800mm x 200 mm, were used as display boards for testing purposes.

iv. Verification:

Rainwater harvesting system

This research promoted the reduce, reuse and recycle (3R)'s ethos. It is considered using a recycled rPET bottle, cut into half size and holes punched to 5mm in diameter. The punched rPET bottle was used as a conduit for RW simulation. A hose pipe and a nose sprinkler were attached at each end, and the faucet was opened slowly so water simulated the rain. The collected water was measured using a gauge (mm). Data was recorded, and the harvested rainwater was measured every 15 minutes. The RWS tank was too small to collect data hourly; the rainwater spilled over, which could have resulted in inconclusive results.

Solar PV output

The energy output was measured using a solar charge controller, which gave energy readings in watts. The data was recorded every 15 minutes. Initially, the readings were recorded every minute, but because the readings did not show much variation, this research opted for 15-minute interval readings.

Data analysis and data interpolation were conducted in Excel.

Mathematical calculations were also done to fulfil the objectives of this research.

The verification of the building panel was to fulfil the objectives of this research:

To determine the volume of rainwater that can be harvested on a 10W panel.

To determine the power output of a 10W solar cell placed on a vertical surface and

To determine the related costs for this technology

The success of this research depended on the design, simulation and the practical verification of the prototype.

The conclusions were drawn from comparing this prototype's theoretical and practical studies, which successfully collected and stored rainwater while simultaneously generating energy. No ethical clearance was required, no data collection permission was needed, and no human studies formed part of this research.

3.3.1. Data

Annual average rainfall data for CT in the WC province of South Africa was obtained online from SAWS over 10 years for CT. The historical data was recorded between 2013 and 2022, from January until December. The average rainfall was measured in millimetres.

A graphical presentation of the annual average 10year rainfall as illustrated in Figure 3.8

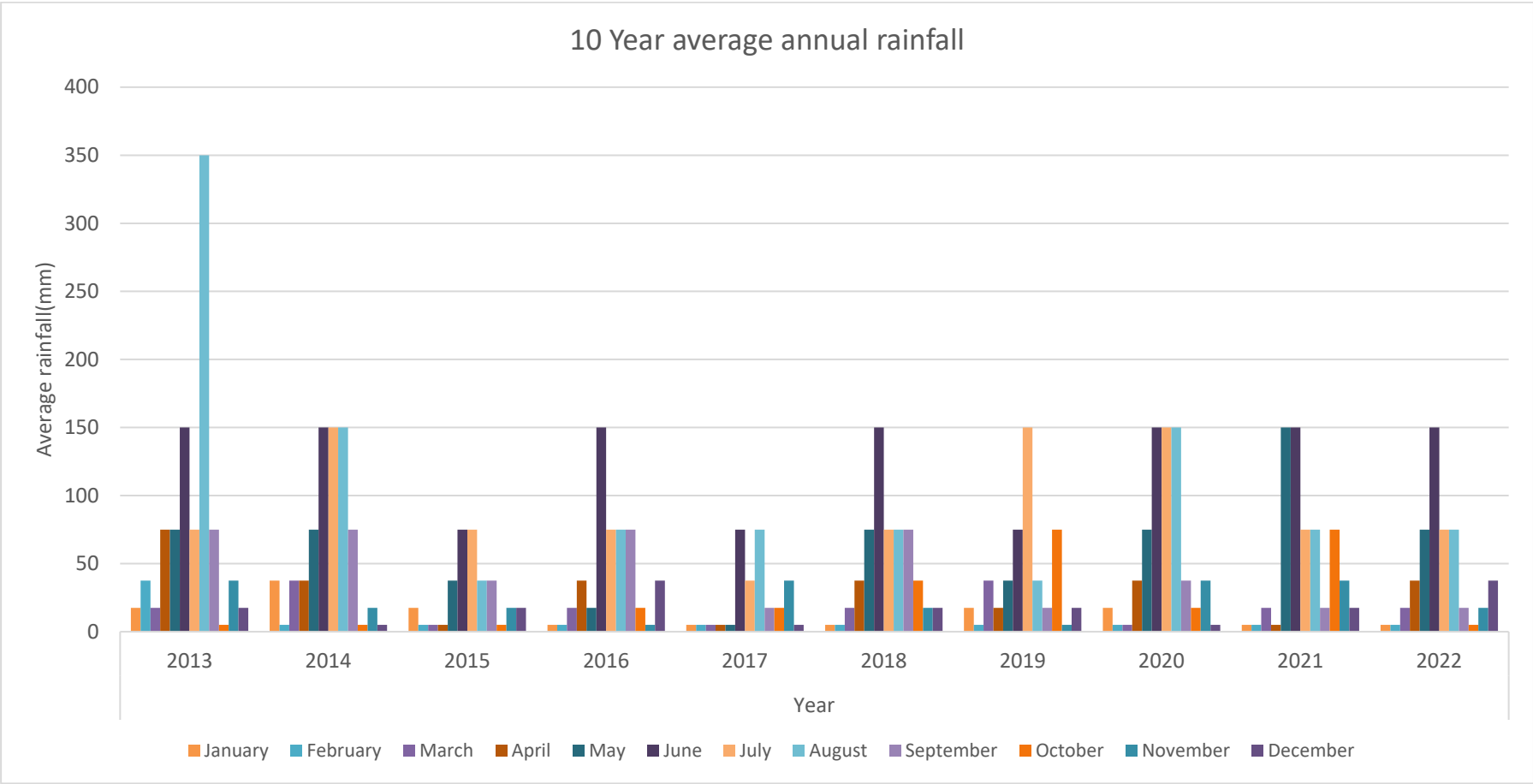


Figure 3.8 Represents a graphical illustration of the annual average rainfall over the 10-years, giving rainfall depth measured in millimetres per month.

3.3.2. Research equipment

The research equipment used in this experimental work for RHW and the building panel, with the help of manufacturing, took place at Netrams Technologies, a 3D model printing company based in Cape Town. The solar PV equipment was imported from China through a CPVT vendor – D&S Solutions. A local electrical company, ACDC, donated the 6mm cable and purchased a display peg from Agrimark Hermanus.

Apparatus required

As detailed, the apparatus used was to accomplish this research's aims and objectives. The equipment used for PV follows the ISO standards ISO9001:2015 and ISO14001:2015.

Building panel: mBP 3D model from APL recycled material, Sika flex 291i, Creality Ender – 3Neo 3D printing machine.

Rainwater harvesting: iBP 3D model embedded in an mBP, a building panel, measuring ruler, hose, nose sprinkler, faucet, and punched rPET bottle for rain simulation.

PV system: MPPT solar charger, a 10W polycrystalline FSC, 12V LiFePO4 solar battery, load, remote meter, RS485 cable, DC cable, AC cable and TE 2way barrier strip connector.

Display: 200m × 800mm × 2no. off. pegboards, cable ties, scissors, bolts and nuts

Recording: Pen, book, stopwatch and a laptop

Personal safety equipment: latex lab gloves, safety goggles, lab coat, and safety boots

Testing Components

Figure 3.9 illustrates various components that were used during the validation process. These components are explained under the required apparatus.



Figure 3.9 Illustrates the all the testing equipment used.

Testing Materials

Water: To simulate the rainwater, water was an agent used for rain simulation.

Sun: To test for the energy generated from the PV system, the sun irradiance was used.

3.3.3. Data collection and analysis

This section presented appropriate data collection relating to the rainwater harvesting and energy generated from PV. Results were interpreted and analysed using a quantitative method. The presentation of results is expressed in graphical and tabulated methods.

Data collection

All data collected for this research were experimental data compared with the theoretical strategies.

The prototype building panel was fixed to a peg board that acted as a vertical wall and is also a rainwater collection tank, simultaneously an energy generation technology with a polycrystalline FSC affixed to its body; simulated rainwater and the latter was harvested during testing. RW collected from the rainwater tank was measured using a scale ruler (mm), and the rainfall data was collected every 15 minutes.

The energy generated from polycrystalline FSC PV was collected, and readings were taken from an MPPT solar charger and recorded in watts. The energy data was collected every 15 minutes. The voltage and amperes of energy generated were displayed, and those readings were also recorded.

Data analysis

A quantitative method was used to analyse the results drawn from the experiment. The quantitative method fulfilled the theoretical strategies used during the research. The data for both RWH and energy generating technologies were autonomously analysed.

The analysis included statistical methods, and results presented in bar graphs and tables.

Other considerations during data analysis that played a pivotal role were:

Time – the time it took to conduct the test, with the urgency due to inclement weather time, to search for sunnier locations for the testing.

Costs – for expertise and equipment

Excel, a Microsoft data analysis program was used.

3.4 Conclusion

This chapter provided a comprehensive overview of the conceptual development process, offering valuable insights into the various phases of planning, design, and construction. Research has meticulously detailed the step-by-step flow of events that motivated their conceptual development, including necessary adjustments that were made along the way. This information is particularly useful for other researchers interested in undertaking similar projects and seeking to understand the complexities of similar conceptual development.

Also, it gave details of equipment, apparatus, conceptual development and methods that were applied for the building of the prototype, the purchasing of the material and other relevant methods to obtain the testing equipment. The experimental equipment collected consistent test data to fulfil this research's aims and objectives. The collected data was presented on an Excel data sheet, and the concluded experimental tests on the prototype were analysed using the quantitative data analysis method developed on Excel. This analysis method aligned with the objectives of this research.

Chapter 4 Model and Design

4.1 Introduction

This chapter details the prototype's modelling and design calculations and covers this research's theoretical strategies. The modelling includes the PV simulation of an off-grid system executed on PVSyst, initial free hand-CAD drawings, 2D and 3D CAD drawings, and the pre-model made from hardboard. Further entailed in this chapter is the final model and its elements & characteristics for the PLA materials used to produce the prototype. This section fulfils this research's theoretical and practical model and design while considering its objectives.

4.2 Modelling

Modelling incorporates simulation of the PV system where PVSyst was utilised as a simulation tool to simulate both a grid-tied and an off-grid PV system, with sizes determined during the preliminary design phase, with the recommendation of a nominal power of 200Wp grid-tied PV system as well as a 76Wp off-grid system. The following loads were applied during the simulation for various periods as part of the simulation process: 1 × 11W Mobile used for 4 hours, 1 x 60W battery (power) bank used for 2 hours; and 1 × 5W LED bulb used for 3 hours. The location was set at CPUT, Bellville campus, with a 90° Tilt – to fulfil the objectives of this research.

4.3 Simulation

PVSyst software was chosen because it is a sophisticated yet user-friendly simulation tool, more so for this project. Andre Mermaid and Co., a Swiss scientist, developed and designed the PVSyst software. A design application globally used largely by engineers providing rapid and accurate results close to actual values (Shrivastava et al., 2023). It is also chosen for designing, simulating, and analysing simplified, sophisticated stand-alone, grid-tied PV systems. This software allows for preliminary design, project design input, and analysis. As a trusted and recognised simulation tool in the industry for developing and optimising PV systems, it provides end-users with more robust PV design, electrical design, energy estimation, and financial analysis, including the return on investment (ROI).

a) Input data

Input data for the simulation was obtained from PVSyst for the CPUT Bellville campus, and the input information is shown in Fig 4.2 with the site's location, latitude, and longitude. Also included were the tilt, the simulation parameters, and the type of module chosen equivalent to the determined nominal power during the preliminary design.

The meteorological data (Meteo) obtained from PVSyst for the CPUT, Bellville campus, with the following coordinates: Latitude: 33.9314S and Longitude: 18.6435E, will be used in the subsequent chapter for output energy. The global horizontal irradiation year-to-year variability was estimated to be 2.9%.

Table 4.1 Incident data by Meteo database

	Jan	Feb	Mar	Apr	May	Jun	Jul	Aug	Sep	Oct	Nov	Dec	Yr
Horizontal Global (W/m ²)	325	293	235	182	135	112	119	147	192	262	311	338	220
Horizontal Diffuse (W/m ²)	95	94	79	54	40	35	35	53	70	79	97	97	69
Extra-terrestrial Solar irradiation (W/m ²)	499	448	378	292	223	190	201	256	337	418	481	510	352
Clearness Index (Ratio)	0.65 1	0.65 3	0.62 1	0.62 3	0.60 6	0.59 0	0.5 91	0.5 75	0.5 69	0.62 6	0.6 45	0.66 2	0.6 26
Ambient Temperature (°C)	22.0	21.9	20.2	17.3	15.1	12.4	12. 2	12. 7	14. 1	16. 8	18. 4	20.8	17. 0
Wind Velocity (m/s)	6.4	6.1	5.3	4.4	3.9	3.9	4.0	4.3	4.7	5.2	6.0	6.3	5.0
Relative Humidity %	66	67	70	74	78	80	78	78	75	69	67	64	72

Table 4.2 Global Horizontal Irradiation table for year 2023

	GlobaHor kWh/m ²	GlobEff kWh/m ²	E_Avail kWh	EUnused kWh	E_Miss kWh	E_User kWh	E_Load kWh	SolFrac ratio
January	241.6	235	6.264	4.252	0.000	1.891	1.891	1.000
February	196.7	190.6	5.185	3.362	0.000	1.708	1.708	1.000
March	174.8	168.1	4.678	2.659	0.000	1.891	1.891	1.000
April	130.9	124.5	3.542	1.616	0.015	1.815	1.830	0.992
May	100.5	93.6	2.714	0.766	0.037	1.854	1.891	0.981
June	80.6	73.9	2.150	0.253	0.013	1.817	1.830	0.993
July	88.6	81.8	2.386	0.470	0.043	1.848	1.891	0.977
August	109.5	103.0	3.020	1.038	0.021	1.870	1.891	0.989
September	138.2	132.4	3.810	1.868	0.000	1.830	1.830	1.000
October	194.8	188.8	5.265	3.263	0.000	1.891	1.891	1.000
November	223.7	216.9	5.959	3.978	0.000	1.830	1.830	1.000
December	251.3	244.2	6.588	4.541	0.000	1.891	1.891	1.000

Year average (Yr)	1931.2	1853.0	51.562	28.066	0.129	22.136	22.265	0.994
-------------------	--------	--------	--------	--------	-------	--------	--------	-------

Legend

- GlobaHor Global Horizontal Irradiation
- GlobEff Effective Global, corr. For IAM and shadings,
- E_Avil Available Solar energy
- E_Unused Unused Solar Energy
- E_Miss Missing Energy
- E_User Energy supplied to the user
- E_Load Energy need of the user (Load)
- SolFrac Solar Fraction (EUsed/ ELoad)

Figure 4.1 demonstrates the path of the sun about the PV vertical tilt of 90° and is also the angle for solar PV modules. According to Figure 4.1, the optimum hours for energy generation under favourable conditions range between 9:30 am and 4:00 pm, with little to no shading probability.

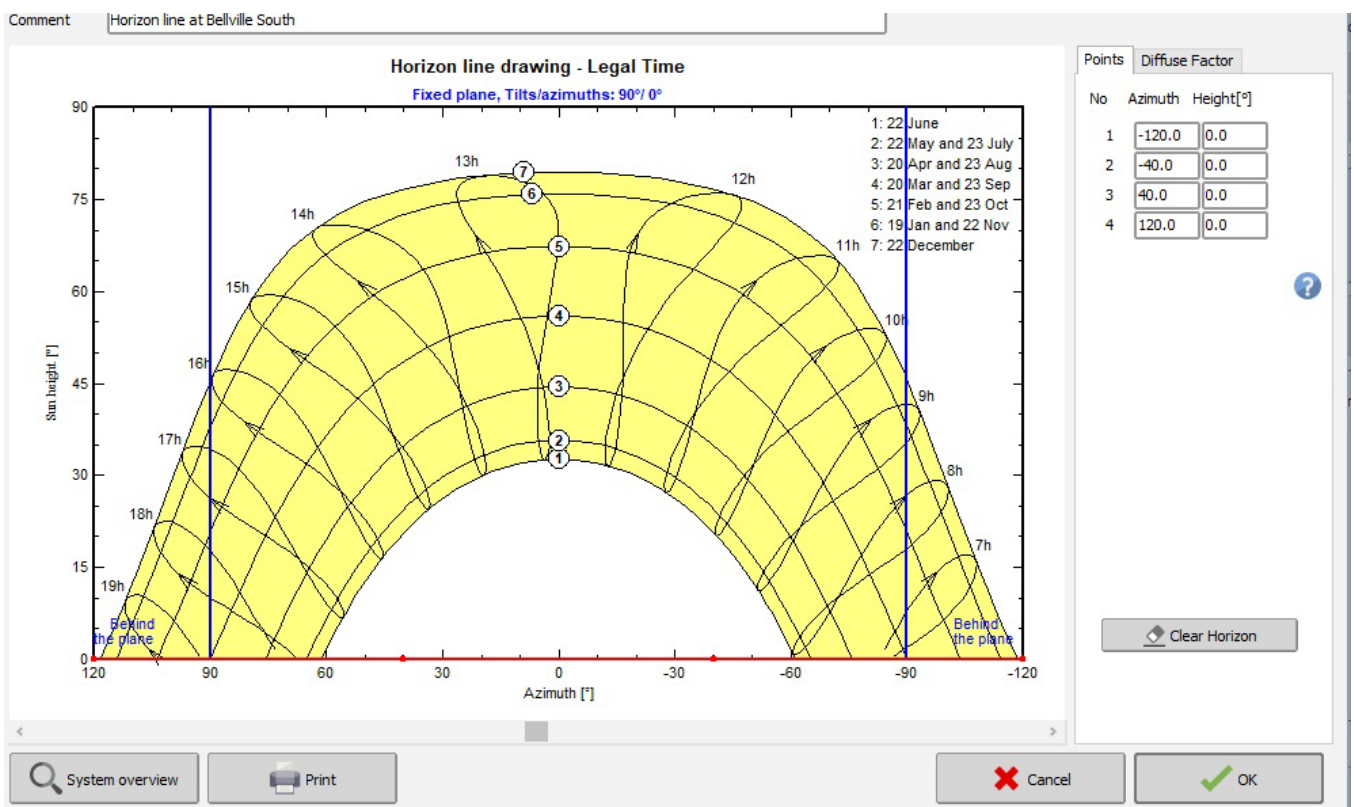


Figure 4.1 Sun paths

With the use of the provided meteorological data, the initial stage is to configure the system. This was achieved by employing orientation which included the following field parameters; plane tilt of 90°, Azimuth 0°, quick optimisation with respect to, a) Annual irradiation yield, b) Summer yield between October and March months, and c) Winter yield between April and September months as shown in Figure 4.2. Table 4.3 provides optimised yield results for transposition factor loss for optimum and global collector plane for annual, summer and winter yields, respectively.

Table 4.3 Optimised yield results

Description	Annual Yield	Summer Yield	Winter Yield
Transposition Factor (FT)	0.73	0.44	1.32
Loss with respect to Optimum	-36.5%	-57.2%	-16.6%
Global on collector plane	1419kN/m2	566kW/m2	853kN/m2

The user needs are defined in Table 4.4, including the LED bulb, mobile phone, battery power bank, and 24-hour standby consumption. The consumption was defined by a year’s consumption, with the hourly distribution also shown in Figure 4.3

Table 4.4 End-user load definition

No	Appliance	Power (W)	Number	Daily use (hr/d)	Daily Energy (Wh/d)
1	LED bulb	5	1	4	20
2	Mobile phone	11	1	3	33
3	Battery power bank	50	1	2	100
4	Standby consumer	1	1	24	24
Total Energy Required					177 Wh/day
Total monthly energy required					5.31kWh/month

The total energy required was 177Wh/d, and the total monthly energy required was 5.31kWh/month, each month having an average of 30 days.

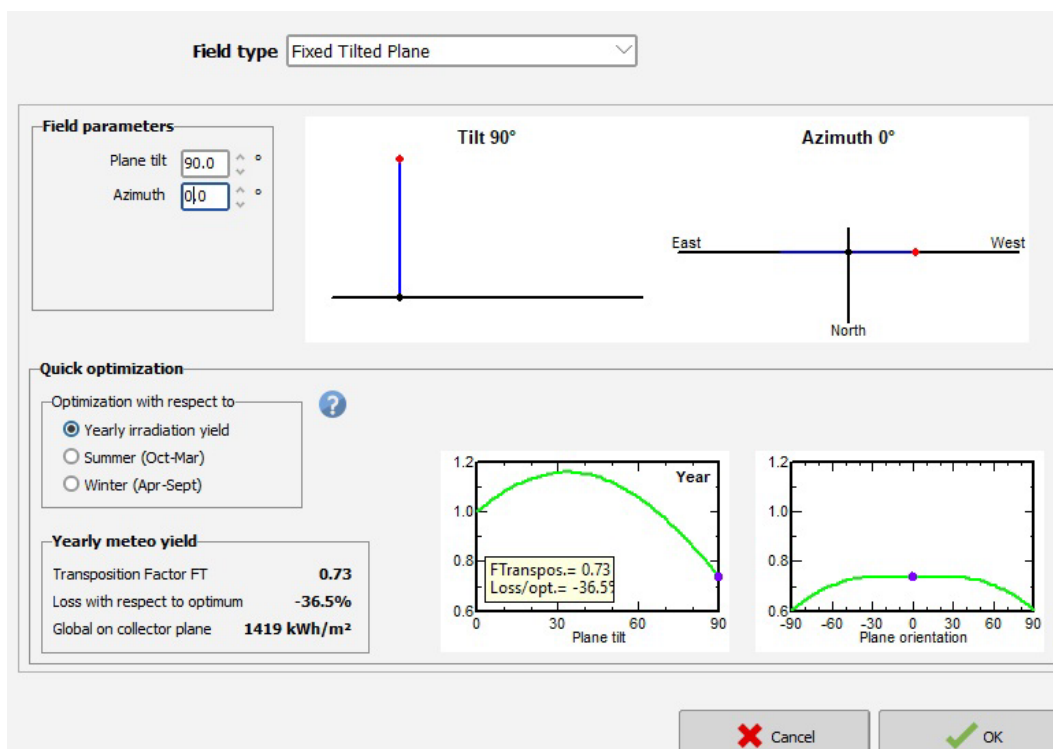


Figure 4.2 PV orientation and tilt angle

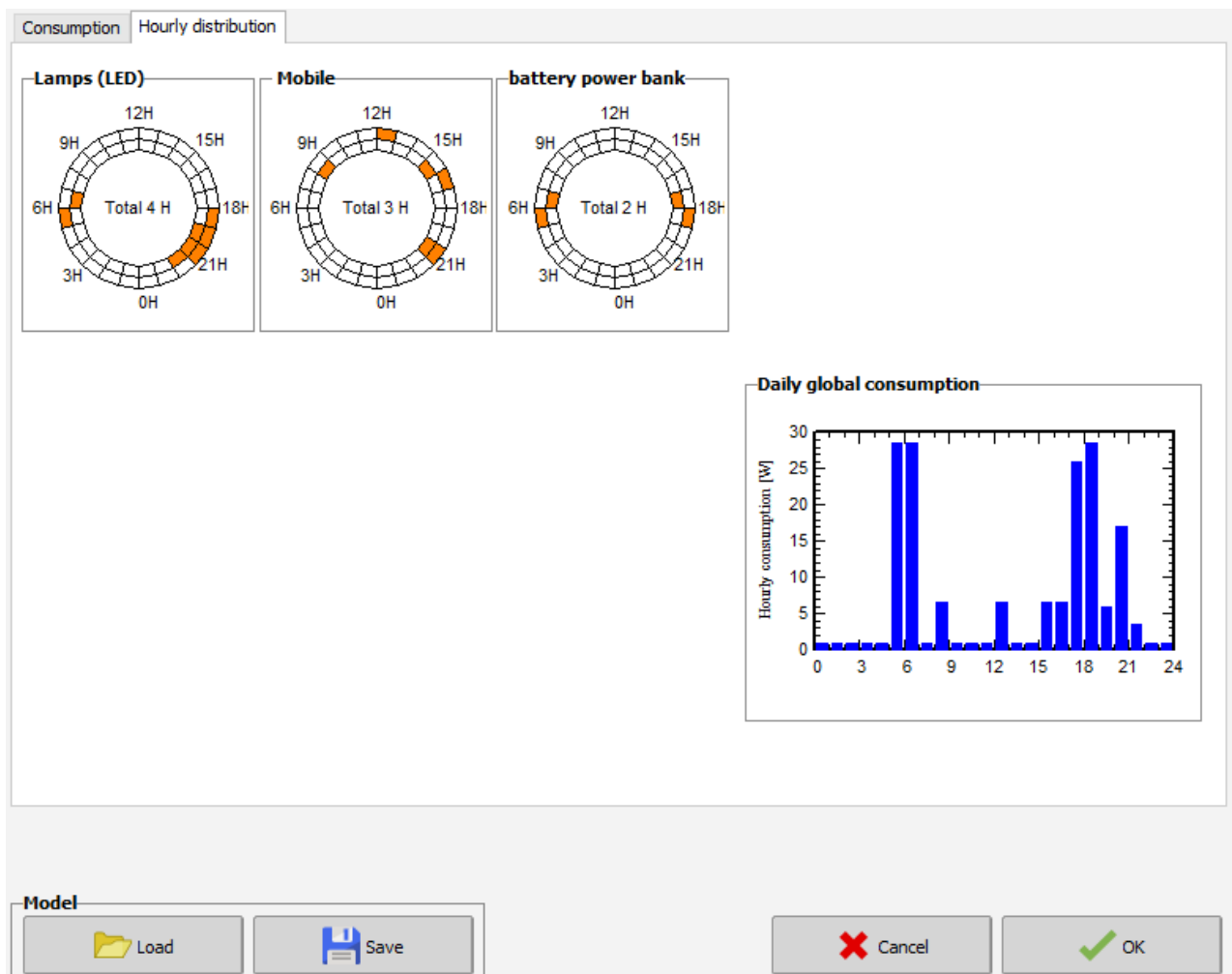


Figure 4.3 Hourly distribution and hourly consumption graph.

As mentioned, the simulation was conducted for both standalone and grid-tied systems. Simulation information is provided. Under standalone and grid-tied PV systems, the input data for each system was similar. The initial stage commenced with the preliminary design for both standalone and grid-tied systems, where the meteorological data was installed for CPUT Bellville South, SA.

b) Preliminary Design for a standalone PV system

The preliminary design is conducted to guide the design phase, laying a foundation for the early-stage design and, where required, resource scheduling and cost estimates.

The meteorological data referred to as the meteo file was employed for CPUT, Bellville Campus, using MN81_SYN MET. This PVSYS meteo file is associated with the corresponding project's geographical sites and determines the required hourly data. The Meteo file may contain geographical coordinates, including longitude, latitude, altitude, Global Horizontal Irradiation (GHI), and ambient temperature for the project location.

The preliminary design simulated results for the off-grid system yielded a nominal power of 77Wp, with a battery capacity of 12V 69Ah, autonomised for 4 days with 5% Loss of Load (LOL), indicating the module's rate of reliability.

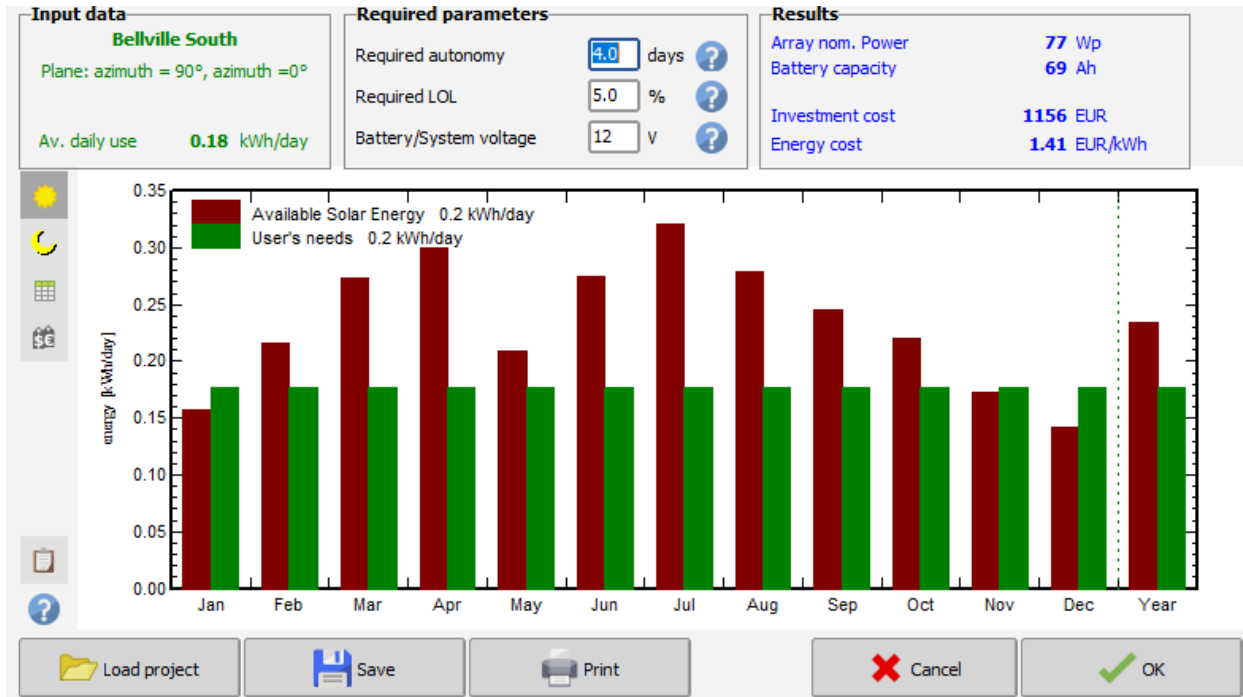


Figure 4.4 Preliminary design results

c) Standalone PV system flow chart diagram

PVSyst was used to simulate PV systems for large and small-scale projects, and it provides a detailed report on the system and assesses the PV system's performance. Figure 4.5 shows a PVSyst flow chart diagram. The simulated standalone system serves as backup power to the grid-tied system, in the event of a grid outage, the standalone system will provide power.

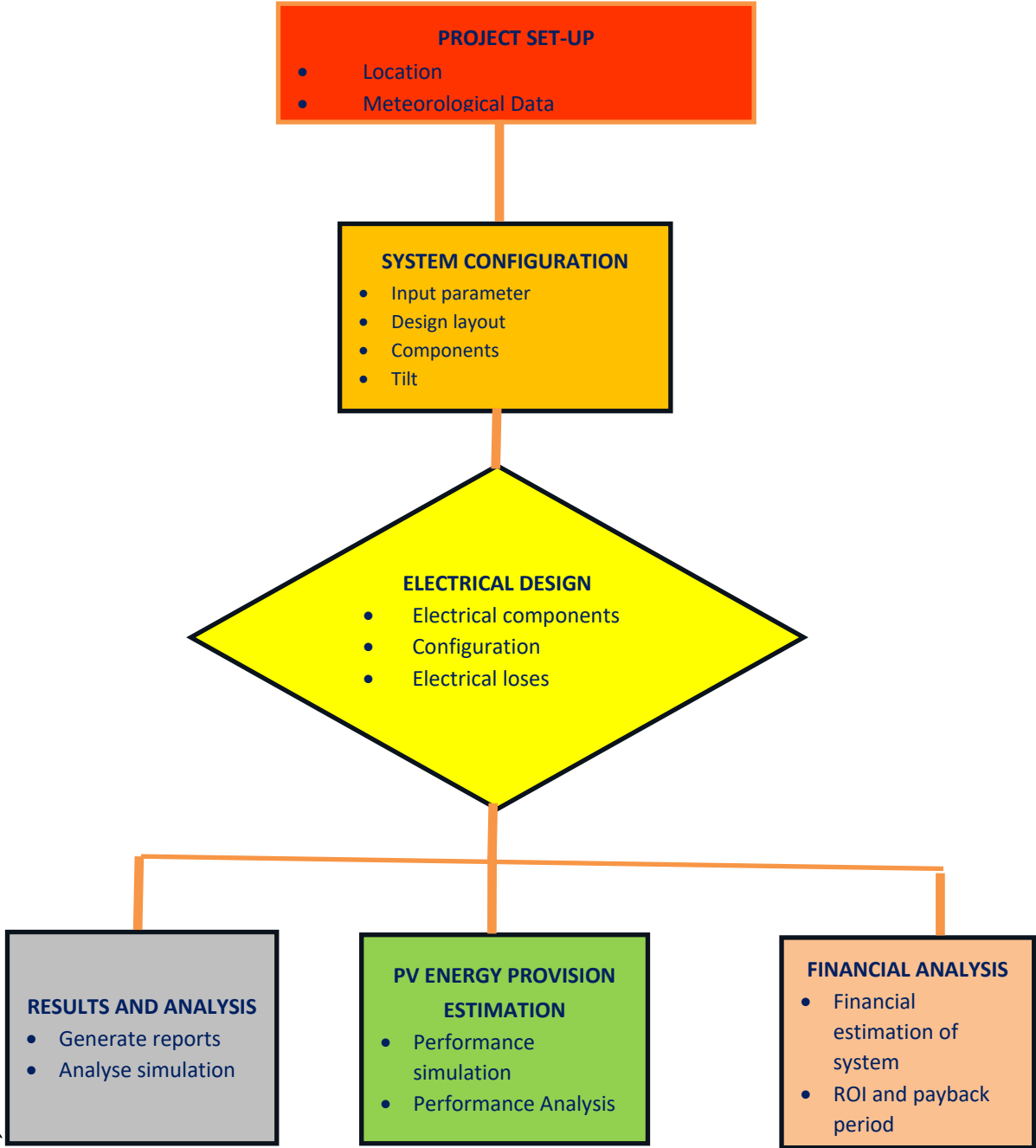


Figure 4.5 Flow chart diagram illustrating a typical PVSyst simulation process flow

PVSyst assists the designer with design results required for each project by optimising the PV design performance analysis, providing energy yield estimations, and offering financial evaluation documentation of PV system projects, and it also calculates carbon offsets or carbon emission reductions (CERs).

d) Detailed pre-sizing

The system pre-sizing contains the Loss of Load Probability (PLOB) as shown in Figure 4.6, which was estimated at 5%, with days of autonomy stipulated at 4 days, the system suggested battery design capacity was estimated at 69Ah, and the battery user voltage was suggested as 12V, while the nominal power was 77Wp and the average daily needs was 200Wh/day.

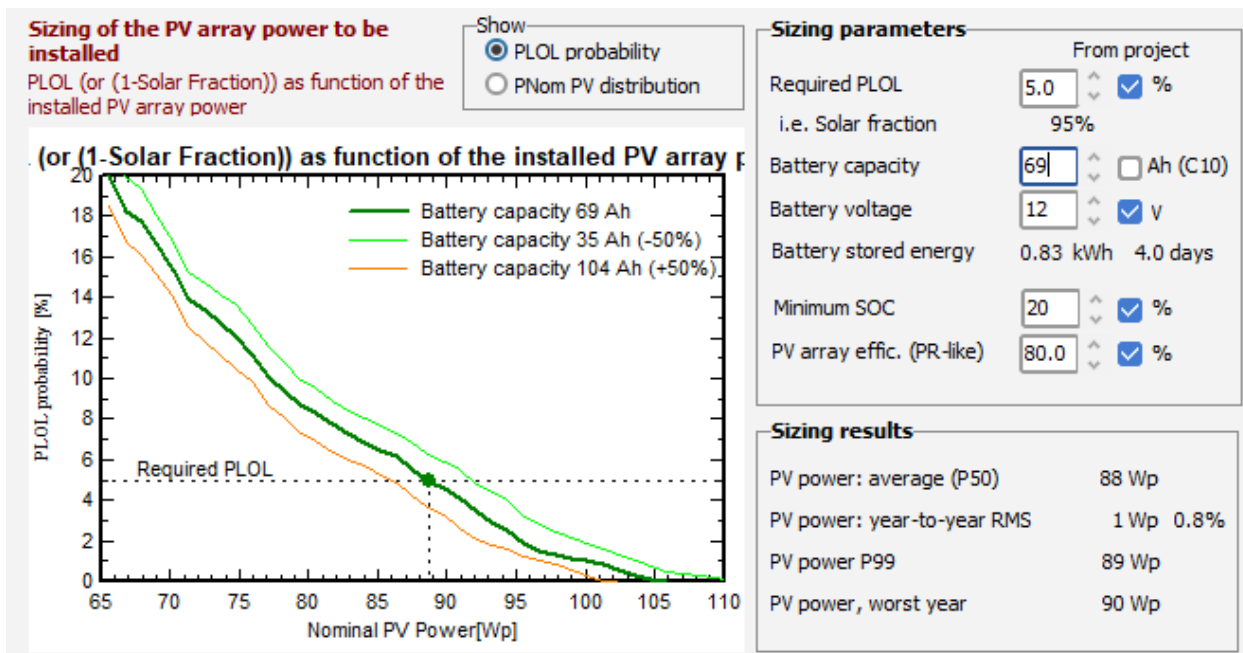


Figure 4.6 Illustration of required PLOL

e) PV System design - Array

The system design included a PV array, controller, storage, and a typical schematic line diagram of a simplified standalone PV system. Despite being designed for an 80Wp polycrystalline (Si-Poly), the preliminary design recommended a module with a nominal power of 76Wp. However, we chose to select an 80Wp 15V module. Choosing this module was more compatible with the MPPT 13V with a maximum charging and discharging current of 7A and 2A, respectively, as shown in Figure 4.7. A battery design with a capacity of 13V 69Ah was determined during the preliminary design. However, during the standalone design, research viewed different battery models where 12.8V 103Ah was selected, as shown in Figure 4.12, a stronger battery design than the recommended 13V 69Ah. The 103Ah battery was able to supply a continuous 1ampere for 103 hours.

PVSyst simulation tool combining both the battery and MPPT to the module design under the generic option indicated that the PV array system is oversized to the user's needs, which promoted high energy losses. When researchers viewed the universal system, which required the nominal pack voltage and the nominal pack capacity as determined during the preliminary design, 13V 69Ah respectively, the system continuously regarded the PV array as strongly oversized. Hence, the research opted for the 12.8V 103Ah, where a 12.8V is considered a LiFePO4 battery. The MPPT controller provided by the design system opted for 1kW 13V with a maximum charging and discharging current of 7A and 2A, respectively. Other options are that the controller power was strongly oversized, the controller output voltage did not match the battery pack voltage, or the MPPT array Voc at -10°C is greater than the maximum input voltage. Coupled with the PV array and the MPPT is battery storage. The battery pack was compatible with the PV operating voltage. Where PV is oversized, regarding user energy needs, the system will lose unused energy. Also, the controller output voltage matched the battery voltage. Thus, the increase in power size.

Av. daily needs
 Enter accepted PLOL: 5.0 %
 Requested autonomy: 4.0 day(s)
 Battery (user) voltage: 13 V
 Suggested capacity: 65 Ah
 Suggested PV power: 89.1 Wp (nom.)

Storage | PV Array | Back-Up | Simplified sketch

Sub-array name and Orientation
 Name: PV Array
 Orient.: Fixed Tilted Plane
 Tilt: 90°
 Azimuth: 0°

Pre-sizing Help
 No sizing
 Enter planned power: 0.1 kWp
 ... or available area: 0 m²

Select the PV module
 Available Now:
 Sort modules: Power Technology
 _Generic | 80 Wp 15V Si-poly Poly 80 Wp 36 cells Since 2021
 Sizing voltages: Vmpp (60°C) 15.8 V, Voc (-10°C) 25.0 V

Select the control mode and the controller
 Universal controller
 MPPT power converter
 Operating mode: Direct coupling, MPPT converter, DC-DC converter
 Max. Charging - Discharging current: MPPT 1000 W 13 V 7 A 2 A
 Universal controller with MPPT conve

PV Array design
Number of modules and strings
 Mod. in series: 1 (should be: No constraint)
 Nb. strings: 1 (should be: between 2 and 2)
 Nb. modules: 1 Area: 1 m²

Operating conditions:
 Vmpp (60°C): 16 V
 Vmpp (20°C): 19 V
 Voc (-10°C): 25 V
 Plane irradiance: 1000 W/m²
 Imp (60°C): 4.4 A
 Isc (60°C): 4.8 A
 Isc (at STC): 4.8 A
 Max. operating power (at max. irrad and 50°C): 73 W
 Array nom. Power (STC): 80 Wp

Figure 4.7 Standalone PV input data

Further information pertaining to the PV array specification were detailed under the selected module, where:

- Basic data*: entail the manufacturer's specifications and the main electrical characteristics.
- Size and technology*: this entails module dimensions and their area, the number of cells and their area, the frame specifics, the maximum average voltage and the bypass protection diode.
- Model parameter*: this includes basic module parameters such as shunt resistance (Rshunt)-series resistance (Rserie), shunt resistance exponential (Rshunt expon) and temperature coefficient (temp. coeff). The parameters define the I/V curve, P/V curve as well as the relative efficiency which passes through Isc, Voc and Mpp as shown in Figure 4.8

The Rshunt default value was based on STC parameters: 0.2 x conductance of MPP given by:

$$V_{mp} / 0.2 (I_{sc} - I_{mp}) \tag{4.1}$$

Where

- V_{mp} = Voltage Maximum Power (V)
- I_{sc} = Short – Circuit Current (A)
- I_{mp} = Current at Maximum Power (A)

For crystalline panels and other technologies, the RShunt value is 4 x Rshunt and 12 X RShunt, respectively. There is some strong interdependency between variables; however, it should be noted that the Rserie value must be less than the maximum value (RSeriesMax), which equals 0.399Ω. Meanwhile, RserieMax depended on RShunt, meaning that to some extent, RserieMax could be increased by increasing RShunt.

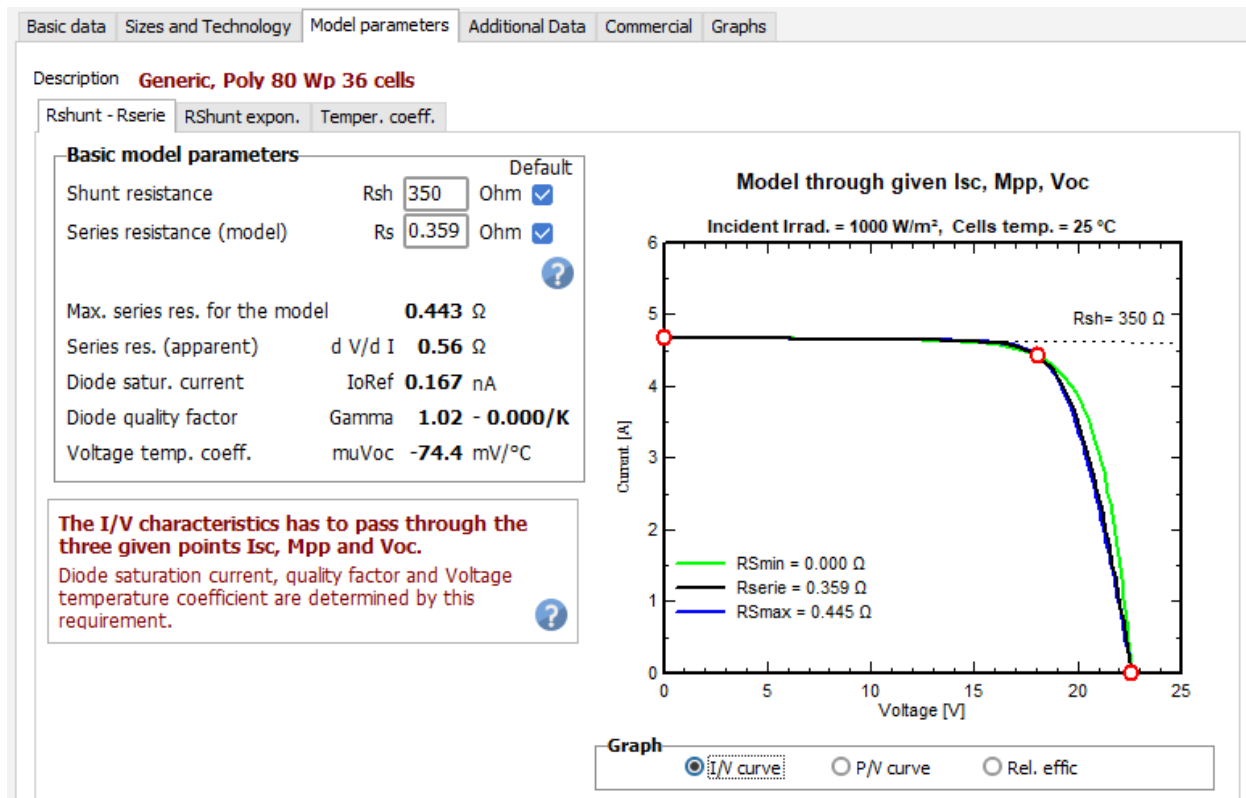


Figure 4.8 Depicts the Isc, Mpp, Voc relationship.

-Additional data: contains additional specifications which include measured lowlight data, measured I/V curve, customised IAM, secondary parameters and degradation, which in summary contain efficiencies, measured I/V points which were obtained from the field study, incident angle modifier, specific losses or gains of crystalline Si-panels, absorption coefficient for temperature, and degradation of PV modules.

Figure 4.9 depicts the relationship for I / V cure for various irradiance relationships ranging between 200W/m² to 1000W/m², while Figure 4.10 illustrates the efficiency vs irradiance relationship, which also ranges between 200W/m² to 1000W/m².

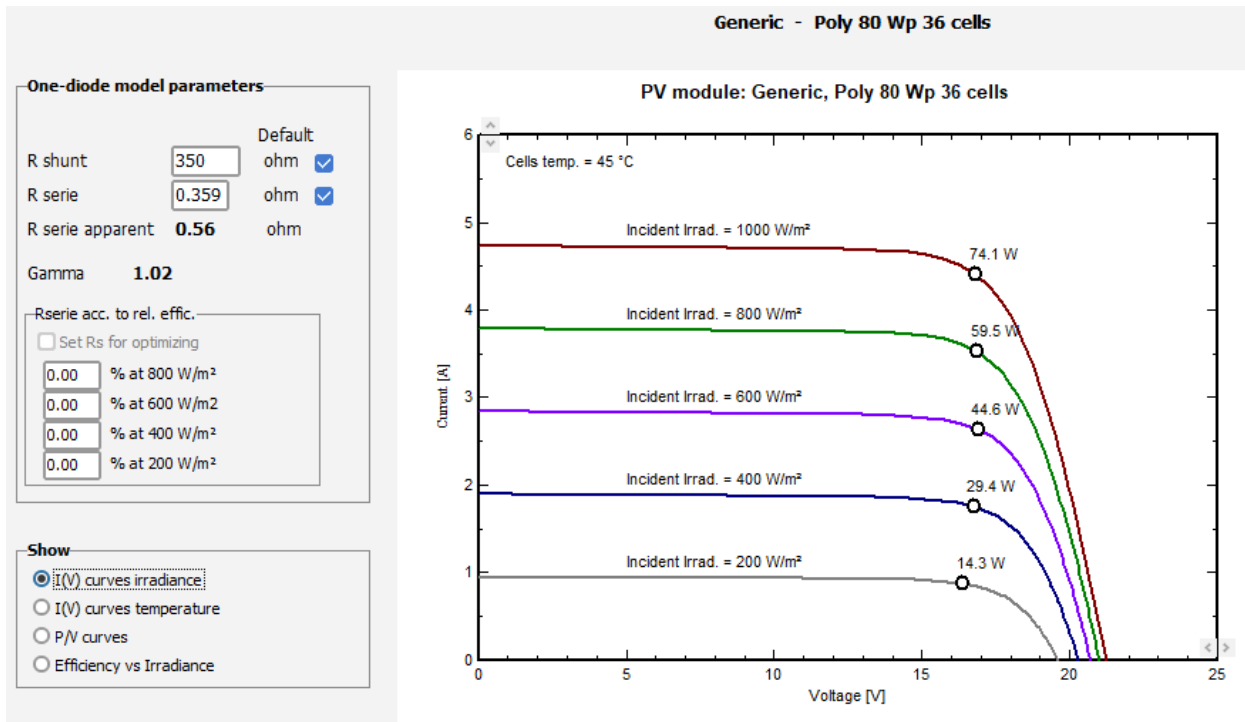


Figure 4.9 I/V curve irradiance relationship

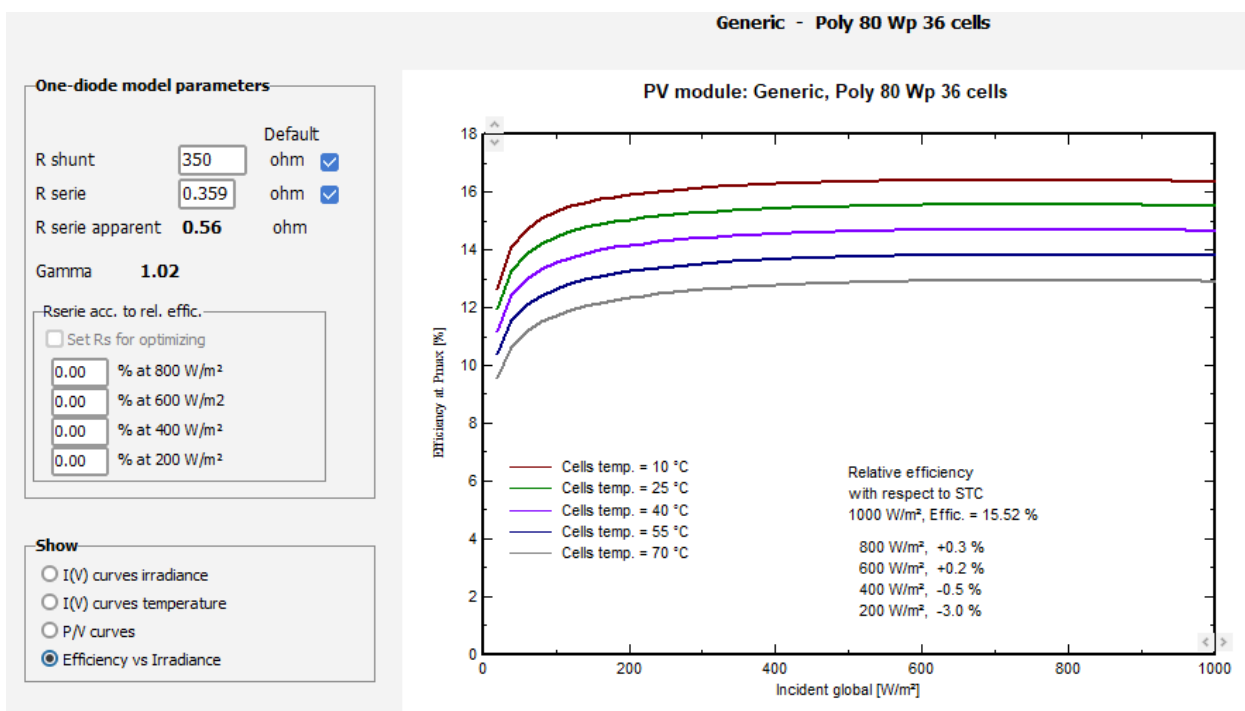


Figure 4.10 Efficiency vs irradiance relationship

f) PV System Design - Controller

The main function of the controller is to protect the battery. It has charge and discharge functions that allow for the disconnection or reconnection of PV when the battery is full, and disconnect or reconnect the load when it is empty. Section 4.2.1 e and Figure 4.7, provide design information about the selected universal charge controller under generic mode. The controller charge or discharge parameters include:

General data, thresholds, MPPT converter, efficiency profile and other data. These parameters specify the manufacturer data, the technology used, and the electrical characteristics such as maximum charging and discharging current, the system's battery pack, the control mode, external control, and the battery control. Define PV input (charging threshold), loading command (discharging threshold) and backup genset command (recharge threshold). Set MPPT operating conditions optimise solar conversion efficiency while cultivating its performance and graphically present the efficiency of the system as shown in Figure 4.10 obtained through

$$\eta = \frac{P_{out}}{P_{in}} \times 100 \tag{4.2}$$

Where :

P_{out} = Power output (W)

P_{in} = Power input (W)

η = efficiency (%)

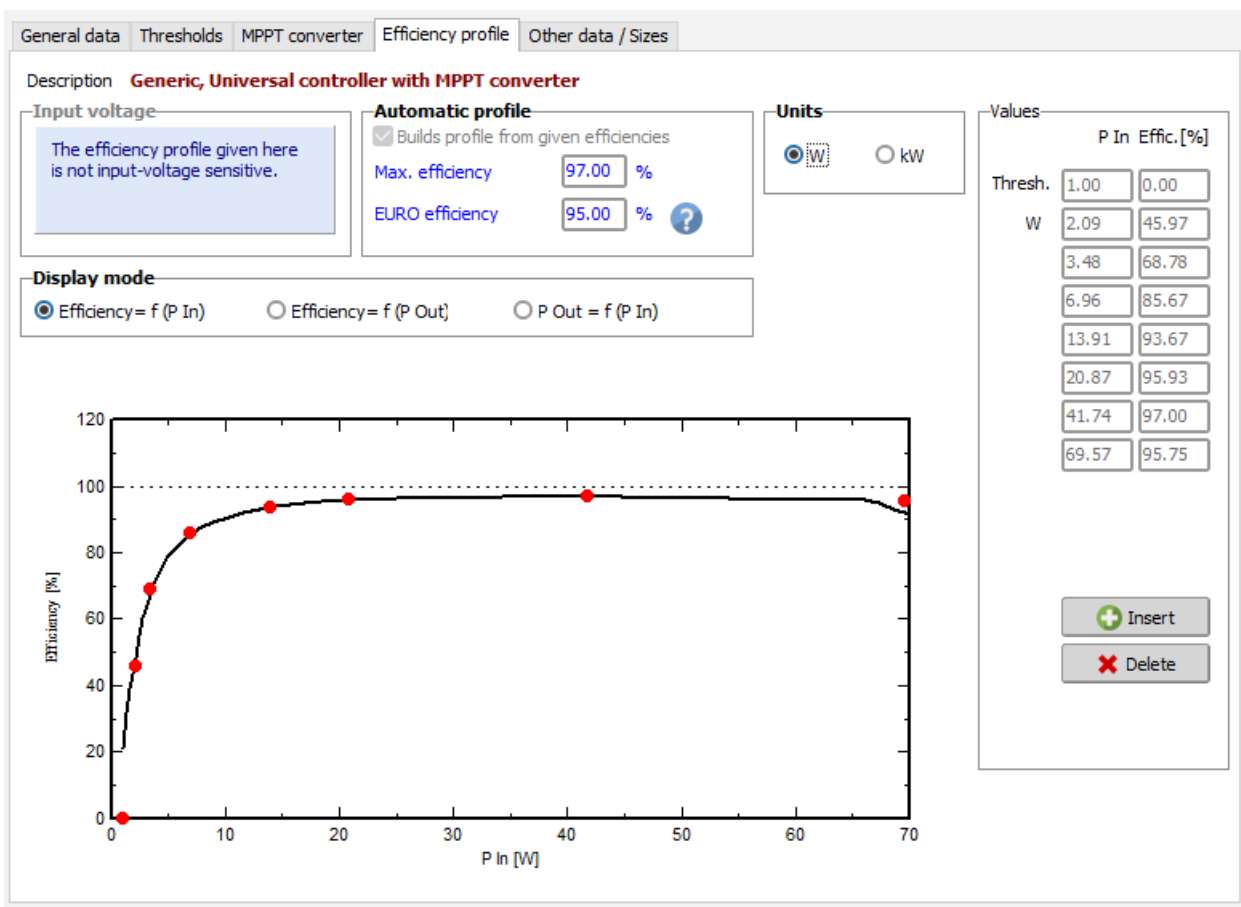


Figure 4.11 Graphical presentation of the systems efficiency profile

g) PV system design - Battery

The battery system served as backup power and entailed basic data, detailed model parameters, graphs, sizes, and technology. The basic parameters include the number of cells, nominal battery voltage, cell capacity, coulombic efficiency, internal resistance at reference temperature, reference temperature, behaviour limits such as maximum charge or discharge voltage, charge or discharge cut-off voltage, minimum charging or discharging temperature, full battery indicators and information renormalisation to C10.

It must be noted that the detailed model parameters are assessed per element, which provides individual characteristics of each component, or whole battery, which collectively characterises all connected components as one unit. Understanding both systems is important during design, selection and battery utilisation for various applications.

The screenshot shows a software interface for battery design. At the top, there are input fields for 'Av. daily needs' (0.2 kWh/day), 'Enter accepted PLOL' (5.0%), 'Requested autonomy' (4.0 days), 'Battery (user) voltage' (13 V), 'Suggested capacity' (65 Ah), and 'Suggested PV power' (89.1 Wp (nom.)). A 'Detailed pre-sizing' button is located below these inputs. Below the button are tabs for 'Storage', 'PV Array', 'Back-Up', and 'Simplified sketch'. The 'Procedure' section lists four steps: 1. - Pre-sizing (Define the desired Pre-sizing conditions), 2. - Storage (Define the battery pack), 3. - PV Array design (Design the PV array and the control mode), and 4. - Back-Up (Define an eventual Genset). The 'Specify the Battery set' section includes a 'Sort batteries by' dropdown (voltage selected), a search bar, and a table of battery specifications. The table shows a 'Lithium-ion' battery with a pack voltage of 13 V, global capacity of 103 Ah, stored energy of 1.2 kWh, total weight of 14 kg, 800 cycles at 80% DOD, and a total stored energy of 856 kWh during battery life. The 'Operating battery temperature' section shows a 'Temper. mode' of 'Fixed (air-conditioned)' and a 'Fixed temperature' of 20 °C. A note states: 'The battery temperature is important for the aging of the battery.'

Figure 4.12 Storage design information

The detailed model parameters focus on the V_{oc} behaviour, the capacity, the lifetime, and the end of charge: resistance increase, which details the internal resistance vs state of charge, internal resistance temperature factor, and self-discharge. Without dwelling too much into detail, these parameters assist with battery management, design and monitoring, and battery optimisation. The formula employed for battery design is:

$$\text{Battery capacity (Ah)} = \frac{\text{Whrs /day}}{(0.85 \times 0.6 \times \text{nominal battery voltage})} \times \text{Days of autonomy} \quad (4.3)$$

Capacity discharge depends on the discharge rate defined by the time (hrs) taken to full discharge. For a lead acid battery with a discharge in 10hrs expressed or specified as C10 depending on each battery capacity. Meanwhile, capacity is rarely defined for lithium-ion (li-Ion) owing to lower capacity dependency. Hence, the Peukert co-efficient of 1.02, a parametrised parameter for li-Ion, is used in PVSyst.

Graphs provide a comparison for the following parameters: a) Charge/Discharge vs SOC, b) Charge voltage vs SOC Ah c) Discharge voltage vs DOD Ah d) Charge voltage vs time and e) Discharge voltage vs time in both whole battery and per element. The detailed graphs are found in Figures A42 – A46. Size and technology provided specific dimensions such as depth, width, height and weight in kg for the LiFePO4 battery.

h) Stand-alone Simulation results

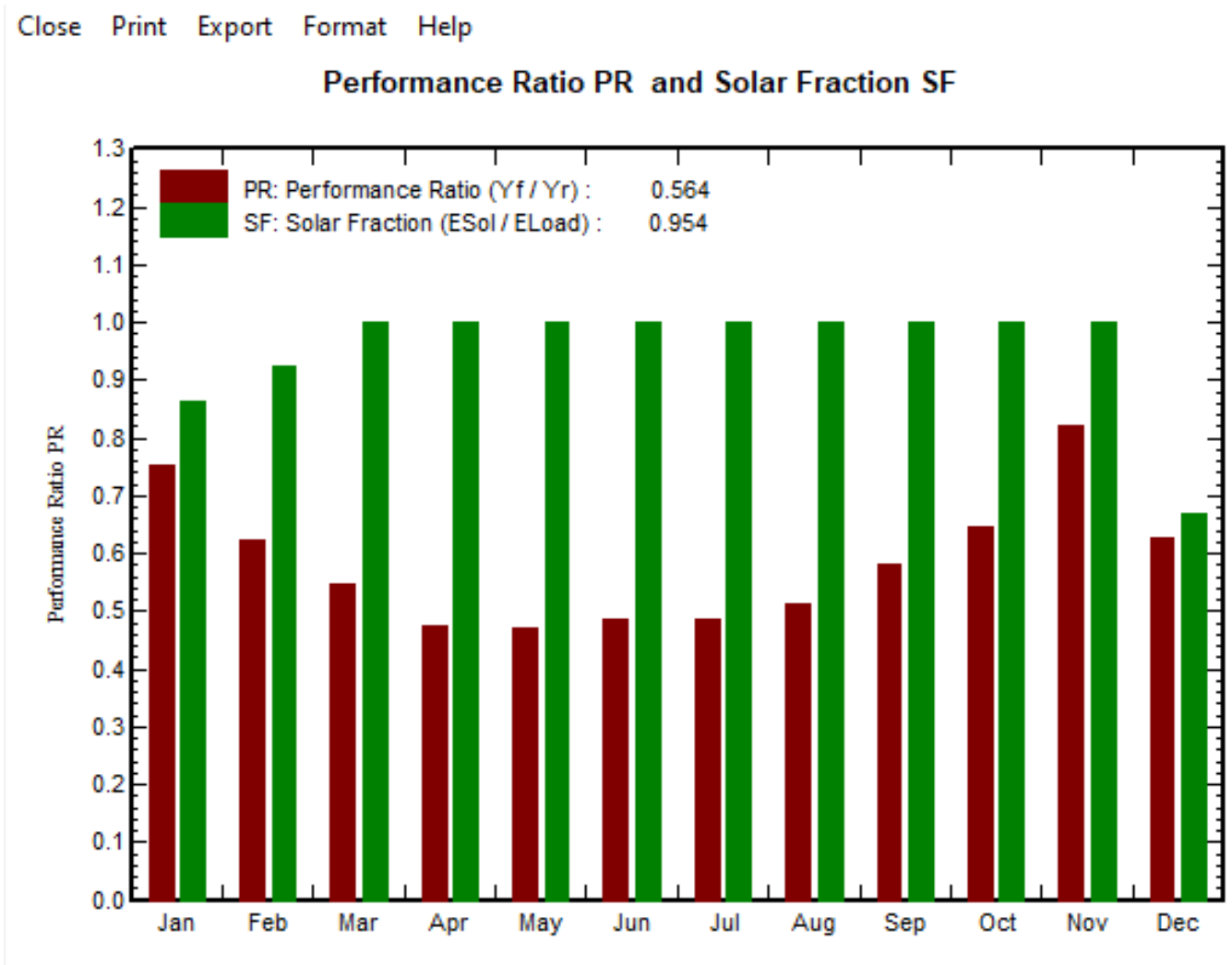


Figure 4.13 Solar performance ratio and solar Fraction

Close Print Export Format Help

Normalized Production and Loss Factors: Nominal power 80 Wp

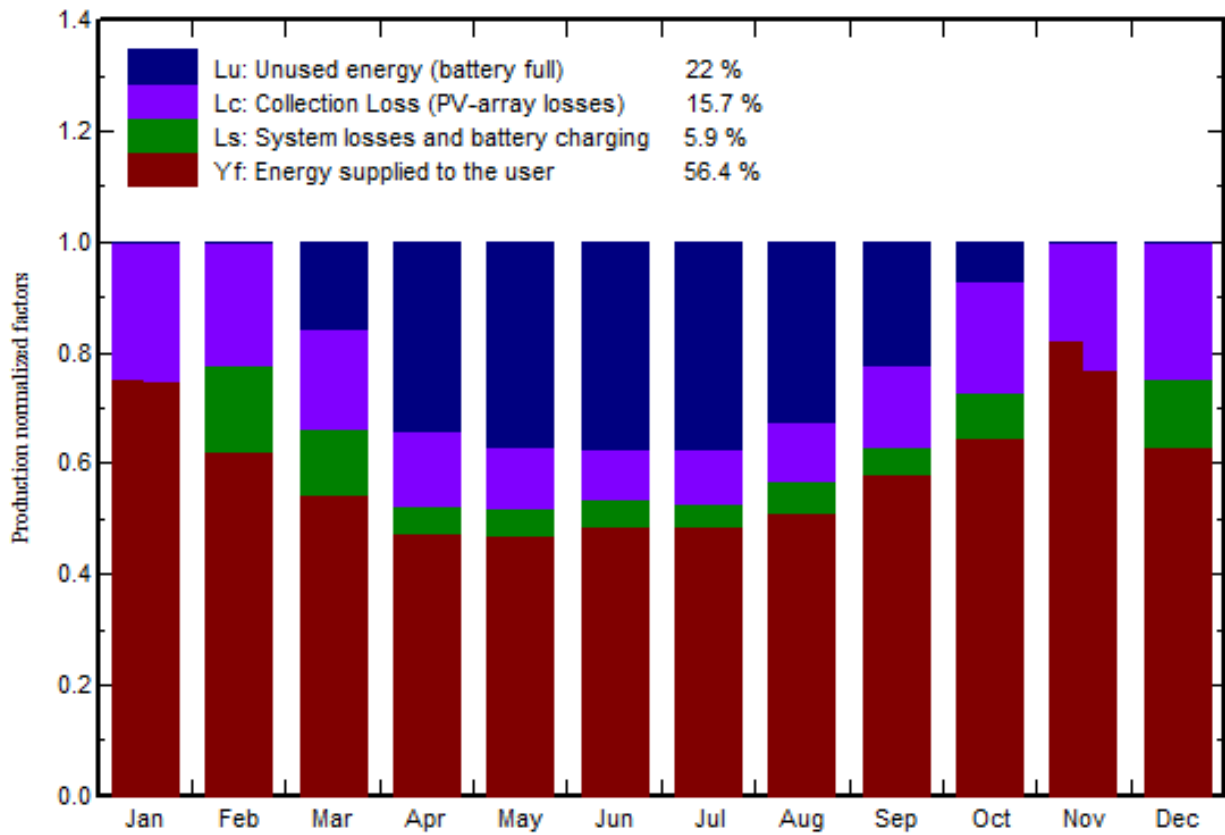


Figure 4.14 Normalised production and loss factor

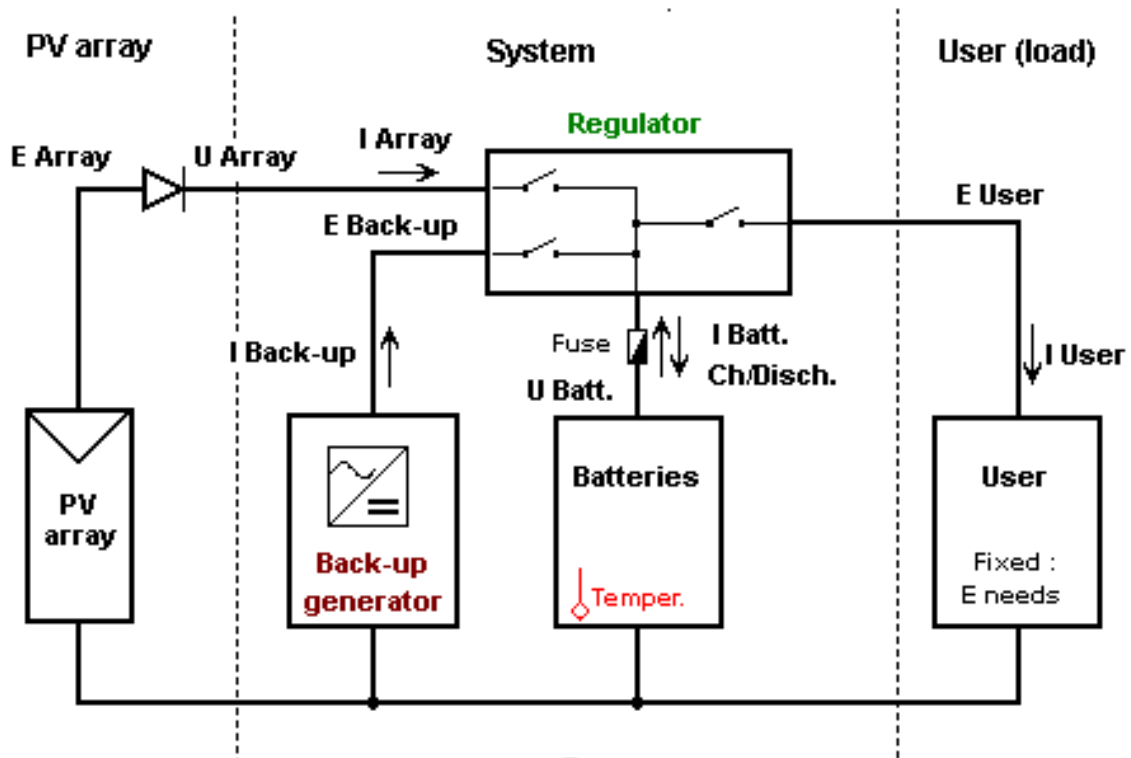


Figure 4.15 Typical layout of a standalone PV system.

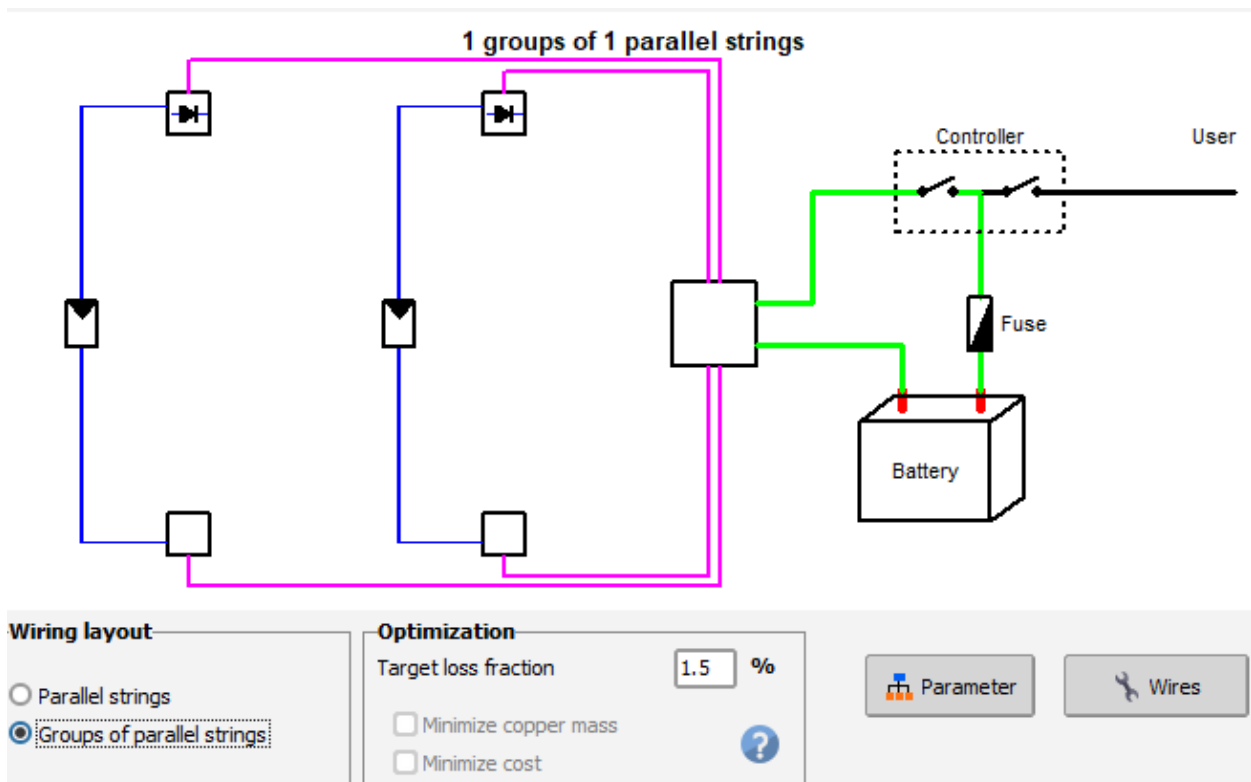


Figure 4.16 Detailed ohmic loss diagram.

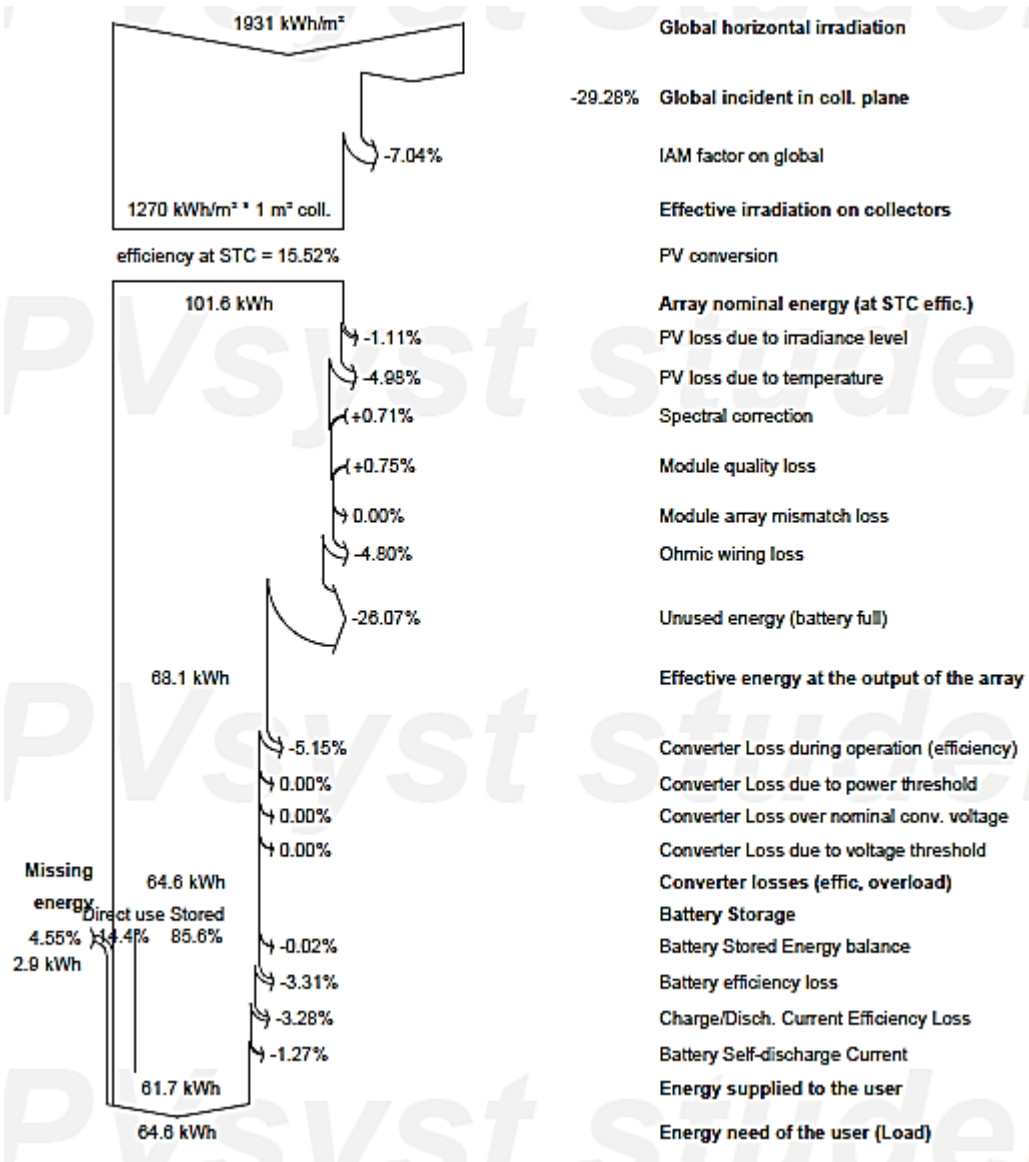


Figure 4.17 Energy loss diagram

Grid-tied system

The grid-tied system allows energy generated from renewable resources to be connected to the grid, where when RE resources are depleted, the grid becomes the energy source for the end-user.

The same orientation parameters used for the standalone system were applied to the grid-tied system. They provided the incident and typical meteorological data, which are the same as tabulated in Table 4.4. In contrast, Table 4.5 provides the same meteo data for CPUT Bellville South, demonstrating the typical meteorological year.

Table 4.5 Meteo data for Bellville South indicating the typical meteorological year (TMY) for plane tilt=90°, azimuth=0°, Albedo=0.2

Interval beginning	GlobaHor kWh/m2/mth	DiffHor kWh/m2/mth	Globinc (Perez model) kWh/m2/mth	RelHum ratio
January	262.1	56.36	81.2	0.647
February	218.2	41.95	98.2	0.626
March	188.1	43.49	135.9	0.661
April	129.6	38.02	142.0	0.669
May	73.7	31.87	99.1	0.804
June	76.1	25.2	128.9	0.805
July	96.1	27.31	155.5	0.780
August	110.6	38.48	134.5	0.793
September	135.8	50.89	112.4	0.762
October	195.3	60.24	108.7	0.741
November	233.5	63.19	82.5	0.629
December	246.2	71.01	72.2	0.691
Year	1965.1	548.02	1351.2	0.721

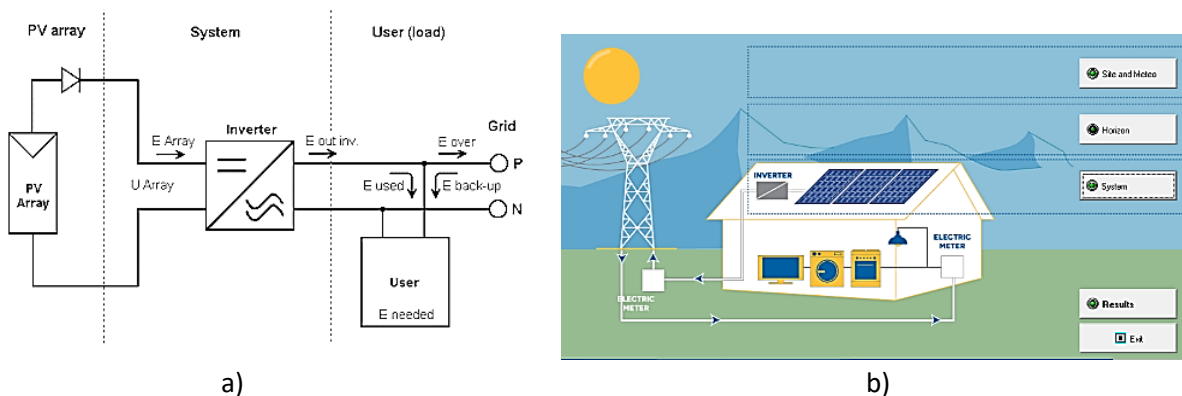


Figure 4.18 a) Typical layout of a grid-tied system b) Grid-tied system configuration

a) Preliminary design for a Grid-tied system

As mentioned, the preliminary design was conducted to guide the design phase, laying a foundation for the early-stage design and where required resource scheduling and cost estimates are required.

The same input data referred to as meteorological data, horizon, and system is used for both standalone and grid-tied systems, yielding the same results as shown in 4.2.1 a). However, the grid-tied system explores further and provides more specified options for module type, mounting position, technology type as well as ventilation property, where for this research, the following options were chosen

Mounting type – standard

Mounting disposition – façade

Technology type - polycrystalline

Ventilation – fully insulated. These options applied to this research and were aligned with the research aims and objectives.

The preliminary design simulated results for a grid-tied system yielding a nominal power of 114kWh per annum, as shown in Figures 4.21

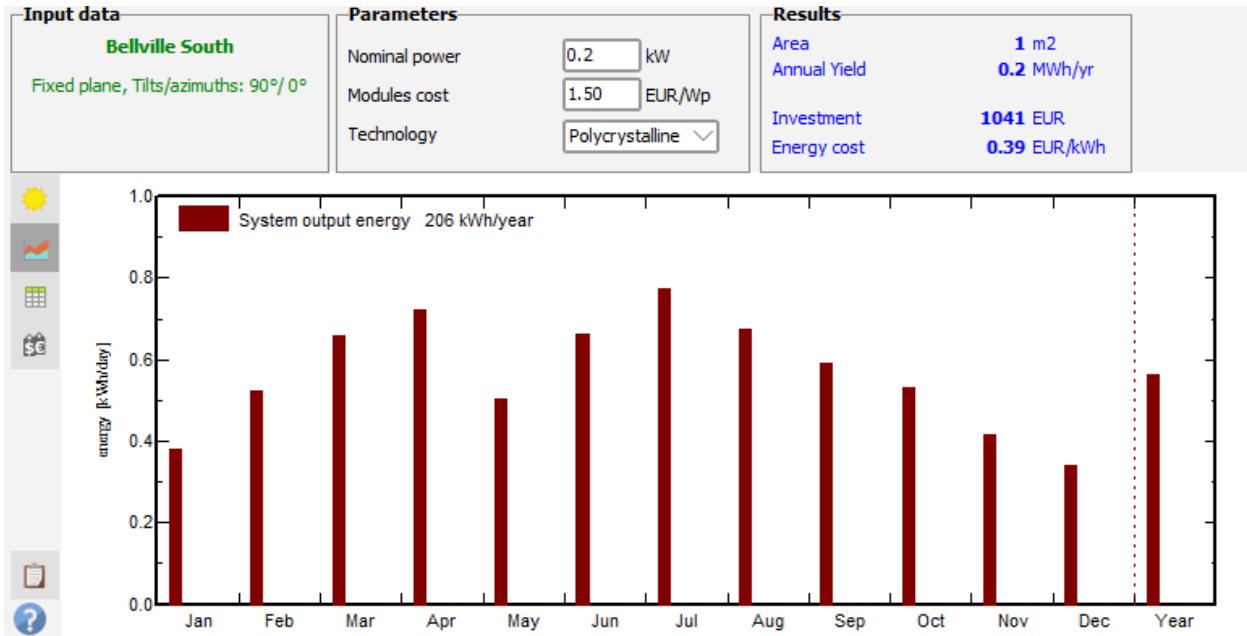


Figure 4.19 Graphical annual energy output

The estimated twelve-monthly energy generated was added together to give a total estimation of 206kWh annual energy generated by the system when the nominal power of the 250W system was utilised as available energy.

b) Grid tied system - PV design.

The grid-tied system was composed of a PV array, an inverter, and a typical schematic line diagram of a simplified grid-tied PV system. During the preliminary design, the nominal power was determined to be 200Wp. A 250Wp PV array system with a 0.25kW 22–55V TL BDM300 inverter was predetermined during the design, and this combination was more compatible with an array of 250Wp. It should be noted that the design considers the worst-case scenario.

Sub-array ?

Sub-array name and Orientation

Name:

Orient.: **Fixed Tilted Plane** Tilt: **90°**
Azimuth: **0°**

Pre-sizing Help

No sizing Enter planned power kWp ?

... or available area(modules) m²

Select the PV module

Available Now: Filter:

Approx. needed modules: **0**

 250 Wp 25V Si-poly Poly 250 Wp 60 cells Since 2015 Typical

Use optimizer

Sizing voltages : Vmpp (60°C) **26.3 V**
Voc (-10°C) **41.7 V**

Select the inverter

Available Now: Output voltage: 240 V Mono 50Hz

 0,25 kW 22 - 55 V 50/60Hz BDM-300 Since 2016

Nb. of inverters: Operating voltage: **22-55 V** Global Inverter's power **0.3 kWac**

Input maximum voltage: **60 V**

50 Hz
 60 Hz

Design the array

Number of modules and strings

Mod. in series: only possibility 1 ?

Nb. strings: between 1 and 2

Overload loss: **0.0 %** ?

Pnom ratio: **1.00**

Nb. modules **1** **Area** **2 m²**

Operating conditions

Vmpp (60°C) 26 V
Vmpp (20°C) 31 V
Voc (-10°C) 42 V

Plane irradiance: **1000 W/m²**

Imp (STC) 8.3 A
Isc (STC) 8.6 A
Isc (at STC) 8.6 A

Max. in data STC

Max. operating power
(at 826 W/m² and 50°C) **0.2 kW**

Array nom. Power (STC) 0.3 kWp

Figure 4.20 Grid tied system input data

Detailed PV design system prompted for the following parameters, which are similar to that of a standalone PV system detailed as:

- Basic data – Provided manufacturers specifications, pertinent measurements, and other main parameters such as RShunt, Rserie model with other model parameters.
- Size and technology - Provided module dimensions including the weight, the number of cells in series and in parallel, the maximum current voltage, maximum voltage, and bypass protection diodes if applicable.
- Model parameter - these included basic module parameters such as shunt resistance (Rshunt)-series resistance (Rserie), shunt resistance exponential (Rshunt expon) and temperature coefficient (temp. coeff). Rserie is adjusted to acquire the main default condition based on the relative efficiency of -3% at 200W/m².
- Additional data includes:

- *Measure low light data*: determine PV module performance for Rserie and Rshunt in low light conditions.
- Measured I/V Curve: the I / V values were obtained during the field study and were pasted in the corresponding columns.
- Also considered in parameters are the Incident Angle Modifier (IAM), the secondary parameters and degradation.

- Graphs were obtained where curve types were compared against parameters as tabulated in Table 4.6:

Table 4.6 Graphs comparing curve types to curve parameters and both parameters were plotted.

Curve Types	Curve Parameters
- Current vs Voltage (I / V)	- Incident Irradiance
- Power vs Voltage (P / V)	- Temperature
- Efficiency vs Irradiance	- Serie resistance
- Efficiency vs Temperature	- Shunt resistance.

The graphs were compared between curve types and curve parameters, the I/V curve is plotted in Figure 4.21, and the remainder can be found in Figure B14 – Figure B26

Close Print Export Format Help

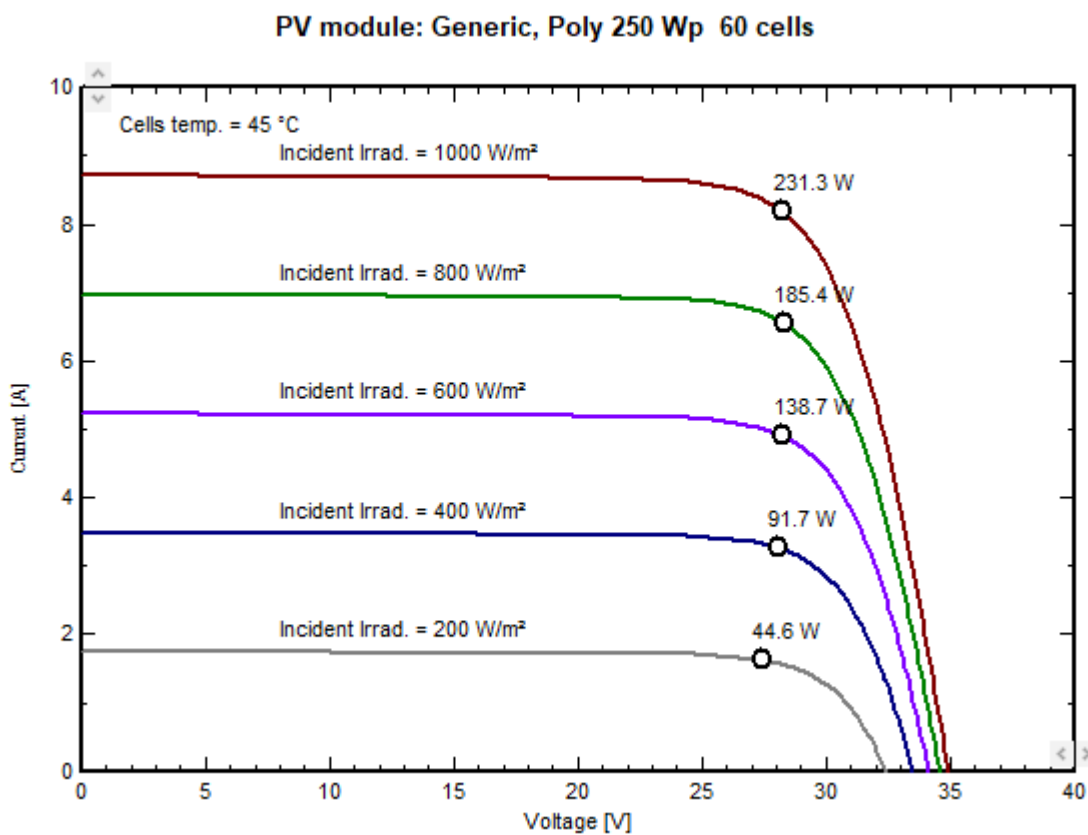


Figure 4.21 I/V curve illustration for a 250Wp Grid tied system

c) Inverter

The main aim of the inverter is to convert DC power to AC power, which is done to change the frequency and voltage of the electricity supply. For this research study, the specified inverter model was a 025kW 22-55V TL BDM 300 Northern Electrical supplier. This model was compatible with the PV system, as detailed in the previous section.

The inverter design was conducted with the use of the following parameters:

Main parameter: The input side (DC PV field) is composed of minimum MPP voltage and maximum MPP voltage of 22 and 55V, respectively, and an absolute maximum MPP of 60V. The frequency was set to 50 and 60Hz, with a Grid voltage of 240V and a nominal AC power of 0.25kVA.

d) Efficiency curve

It is a presentation of a relationship between efficiency and input power (Pin) (W); the output power (pout) was measured along the x-axis while the efficiency was plotted along the y-axis.

The efficiency curve is given by:

$$P_{out} = \eta \times P_{in}$$

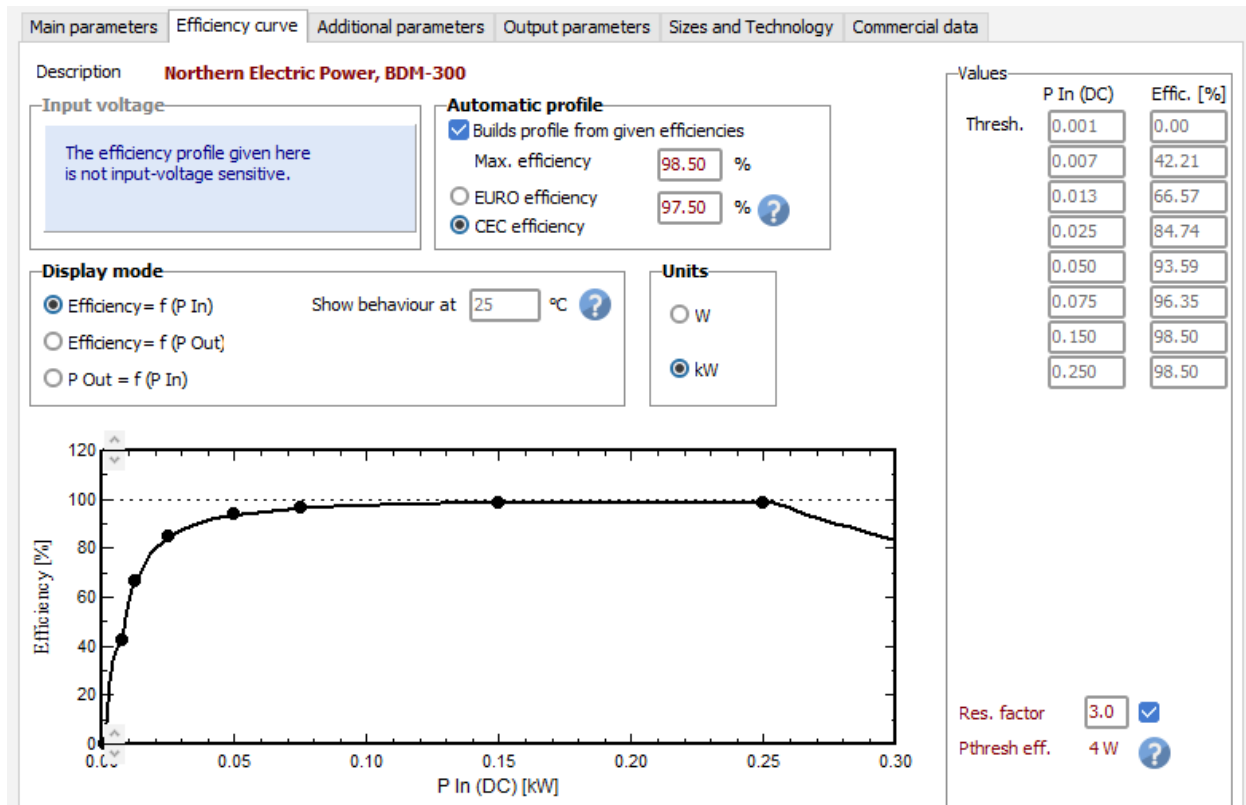


Figure 4.22 illustrates the efficiency curve

e) Additional parameters

More inverter specifics are defined, such as secondary parameters for converting DC to AC for grid-tied connections. The latter is of primary importance and highly impacts safety, performance, and inverter functionality i.e. MPPT, input voltage and current, power factor grid support functions and other features.

f) Inverter output parameters

Typically adhere to and comply with standard electrical specifications and are responsible for safe and efficient PV system operations that the manufacturer normally specifies. For the system's overall performance, the inverter is adequately selected and sized based on the PV's electrical characteristics, and the main characteristics are power factor and maximum AC Power (temperature). Figure 4.23 illustrates an example of an inverter output parameter.

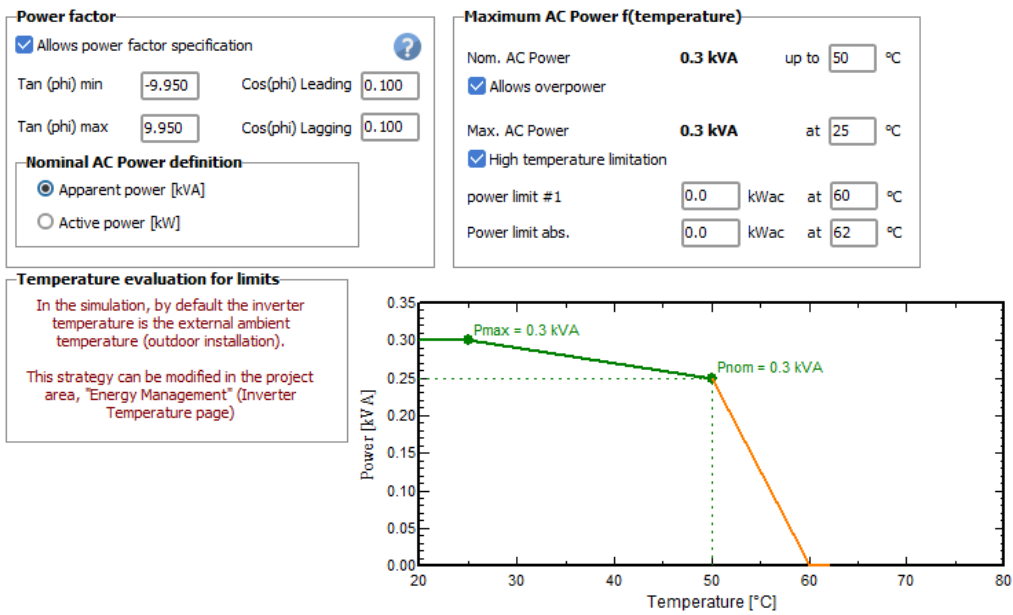


Figure 4.23 Inverter output parameters

g) Size and technology

Provides more specification on the selected technology and its corresponding dimensions, including operating conditions or behaviour limits. The operating conditions or behaviour limits are further employed through behaviour at nominal power, behaviour at minimum or maximum voltage and operating mode.

h) Grid tied system simulation results

The grid-tied system simulation results are presented graphically as follows:

Close Print Export Format Help

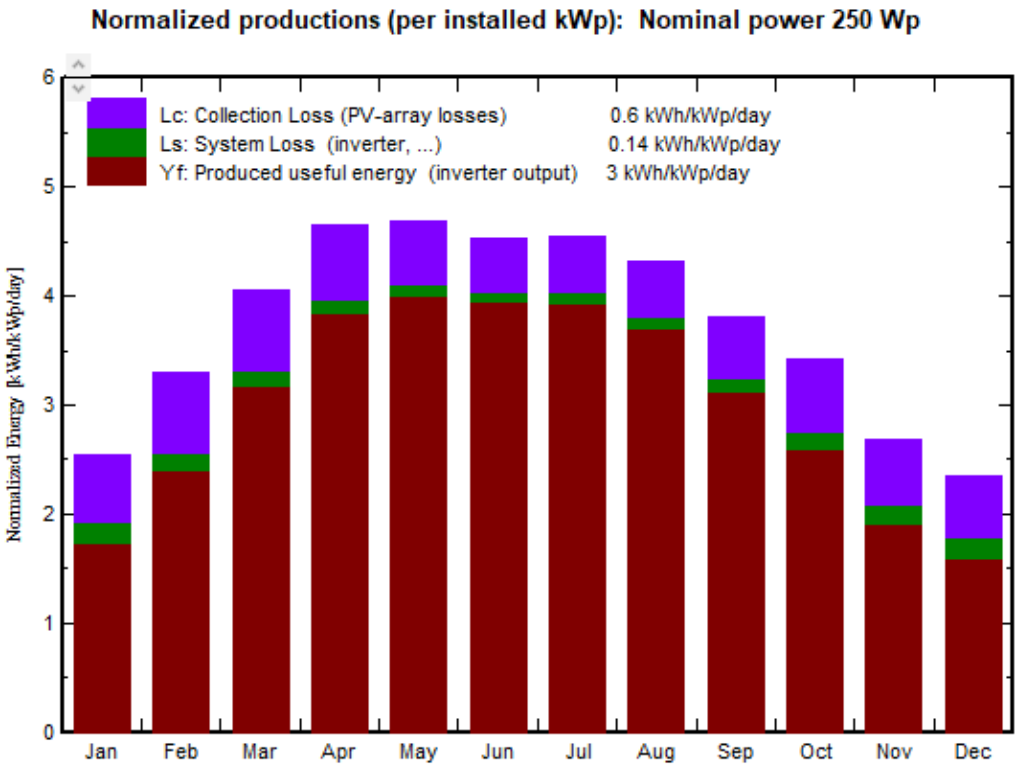


Figure 4.24 Normalized productions per installed 250Wp

Close Print Export Format Help

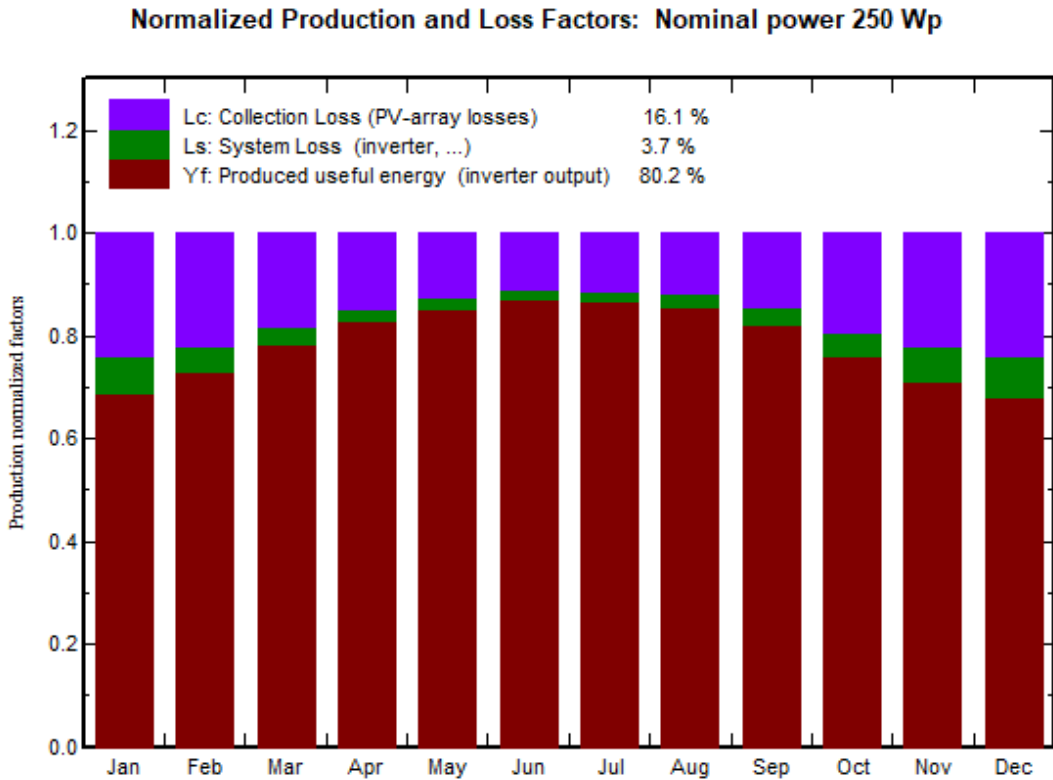


Figure 4.25 Normalized production and loss factors: Np 80Wp

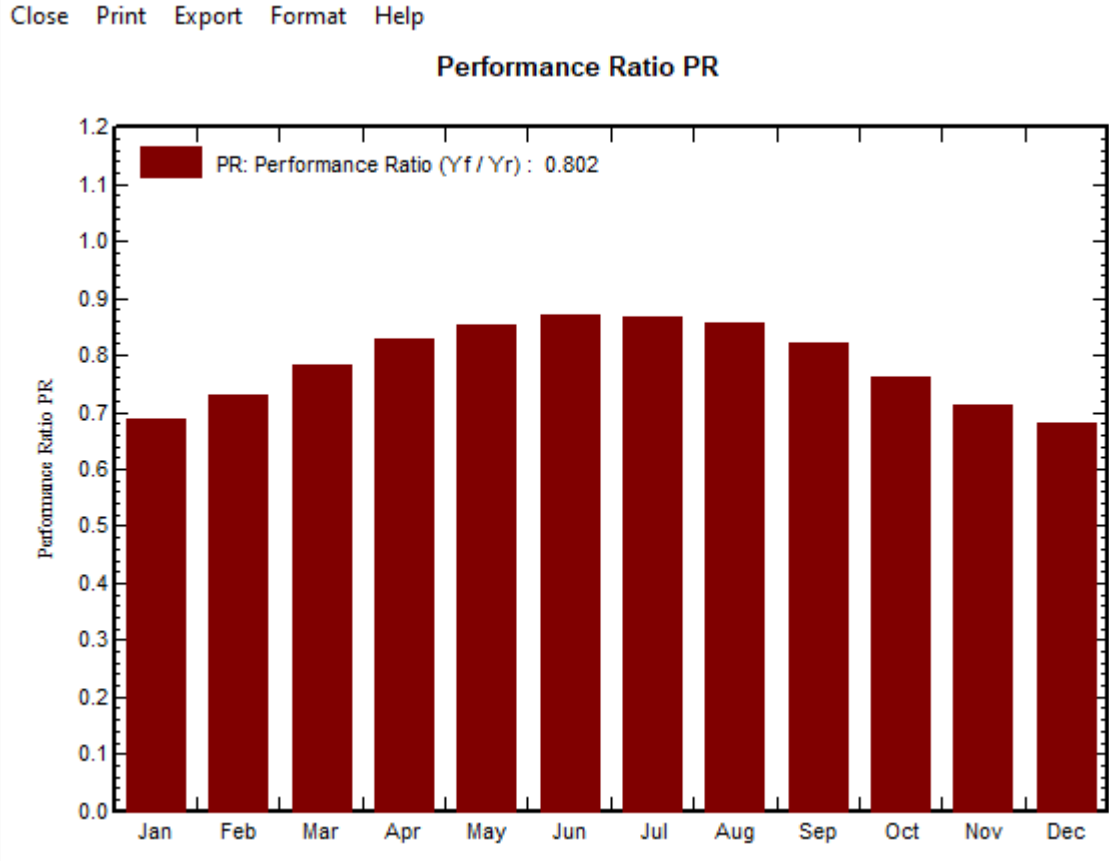


Figure 4.26 Performance ratio

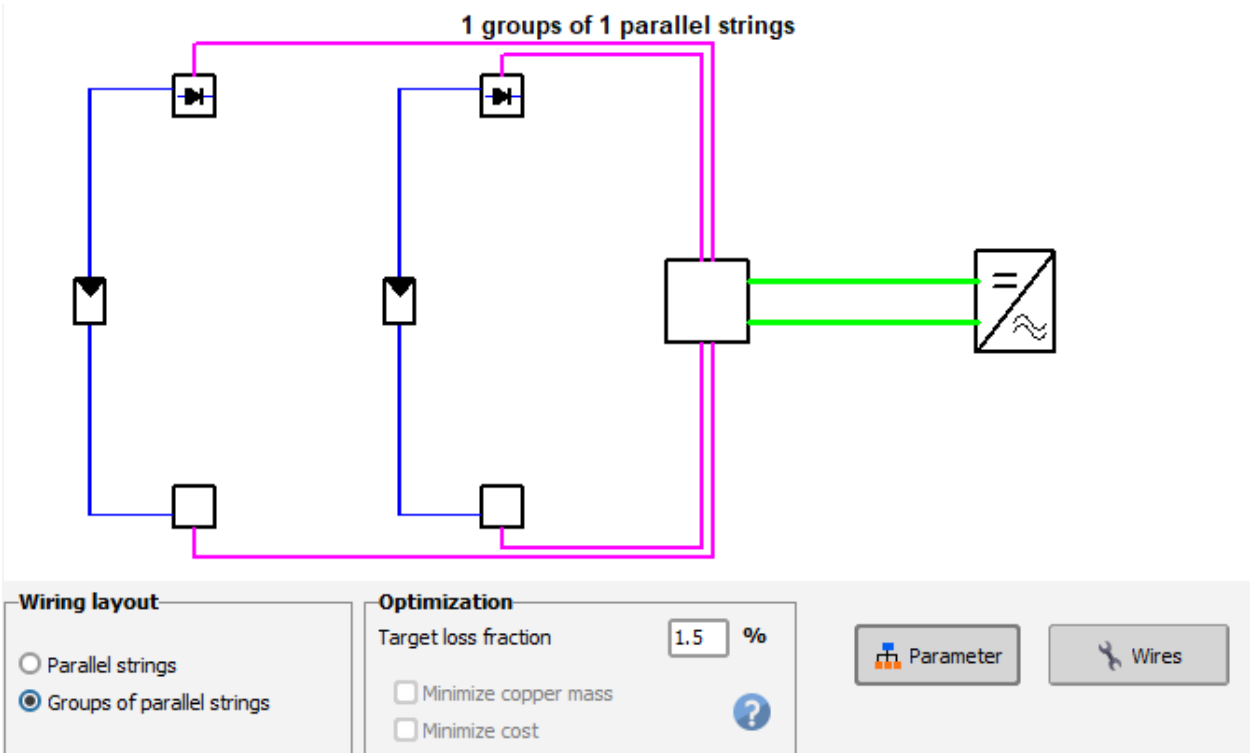


Figure 4.27 Losses in group of parallel strings

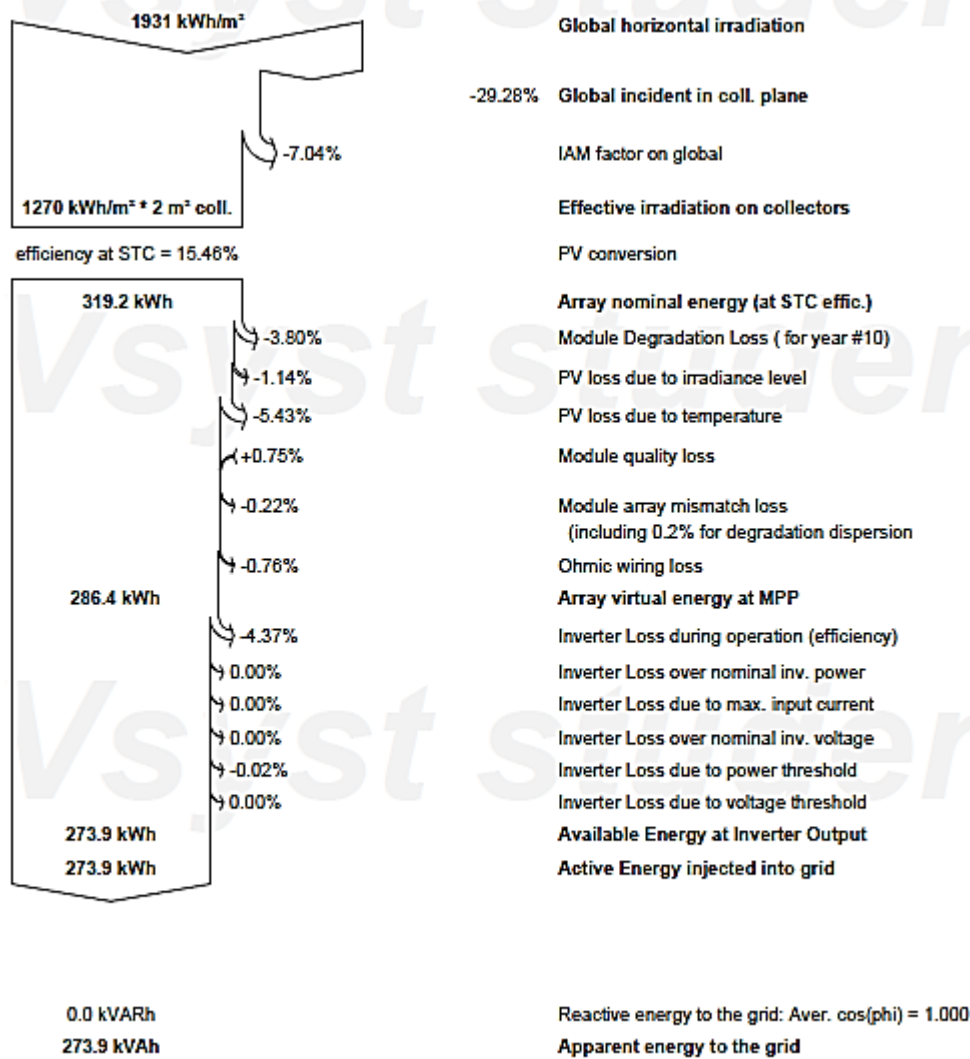


Figure 4.28 Energy loss diagram

4.4 Model

The Computer-Aided Drawing (CAD) 2D and CAD 3D software is software used to draft the concept and prepare the final 3D CAD drawing for 3D printing, used for converting 3D to a stereolithography (STL) 3D printing file. PVSyst is an accurate and flexible software used in the solar energy industry for simulating and analysing PV systems, which provides a theoretical design system that gives the PV output.

Drawings

The drawings are illustrations of work to complete the research prototype. They serve as a guide on the model layout and aid in the design calculations. The research drew the concept for discussion, and the discussed CAD drawing layout indicated what the final prototype would look like, with finer details improved. The research considered various stages in the drafting of the drawings, and this consent for further improvements as more works progressed with the diagrams.

Freehand drawing

In the build-up of the research project, a free hand drawing was prepared as an initial conceptualisation process. The freehand drawing guides the design requirements, assists in the clarification and development of the prototype, and documents any previous, new, and revised work relating to the development of the prototype. Figure 4.29 illustrates the freehand drawing for the prototype.

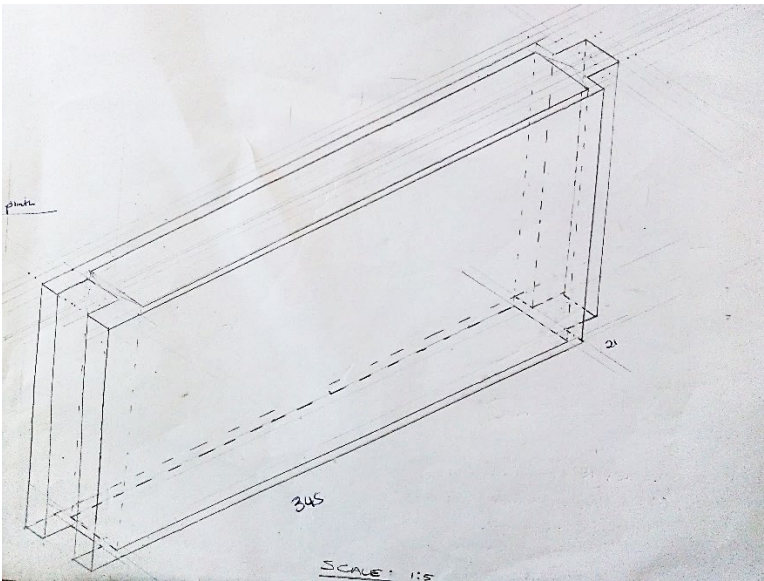


Figure 4.29 Freehand drawing for the revised concept

CAD drawing

The CAD drawing was developed as a final technical document after finalising the freehand drawing technical data. Fig 4.29 illustrates the CAD drawing with dimensions.

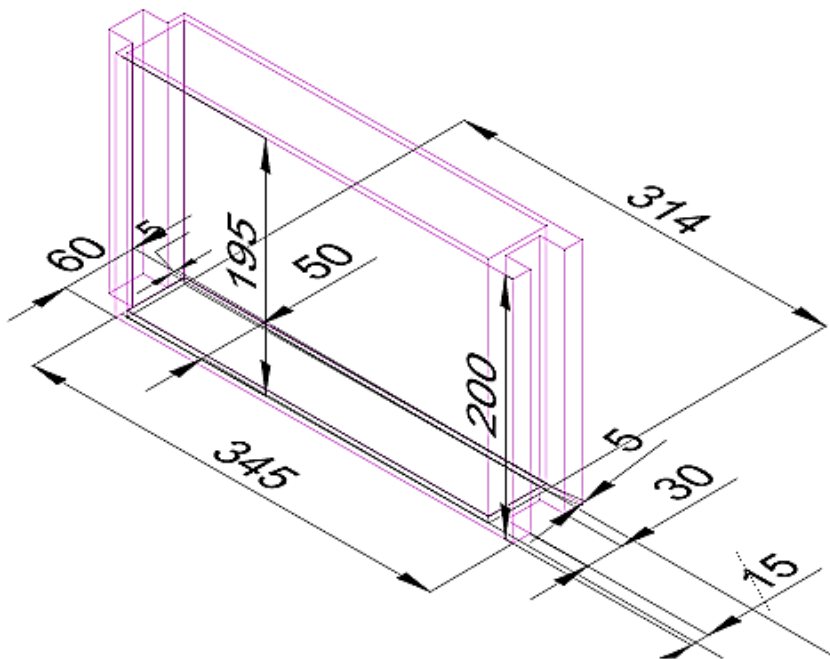


Figure 4.30 Prototype CAD drawing with dimensions.

Pre-model

This research drew a presentation of the conceptual freehand schematic after discussing the functions of the model. The initial concept shows the flattened rainwater tank with solar PV attached to the front of the rainwater tank, and both these technologies are built into the building panel. The dimensions of the building panel were 345mm x 60mm x 200mm. However, the dimensions of the rainwater tank were 315mm x 195mm x 50mm, and the dimensions for the solar cell were 345mm x 200mm. These dimensions can be altered and are adaptable to any size building panel. Considerations for further development of the building panel and adjoining building panels can be implemented once the building of the initial prototype is complete and concluded. The latter resulted in the alteration of the initial design. Research reduced the initial dimensions to a portable-sized building panel for ease of construction. The preliminary model is shown in Figure 4.31, and Figure 4.30 illustrates the conceptual layout for the prototype building panel.



Figure 4.31 Illustration of a Pre-model

Model

Research implemented changes to the initial prototype concept. All dimensions changed, and the panel size was now half the original size. Figures 7.1, 7.2a, and 7.2 bs original design drawings are shown in Chapter 7, and an amended image drafted on AutoCAD is shown in Figure 4.30. Dimensions of the amended concept are 345mm x 60mm x 200mm, and the outside wall thickness is 5mm all around. The rainwater collection tank dimensions are 314mm x 50mm x 195mm.

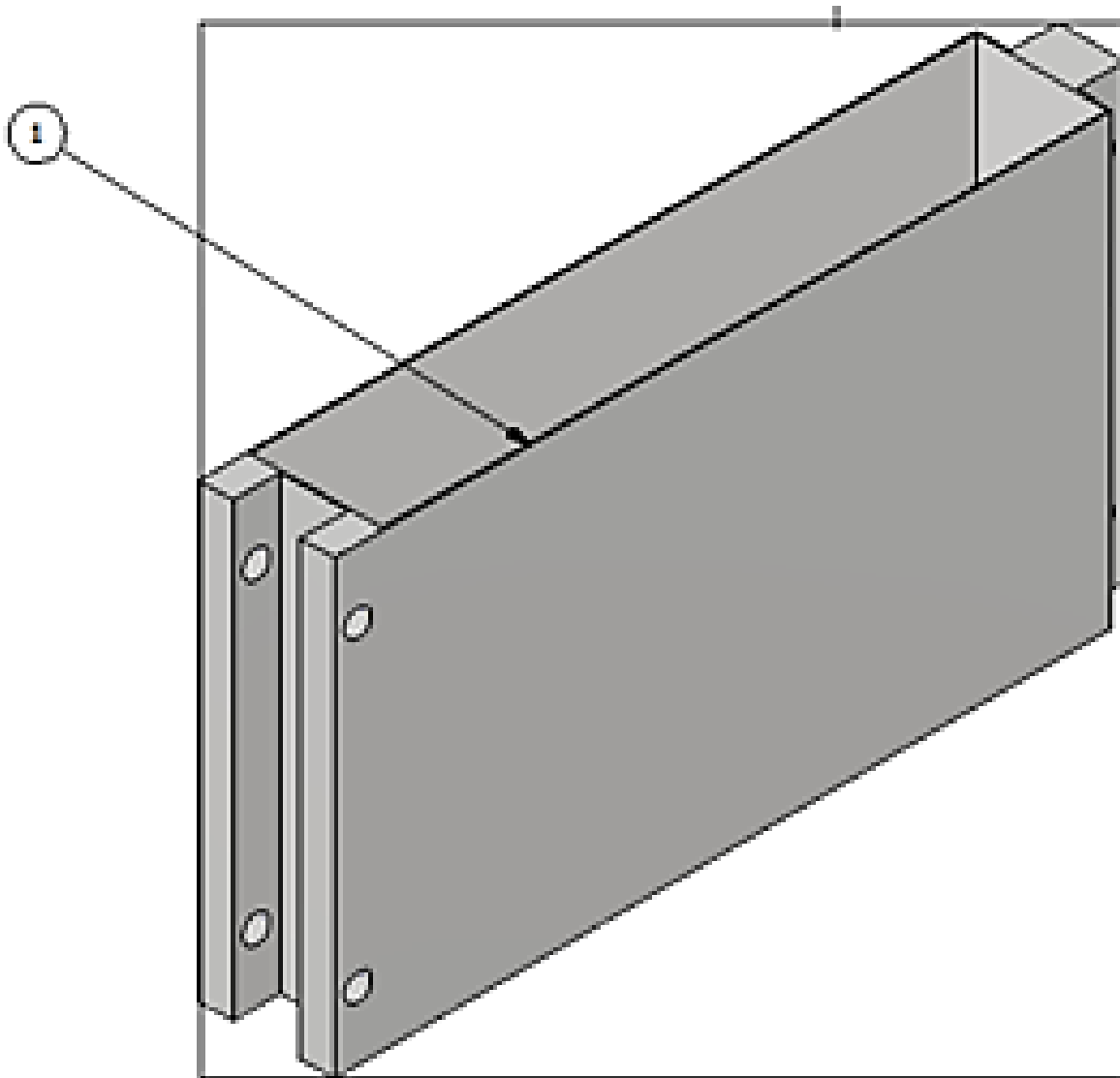


Figure 4.32 Prototype building panel isometric view.

During printing, a 315mm x 195mm x 60mm with a 5mm thick wall was printed instead of a building panel with a 1mm thick wall, which would have increased the volume of the water collected. However, the calculations and verifications followed the 5mm thick wall building panel.

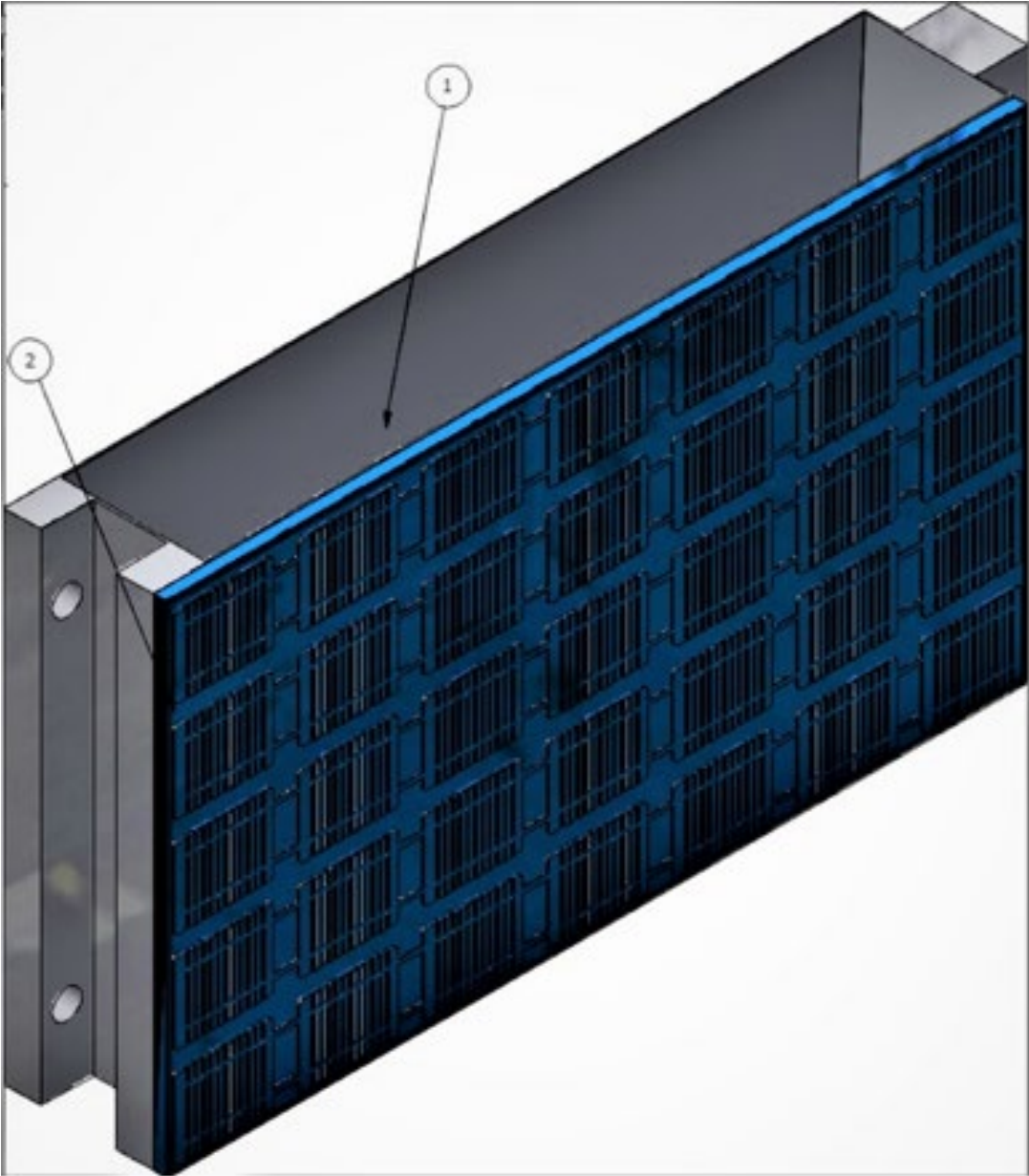


Figure 4.33 Prototype building panel with PV isometric view

4.5 Building panel design

The building panel

All building panel designs were in accordance with SANS 10100-1. For structural steelwork, SANS 10162 Measurements from the conceptual design with the following dimensions, length = 345mm, breadth = 60mm and depth = 200mm, were used to determine the self-weight by calculating the volume of the material, which yielded $4.14 \times 10^{-3} \text{m}^3$. From the density of PLA material, which equals 1250kg/m^3 , and a volume of $4.14 \times 10^{-3} \text{m}^3$, the weight of the material was determined to be 5.15kg. Also, the pressure the panel can withstand was determined to be $735.75 \times 10^{-3} \text{kN/m}^2$. The surface area was calculated to be $69 \times 10^{-3} \text{m}^2$. The bolt was designed using the following parameters: $\phi_b = 0.8$; $n = 1$; $m = 1$; Bolt size = M12, nominal diameter (ND) = 13mm, Class = 4.8, Grade300W

RWH

The surface area for the RWH system was calculated from length = 314mm, breadth = 50mm and depth = 195mm, which yielded a surface area of $61.23 \times 10^{-3} \text{m}^2$. The volume of rainwater that was calculated was determined as $6.0615 \times 10^{-3} \text{m}^3$. The weight of the water was calculated as 3.06kg \approx 3.0kg.

Flexible solar cell.

The optimum power generated by a 10W polycrystalline FSC panel was calculated to yield 0.055kWhrs over an optimum of 5.5 sun hours per day for CT, SA. The flexible solar cell covered 372mm x 157mm of the panel. Thus, the calculated area that it covered was 0.069m². Further, the practical aspect of work still needs to be investigated.

4.6 Design Calculations

To fulfil the objectives of this study, design calculations were conducted. The system design entails three technologies, each calculated autonomously, the building panel, the rainwater collection system and the PV system, and made use of the following known variables for the prototype design in the following sequence 1) Building panel design, 2) Rainwater harvesting system design and 3) PV design:

Building panel design and RWH design: γ Polylactic Acid (PLA) filament 1250kg/m^3 , γ water = 1000kg/m^3 , Panel outside dimensions (O/D) ($L \times W \times H$) = $0.345 \times 0.060 \times 0.200$; RW system inside dimensions (I/D) (m);

($L \times W \times H$) = $0.314 \text{m} \times 0.05 \text{m} \times 0.195 \text{m}$; Study Area = CPUT, South Africa; PV power output = 10W; Bolt diameter (ϕ) = M12mm; nominal diameter (DN) = 13mm; $\phi_b = 0.8$; $n=1$; $m=1$; $\phi_{br} = 0.67$; $t = 15 \text{mm}$; $g = 9.81 \text{ms}^{-2}$; $f_u = 420 \text{MPa}$; $a = 10.5 \text{mm}$; $e = 167.5 \text{mm}$;

PV Design: Cell type = Polycrystalline; PV dimensions = ($L \times H$) = $0.314 \times 0.2 \text{m}$ 158 where the solar cell dimensions were 0.377×0.158 ; STC = 25°C ; $T_{\text{max}} = 40^\circ \text{C}$; $T_{\text{min}} = 5^\circ \text{C}$; $T_{\text{coeff}} = -0.137\%/^\circ \text{C}$; NOCT = 45°C ; Irradiance (G) = 1000W/m^2 ; Panel $I_{\text{sc}} = 3 \text{A}$; optimum hours = 5.5hrs; System performance ratio = 0.75; DOD = 0.85, energy loss in the system = 1.3; Energy usage: 1 x 11W Mobile phone used for 3hours, 1x 50W battery power bank used for 2hrs; 1x 5W LED used for 4hours and a standby load of 1W used for 24hours..

Bolt design following SANS 10162-1 and SANS 2001:CS1; RWS design following SANS 1739-2017; PV Design following SANS 10142-1 and SANS 101066

Building panel design Calculations

The building panel design incorporated providing a solution for bolted members as well as eccentric connections, rainwater harvesting design and PV design with the application of first principle. Table 4.7 provides standardised calculations for surface area, volume, weight and power output.

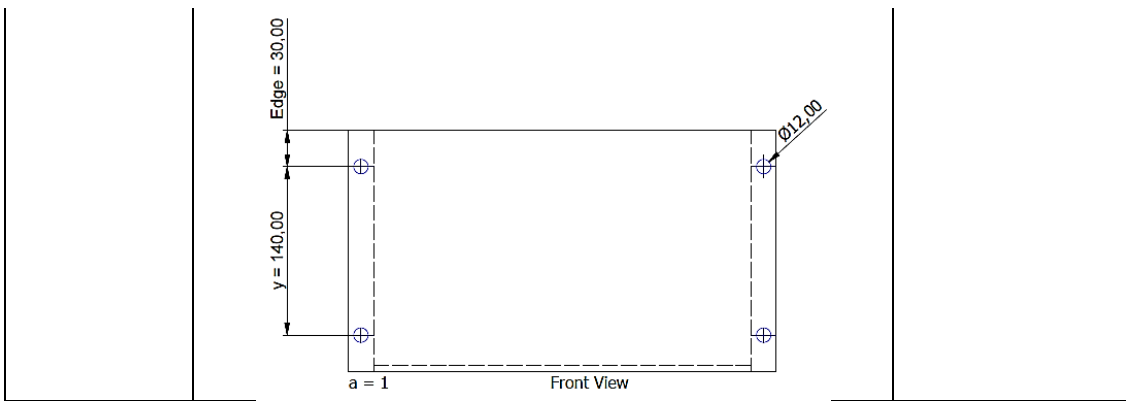
Table 4.7 Details mensuration for building panel components

Location			Surface Area	Volume	Weight
	Cape Town	South Africa			
Dimensions	Building Panel				
	Length	345 mm	0.021 m ²	0.00414m ³	5.175 kg
	Breadth	60 mm			
	Depth	200 mm			
Material	r-PET Plastic	Density: 1250 kg/m ³			
	Flexible Solar Cell	10 W			
Rain Water Harvesting	Length	314 mm	0.0157m ²	3.062x10 ⁻³ m ³	3,062 kg
	Breadth	50 mm			
	Length	195 mm			
Flexible Solar Cell		Power output 0,55kWhrs	0.021m ²		

Detailed design calculations for the prototype are provided in table 4.8, the calculations have been conducted autonomously for each technology, however, validating if the building panel will be able to carry the load of the harvested rainwater at full capacity. The calculations also determines the amount of power the 10W will supply.

Table 4.8 Design table for non-load bearing building panel, RWH and PV system

Reference	Calculation	Output
SANS 10162-1	<p>Building panel</p>	



Reference	Calculation	Output
SANS 10162	<p>1. Self-weight</p> <p>a) Mass per unit length</p> <p>b) Force</p> <p>c) Pressure</p> <p>2. Live load</p> <p>a) Area</p> <p>b) Volume</p> <p>c) Mass</p> <p>d) Force</p> <p>e) Pressure</p> <p>3. Load Calculation</p> <p>a) Ultimate load (P_u) = (1.2 x Dead-Load) + (1.6 x Live-Load)</p> <p>4. Bolt Calculations</p> <p>a) Check for minimum pitch $= 0.27 \times \phi_b$ $140\text{mm} > 32.4\text{mm}$ \therefore Design is Ok</p> <p>b) Edge Distance $= 1.5 \times \phi_b$ $18\text{mm} > 10.5\text{mm}$</p>	<p>147.15N/m</p> <p>50.767N</p> <p>735N/m²</p> <p>0.06123m²</p> <p>3.0615x10⁻³m³ Equivalent to 3.06 litres</p> <p>3.062kg</p> <p>30.033N</p> <p>490N / m²</p> <p>1.668kN/m²</p> <p>32.4mm</p> <p>18mm</p>

	<p>Minimum edge distance is not OK \therefore Recommendation: to prevent edges from tearing, increase the plate size to 32mm; this will give enough clearance. Reduce the bolt size to M4, but further loading calculations must be verified against the choice of an M4 or M6 bolt. Meaning if M4 bolt is used, then minimum edge distance = $1.5 \times \phi_b(M4) = 6\text{mm}$. \therefore The minimum edge distance is OK. However, the M4 bolt must comply with the minimum tensile strength of the bolt in accordance with SANS 10162, and the holes must be punched in accordance with SANS 2001:CS1</p>	
Reference	Calculation	Output
	<p>$\Sigma y = 140\text{mm}$ $a = 1$ $n = 2$</p> <p>5. Maximum Tension (T_u) = $\frac{P \times e \times y}{a \times \Sigma y^2}$</p> <p>6. Tension resistance (T_r) = $0.75 \times \phi_{br} \times A_b \times f_u$</p> <p>$T_r > T_u \therefore$ Design is Ok</p> <p>7. Maximum Shear (V_u) = $\frac{P}{N}$</p> <p>8. Shear resistance (V_r) = $0.6 \times \phi_b \times n \times m \times A_b \times f_u$</p> <p>$V_r > V_u \therefore$ Design is OK</p> <p>9. Combined Action = $\frac{V_u}{V_r} + \frac{T_u}{T_r}$</p> <p>10. Bearing of bolts (B_r) = $\phi_{br} \times a \times t \times n \times f_u$ if $a < 3d$ and</p> <p>11. Bearing of bolts (B_r) = $3\phi_{br} \times t \times d \times n \times f_u$ if $a > 3d$</p> <p>Check for bearing of bolts if $a > 3d$ or $a < 3d$ $10.5\text{mm} < 36\text{mm}$ $\therefore a < 3d$</p> <p>12. Use Bearing of bolts (B_r) = $\phi_{br} \times a \times t \times n \times f_u$</p> <p>$94.975 > 0.834$ \therefore Design is Ok.</p>	<p>= 1.995kN</p> <p>= 28.5kN</p> <p>0.834kN</p> <p>15.96kN</p> <p>0.0792</p> <p>36mm</p> <p>94.975kN</p>

SANS 1739	<p>Rainwater storage calculations</p> <p>a) Area</p> <p>b) Volume</p> <p>c) Rainfall intensity (i) = $\frac{\text{Average Rainfall (mm)}}{\text{Time (hr)}}$</p> <p>d) Wetted perimeter (P_w) = $2 \times (L + H)$</p> <p>e) Flow rate (Q) = $\frac{\text{Volume (V)}}{\text{Time (t)}}$</p> <p>f) Velocity ($V$) = $\frac{\text{Flow rate (Q)}}{\text{Area (A)}}$</p>	<p>0.0612m²</p> <p>3.0615x10⁻³m³</p> <p>104mm/hr</p> <p>1.018m</p> <p>3.4017x10⁻⁶ m³/s</p> <p>0.0556 x 10⁻³ m/s</p>
Reference	Calculations	Output
SANS 10142	<p>PV Design Calculations</p> <p>a) Energy generated per hr = Watt x optimum hours</p> <p>b) Energy generated considering performance ratio = Watt x hrs x per ratio</p> <p>c) Energy generated per day = Total energy generated / 24hr</p> <p>d) $V_{ocmax} = [(T_{ocmin} - STC) \times T_{coeff}] + V_{oc}$</p> <p>e) $V_{mpp} = (T_{localmin} + NOCT - T_{STC}) \times T_{coeff} + V_{oc}$</p>	<p>55Whrs</p> <p>41.25Whrs</p> <p>2.29W/Day</p> <p>12.74V</p> <p>2V</p>
SANS 10142-1-2	<p>Battery calculation design</p> <p>a) Total usage = Sum of energy use W x number of hours per day</p> <p>b) Total PV panel energy needed = Total usage x 1.3 factor</p> <p>c) Battery capacity (Ah) = $\frac{\text{Whrs /day}}{(0.85 \times 0.6 \times \text{nominal battery voltage})} \times \text{Days of automy}$</p> <p>d) Solar controller rating = $T_{soc} \times 1.3$</p> <p>Rating: 4A @12V or greater</p>	<p>177Whrs</p> <p>230Whrs</p> <p>29Ah</p> <p>4A</p>

4.7 Materials

Table 4.9 gives a breakdown of elements for the polylactic acid prototype material, mostly used for 3D printing. The material is widely known as PLA and defines thermal and mechanical properties.

Table 4.9 PLA material elements

PLA	Description	Value
Technical Name	Poly(lactic Acid (PLA) or poly l-lactic Acid (PLLA)	
Chemical formula		$(C_3H_4O_2)_n$
Characteristics	A biodegradable material popularly used in 3D printing, packaging and other industries. It is made from renewable materials such as cornstarch and sugarcane.	
	Panel weight	644g
	Panel weight with water	4880g
	Net filament weight	750g
	Density	1210 – 150kg/m ³
	Colour information	Green, Black, Metallic Silver, White, Transparent, Orange, Yellow, Blue, Magenta, Red, Pearl white.
Thermal Properties	Melting Temperature	157 - 170°C
	Injection mould temperature	178 - 240°C
	Heat Deflection Temperature (HDT)	49 - 52°C @ 0.46MPa
Mechanical Properties	Tensile Strength	61 – 66MPa
	Flexural Strength	48 – 110MPa
	Specific Gravity	1.24
	Yield Strength	70MPa
	Young Modulus	2.7 – 16GPa
	Elastic Modulus	3750 MPa
	Shrink ratio	0.37 – 0.41%

The model was printed as a single unit, a building panel and a rainwater harvesting system. The PV and its components were joined using a marine adhesive sealant, which was spread on the face of the building panel measured at 0.069m².

4.8 Prototype costs

The prototype costs vary, and these depend on a number of variables such as materials, labour costs, licencing, IP, transport and shipping, market research, software, testing and so forth. For this study, which assesses the veracity of the building panel for the prototype for rainwater storage and energy generation, the prototype's size was only developed knowing well that it can be scaled to any size. The prototype's size directly affects the costs and the duration of the prototype development and all other aspects relating to the fruition of the sizeable product including mass production. The costs herein only give a synopsis for

building a small-scale prototype. Without delving into much detail on the product development costs, this research only highlights the pertinent aspects relating to this research and briefly illustrates the potential of profit/loss options (Ashton, 2012:249) (Brown, 2010:40).

Table 4.10 provides the actual material costs which incorporate raw materials, occupational health and safety and other components required to produce the prototype, these costs are inclusive of a 15% VAT.

Table 4.10 Prototype building costs

Description	Qty	Tax	Rate	Amount
Materials for a 345 × 50 × 195				
3D Printing - Prototype	1	15%	R1 631,74	R 1 876,50
MPPT Triron 10A with MT50	1	15%	R3 553,12	R 4 086,09
10W 12V Flexible Panel	2	15%	R641,97	R 1 476,52
12V Lithium Ion Battery	1	15%	R651,30	R 749,00
Subtotal				R 8 188,11
Miscellaneous				
Peg Board	2	15%	R25,00	R 57,50
Peg Board lots	1	15%	R193,00	R 221,95
Eureka Screws	1	15%	R19,13	R 22,00
12V Male Plug	1	15%	R41,10	R 47,27
Sika Flex Sealant	3	15%	R230,75	R 796,09
Subtotal				R 1 144,80
OH&S				
Heating Gloves	1	15%	R105,05	R 120,81
Safety Goggles	1	15%	R15,94	R 18,33
Duster Coat	1	15%	R239,13	R 275,00
Subtotal				R 414,14
Total				R 9 747,05
VAT 15%				R 1 462,06
Total				R 11 203,11

When conducting product development and to validate its profitability, a suitable and detailed financial study needs to be conducted (Ashton, 2012:249). For the benefit of this research study, only a brief indication is detailed in table 4.11

Table 4.11 Revenue table

Description	Unit	Qty	Rate	Amount
Building Panel (RWS & RE) and components with Installation	Sum	1	R37 769,83	R37 769,83
Other costs				0

Grid-Connection	Sum	1	R15 000	R15 000,00
Certificate of Compliance	Sum	1	R15 000	R15 000,00
Subtotal				R67 776,83
VAT			15%	R10 165,47
Total				R77 935,30

As mentioned previously a detailed financial model required a studying to validate its profitability (Brown, 2010:40). For the purpose of this research, a rule of thumb is used to measure the financial feasibility of this prototype. The rule of thumb included figures for operating costs as detailed in table 4.12

Table 4.12 Expenses table

Expenses	
Administration	R8 000,00
Stationery	R5 000,00
Communications	R3 000,00
Transport	R5 000,00
Rental Space	R9 000,00
Services	R1 200,00
Insurance	R2 500,00
Other	R5 000,00
Total	R38 700,00

The financial statement is composed of an income statement which highlights the revenue and expenses of an organisation during a certain period (Brown, 2010:40). Table 4.13 illustrates the profit and losses where revenue is measured against expenses. And the resulting difference is profits for the purpose of this study.

Table 4.13 Profit and losses table

Profit and losses	
Revenue	R89 138,41
Expenses	-R38 700,00
Total Profits	R50 438,41

4.9 Conclusion

In conclusion, this chapter covered the theoretical component of this research project. These theoretical strategies included simulation, model, design calculations, material selection, and costs.

A simulation was conducted for both a grid-tied system and a standalone system. PVSyst software was used as a simulation tool. The location was set at the CPUT Bellville campus with a tilt of 90° and Azimuth of 0°, the latter fulfilling the objectives of this research study. A preliminary design for both systems was conducted as the initial design step to provide guidance. Orientation and user loads were incorporated to determine the equivalent total energy of 177Wh/day. Common to both systems, standard data included meteorological data and orientation, which entails field parameters and quick optimisation. The

process included the PV array, an inverter, detailed losses, self-consumption, storage, horizon, near shading and energy management to achieve full simulation for the grid-tied system. In contrast, the system design included PV design, controller, storage, detailed loss, horizon, and near shading for the standalone system.

The model incorporated drafting, drawings involving various technologies such as 2D and 3D CAD drawings, SolidWorks, and pre-model preparations.

The design calculation included autonomous calculations for the building panel design, RWH and PV design. The building panel design incorporated non-loadbearing design calculations, commencing with self-weight, load calculations, and bolt design. In contrast, the RW storage calculation incorporated the area and volume of the RW tank with storable water, respectively, and the PV design calculations included energy generated, which were in line with the aims and objectives of this research work.

This section also included detailed technical information for the chosen prototype materials and their elements. Lastly, it provided detailed prototype calculations, which included building costs, revenue, expenses, and predicted profit and losses.

The concluded information conforms to the aims and objectives of this study.

Chapter 5 Construction System and Validation

In this chapter, research presents the construction and validation process for the building panel that harvests rainwater and generates energy from PV. The construction of the building panel with the rainwater system occurred at Netram Technologies, Cape Town. Netram Technologies has 3D printing facilities and is limited to APL, with sizes of up to 1m for prototype modelling. The equipment used for the panel production is the Creality Ender – 3Neo 3D printer.

The PV technology was purchased through D&S Solutions, a CPUT vendor, and an import/export company for green technologies. The PV technology equipment was imported from China and sourced from different suppliers.

5.1 Prototype Construction and Assembly

The building panel prototype was constructed in 4 different phases in total, ranging from equipment i) procurement & logistics, ii) the CAD drawing and printing phase, iii) the wiring of PV and its components and iv's) the assembling phase. The process flow chart is depicted in Fig 5.1, providing an interpretation of stages during the prototype construction.

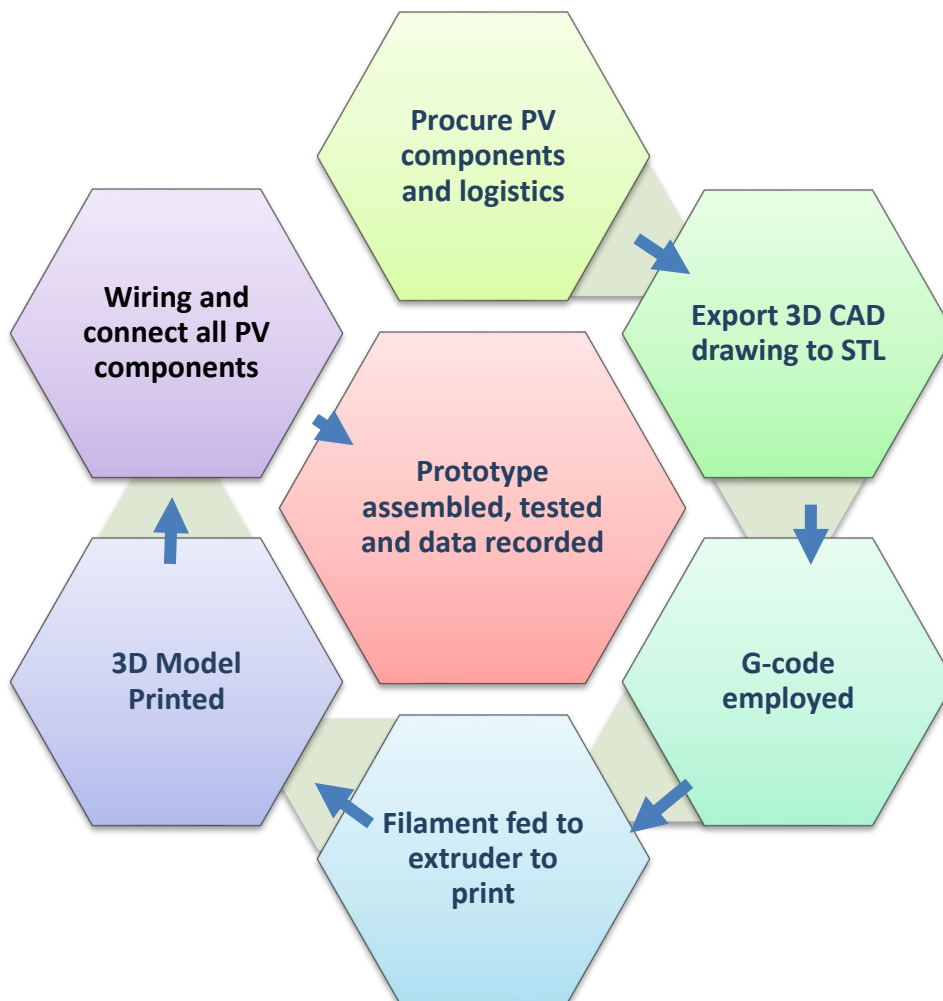


Figure 5.1 Flow chart diagram for construction and assembling of the prototype, including design and procurement phases.

The project images portray the construction and assembly process in the flow chart diagram. The project commenced with the CAD drawing phase. After the drawings were completed, the procurement of PV materials and their components took place, and the process took six weeks to conclude. While waiting for materials to arrive in SA, the CAD drawing was exported into an STL file, which was deployed onto the 3D printer, which took almost 4hrs to complete. The transparent PLA was employed on the 3D printer, and the G-code instructed the printer on how much filament to extrude. Subsequently, the prototype. The transparent-to-white prototype is produced with geometric lines visible, the thickness wall is 5mm, these dimensions can be altered depending on the needs. The prototype was collected. Two pegboards measuring 800mm x 200mm were affixed using cable ties for wall stability.

The prototype building panel was weighed before assembly, and it weighed 644g. The wiring of the PV panel and its components occurred with the assistance of a qualified PV technician. The MPPT was placed on the pegboard to ensure the parts were aligned for the final assembly. One side of the building panel measuring 345mm x 200mm was pasted with the Sika 219i marine adhesive sealant. Subsequently, the polycrystalline FSC was affixed to the building panel, which was left for 24 hours to allow sufficient curing time. Subsequently placed on to the pegboard, the 2ℓ rPET bottle was cut, and only a two-thirds of the bottle remained, the one-third was discarded. The remaining rPET was perforated with holes measuring 5mm, using a star screw driver. After completion, the rPET was fixed onto the pegboard with a bolt and nut. Three of the crucial components were affixed onto the pegboard, and the MPPT was affixed with bolts and nuts; however, the building panel for RWH and energy generation was affixed to the pegboard using a cable tie, as well as the LiFePO₄ battery. The polycrystalline FSC is subsequently connected to the MPPT. The LiFePO₄ battery was the last component to be connected. The objectives of this study do not consider the use of a battery, but the battery was needed if there was no load, then the battery could be used as an energy storage.

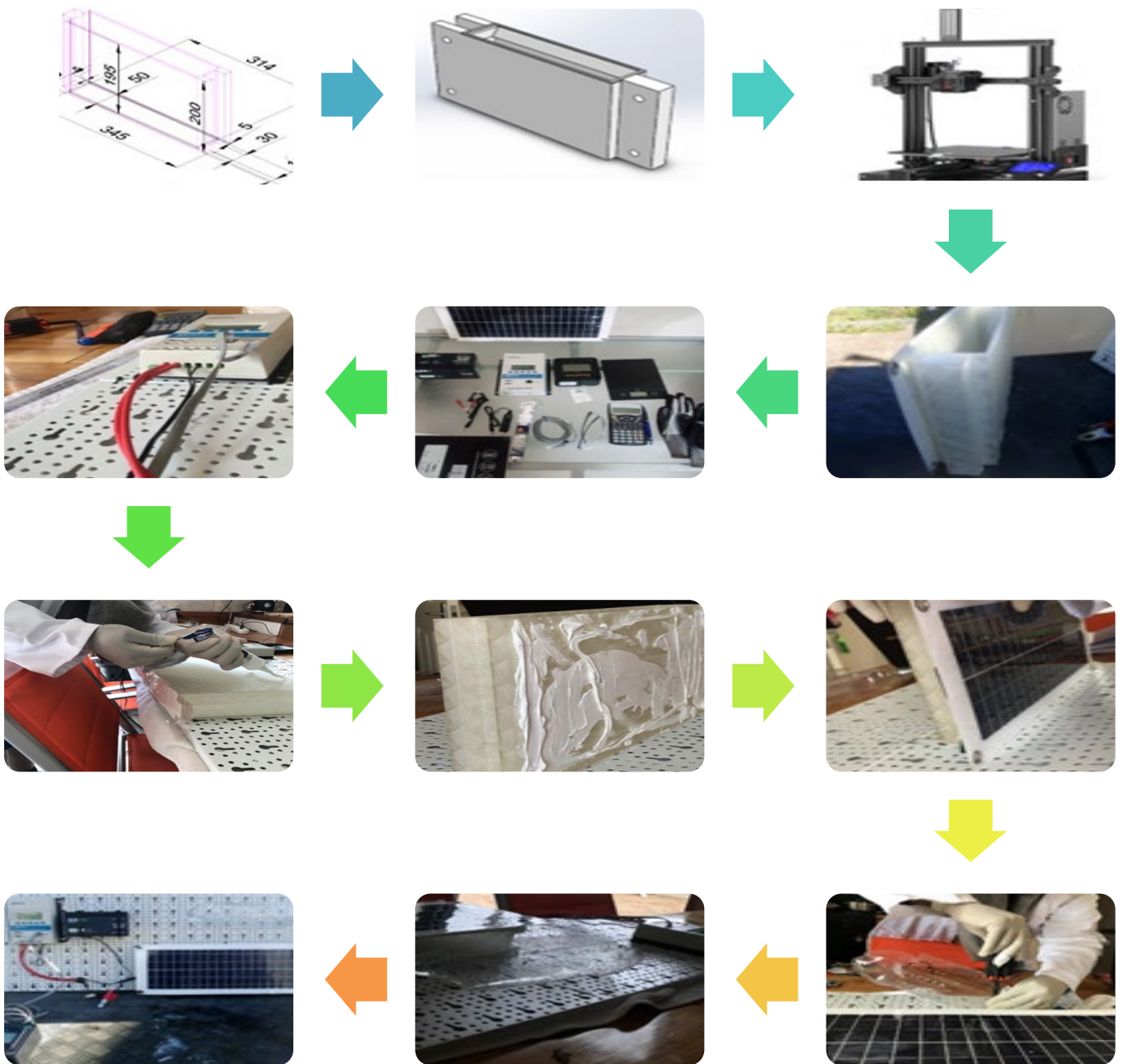


Figure 5.2 An illustration of a flow chart diagram with project images on the sequence for system construction and assembly.

Building panel final product

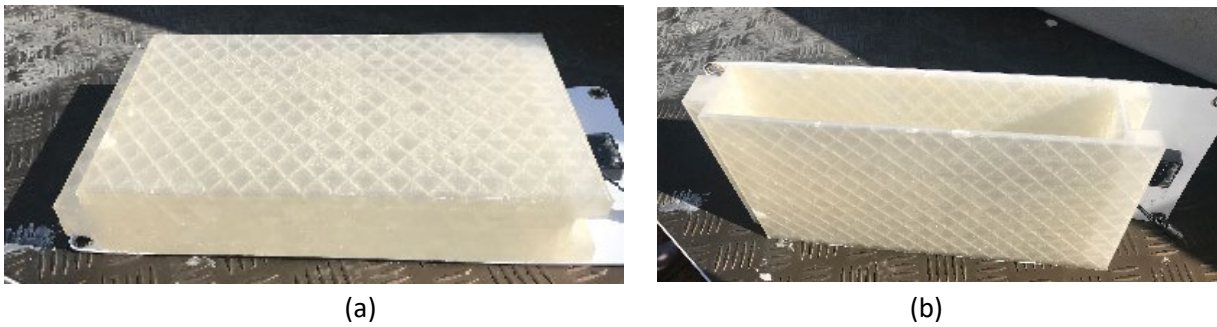


Figure 5.3 Completed building panel and its openings

Figure 5.3 (a) illustrates the final building panel, placed horizontally on a flat surface, presenting the bottom part of the building panel, whereas (b) illustrates the back of the building panel and its opening to the RWS tank.



(a) Connection side of Panel

(b) PV panel junction vox

Figure 5.4 Connection side of Panel and PV panels junction box

Figure 5.4 (a) Presents one of the connecting sides with the opening to the RWS and (b) illustrates the alternating side of the building panel with the PV panel's junction box.

5.2 Validation

The tests were conducted on both the RWH and the PV systems. All tests were conducted on different days, due to inclement weather. The planned starting time for conducting the tests was from 8 am to 5 pm. All data was recorded with their corresponding times. For the RWH system, the collected data was the depth of the rain and the time it took to reach that dept. For PV, the collected data was Wattage, Voltage and Amps. The battery readings were not recorded. This research kept to the study's objectives to determine the power output for a 10W on a vertical surface.

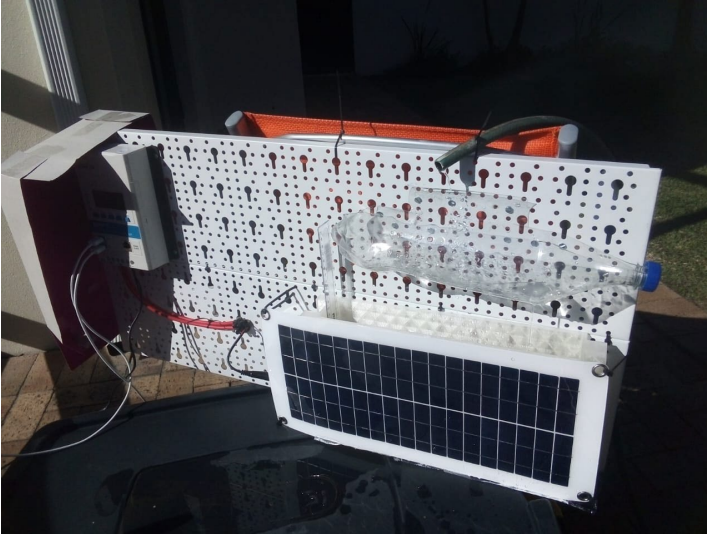


Figure 5.5 Assembled prototype building panel being validated

5.5.1. Rainwater harvesting data

Rainwater harvesting data is detailed in Table 5.1. The data is recorded at 15-minute intervals. The 30-minute and 1-hour intervals were first tested; for the 1-hour interval, the rainwater tank was filled before reaching the 1-hour mark. And for the 30-minute interval, the water needed to be released often. The 15 minutes worked better in the data collection.

Water was slowly released from the faucet, through the sprinkler head, onto the bottle, punched with 5mm holes into the collection tank.

The stop watch was used to start/stop the recording time, the ruler was used to measure the depth of water collected. All measurements were in mm, and the times were recorded in minutes. The prototype validation was conducted from July 10, 2023 marking this day as day1 of the validation process up to August 2, 2023. Two separate days were also used for conducting tests, August 3rd and 4th 2023.

Table 5.1 RWH data set

Time		Day1	Day2	Day3	Day4	Day5	Day6	Day7	Day8	Day9	Day10
From	To	Rainfall (mm)_Day1	Rainfall (mm)_Day2	Rainfall (mm)_Day3	Rainfall (mm)_Day4	Rainfall (mm)_Day5	Rainfall (mm)_Day6	Rainfall (mm)_Day7	Rainfall (mm)_Day8	Rainfall (mm)_Day9	Rainfall (mm)_Day10
08:00	08:15	27	25	26	29	26	26	27	26	29	29
08:15	08:30	28	24	24	30	27	25	26	26	28	29
08:30	08:45	27	25	26	30	26	26	27	25	29	27
08:45	09:00	26	23	25	31	27	27	27	26	28	27
09:00	09:15	26	27	24	29	27	27	26	25	27	27
09:15	09:30	25	22	25	29	28	28	25	26	28	28
09:30	09:45	27	25	26	28	27	27	27	27	27	28
09:45	10:00	28	26	26	30	26	28	26	27	29	29
10:00	10:15	27	26	26	31	27	27	25	26	28	29
10:15	10:30	28	27	27	30	26	27	26	27	28	28
10:30	10:45	25	25	26	31	26	26	27	26	27	27
10:45	11:00	26	24	27	30	25	27	27	25	28	27
11:00	11:15	25	23	27	30	25	27	23	26	28	27
11:15	11:30	28	27	25	31	28	28	27	26	27	28
11:30	11:45	27	25	26	29	27	8	25	25	27	28
11:45	12:00	25	25	26	30	25	27	25	26	26	29
12:00	12:15	29	26	26	31	29	26	26	25	25	27
12:15	12:30	27	27	25	31	27	25	27	27	27	26
12:30	12:45	27	27	27	32	27	25	27	28	28	28
12:45	13:00	28	28	25	32	28	26	28	27	29	26
13:00	13:15	27	27	26	32	27	26	27	28	25	27
13:15	13:30	25	27	26	31	25	26	27	27	25	28
13:30	13:45	26	25	25	31	26	26	25	26	25	28
13:45	14:00	26	26	25	30	26	27	26	25	26	29
14:30	14:45	23	28	27	20	19	20	30	29	25	27
14:45	15:00	24	28	27	19	18	19	31	28	24	27
15:00	15:15	22	29	28	19	19	20	30	29	26	25
15:15	15:30	22	28	28	20	18	20	31	29	25	25
15:30	15:45	21	27	27	20	17	20	29	27	24	25
15:45	16:00	20	28	27	19	16	21	30	28	25	25
16:00	16:15	20	27	27	19	17	20	29	27	25	26
16:15	16:30	21	27	27	20	17	20	29	26	24	26
16:30	16:45	20	27	26	20	16	20	28	27	25	26
16:45	17:00	20	28	27	20	16	21	29	26	26	26

5.5.2. PV data

PV recorded data is detailed in Table 5.2. The data was recorded a 15minute intervals. The recording time started at 8am, till 5pm. The data recorded on a 15minute interval coincides with the RWH data. The zero readings are a result of shading from buildings as well as winter solstices in winter months. To get the appropriate reading the PV panel orientation was set to the North facing direction. Remembering the objectives of this research, to verify the power output of a 10W polycrystalline FSC on a vertical surface Meaning the inclination angle is ninety degrees. The collected data included the Voltage and the amperes; however, the recorded data only focuses on the output in Watts. The readings were collected from the MPPT solar charge controller, and were recorded for every 15minute interval that the tests were conducted.

The stop watch was used to start/stop the recording time.

Table 5.2 PV data set

Time (m)-From	Time(m)-To	Power output (W) Day1	Power output (W) Day2	Power output (W) Day3	Power output(W) Day4	Power output (W) Day5	Power output (W) Day6	Power output (W) Day7	Power output (W) Day8	Power output (W) Day9	Power output (W) Day10
11:00	11:15	5	0	2	4	4	4	4	2	4	4
11:15	11:30	4	4	3	4	4	4	4	2	4	4
11:30	11:45	5	3	3	3	3	4	3	2	4	4
11:45	12:00	5	4	3	4	4	3	4	3	4	3
12:00	12:15	5	5	3	4	5	3	5	3	4	3
12:15	12:30	4	2	4	4	2	3	2	3	4	3
12:30	12:45	4	4	4	4	4	4	4	4	4	4
12:45	13:00	4	4	4	3	3	4	3	4	3	4
13:00	13:15	4	4	4	4	3	3	3	4	4	3
13:15	13:30	5	3	4	4	3	4	3	4	4	4
13:30	13:45	4	4	4	3	4	3	4	5	3	3
13:45	14:00	4	4	5	4	4	4	4	5	4	4
14:30	14:45	5	4	5	4	4	5	3	5	4	4
14:45	15:00	4	4	4	4	4	2	3	3	4	4
15:00	15:15	4	4	4	4	4	4	4	4	4	4
15:15	15:30	4	4	3	3	3	3	4	3	3	3
15:30	15:45	4	3	3	3	3	3	4	3	2	2
15:45	16:00	4	3	3	3	3	3	4	3	2	2

Table 5.3 Rainfall & PV data set when storage is 0% & 100% respectively

Time		Rainfall (mm)		PV		
From	To	Rain	Cumulative	Voltage (V)	Amperes (A)	Watts (W)
11:00	11:15			13,6	0,2	3,0
11:15	11:30			13,3	0,1	1,0
11:30	11:45			13,3	0,2	2,2
11:45	12:00			13,1	0,2	1,5
12:00	12:15			12,2	0,1	1,0
12:15	12:30	195	195	12,8	0,1	1,5
12:30	12:45	195	195	13,0	0,3	2,5
12:45	13:00	195	195	11,0	0,3	3,6
13:00	13:15	195	195	13,2	0,2	3,2
13:15	13:30	195	195	13,3	0,3	3,8
13:30	13:45	195	195	13,5	0,3	3,6
13:45	14:00	195	195	13,6	0,2	4,0
14:30	14:45	195	195	13,5	0,1	4,2
14:45	15:00	195	195	13,2	0,1	3,8
15:00	15:15	195	195	12,0	0,3	3,5
15:15	15:30	195	195	12,0	0,3	2,7
15:30	15:45	195	195	12,0	0,3	2,0
15:45	16:00	195	195	12,0	0,3	1,8
16:00	16:15	195	195			
16:15	16:30	195	195			
16:30	16:45	195	195			
16:45	17:00	195	195			

Table 5.4 Combined cumulative data for Rainwater collection, energy generation, and when the storage is 0% & 100% respectively at 15 minutes intervals

Time(hrs)	Water Depth in panel_D	Hourly total RWC_D1	Energy Generated (W)_D1	Hourly Energy generated (W)_D1	Water Depth in panel_L	Hourly total RWC_D2	Energy Generated (W)_D2	Hourly Energy generated (W)_D2	Water Depth in panel_D	Hourly total RWC_D3	Energy Generated (W)_D3	Hourly Energy generated (W)_D3	Water Depth in panel_D	Hourly total RWC_D4	Energy Generated (W)_D4	Hourly Energy generated (W)_D4	Water Depth in panel_D	Hourly total RWC_D5	Energy Generated (W)_D5	Hourly Energy generated (W)_D5	Water Depth in panel_D	Hourly total RWC_D6	Energy Generated (W)_D6	Hourly Energy generated (W)_D6
	27				25				26				29				26				26			
	28				24				24				30				27				25			
8:00-9:00	27				25				26				30				26				26			
	26	108			23	97			25	101			31	120			27	106			27	104		
	26				27				24				29				27				27			
	25				22				25				29				28				28			
	27				25				26				28				27				27			
9:00-10:00	28	106			26	100			26	101			30	116			26	108			28	110		
	27				26				26				31				27				27			
	28				27				27				30				26				27			
	25				25				26				31				26				26			
10:00-11:00	26	106			24	102			27	106			30	122			25	104			27	107		
	25		4,1		23		3,5		27		2,1		30		3,7		25		3,5		27		3,9	
	28		3,7		27		4,0		25		2,7		31		3,5		28		4,0		28		3,9	
	27		4,1		25		2,8		26		2,5		29		3,1		27		2,8		8		3,5	
11:00-12:00	25	105	4,2	16,1	25	100	3,9	14,2	26	104	2,5	9,8	30	120	4,2	14,5	25	105	3,9	14,2	27	90	3,0	14,3
	29		4,2		26		5,0		26		2,9		31		4,2		29		5,0		26		2,5	
	27		3,5		27		1,5		25		3,5		31		3,5		27		1,5		25		2,5	
	27		3,6		27		4,0		27		3,6		32		3,6		27		4,0		25		3,5	
12:00-13:00	28	111	3,4	14,7	28	108	3,3	13,8	25	103	4,0	14	32	126	3,4	14,7	28	111	3,3	13,8	26	102	4,0	12,5
	27		4,0		27		3,2		26		4,0		32		4,0		27		3,2		26		2,8	
	25		4,1		27		3,0		26		4,1		31		4,1		25		3,0		26		3,9	
	26		3,4		25		4,0		25		4,4		31		3,4		26		4,0		26		3,0	
13:00-14:00	26	104,0	3,7	15,2	26	105,0	4,0	14,2	25	102,0	4,7	17,2	30	124,0	3,7	15,2	26	104,0	4,0	14,2	27	105,0	4,0	13,7
	23		4,1		28		4,0		27		4,5		20		3,9		19		3,9		20		5,0	
14:30-15:00	24	47,0	3,9	8,0	28	56,0	4,0	8,0	27	54,0	4,3	8,8	19	39,0	3,9	7,8	18	37,0	3,9	7,8	19	39,0	1,5	6,5
	22		3,5		29		3,5		28		3,5		19		3,5		19		3,5		20		4,0	
	22		3,1		28		3,3		28		3,3		20		3,0		18		3,0		20		3,3	
	21		3,4		27		2,9		27		2,9		20		2,5		17		2,5		20		3,2	
15:00-16:00	20	85	3,1	13,1	28	112	2,5	12,2	27	110	2,5	12,2	19	78	2,5	11,5	16	70	2,5	11,5	21	81	2,9	13,4
	20				27				27				19				17				20			
	21				27				27				20				17				20			
	20				27				26				20				16				20			
16:00-17:00	20	81			28	109			27	107			20	79			16	66			21	81		

Table 5.4 Continued

Time(hrs)	Water Depth in panel_D	Hourly total RWC_D7	Energy Generated (W)_D7	Hourly Energy generated (W)_D7	Water Depth in panel_D	Hourly total RWC_D8	Energy Generated (W)_D8	Hourly Energy generated (W)_D8	Water Depth in panel_D	Hourly total RWC_D9	Energy Generated (W)_D9	Hourly Energy generated (W)_D9	Water Depth in panel_D	Hourly total RWC_D1	Energy Generated (W)_D10	Hourly Energy generated (W)_D10	0-100% full tank	Energy (W) generated	Hourly Energy (W) generated	
	27				26				29				29							
	26				26				28				29							
	27				25				29				27							
8:00-9:00	27	107			26	103			28	114			27	112						
	26				25				27				27							
	25				26				28				28							
	27				27				27				28							
9:00-10:00	26	104			27	105			29	111			29	112						
	25				26				28				29							
	26				27				28				28							
	27				26				27				27							
10:00-11:00	27	105			25	104			28	111			27	111						
	23		3,5		26		1,7		28		4,1		27		3,9			3,0		
	27		4,0		26		1,5		27		3,7		28		3,9			1,0		
	25		2,8		25		2,0		27		4,1		28		3,5			2,2		
11:00-12:00	25	100	3,9	14,2	26	103	3,3	8,5	26	108	4,2	16,1	29	112	3,0	14,3		1,5	7,7	
	26		5,0		25		3,2		25		4,2		27		2,5			1,0		
	27		1,5		27		3,0		27		3,5		26		2,5		195	1,5		
	27		4,0		28		4,0		28		3,6		28		3,5		195	2,5		
12:00-13:00	28	108	3,3	13,8	27	107	4,0	14,2	29	109	3,4	14,7	26	107	4,0	12,5	195	3,6	8,6	
	27		3,2		28		4,0		25		4,0		27		2,8		195	3,2		
	27		3,0		27		4,2		25		4,1		28		3,9		195	3,8		
	25		4,0		26		4,6		25		3,4		28		3,0		195	3,6		
13:00-14:00	26	105,0	4,0	14,2	25	106,0	4,6	17,4	26	101,0	3,7	15,2	29	112,0	4,0	13,7	195	4,0	14,6	
	30		3,2		29		5,0		25		4,1		27		4,1		195	4,2		
14:30-15:00	31	61,0	3,0	6,2	28	57,0	3,3	8,3	24	49,0	3,7	7,8	27	54,0	4,0	8,1	195	3,8	8,0	
	30		4,0		29		4,0		26		3,7		25		3,7		195	3,5		
	31		4,0		29		3,3		25		3,0		25		2,9		195	2,7		
	29		4,0		27		3,2		24		2,3		25		2,3		195	2,0		
15:00-16:00	30	120	4,2	16,2	28	113	2,7	13,2	25	100	2,1	11,1	25	100	2,1	11	195	1,8	10	
	29				27				25				26				195			
	29				26				24				26				195			
	28				27				25				26				195			
16:00-17:00	29	115			26	106			26	100			26	104			195			

5.3 Conclusion

The building panel construction occurred at Netram Technologies, a 3D printing facility specializing in models and prototypes. The Creality Ender-3Neo 3D printing machine was employed for fabricating the final product—an innovative building panel designed for rainwater collection and energy generation. The PV technology and its components were sourced from China through D&S Solutions, a vendor associated with the Cape Peninsula University of Technology (CPUT).

The technical process involved the preparation of 3D drawings, which were then exported to an STL file. The G-code was generated and utilized for printing after loading filament onto the 3D printer. The assembly phase encompassed intricate wiring, connecting the Maximum Power Point Tracker (MPPT) to the PV system and the battery. The attachment of the building panel to the PV system was facilitated by applying SIKA 291i, a specialized adhesive marine sealant.

A validation process ensued post-construction, immediately after all components were adequately dried. The recording spanned from 8 am to 5 pm, encompassing simulated rainwater events at 15-minute intervals. Additionally, PV recordings commenced post-11 am due to shading from nearby structures, with data collected at the same 15-minute intervals. All recorded data was documented using Microsoft Excel, a comprehensive data analytics tool.

Chapter 6 Results and Discussion

This chapter presents the results from the tests conducted and presented in Chapter 5. The results were compared with the design calculations, and conclusions were drawn. The test results verified if the experiment fulfilled the objectives of this study. This chapter discussed a thorough analysis and precise interpretation of the results.

6.1 RWH and PV results

This section determined the analysis of practical work as detailed in Chapter 5.2. The work was presented graphically. The analysis interpreted the data in the following manner: a wholistic view of recorded water depth data over the total duration of study; -A wholistic view of generated energy over a total duration of study; -A comparative assessment between water depth data and generated energy over the total duration of study; -A daily comparative analysis of rainfall data against generated energy per day from 8 am till 5 pm; - An hourly comparative evaluation of rainfall data with the generated energy as well as the statistical analysis for both the rainfall and generated energy. This measured and verified if the conducted test fulfilled the objectives of this research work.

The subsequent graphs show results for RWH conducted over 10 days and on an hourly basis of how much rain was harvested per hour.

Figure 6.1 - provides a graphical presentation of rainfall harvested over a ten day of study.

Figure 6.2 – provides an illustration of rainfall and power generated over a ten day of study.

Figure 6.3 – gives an indication of how much rainfall was collected and energy generated during the third hour of the experiment.

Figure 6.4 - shows what the experimental readings were during the eighth hour of the study over ten days.

Figure 6.5 -provides an indication of power generated over a tenday study.

Figure 6.6 – illustrates cumulative energy generated over a ten day of study.

Figure 6.7 – shows energy generated against rainfall when storage is 0% and 100%full.

Figure 6.8 – shows the relationship between PV and rainfall depth when storage tank is 0 % and 100% full.

Figure 6.9 – provides cumulative energy generated against actual rainfall depth during day seven.

Figure 6.10 – illustrates rainfall depth and energy generated during day 3 of validation.

Table 6.11 and table 6.12 provide the statistical analysis for both rainwater harvesting and power generation respectively.

For rainwater the mean values varied between 25 and 27. The median values ranged between 26 and 30 and the mode was 25 which appeared once, 26 appearing twice, 27 which appeared 6 times, and 30 appearing once. Thus the mode was 27 with the highest number of appearances. The minimum and maximum values were 8 and 32.

For table 6.12 – power generation the mean values ranged between 1.752 and 1.970. The median values were between 1.6 and 3.1 while the mode was 0. The minimum and maximum values ranged between 0 and 5.

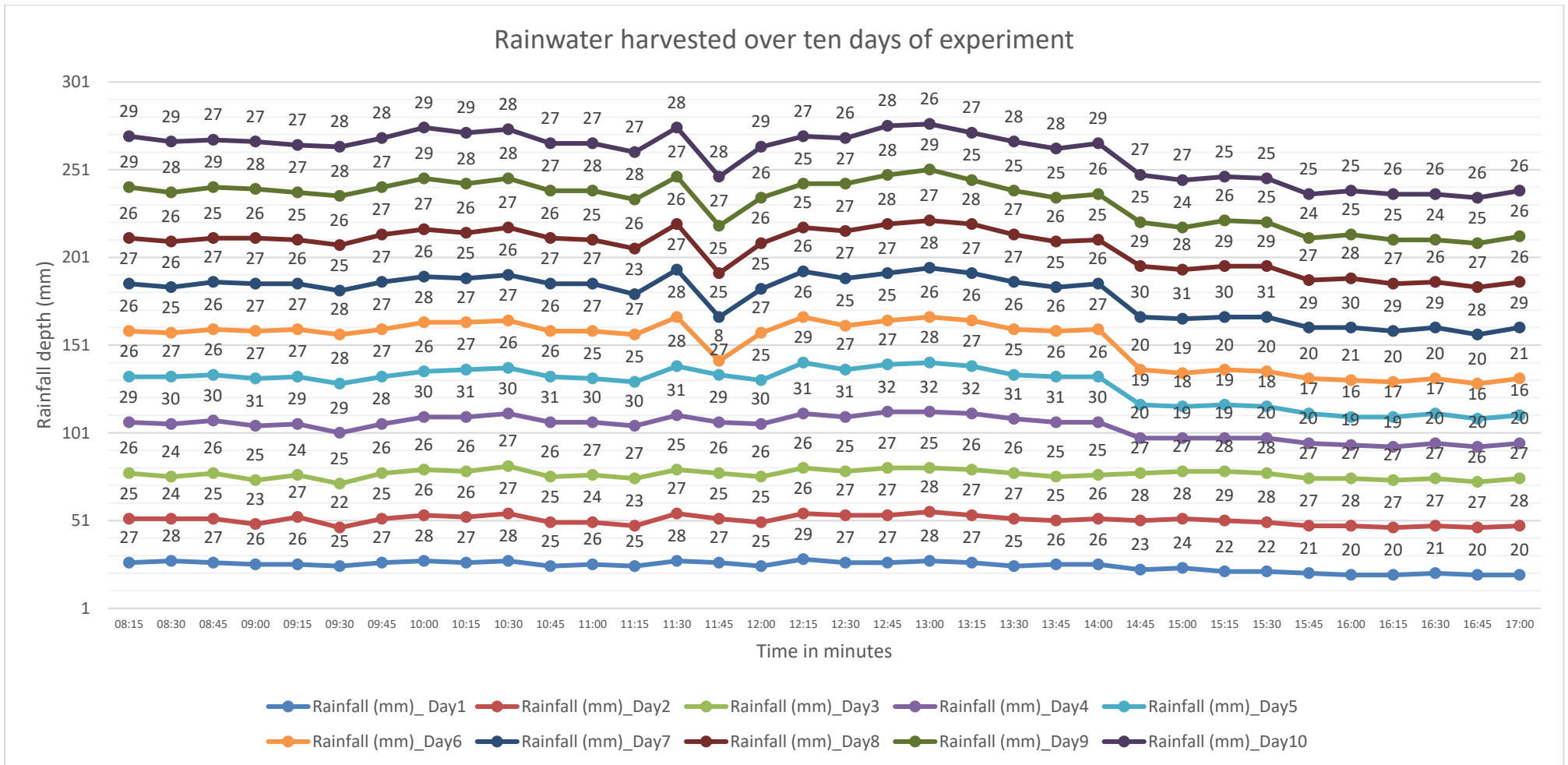


Figure 6.1 Recorded rainfall depths (mm) over a total duration of ten days of practical experiment

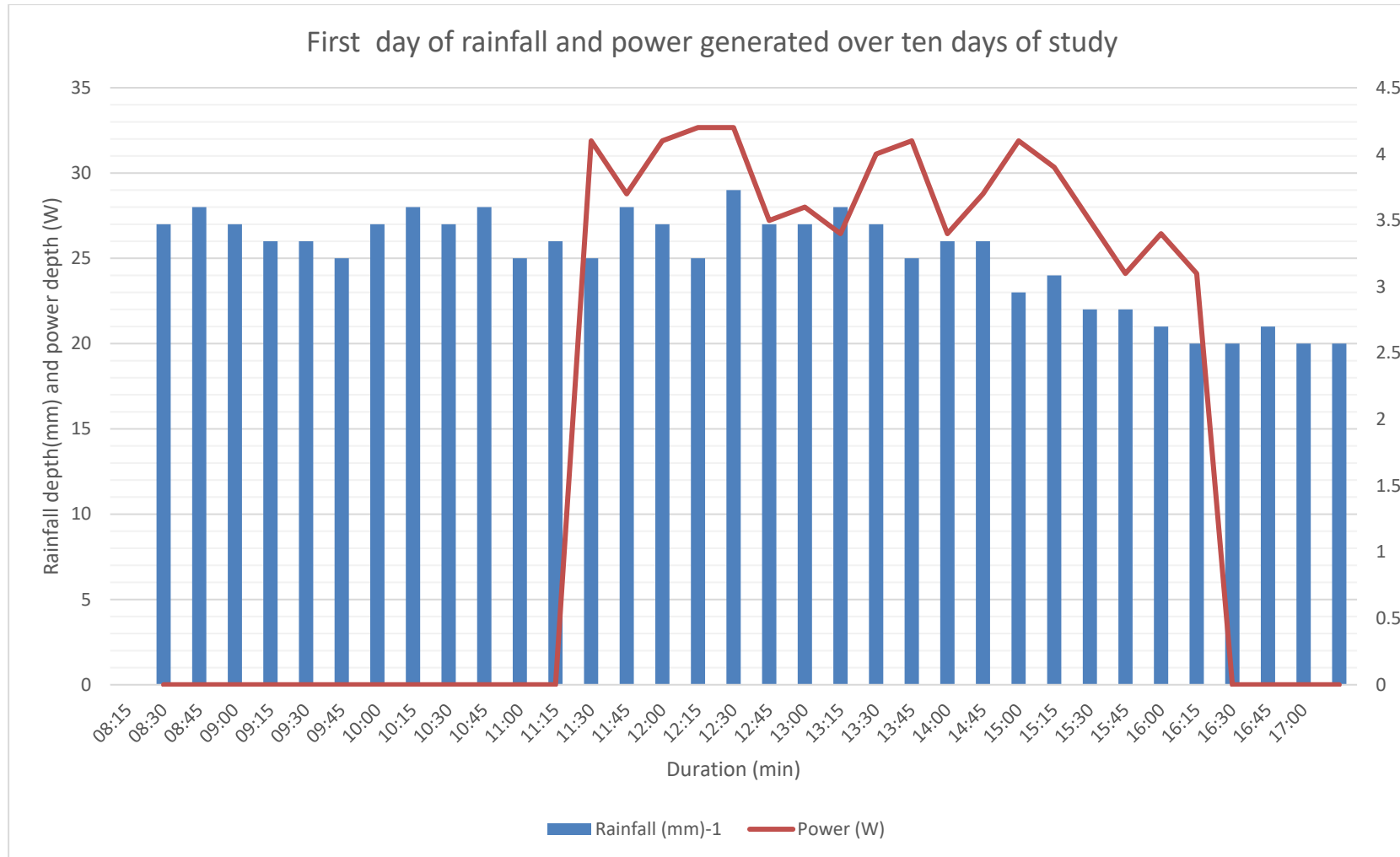


Figure 6.2 Graphical illustration of rainfall depth (mm) and energy generated (W) on the first day of the experimental work, resuming from 08:00 up to 17:00

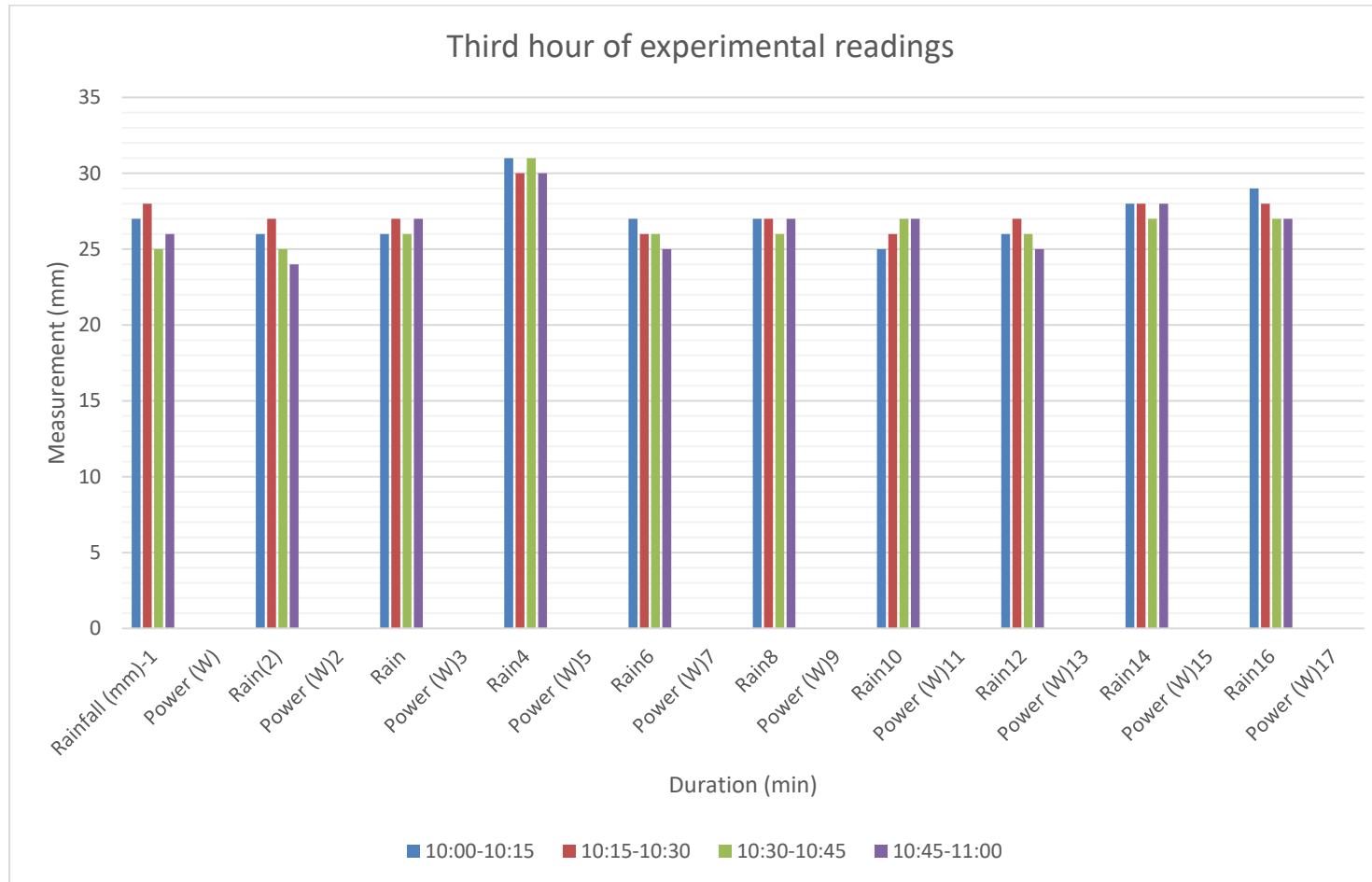


Figure 6.3 Graphical illustration of rainfall depth (mm) and energy generated (W) during third hour of experimental, resuming from 10:00 up to 11:00

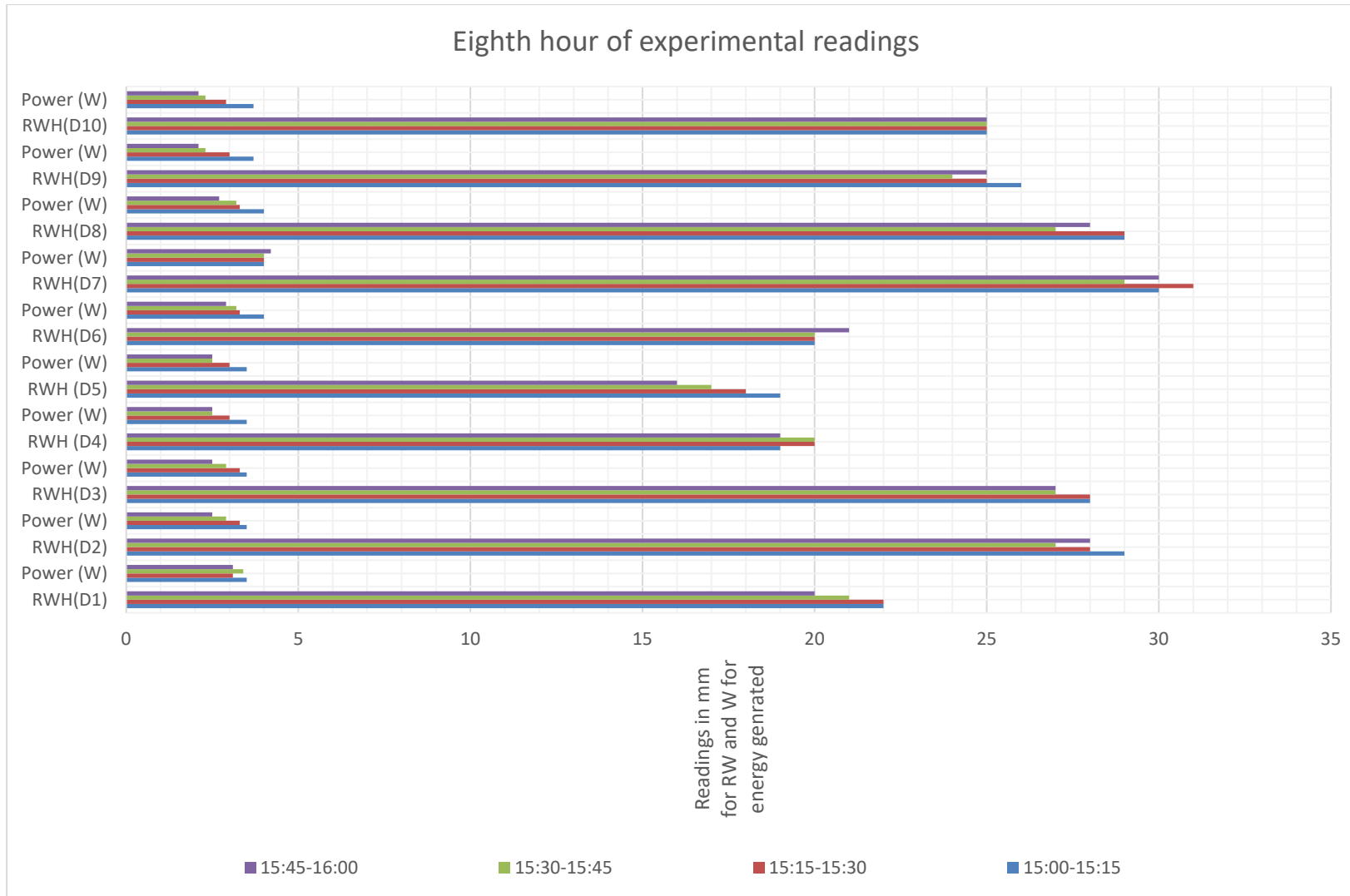


Figure 6.4 A bar graph presentation of rainfall depth (mm) and power generated (W) during eight hour of the experimental work, which took place between 15:00-16:00

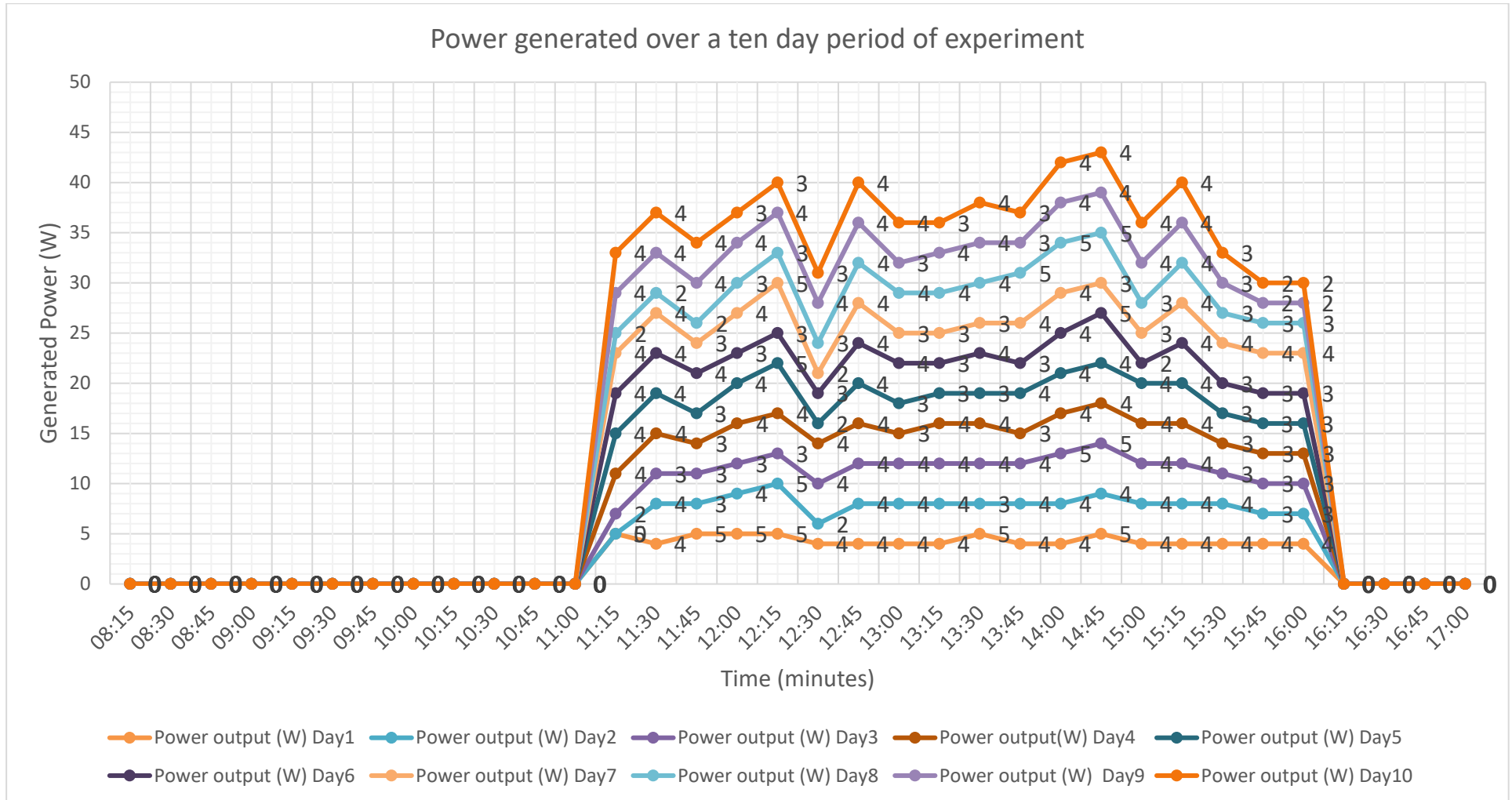


Figure 6.5 Energy generated presented graphically for the total duration of the experiment between 08:00 and 17:00

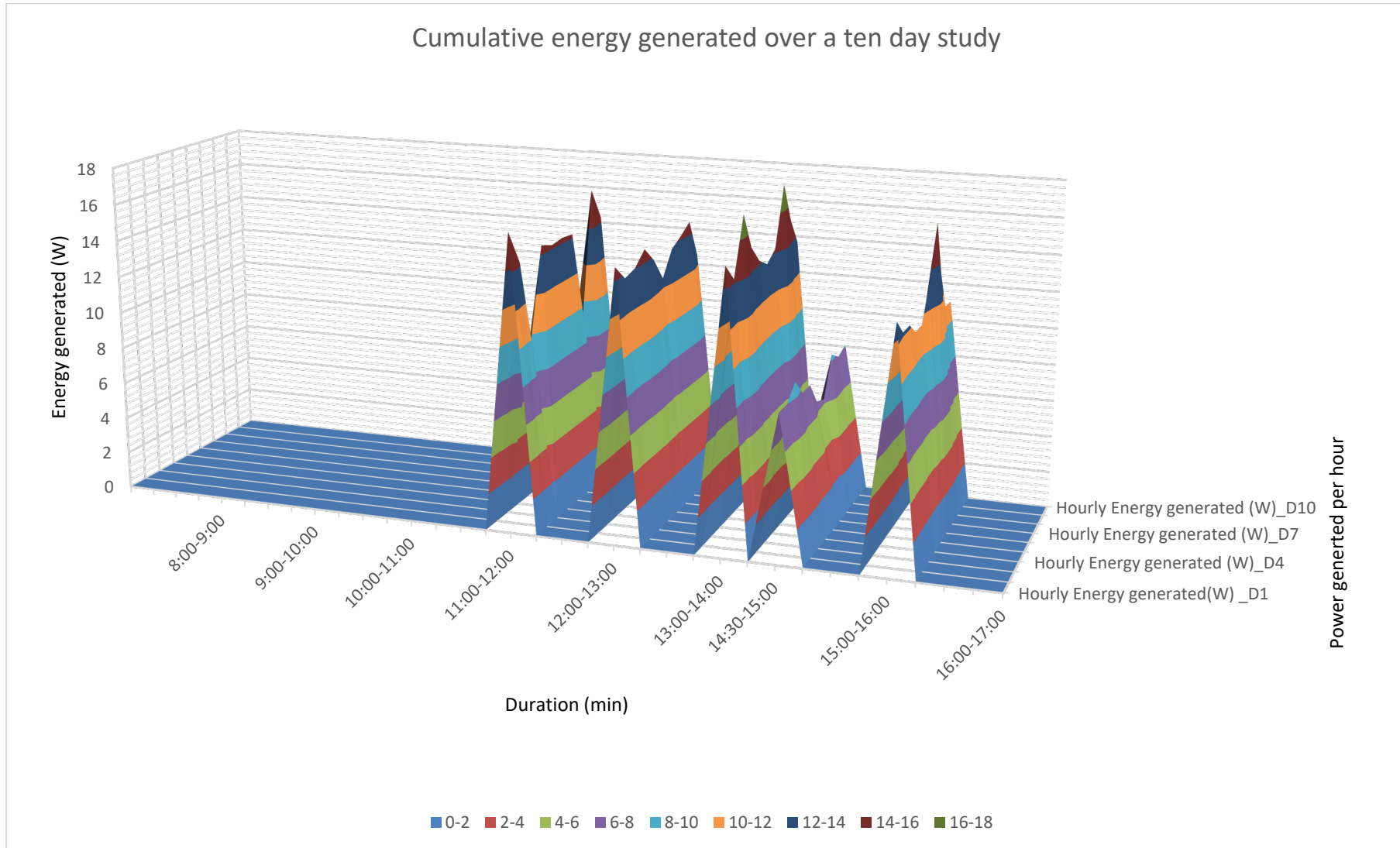


Figure 6.6 Graphical illustration of cumulative energy generated (W) during the 10 day period of study, depicting the total hourly energy generated

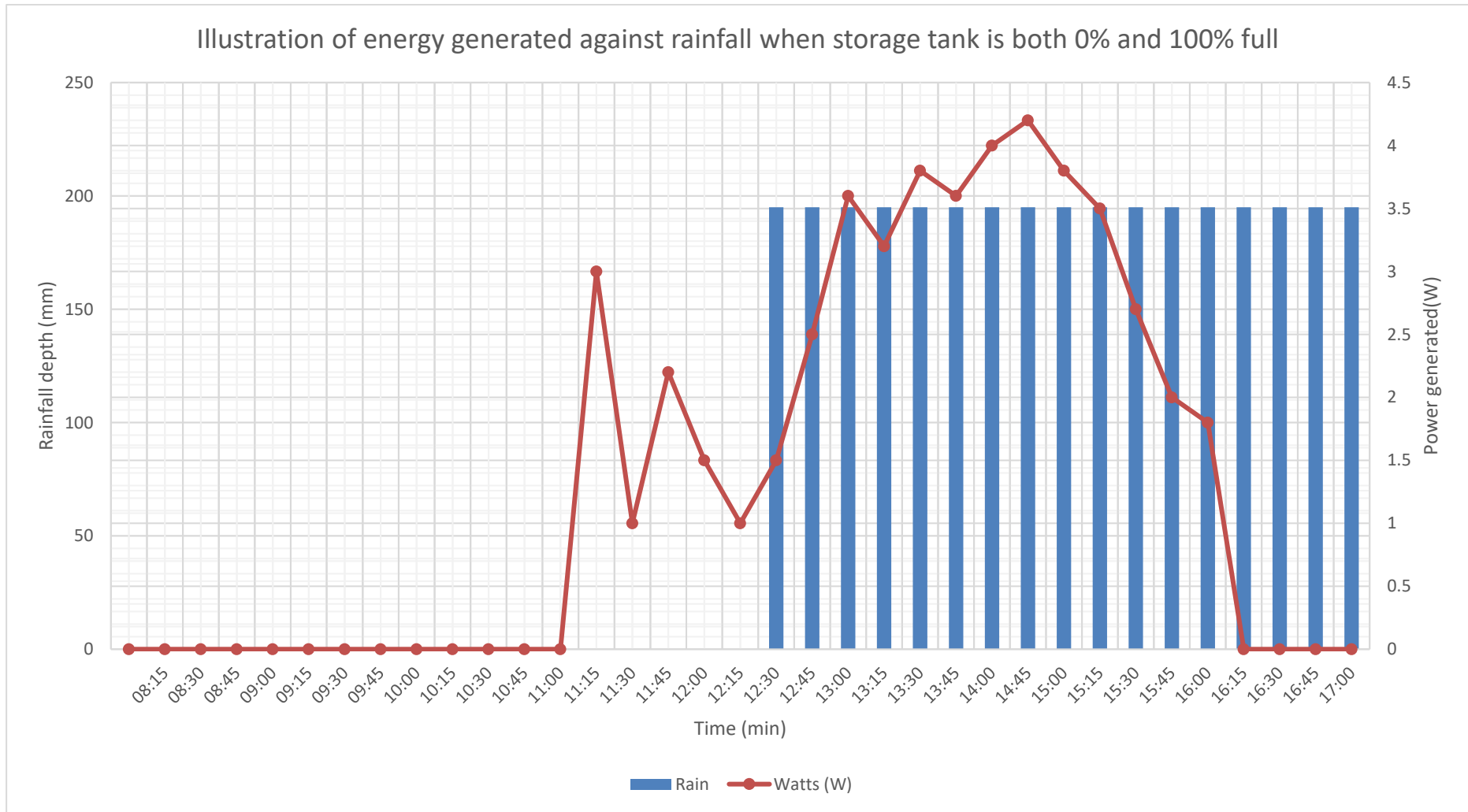


Figure 6.7 A clear graphical presentation of energy generated in Watts when the rainwater storage is both 0% and 100% full. Experiments were conducted from 08:00 – 12:00 when water storage was 0% and from 12:00 - 17:00 when water storage was 100% full.

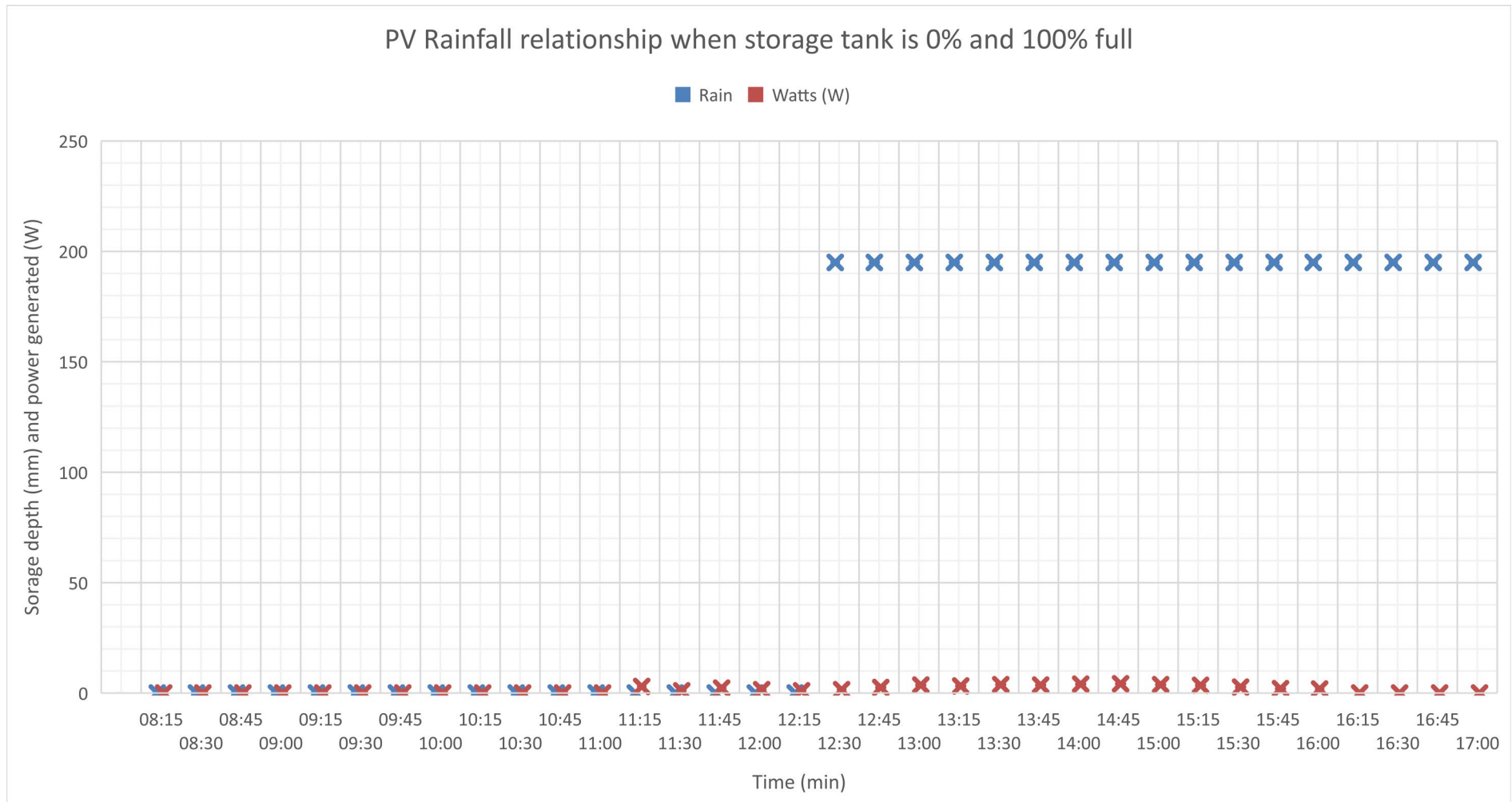


Figure 6.8 Graphical illustration of rainfall depth (mm) and energy generated (W) on the first day of the experimental work, resuming from 08:00 up to 17:00

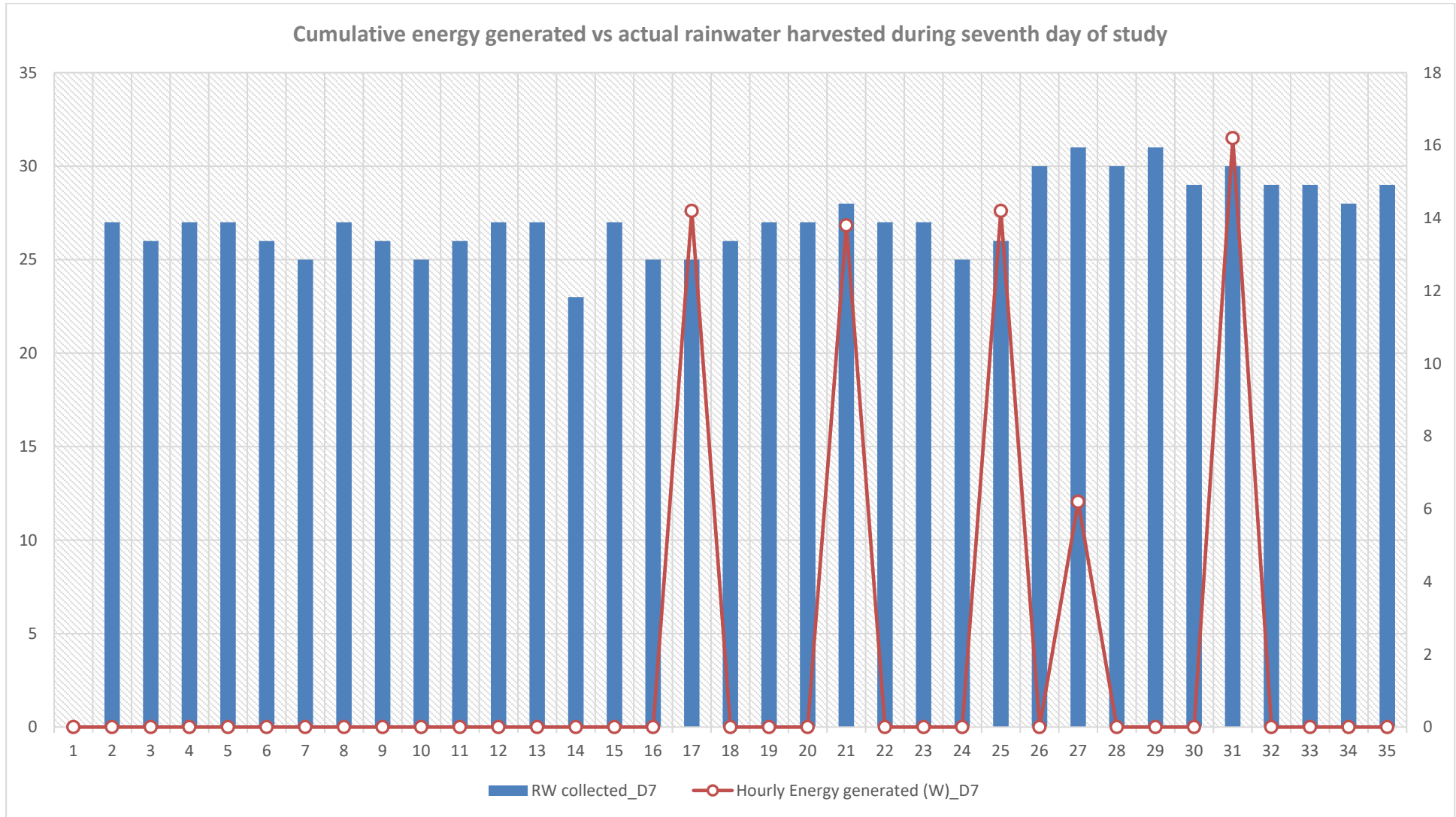


Figure 6.9 Graphical illustration of rainfall depth (mm) and energy generated (W) on the first day of the experimental work, resuming from 08:00 up to 17:00

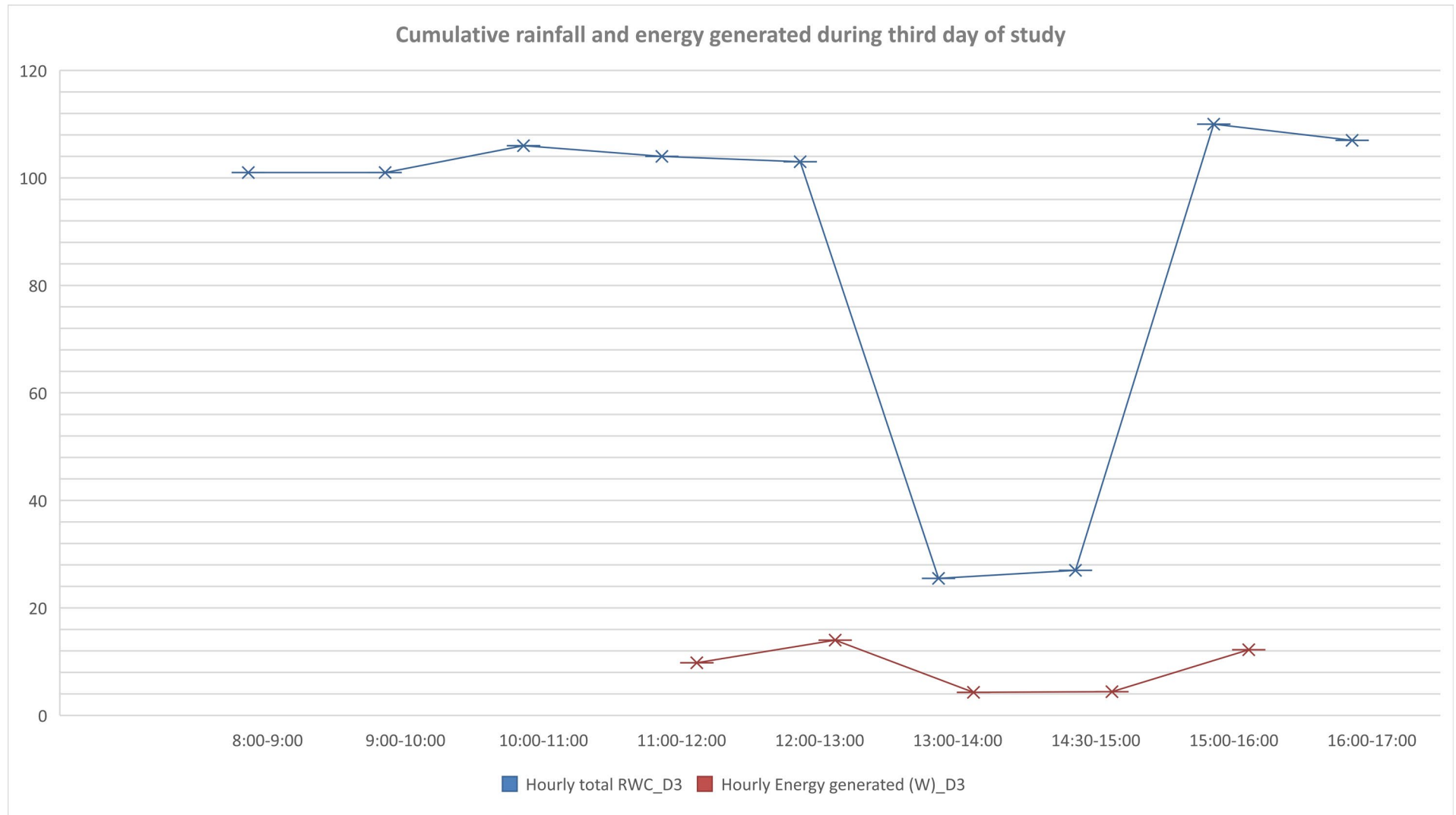


Figure 6.10 Graphical illustration of rainfall depth (mm) and energy generated (W) on the first day of the experimental work, resuming from 08:00 up to 17:00

Table 6.1 Statistical analysis for rainfall during the 10 days of study.

<i>Description</i>	<i>Rainfall - Day1</i>	<i>Rainfall - Day2</i>	<i>Rainfall - Day3</i>	<i>Rainfall - Day4</i>	<i>Rainfall - Day5</i>	<i>Rainfall - Day6</i>	<i>Rainfall - Day7</i>	<i>Rainfall - Day8</i>	<i>Rainfall - Day9</i>	<i>Rainfall - Day10</i>
Mean	25,08824	26,14706	26,11765	27,17647	23,85294	24,08824	27,20588	26,58824	26,55882	27,17647
Standard Error	0,47461	0,286762	0,172869	0,865738	0,758942	0,715711	0,323691	0,202997	0,274239	0,21722
Median	26	27	26	30	26	26	27	26	27	27
Mode	27	27	26	30	27	27	27	26	25	27
Standard Deviation	2,767426	1,672095	1,007989	5,048075	4,425356	4,173275	1,887429	1,183668	1,599075	1,266601
Sample Variance	7,658645	2,7959	1,016043	25,48307	19,58378	17,41622	3,562389	1,40107	2,557041	1,604278
Kurtosis	-0,72379	-0,08758	-0,37347	-1,18411	-1,00818	5,246636	-0,18958	-0,38112	-1,29779	-0,87409
Skewness	-0,74424	-0,65987	-0,24802	-0,85483	-0,86999	-1,93722	0,28776	0,533663	-0,01888	-0,16185
Range	9	7	4	13	13	20	8	4	5	4
Minimum	20	22	24	19	16	8	23	25	24	25
Maximum	29	29	28	32	29	28	31	29	29	29
Sum	853	889	888	924	811	819	925	904	903	924
Count	34	34	34	34	34	34	34	34	34	34

Table 6.2 Statistical analysis for energy generated from PV during the ten days of study.

	<i>PV - 1</i>	<i>PV - 2</i>	<i>PV - 3</i>	<i>PV - 4</i>	<i>PV - 5</i>	<i>PV - 6</i>	<i>PV - 7</i>	<i>PV - 8</i>	<i>PV - 9</i>	<i>PV - 10</i>
Mean	1,973529	1,835294	1,823529	1,873529	1,808824	1,776471	1,9	1,811765	1,908824	1,752941
Standard Error	0,327098	0,315886	0,315326	0,313803	0,312553	0,30731	0,325423	0,321449	0,32213	0,299442
Median	3,1	2	2,3	2,5	2	2	2,15	1,6	2,2	2,2
Mode	0	0	0	0	0	0	0	0	0	0
Standard Deviation	1,907292	1,841916	1,838652	1,829772	1,82248	1,791911	1,897526	1,874351	1,878324	1,746032
Sample Variance	3,637763	3,392656	3,380642	3,348066	3,321435	3,210945	3,600606	3,513191	3,528102	3,048627
Kurtosis	-2,04195	-1,82797	-1,75221	-1,99084	-1,79384	-1,75423	-1,8894	-1,68639	-1,99099	-1,87295
Skewness	-0,06358	0,125945	0,171083	-0,00852	0,148875	0,162582	0,092374	0,262732	0,018711	0,097375
Range	4,2	5	4,7	4,2	5	5	5	5	4,2	4,1
Minimum	0	0	0	0	0	0	0	0	0	0
Maximum	4,2	5	4,7	4,2	5	5	5	5	4,2	4,1
Sum	67,1	62,4	62	63,7	61,5	60,4	64,6	61,6	64,9	59,6
Count	34	34	34	34	34	34	34	34	34	34

6.2 Discussions

This chapter compares the outcomes obtained in Chapter 5, integrating the following design aspects of the research: the simulation, the autonomous design calculations for the building panel, the rainwater harvesting system, and the PV system. It should be noted that the applied theoretical strategies mentioned in Chapter 3 all form part of the verification and discussion process to conclude the verification of the design of a prototype building panel for rainwater storage and energy generation.

The research project conformed to the aims and objectives of this study to ascertain the success of the design of the prototype building panel for rainwater storage and energy generation. The objectives were;

- To determine the volume of rainwater harvested in a rainwater storage tank with inside dimensions of 314 × 50 × 195mm embedded in a building panel.
- To determine the power output of a 10W solar cell placed on a vertical surface of a building panel with 345 × 60 × 200mm outside dimensions.
- To determine the related costs for this technology.

6.2.1. Simulation

The simulation was employed in two stages: the standalone and grid-tied systems. Assessing both systems without bias is recommended when designing a system of this nature. However, for this research, the standalone system design was employed as a backup system to the grid-tied system; in the event of grid system failure, continuous power will be accessible through the battery system. The simulation process commenced with meteorological data employed for off-grid and grid-tied systems.

The simulation commenced with the meteorological data employed for both the off-grid and grid-tied systems. The location coordinates were Latitude: 33.93145S and Longitude: 18.6435E, both coordinates obtained from PVSyst. The tilt was 90°, Azimuth 0° and Albedo 0.200.

The optimal yield for transposition factor (FT) was 0.44, 0.73 and 1.32 for summer, annual, and winter, respectively. These factors are dependent on the transposition model that was selected. Depending on the transposition model chosen, FT typically ranges between 0 and 2.00 for the Perez model, whereas, for the Hay Model, FT ranges between 0.00 and 1.00. The transposition model chosen for this research was the Perez model, which could potentially have resulted in the high transposition factor, more so for the winter yield. Because FT was not part of the aim or objective of this study, a detailed review of the FT can be investigated further in another study; maybe these factors may impact this research simulation's results.

The loss concerning optimum values indicated high losses for summer yield and lower losses for winter yield. They were recorded as follows: 16.6%, 36.5%, and 57.2% for winter optimisation, annual optimisation, and summer optimisation, respectively. The summer losses were very high, followed by annual yield, then winter optimisation, a number of factors could have contributed, such as temperature, soiling, degradation, and wiring losses, amongst others, or there could be other factors resulting in such yields, that also could be examined. But, because this research is only limited to the aims and objectives of this study, no further investigations could be pursued in this regard, and time was limited to the main research.

Standalone System

A very detailed system design was employed for this study, and this process started with the preliminary design, which provided early-stage design results as a foundation for the system design. The same process was implemented for the grid-tied system.

A defined consumption composed of a 5W LED bulb, used for 4 hrs a day; an 11W mobile phone consuming power for 3 hrs a day; a 50W battery power bank consuming power for 2hrs a day and a 1W standby consumer using power for 24hrs a day had a total energy requirement of 177Wh per day. With the required consumption of 177Wh per day, the simulated preliminary design resulted in a nominal power of 77Wp with a battery capacity of 12V 69Ah autonomised for 4 days and a load loss of 5%, with power (P50) averaging 88Wp, meaning the system is expected to produce 88Wp on average.

The array was designed for an 80Wp 15V polycrystalline as the available power under generic PV modules, with V_{mpp} at 60°C equivalent to 15.8V and a V_{oc} at -10°C of 25V.

It must be noted that the V_{mpp} of 15.8V is greater than the PV voltage, which may mean the PV may be underperforming due to energy losses caused by improper harnessing of generated voltage. Safety concerns may also be created due to voltage discrepancies.

The charge controller, one of the critical components for the standalone system's voltage, must be compatible with the system's voltage to reduce mismatch or losses. It is vital to ensure compatibility between components is adhered to.

It is important to note that this research only adjusted values applicable to this study, such as the Wp, tilt, Azimuth, and battery capacity per the preliminary design for the MPPT controller. The generic system under the Universal Controller system was selected so that the research does not interfere with other values and only focuses on the aspects applicable to the aims and objectives of this study.

Upon selection of the 80Wp 15V PV module, the design parameters such as basic data, size and technology, and module parameters, no values were altered at this stage. The additional data and graphs were also explored. Under measured I/V in additional data, only the current and voltage information obtained from the field study were added.

MPPT controller

The universal controller was selected in generic mode, resulting in a yield and Maximum Power Point Tracking (MPPT) configuration with specified values of 1000W, 13V, 7A, and 2A for maximum charging and discharging currents, respectively. The design parameters of the controller, encompassing general data, thresholds, MPPT converter settings, efficiency profiles, and other relevant data, remained unchanged from their default values. Notably, the only modification pertained to the MPPT input value, adhering strictly to the applicable specifications.

Storage

According to the preliminary design, the battery storage capacity of 12V 69Ah is recommended. However, the closest battery capacity to the recommended design was 12.8V 103Ah

When we look at the charging time between the two

12.8 V 103Ah

$12.8 \times 103 = 1318,4Wh$

(6.1)

$1318.4Wh / 80$

= 15.45 hours to charge a 103Ah battery

But with the 12V 69Ah battery system

$12 \times 69 = 828Wh$

(6.2)

$828 / 80$

= 10.35hours to charge a 69Ah battery, on average PV sun-hours is available for 8hrs a day. This research points out certain issues that could be remedied within the study, but because storage was not part of the aims and objectives of this study, time and study were allocated to pertinent components aligned with the aims and objectives of this study.

The research analysed the battery pack system under the whole battery instead of the per-element option. The battery design parameters and the default information contained under basic data, detailed parameters, graphs, size and technology were not altered. All default values remained. This research mandate was to adhere to the aims and objectives and to obtain the corresponding results.

Standalone Simulation Results

The 80Wp solar performance ratio was rated 0.56, while the fraction was 0.954. The value of 0.954 meant the solar energy system met 95.4% of the solar demand. However, the solar performance value of 0.56 expressed as 56%, suggesting that the system suffered energy losses, hence the underperformance. The recommendation is to improve the voltage, as previously mentioned, as the voltage variation would impact the energy losses. And other factors need to be observed to improve the system's performance and efficiency.

There are default values that were not altered, and for the next phase of this study, these default figures may require amending to accommodate in-depth research of this project.

For the normalised production and factor loss, the simulated results yielded the following:

Unused energy was 22%, PV array losses accounted for 15.7%, the system loss battery charge was 5.9%, and energy supplied to the user was 56.4%

The energy lost in the system with unused power in total was equivalent to 43.6%, and only 56.4 % of power was supplied. Some contributing factors to the factor loss include thermal parameters, string mismatch voltage, soiling IAM losses, degradation and module quality mismatch, which include string voltage mismatch and module mismatch losses.

Loss Diagram outcomes produced the following: GHI produced 1931kWh/m², with a loss of -29.28% from the Global incident collector plane and a further -7.04% loss from the IAM factor on Global, bringing a total of 1270kW/m². Effective irradiation on collectors for PV conversion was 15.52% efficiency at STC.

The array's nominal energy at STC efficiency was 101.6kWh. With losses in the system which included the following: -1.11% PV loss due to irradiance level, -4.98% PV loss due to temperature, +0.71% Spectral correction, +0.75% module quality loss, -0.00% module array mismatch losses, -4.80% Ohmic wiring loss, -26.07% unused energy (battery full), 68.1 Effective energy at output of the array, -5.15% converter loss during operation (efficiency). 64.6kWh converter losses efficiency overload. 85.6% of Battery storage. 4.4% was directly stored, and 4.55% was missing energy, equivalent to 2.9kWh. From the battery storage of 64.4kWh -0.02%, -3.31%, -3.28% and -1.27% were losses incurred due to battery stored energy balance, battery efficient loss, charge/discharge current efficiency and battery self-discharge current, respectively. 61.7kWh of energy was supplied to the user, and 64.6kWh of the user's energy needs were supplied.

Grid-tied system

The grid-tied system also commenced with the preliminary design. The site's meteorological data was defined as similar to that of the off-grid system. The system design required nominal power. Thus, based on the consumption, as detailed in the standalone system, of 177Wh/d, the nominal power was established at 0.18kWp, tilt of 90°, Azimuth 0° and Albedo 0.200. During the preliminary design, the system specifications were required to ensure adequate and relevant information was added for preliminary analysis when generating simulation results. The relevant information included module type, where the standard was selected; technology, polycrystalline was chosen; ventilation, fully insulated was selected; and mounting disposition, where façade / tilted roof was selected. The façade was more relevant to the research project specifications. With the specified information, the research attempted to adhere to conditions similar to those at the practical site.

A) Preliminary design

The input values were the tilt 90°, Azimuth 0°, and the estimated total required energy from the standalone load determination of 177Wh per day. The simulated preliminary results yielded a PV system with a nominal power 200Wp.

B) The PV system designs

A 200Wp 25V polycrystalline system was selected under generic PV modules, sizing voltage at operating conditions, where V_{mpp} at 60°C was 26.3V r.u.t 26V and V_{oc} at -10°C was 41.7V r.u.t.47V. The design parameters included basic data, sizes and technology, model parameters, and additional data, incorporating IAM, measured I/V, low light data, commercial data, and graphs.

The important aspect in this regard is the P_{mpp} of the model, which should not be greater than the $V_{mpp} \times I_{mpp}$ specified data at STC. This may present a discrepancy resulting from numerous reasons, such as inconsistent manufactured data or the RShunt value that has not been gauged appropriately.

Some of the manufacturer's specifications included:

Irradiation reference measured at 1000W/m², temperature reference of 25°C, $I_{sc} = 8.630A$; $I_{mpp} = 8.330A$; $V_{oc} = 37.40V$; $V_{mpp} = 30.00V$, Temperature coefficient = 4.3mA/°C or 0.050%/°C with 60cells in series. Whereas the internal resulting tools was measured as follows: $P_{mpp} = 251.5W$; Operating temperature = 25°C; $V_{oc} = 37.4V$; $V_{mpp} = 30.7V$; $I_{mpp} = 8.18A$; $I_{sc} = 8,63A$; cell area = 17.07m²;

To evaluate if the P_{mpp} is not greater than $V_{mpp} \times I_{mpp} = 30.00V \times 8.330A = 249.9W$, whereas the maximum power point under operating conditions was 251.5W >249.9W therefore, we first verify if nominal power falls within 0.2% of nominal power given by: (+/-) 0.2/100 x 250 = (+/-)0.5 +250 = 250.5 or 249.5. This value is compared to the P_{mpp} , thus 251.5W > 0.2 x Nominal Power. Therefore, in this regard, V_{mpp} or I_{mpp} or both V_{mpp} and I_{mpp} will need to be adjusted. The resulting value may impact the performance ratio when not adjusted.

The model parameter examined in detail is the RShunt – Rserie. RShunt exponential examines the relative efficiency, which measures the low light performance. Low light performance depends on increasing RShunt, increasing RShunt (0) and increasing Rserie. RShunt is given by the following formula:

$$RShunt = V_{mpp} / 0.2 \times (I_{sc} - I_{mp}) \quad (6.3)$$

The low light performance is vital for module performance, and it guarantees effective energy production under several lighting conditions.

C) Inverter

The compatible inverter to the 250W 25V polycrystalline module was a 0.25kW 22-55V 50/60Hz BDM-300 manufactured by Northern Electric Power inverter. With an input maximum voltage of 60V, an output voltage of 240V, and a global invert power of 0.3kWac.

The inverter design parameter included main parameters which provide specific inverter design details such as:

Input side (DC PV field) - Minimum MPP voltage of 22V; Maximum MPP voltage of 55V; the absolute maximum power of PV voltage was 60V; Power Threshold given as 1.250, which was calculated from:
 $= 0.5\% \times Np$
 $= 0.5/100 \times 250W = 1.250W$ (6.4)

It should be noted that the power threshold may not necessarily be a model requirement. However, maintain consistency in automatically built profiles.

The Output side AC grid – Monophase with a 50 and 60 Hz frequency. A grid voltage of 240V, nominal AC power of 0.250kVA, maximum AC power of 300kVA, nominal AC 1.040A, maximum AC 1.040A.

The maximum efficiency was measured to be 98.50%.

Grid-tied system simulation results

For the Performance ratio of a 250Wp grid-tied system, the performance ratio was 0.802, which translates to 80.2%. This is 80.2% of the energy produced for the energy production of an ongoing system at nominal STC efficiency.

In normalised production and loss factors, the collection loss (PV-array losses) amounted to 16.1%, the system loss in the inverter was 3.7%, and the useful energy produced was 80.2%.

Under normalised production per installed 250Wp, PV array losses accounted for 0.6kWh/kWp/d, whereas inverter system loss was 0.14kWh/kWp/d while produced useful energy was 3kWh/kWp/d.

Loss Diagram outcomes produced the following: GHI produced 1931kWh/m², with a loss of -29.28% from the Global incident collector plane and a further -7.04% loss from the IAM factor on Global, bringing a total of 1270kWh/m². Effective irradiation on collectors for PV conversion was 15.46% efficiency at STC.

The array's nominal energy at STC efficiency was 319.2kWh. With losses in the system amounting to 273kWh, these losses included the following: -3.81% module degradation, -1.14% PV loss due to irradiance level, -5.43% PV loss due to temperature, -0.22% Array mismatch losses, -0.76% Ohmic wiring loss (Array virtual Energy Np) amounted to 286.4kWh. Inverter loss during operation (efficiency) was -4.73%. The ultimate yielded power was 273.9 kWh of active energy at inverter output and 273.9 kWh of Active energy injected into the grid.

6.2.2. Calculations

One of the theoretical strategies applied was design calculations. These are detailed in Chapter 4, including the NLB building panel design calculations, the bolt design calculations, the rainwater storage calculations and the solar PV calculations. The latter were autonomously designed.

The NLB building panel and bolt design

The designs were in accordance with SANS 10162 and SANS 2001:CSI, which provide guidelines for structural steel design and punching of holes for bolts, respectively. The corresponding codes were used as a guideline in compiling the designs for building and the structural use of steel. For the building panel design, it must be noted that the structural design only focused on the NLB structures, utilising both external and internal dimensions of the building panel and rainwater storage tank, respectively. The design encompasses self-weight and live load, resulting in ultimate load (Pu). These design calculations also included bolt calculation, assessing the bolt in shear and tension.

The design took into cognisance the self-weight of the panel to assess if the panel would withstand the loading of the RW storage tank, which is one hundred percent full. It was determined that the panel weighed 5.175kg with a strength of 735 N/m².

The calculations were based on the 3D-printed prototype building panel for an mBP.

It was determined that the area of the building panel was 0.069m² with a volume of 4.14x10⁻³m³. The mass composition was calculated to be 5.175kg, yielding a self-weight of 50.757N. Thus, the NLB panel strength was calculated as 735N/m². Therefore, the self-weight of the panel is 50.757N.

The live load was calculated assuming the RW storage tank was 100% full. An iBP produced an area of 61.23x10⁻³m², and the volume was calculated as 3.0615x10⁻³ m³ of rainwater the tank can collect, which was converted to litres, yielding a rounded figure of 3,0ℓ. The latter yields the force and strength of an RW collection system as 30.33N and 490.5kN/m², respectively.

This means the NLB building panel with a self-weight of 50.757N can withstand a RW storage tank with a self-weight of 30.33N when it is 100% full.

The rainwater storage tank is made from a polymer-based product called PLA; bolts are required to affix the panel to the connecting wall. Therefore, the design includes bolt design calculations that can

withstand the ultimate load, a combination of the dead load and the live load given by $P_u = (1.2 \times \text{Deadload}) + (1.6 \times \text{Live load})$ equation, yielding 1.67 kN/m^2 .

Once the bolt diameter is known, the first requirement is to check the minimum pitch, which is a distance between bolt hole centres taken to be $2.7 \times$ the bolt diameter. Bolt pitch is usually located along the longitudinal axis of the plate.

The next requirement is to calculate the minimum edge distance, defined as the minimum permissible distance between the centre of the bolt and the edge of a load-carrying element. The minimum edge distance was calculated in accordance with Table 8 of SANS10162 clause 22.3.2 and is taken as $1.5 \times$ bolt diameter.

During design, when determining the edge distance, the design is okay if the calculated value is less than the edge distance. However, if the calculated design value exceeds the minimum edge distance, the edges will likely tear, collapsing the structure. Bolt shear failure must be avoided. Therefore, to prevent the edges from tearing, several options can be considered, such as reducing the bolt size provided the tensile strength of the bolt was in accordance with SANS10162, a study provided and option highlighted (Puthli and Fleischer 2001) the need to suitably reduce the design bearing resistance by $2/3$ for loads in shear. The design shear force must be smaller than the design shear resistance.

The next step was calculating maximum tension (T_u) and tension resistance (T_r). The design was okay when the tension resistance exceeded the maximum. Also, the maximum shear (V_u) and shear resistance (V_r) were simultaneously calculated where the design was safe. Therefore, this results in shear resistance greater than the maximum shear. Furthermore, the factored bearing resistance was determined as given in SANS 10136-1 clause 13.10(c), referred to as the maximum load the support can endure given by Bearing of bolts (B_r) = $\phi_{br} \times a \times t \times n \times f_u$ if $a < 3d$ and Bearing of bolts (B_r) = $3\phi_{br} \times t \times d \times n \times f_u$ if $a > 3d$, where ϕ_{br} Equals to 0.67. When a is greater than $3d$, the design is safe. However, when it is less than $3d$, the plate is tearing. Change plate thickness or bolt sizes.

The rainwater storage system design

The designs were conducted per SANS10400, a set of National Building Regulations, and SANS10400 - part H, a National Building Regulations for rainwater harvesting and water storage systems design and construction.

The dimensions of the rainwater storage tank are as detailed with iBP, which produced an area of $61 \times 10^{-3} \text{ m}^2$ and a volume of $3 \times 10^{-3} \text{ m}^3$ which, when converted to litres, yielded 3ℓ . The storage tank mass was 3.0615 kg , and it possessed a self-weight of 30.033 N . The self-weight calculations were conducted to verify if the NLB panel can withstand the RWS tank self-weight.

From the simulated rainfall, the average value of maximum and minimum / $2 = (120 + 66) / 2 = 93 \text{ mm/hr}$ signifies heavy rainfall for the measured period. This amount of rain can lead to flash floods and other weather-related risks. However, the calculated flow rate of $3.4 \times 10^{-6} \text{ m}^3$ is significantly low for practical rainfall applications and may be considered rainfall showers. In some instances, it may include extremely light rain with very fine raindrops, resulting in a significantly slow flow rate compared to other rainfall events. Also, the corresponding velocity of $5.6 \times 10^{-6} \text{ m/s}$ is significantly low, which results in stagnating rainfall movements or may even pose as a misty rainfall or light drizzles.

PV Design

The PV design was in accordance with the SANS 10400-XA and SANS10142, which provide guidelines on energy usage in building and wiring of premises, respectively. The PV panel dimensions were given as $345 \text{ mm} \times 200 \text{ mm}$.

The objective was to determine how much power a 10W polycrystalline FSC can generate when placed on a 90° vertical surface.

The initial design calculation was to determine how much energy was generated per hour, given an average period of 5.5 hours, an average sun hour, and an average sun hour value for South Africa for optimum sunshine hours and optimum power output. The energy generated yielded 55Whrs, and the energy generated considering a performance ratio of 75% yielded 41.25Whr. For a full day's operation, the total energy generated per day was 2.29W/day.

Further, the system viewed the maximum open circuit voltage (V_{ocmax}), a fundamental design parameter for PV, and considered safety, system design, compliance, and efficiency. Meanwhile, V_{mpp} describes the module performance and is typically provided in the datasheet. Where maximum power output, system design, matching inverter, and energy output all highlight the significance of the V_{mpp} and the input V_{mpp} has on each latter, it is also described as the point of the current-voltage (I-V) curve when PV operates efficiently; thus, it is the voltage at a specific point.

V_{ocmax} is the maximum open circuit voltage, which takes into account a minimum operating temperature of 5°C, standard test conditions of 25°C, temperature coefficient of -0.137%/°C, and the open circuit voltage of 10V, all yielding a maximum operating voltage of 12.7V. While the V_{mpp} considers the local minimum temperature given as 40°C, nominal operating cell temperature (NOCT) assists in estimating performance to calculate efficiency to size and design the system and provide durability and warrants the system. The NOCT was 45°C, the STC was 25°C, temperature coefficient was -0.137%/°C and the voltage was 10V which all yielded 2V

V_{mpp} was calculated as 2V, and the V_{oc} was determined as 12.7V. It must be recognised that V_{oc} is always bigger than V_{mpp} .

6.2.3. Systems Validation

The analysis was subdivided into three categories: hourly evaluation, daily evaluation and the evaluation where the RWS tank was zero percent full and one hundred percent full. Where the RWS tank was one hundred percent full, the FSC was evaluated for improved efficiency when energy values were in their raw and cumulative forms. The evaluation period was conducted every fifteen minutes to assess how long it took to fill the RWS tank while evaluating the energy generation and how it impacted its efficiency. Also, in this same evaluation, the energy generation was compared in two stages, in its raw and cumulative values, to assess if the efficiency of the FSC is influenced by water in the RWS tank.

The readings were taken every 15 minutes, and hourly output data was computed for water collected and PV generated. Because of the size of the prototype building panel with a depth of 200mm, water spillage will occur once the depth reaches the maximum depth.

During the initial three hours of the validation process as shown in figure 6.3, the RWS tank underwent three fillings, reaching water levels of 108mm, 106mm, and 106mm for hours one, two, and three, respectively. No energy was generated during this period, as shading from adjacent buildings resulted in zero readings from the PV system. However, starting at 11:00, corresponding to the fourth hour of validation, the PV system recorded its first reading of 4.1W. On the first day, with an accumulated rainfall of 105mm, the PV generated an average of 4.1W, while a cumulative of 16.1W was recorded against 105mm of collected rainwater (RW).

Between days 2 and 4, cumulative energy generation during the fourth hour was 14.2W, 9.8W, and 14.5W, with corresponding RW collection of 100mm, 104mm, and 120mm. From days 5 to 7, cumulative energy generation at the fourth hour was 14.2W, 14.3W, and 14.2W, matched with RW storage at 105mm, 90mm, and 100mm. Days 8 to 10 as shown in figure 6.5 have a cumulative RW collection of 103mm, 108mm, and 112mm, alongside cumulative energy generation of 8.5W, 16.1W, and 14.3W.

In the fifth hour, cumulative harvested RW from day 1 to day 4 was 111mm, 108mm, 103mm, and 126mm, with corresponding cumulative energy values of 14.7W, 13.8W, 14W, and 14.7W. From day 5 to day 10, cumulative energy against RW harvested was 13.8W, 12.5W, 13.8W, 14.2W, 14.7W, and 12.5W, while RW values were 111mm, 102mm, 108mm, 107mm, 109mm, and 107mm.

Hour six resulted in cumulative RW collection and energy generation for days 1 to 10. Despite a 30-minute loss, in the seventh hour, they provided conclusive data with the lowest values during the 10-day validation. In the eighth hour as shown in figure 6.4, from 15:00 to 16:00, they demonstrated higher PV generation than stored RW quantities. Seasonal sum-hours variations were considered, with energy generation ranging from 11.0W to 16.2W.

The ninth hour, between 16:00 and 17:00, it yielded 0W due to sunset, orientation, and shading from surrounding buildings. Subsequent testing of the RWS tank showed increased energy generation when filled, ranging from 8.6W to 14.6W, indicating the cooling effect on the FSC and the enhanced efficiency of direct contact between FSC and simulated rainwater during the verification process.

The volume of water a panel of this size can generate is 3 litres. A collection of rainwater from ten building panels can generate 30 litres. However, as previously mentioned, the building panel size can be adjusted according to end-user needs. With the water consumption in SA amounting to 237 litres per capita per day (Jay Gohel, Hina Bhatu, 2020), with sufficient rainfall and rainwater collection, the building panel is built to size in accordance with end-user needs, the building panel is capable of storing sufficient rainwater to meet the demand.

6.2.4. Costs

The prototype costs provide a baseline for estimating the actual scalable model. The cost analysis developed for this study was to fulfil the objectives of this research.

The prepared project costs included some pertinent aspects required in prototype development. These formed the material costs, the import costs and components, sundries, health and safety, and the revenue table, with profit valued at 2.5x costs. These engineering fees account for 15% of the costs, accounting fees account for 15%, installation fees account for 10%, and wastage account for 15% of the total cost. The professional fees at 15% yielded R3655.14 each, whereas installation and wastage yielded R2436.76 and R3655.14, respectively. The total for the revenue was recorded as R37 769.83. The expense, including administration, stationery, communications, insurance, rental space, transport, services and other unaccounted expenditures, roughly equated to R38700.00.

The profit margin was calculated as the difference between revenue and expenses, which yielded R39235.30. This means this project can profit 36%. Other factors that need to be considered are exchange rates, consumer price index, which affects inflation, labour costs, excise and duties, and logistics to understand the profit margin fully. However, a well-written business plan needs to be put in place, and utilising the preceding information as a guide for this business model, implementing a proper business plan will modify the financial implications.

6.3 Conclusion

The main purpose of this research was to design a prototype building panel for rainwater storage and energy generation. Practical and theoretical strategies were employed. These strategies were aligned with the aims and objectives of this study. Detailed discussion and results are contained in this chapter and the

preceding chapter (Chapter 6 and Chapter 5). An in-depth study of a building panel for rainwater storage and energy generation is required. The building panel emulates the conventional-sized building panel, which will further assess the performance of these combined components for four complete seasonal cycles and provide more accurate readings. With this research work objectives, the results discussed under the results and discussion chapter show the research's success and that the goals have been met. The design of a prototype building panel for rainwater storage and energy generation is novel and unique. The engineering body of knowledge has illustrated autonomous designs for building panels, rainwater storage and energy generation. However, it has not shown a design for a building panel with combined crucial and value-added technologies working in unison. Therefore, the design of a building panel for rainwater storage and energy generation is exceptional and innovative.

Chapter 7 Conclusions and recommendations

South Africa's population growth has resulted in an amplified dependence on fundamental services such as water and electricity from municipalities. This surge is directly correlated to the effects of climate change. Providing clean, sustainable, and reasonably priced water and electricity to rural communities is pivotal. Against this backdrop of challenges, this research has developed a prototype building panel that facilitates rainwater storage and energy generation. The study employed an innovative design approach that was geared towards achieving the research objectives. The study's outcome summarizes the work conducted to accomplish various design aspects and recommends areas for further research to improve the prototype.

7.1 Conclusions

This research aimed to design a prototype building panel for rainwater storage and renewable energy generation. The prototype design was conducted at CPUT computer labs with the assistance of the mechanical engineering department. The 3D printing for the prototype was done at Netram Technologies, while the flexible solar cell and its components were imported from China through D&S Technologies. The PV system and its components were interconnected under the guidance of a skilled technician. Conclusions were independently derived as measurements were taken autonomously despite the symbiotic nature of the system.

The following conclusions were drawn from the study, which incorporated theoretical and practical studies, and these conclusions were aligned with the objectives.

1. Upon thorough examination, it has been ascertained that the building panel can harness a total of 3.06ℓ of rainwater. From a practical standpoint, the panel was observed to achieve a depth of 195mm, thereby resulting in the successful harvesting of 3.0ℓ of rainwater.
2. Based on theoretical analysis, it has been determined that a photovoltaic (PV) panel with a power rating of 10W can generate 55Whrs of energy. In contrast, empirical data from practical experimentation indicates that the maximum cumulative power output obtained from a vertical surface was 16W. Nevertheless, the research objective has been successfully achieved.
3. It has been determined that the cost estimate associated with the building panel is valued at eleven thousand two hundred and three rands and eleven cents (R11203,11). However, in light of the findings, it is recommended that further research be conducted to assess the feasibility of the system and to explore available incentives for rural communities. Furthermore, a research and development study is suggested to accommodate affluent communities and businesses.

The construction of a prototype and its testing process described the equipment and methods used to collect consistent test data, which were analyzed utilising a quantitative data analysis method developed in Excel.

The theoretical component of the research project included simulation, model, design calculations, material selection, and costs. The simulation was conducted for both grid-tied and standalone systems.

The model incorporated drafting and drawings such as 2D and 3D CAD, SolidWorks, and pre-model preparations. The design calculation included autonomous calculations for building panel design, RWH and PV design. Lastly, it provided detailed prototype calculations, including building costs, revenue, expenses, and predicted profit and losses.

A rainwater collection and energy generation building panel was constructed using 3D printing technology at Netram Technologies. The PV technology and components were sourced from China through D&S Solutions. The assembly process involved intricate wiring and connecting the Maximum Power Point Tracker (MPPT) to the PV system and battery. At the same time, the building panel was attached using a specialized adhesive marine sealant. The validation process included simulated rainwater events and PV recordings, with data documented using Microsoft Excel.

The design calculations followed SANS codes of practice. Calculations were conducted to verify the structural strength of the NLB building panel, bolt, and RWS system design. The link between the NLB building panel and the rainwater harvesting system was considered to ensure that the building panel's structural strength and the bolt design could withstand the RW harvesting system when the rainwater tank is filled to 100% capacity. The calculations showed that the NLB panel could withstand the RWS with 100% water capacity.

The prototype building panel with a flexible solar cell was tested for collecting rainwater and generating energy. The highest cumulative rainwater harvested was 126mm, with 15W energy. The prototype was assessed with 0% and 100% full capacity, generating a cumulative of 7W and 15W, respectively. The results show this project is doable and has room for improvement.

The cost analysis was conducted to provide a baseline. Costs were broken down into direct and indirect categories, including materials, miscellaneous expenses, OH&S, estimated revenue, estimated expenses, and estimated profit/loss. Other cost considerations should be factored in for a more accurate estimate. The project looks profitable, and government incentives may be available.

This research aimed to design a unique building panel for rainwater storage and energy generation. The results of the study show that the objectives were met. The design is exceptional and innovative, combining crucial technologies. Further in-depth study is needed to assess performance over seasonal cycles.

In summary, integrating rainwater storage and energy generation within a building panel presents a promising and sustainable solution for addressing water scarcity and energy needs. This approach contributes to resource conservation, promotes environmentally friendly practices in the construction industry, and is affordable. The design of this panel emphasizes the optimization of rainwater collection and storage efficiency while also incorporating energy generation components to harness renewable energy. This dual functionality enhances the panel's versatility, making it ideal for a wide range of applications in both rural and urban settings. Thus, this innovative solution is highly recommended, prioritising sustainability and conservation and working towards a more environmentally conscious future.

7.2 Recommendations

Selecting durable and weather-resistant materials for building panels is essential to ensure longevity and resilience to environmental elements. In alignment with eco-friendly principles, recycled or sustainable materials can be considered. The design should be optimised to optimise the efficiency of rainwater collection systems, and a filtration system should be incorporated to minimise the maintenance requirements and ensure water quality. Integrating solar cells and wind turbines into the panel design is recommended to generate energy and select high-efficiency components to maximise energy output. For remote monitoring and control, smart technology can be implemented to monitor and control rainwater storage and energy generation, including sensors for water level, energy output, and system health. The building panel design should be modular, capable of integrating various architectural designs, and scalable to accommodate different building sizes and energy demands. Advocating for government incentives and community programs that encourage sustainable building practices can promote widespread adoption. Educational initiatives can raise awareness about the benefits of rainwater harvesting and renewable energy generation, providing resources and guidelines for architects, builders, and homeowners. Collaboration between researchers, architects, and industry stakeholders can continually improve the design and efficiency of building panels for rainwater storage and energy generation. Ongoing research can refine technology and address emerging challenges. By implementing these recommendations, building panels can become a mainstream solution for sustainable construction, contributing to water conservation, renewable energy generation and environmental sustainability.

References

- Adham, A., Riksen, M., Abed, R., Shadeed, S., and Ritsema, C. (2022) 'Assessing a suitable technique for rainwater harvesting using Analytical Hierarchy Process (AHP) methods and GIS techniques, *Water*, 14(13), pp 2110. doi: 10.3390/w14132110.
- Aladenola, O.O and Adiboye, O.B (2010) 'Assessing the potential for rainwater harvesting', *Water Resource Management*, 24, pp. 2129 – 2137. doi: 10.1007/s11269-009-9542-y.
- Alawad, O.M., Gombeda, O.J., Quiel, S.E., and Naito, C.J., (2020) 'Flexural performance of non-load-bearing blast resistant precast concrete cladding panels with discrete connections', *Journal of Building Engineering*, 32, p. 101438. doi: 10.1016/j.jobbe.2020.101438.
- Almeida, A. P. et al. (2021) 'Dynamic modelling of rainwater harvesting with green roofs in university buildings', *Journal of Cleaner Production*, 312, p. 127655. doi: 10.1016/j.jclepro.2021.127655.
- Al-Shaleh, M. and Attiogbe, E.K. (1997) ' Flexural strength characteristics on non-load bearing masonry walls in Kuwait', *Materials and Structures*. 30, pp. 277–283. doi: 10.1007/BF02486352.
- Anchan, S.S and Prasad, H.G.S., (2021) 'Feasibility of rooftop rainwater harvesting potential: A Case Study of South Indian University. *Cleaner Engineering Technology*,4, pp. 100206. doi:10.1016/j.clet.2021.100206.
- Andoh, P., Nyarko, F., and Agyei-Agyamang, A. (2016) 'Characterization of recycled plastics for structural applications', *International Journal of Science and Technology*, 5 (6) pp. 259-267.
- Ariyanayagam, A.D and Mahendran, M., (2018) 'Experimental study of non-load bearing light gauge steel framed walls in fire', *Journal of Constructional Steel Research*, 145, pp. 529-551. doi:10.1016/j.jcsr.2018.02.023.
- Ashton, R. 2012. How to start your own business for entrepreneurs. 2nd Ed. UK.Pearson Education Limited.
- Attoye, D. E. and Hassan, A. (2017) 'A Review on Building Integrated Photovoltaic Façade Customization Potentials', *Sustainability*, 9(12), p. 2287. doi: 10.3390/su9122287.
- Ayadi, O., Shadid, R., Bani-Abdullah, A., Alrbai, M., Abu-Mualla, M., and Balah, N.A. (2020) ' Experimental comparison between Monocrystalline, Polycrystalline, and Thin-film solar systems under sunny climatic conditions', *Energy Reports*. 8. pp. 218-230. doi.10.1016/j.egyr.2022.06.121.
- Bagher, A.M., Vahid, M.M.A., and Mohsen, M. (2021) 'Types of Solar Cells and Application', *American Journal of Optics and Photonics*, 3 (5), pp. 94-113. doi: 10.11648/j.ajop.20150305.17.
- Betasolo, M & Smith, C. (2020), 'Rainwater harvesting infrastructure management', *Environmental Health - Management & Prevention Practice*. doi: 10.5772/intechopen.90342.
- Bida, S.M., Aziz, F.N.A.A, Jaafar, M.S., Hejazi, F., and Bakar, N.A. (2021) 'Thermal resistance of insulated precast concrete sandwich panels', *Internatinal Journal of Concrete Structures and Materials*. 15(1):41. doi:10.1186/s40069-021-00477-6.
- Brown, B. 2010. Key financial skills for South African Managers and Entrepreneurs with no financial background. SA. Bookstorm
- Campisano, A. et al. (2017) 'Urban rainwater harvesting systems: Research, implementation and future perspectives', *Water Research*. doi: 10.1016/j.watres.2017.02.056.
- Chandramouli, S. (2015) 'Design of Rainwater Harvesting System (RWH)', *International Journal for Research and Development*', 3(07), pp. 351-353.
- Chowdhury. S.A and Mounshed. M. (2016) 'Off-grid electrification with Solar Home Systems: An appraisal of the quality components', *Journal of Renewable Energy*. 97, pp.585-598. doi:10.1016/j.renene.2016.06.017.
- City of Cape Town. (2016) Guidelines for the installation of alternative water systems. [ONLINE] available
-

from

<https://resource.capetown.gov.za/documentcentre/Documents/Procedures,%20guidelines%20and%20regulations/Guidelines%20for%20Alternative%20Water%20Installations.pdf> [Accessed 18/09/2022].

City of Cape Town. (2021) Requirements for small scale embedded generation [ONLINE] available from <https://resource.capetown.gov.za/documentcentre/Documents/Procedures,%20guidelines%20and%20regulations/Requirements%20for%20Small-Scale%20Embedded%20Generation.pdf> [Accessed 24/04/2023].

Dem'yanov, A., Kolchunov, E., Iakovenko, I., and Kozarez, A., (2019) 'Load bearing capacity calculation of the system "Reinforced Concrete Beam - Deformable base" under torsion with bending', *E3S Conference*. doi:10.1051/e3sconf/20199704059.

DMRE. (2020) Licensing exemption and registration for public comment . [ONLINE] available from <https://www.energy.gov.za/files/policies/Gazette46850-Licensing-Exemption-and-Registration-Notice-for-Public-Comment.pdf> [Accessed 24/04/2023].

DoE. (2022) South African energy sector report. [ONLINE] available from <https://www.energy.gov.za/files/media/explained/2021-South-African-Energy-Sector-Report.pdf> [Accessed 02/06/2023].

van Eekelen, M. W. *et al.* (2015) 'A /novel approach to estimate direct and indirect water withdrawals from satellite measurements: A case study from the Incomati basin', *Agriculture, Ecosystems & Environment*, 200, pp. 126–142. doi: 10.1016/j.agee.2014.10.023.

El Ansary, A.M., El Damatty, A.A., and Nassef, A.O. (2009) 'A coupled finite element genetic algorithm technique for optimum design of steel conical tanks', *Journal of Thin-walled Structures*, Vol 48, pp. 260-273. doi:10.1016/j.tws.2009.10.004.

Garhwal, A., Sharma, S., and Danie Roy A B. (2022) 'Performance of Expanded Polystyrene (EPS) sandwiched concrete panels subjected to accelerated corrosion', *Structures*, 43, pp. 1057-1072. doi:10.1016/j.istruc.2022.07.020.

Gibberd, J. T. (2020) 'An alternative rainwater harvesting system design methodology', in P. De Jager (ed.) *In Sustainability Handbook*. 1st edn. Ed. S.I.: Alive2green. doi: <http://hdl.handle.net/10204/12102>.

Gobin, A., Sparks, D., Okedi, J., Armitage, N., and Ahjum, F. (2019) 'Assessing the energy carbon footprints of exploiting and treating brackish groundwater in Cape Town', *Water SA*, 45(1), pp. 63-74. doi:10.4314/wsa.v45i1.08.

Gohel, J., Bhatu, H., Kapupara, P., and Ramsamy, B. (2020) ' Designing of rooftop rainwater harvesting system at RK University', *Journal of Pharmacognosy and Phytochemistry*, 9(2) pp 351 - 353.

Guangul, F.M., Chala, T.M.(2019) ' Solar Energy as Renewable Energy Source: SWOT Analysis', *ICBDSC*. doi:10.1109/ICBDSC.2019.8645580.

Gunkler, E and Dashkhuu, O. (2014) 'On the load-bearing capacity of masonry walls subjected to concentrated end strip loads', *Mauwerk*, 18. doi: 10.1002/dama.201400623.

Gurkalo, F., Du, Y.G., Poutos, Y., and Timenez-Bescoc, C. (2016) 'The nonlinear analysis of innovative slit reinforced concrete tower in seismic regions', *Journal of engineering structures*, Vol 134, pp. 138-149. doi:10.1016/j.engstruct.2016.12.033.

Hänig, J. and Weller B. (2019) 'Load-bearing behaviour of innovative lightweight glass-plastic-composite panels', *Glass Structural Engineering*, 5, pp. 83-97. doi: 10.1007/s40940-019-00106-5.

Helmreich, B. and Horn, H. (2009) 'Opportunities in rainwater harvesting', *Desalination*, 248(1–3), pp. 118–124. doi: 10.1016/j.desal.2008.05.046.

Hendry, A.W. (2001) 'Masonry wall: Materials and Construction', *Construction and Building Materials*, 15 (8) pp 323-330. doi:10.1016/S0950-0618(01)00019-8.

- Huld, T. (2017) 'PVMAPS: Software tools and data for the estimation of solar radiation and photovoltaic module performance over large geographical areas', *Solar Energy*, 142: pp. 171 - 181. doi:10.1016/j.solener.2016.12.014.
- Gohel, J., Bhatu, H., Kapupara, P. and Barath, R. (2020) 'Designing rooftop rainwater harvesting system at RK University', *Journal of Pharmacognosy and Phytochemistry*, SP9(2), pp. 351–353.
- Johnson, D. O. and Ogunseye, A. A. (2017) 'Grid-connected photovoltaic system design for local government offices in Nigeria', *Nigerian Journal of Technology*, 36(2). doi: 10.4314/njt.v36i2.33.
- Jon Franke. (2021) *The 2021 Empower Virtual Summit: Moving Solar Forward*, aurorasolar. Available at: <https://www.aurorasolar.com/blog/the-2021-empower-virtual-summit-moving-solar-forward/>.
- Jurasz, J., Cheran. B., and Orłowaska. A. (2020) 'Component degradation in small-scale off-grid PV-battery system operation in terms of reliability, environmental impact and economic performance', *Journal of Sustainable Energy Technologies and Assessments*, 38. doi: 10.1016/j.seta.2020.100647
- Jury, M.R., (2020) 'Climate trends in the Cape Town area, South Africa', *Water SA*, 46(3) pp. 438–447. doi: 10.17159/wsa/2020.v46.i3.8654.
- Kaiser, G., and Macleod, N. (2018) 'Cape Town: Where we've been and where we want to go', *Sabinet African Journals*, 2018(9).
- Kahindra, J.M., and Taigbenu, A.E (2011), 'Rainwater harvesting in South Africa: challenges and opportunities', *Physics and Chemistry of the Earth*, 36(14-15), pp 968 - 976. doi: 10.1016/j.pce.2011.08.011.
- Kanno, G. G. et al. (2021) 'Estimation of rainwater harvesting potential for emergency water demand in the era of COVID-19. The case of Dilla town, Southern, Ethiopia', *Environmental Challenges*, 3. doi: 10.1016/j.envc.2021.100077.
- Kim, S., Lee, D., Kim, Y., and Kim, S. (2020) 'Development and application of precast concrete double wall system to improve productivity of retaining wall construction', *Sustainability* 12, pp 2-12. doi: 103390/su12083454.
- Kinnane, O., West, R.P., and O'Hegarty, R. (2022). 'Failure Modes of Load-Bearing Sandwich Panels in Shear'. In: Singh, S.B., Barai, S.V. (eds) *Stability and Failure of High Performance Composite Structures*. Composites Science and Technology . Springer. doi:10.1007/978-981-19-2424-8_3
- Kinnane, O., West, R.P., and O'Hegarty, R. (2022) 'Stability and Failure of High Performance Composite Structures', *Composites Science and Technology*, pp. 39 -66. doi: 10.1007/978-981-19-2424-8_3
- Kumar, A. et al. (2019) 'Solar energy for all? Understanding the successes and shortfalls through a critical comparative assessment of Bangladesh, Brazil, India, Mozambique, Sri Lanka and South Africa', *Energy Research & Social Science*, 48, pp. 166–176. doi: 10.1016/j.erss.2018.10.005.
- Lamnini, S., and Kadar, P. (2017) 'Perspectives of PV technology and their applications', *International Symposium on Applied Machine Intelligence and Informatics*. doi:10.1109/SAMI.2017.7880362.
- Lavaa, A. (2023) Everything you need to know about monocrystalline solar panel. [ONLINE] available from <https://www.linquip.com/blog/what-is-a-monocrystalline-solar-panel> [Access 01/06/2023].
- Lamer, G. (2021) Cells and building structures. Part II. The load-bearing units in cells of the building – The cells in the load-bearing elements of the building, *International Review of Applied Sciences & Engineering*, 13(2022) 1, 11-21 doi: 10.1556/1848.2021.00224
- Laurenço, B.P., Vasconcelos, G., Medeiros, J., and Gouveia, J. (2010) 'Vertically perforated clay brick masonry for load-bearing and non-load-bearing masonry wall', *Construction and Building Materials*, 24, pp2317-2330. doi:10.1016/j.conbuildmat.2010.04.010.
- Leutnat, D., Muschalla, D., and Uhl, M. (2012) 'Statistical distribution of Tand S
- Maity, P.K., Das, S., and Das, R. (2018) 'Remedial measures for saline water in coastal aquifers in South
-

- West Bengal in India', *MOJ Ecology and Environmental Science*. 6(1):00061 doi:10.15406/mojes2018.03.00061.
- Li, X., Li, P., Wu, Z., Luo, D., Yu, H.Y., and Lu, Z.H. (2021) 'Review and perspective of materials for flexible solar cells', *Materials Reports: Energy*. doi:10.1016/j.matre.2020.09.001.
- Ma, T., Yang, H., and Lu, L. (2014) 'Solar photovoltaic system modelling and performance prediction', *Renewable and Sustainable Energy Reviews*. 36 pp304 - 315. doi:10.1016/j.rser.2014.04.057.
- Majesty, D., Chioma, A., Benjamin A., Chijioke, N., and Humpfrey, N. (2013). 'Effect of different storage vessels on water quality', *Global Research Journal of Science*. 2(2), pp. 9-13.
- Mansur, A.A., Islam, M.I., Kiron, K., ul Haq, M.A., Maruf, H., Shihavuddin A.S.M., Ashieque, R.H., and Amin, R. (2022) 'Electrical experimental data collection of polycrystalline and monocrystalline photovoltaic modules in an indoor environment using artificial sun simulators', *Data in Brief*. 423. 108389. doi:10.1016/j.dib.2022.108389.
- Mathur, G.C. (1984) "One-brick thick load-bearing walls for seismic areas", *Batiment International, Building Research and Research*. 12:2, pp 102-107. doi: 10.1080/09613218408551203.
- Miccolli, L., Fontana, P., Silva, N., Kocadag, R., Cedeqvist, C., Kreft, O., Qvaeschning, D. (2016). 'UHPC - AA/CLC composite panel-self cleaning properties. Materials and production technology', *World Sustainable Energy Days*. pp 1-14.
- Mishra, S.S., Shruthi B. K., Rao, H. J. (2020) 'Design of Rooftop Rainwater Harvesting Structure in a University Campus', *International Journal of Recent Technology and Engineering*, 8(5), pp. 3591–3595. doi:10.35940/ijrte.E6519.018520.
- Motteu, H., (1997). 'Load-bearing walls and structural response', *Batiment International, Building Research and Practice*, 5:5 pp 290-290, doi:10.1080/0961327708550606.
- Mousakhani, F., Simons, A., Harris, D., Yavarkhani, M., and Anvari, A. (2022). 'The use of discarded plastic water bottles as an insulating material for external walls in buildings', *Journal of Physics:Materials Science and Engineering* pp. 1-7, doi:10.1088/1757-899x/1218/1/012051.
- Moutassem & Al Mara, (2021). 'Design and production of sustainable lightweight concrete precast sandwich panels for non-load bearing partition walls', *Cogent Engineering*, 8:1 1993565, doi: 10.1080/23311916.2021.1993565.
- Mukheibir, P. and Ziervogel, G. (2007). 'Developing a Municipal Adaptation Plan (MAP) for climate change: the city of Cape Town', *Environment and Urbanisation*, 19(1), pp. 143–158. doi: 10.1177/095624780707691.
- Mukheibir, P. and Ziervogel, G. (2007). 'Municipal Adaptation Planning (MAP), Green citynomics The urban water against climate change, 1st Edition, pp 17.
- Mutafchieva, G., Lakov, L., Aleksandrova, M., Dimitrova, R., and Peev, G. (2022). 'Foam ceramic blocks with low thermal conductivity suitable for the construction of roads and urban square pavements and non-load-bearing partition walls', *International Scientific Journal "Machines. Technologies. Materials"*, 5, pp. 186-188.
- Mutombo, N. M.-A. and Numbi, B. P. (2019) 'Assessment of renewable energy potential in Kwazulu-Natal province, South Africa', *Energy Reports*, 5, pp. 874–881. doi: 10.1016/j.egy.2019.07.003.
- NERSA. (2020). Registration procedure in terms of schedule 2 of the electricity regulation. [ONLINE] available from <https://www.nersa.org.za/wp-content/uploads/2021/02/Registration-Procedure-.pdf> [ACCESSED 24/04/2023].
- Nogueira, C. E. C. et al. (2015) 'Performance of monocrystalline and polycrystalline solar panels in a water pumping system in Brazil', *Renewable and Sustainable Energy Reviews*, 51, pp. 1610–1616. doi: 10.1016/j.rser.2015.07.082.
-

- Noor Jamal (2015) 'Options for the supply of electricity to rural homes in South Africa', *Journal energy South. Africa*, 26(3). Available at: http://www.scielo.org.za/scielo.php?script=sci_arttext&pid=S1021-447X2015000300006.
- Novak, C., Van Giesen, E., and DeBusk, K.M. (2021) 'Designing rainwater harvesting systems; integrating rainwater into building system. Wiley.
- O'Hagarty, R., and Kinnane, O. (2020) 'Review of precast concrete sandwich panels and their innovation', *Construction and building materials*, 233, 117145. doi: 10.1016/j.conbuildmat.2019.117145.
- Opoku, R., Mensah, G., Adja, E.A., Dramani, J.B., Kornyo, O., Nijhar, R., Addai, M., Marfo, D., Davis, F., and Obeng, G.Y. (2023) 'Machine learning redundant energy of a solar PV mini-grid system for cooking applications', *Journal of Solar Energy* 262. doi:10.1016/j.solener.2023.06.008
- Pala, G.K., Pathivada, A.P., Velugoti, S.J.H., Yerramsetti, C., and Veeranki, S. (2020) 'Rainwater Harvesting-A review on conservation, creation and cost-effectiveness', *Materials to day proceeding*, 45 (7), pp. 6567 - 6571. doi: 10.1016/j.matpr.2020.11.593.
- Pečur, I.B, Bagarić M., and Milovanović, B. (2020) 'Development and application of a prefabricated façade panel containing recycled construction and demolishing waste', *Journal façade design and energy*, 8(2) doi: 10.7480/jfde.2020.2.4788.
- Pitroda, J., Bhut, K.A., Bhimani, H.A., Chhayani, S.N., Bhatu U.R., and Chauhan, ND. (2016) 'A Critical Review on Non-Load Bearing Wall Based on Different Materials', *ARC*, 2 (4), pp 33-40. doi: 10.20431/2454-8693.0204005
- Du Plessis, J. A. (2017) 'An investigation into the evidence of seasonal rainfall pattern shifts in the Western Cape, South Africa', *Journal of the South African Institution of Civil Engineering*, 59(4), pp. 47–55. doi: 10.17159/2309-8775/2017/v59n4a5.
- Premrov, M., Ber, B. & Kozem Šilih, E. (2021) 'Study of load-bearing timber-wall elements using experimental testing and mathematical modelling', *Advances in Production Engineering & Management*, 16 (1) pp 67-81. doi: 10.14743/apem2021.1.385
- Qin, J., Lan, Linkai., Chen, Shanshan., Huang, Feinan., Shi, Huanrong., Chen, Wenjie., Xia, Haibo., Sun, Kuan., and Yang, Changduk. (2020) 'Recent progress in flexible and stretchable organic solar cells', *Advanced Functional Materials*. 30 (2002529) pp. 1-22. doi:10.1002/adfm.202002529.
- Radcliffe J.G (2020) 'Water reuse and recycling in Australia - history, current and future perspectives', *Journal Water Cycle*, (1), pp. 19-40. doi:10.1016/j.watcyc.2020.05.005.
- Ramos Heranz, R., Campayo Martín, J.J., Zamora Belver, I., Larranaga Lesaka, J., Zulueta Guerrero, E., Puelles Pérez, E. (2010) 'Modelling of Photovoltaic Module', *International Conference on Renewable Energie and Power Quality*. 1 (8), pp1186 - 1190. doi:10.24084/repqj08.619
- Rehman, S., Bader, M. A. and Al-Moallem, S. A. (2007) 'Cost of solar energy generated using PV panels', *Renewable and Sustainable Energy Reviews*. doi: 10.1016/j.rser.2006.03.005.
- Richman, M.B., and Leslie M.R., (2018) 'The 2015-2017 Cape Town Drought: Attribution and Prediction Using Machine Learning', *Procedia Computer Science*, 140, pp. 248–257. doi: 10.1016/j.procs.2018.10.323.
- Roffe, S.J., Steinkopf, J., and Fitchett, J. (2021) 'South African winter rainfall zone shifts: A comparison of seasonality metrics for Cape Town from 1841 - 1899 and 1933 - 2010', *Research Square*. pp 1-19. doi:10.21203/rs.3.rs-867223/v1.
- Sainthiya, H. (2017) 'Different types of cooling systems used in photovoltaic module solar system: A review', *IEEE WiSPNET Conference*. doi:10.1109/WiSPNET.2017.8300012.
- Santos, C., Imtaz, C.A., Ghisi, E., Matos, C., (2020) 'The effects of climate change on domestic Rainwater Harvesting', *Science of the Total Environment*, 729, pp. 1-8. doi:10.1016/j.scitotenv.2020.138967.
- Santos, P. and Mateus, D. (2020) 'Experimental assessment of thermal break strips performance in load
-

- bearing and non load-bearing LSF walls', *Journal of Building Engineering*, 32, doi: 10.1016/j.jobbe.2020.101693.
- Savelli, E. *et al.* (2021) 'Don't blame the rain: Social power and the 2015–2017 drought in Cape Town', *Journal of Hydrology*, 594, p. 125953. doi: 10.1016/j.jhydrol.2020.125953.
- Schmitt, M, (2018) 'Load-bearing capacity of infill masonry wall considering the deformation-based membrane effect,' *Mauwerk*, 22, pp 151-161. doi: 10.1002/dama.201800003.
- Semenov, V., Zhukov, A., Pilipiako, A., and Mednikova, E. (2021) 'Effective thermal insulation based on recycled polyethylene', *Journal of Physics: Materials Science and Engineering*, pp 1-8. doi:10.1088/1757-899X/1030/1/012026.
- Sheng, L.X., Mari, T.S., Ariffin, A.R.M., and Hussein, H. (2011) 'Integrated sustainable roof design', *International Conference of Greenbuildings and Sustainable cities. Procedia Engineering*. 21 pp 846 - 852. doi:10.1016/j.proeng.2011.11.2086.
- Shrivastava, A., Sharma, R., Saxena, M.K., Shanmugasundaram, V., and Ankit, M.L.R. (2023) 'Solar energy capacity assessment and performance evaluation of a standalone PV system using PVSYST', *Materials Today Proceedings*. 80. pp 3385 - 3392. doi:10.1016/j.matpr.2021.07.258.
- Singh, S., Yadav, R., Kathi, S., and Singh, A.N., (2022) 'Chapter14-Treatment of harvested rainwater and reuse: Practices, prospects, and challenges', *Advances in Environmental Pollution Research, Pages 161-178*. doi: 10.1016/B978-0-12-822933-0.00003-6.
- Sousa, P.M., Blamey, R.C., Reason, C.J.C., Ramos, A.M., and Trigo, R.M. (2018) 'The 'Day Zero' Cape Town drought ad the poleward migration of moisture corridors', *Environmental Research Letters*. 13. 124025. doi:10.1088/1478-9326/aaebc7.
- South African Weather Services. [ONLINE] available from <https://www.weathersa.co.za/home/historicalrain>. [Accessed 29/05/2023]
- Sreega, R., Nithyananthan, K., and Nandini, B. (2017) 'Design and development of automated solar panel cleaner and cooler', *International Journal of Electrical ad Electronics Engineers*. 9(2).
- Supian, B. A., Ekaputri, C. and Priharti, W. (2020) 'Increasing the output power of solar panel by using cooling system', *IOP Conference Series: Materials Science and Engineering*, 830, p. 032039. doi: 10.1088/1757-899X/830/3/032039.
- Taşçioğlu, A., Taşkın, O. and Vardar, A. (2016) 'A Power Case Study for Monocrystalline and Polycrystalline Solar Panels in Bursa City, Turkey', *International Journal of Photoenergy*, 2016, pp. 1–7. doi: 10.1155/2016/7324138.
- Tawiah P. O. , Andoh P. Y., A.-A. A. and N. F. (2016) 'Characterization of Recycled Plastics for Structural Applications', *International Journal of Science and Technology*, 5(6), pp. 259–267.
- Veeranna, J., and Jeet, P. (2020) 'Groundwater recharge technology for water resource management: A Case Study', *Groundwater Management and Resources*. doi: 10.5772/intecopen.93946.
- Vuong, N. M., Ichikawa, Y. and Ishidaira, H. (2016) 'Performance assessment of rainwater harvesting considering rainfall variations in Asian tropical monsoon climates', *Hydrological Research Letters*, 10(1), pp. 27–33. doi: 10.3178/hrl.10.27.
- Wang, X. H. *et al.* (2017) 'The Design, Simulation and Testing of V-shape Roof Guide Vane Integrated with an Eco-roof System', *Energy Procedia*, 105, pp. 750–763. doi: 10.1016/j.egypro.2017.03.386.
- Wolski, P. (2018). 'How sure is Cape Town's "Day Zero" drought?', 15(2), pp. 24-27 doi 10.1111/j.1740-9713.2018.01127.x
- Xing, C. *et al.* (2021) 'Environment-friendly Cu-based thin film solar cells: materials, devices and charge carrier dynamics', *Physical Chemistry Chemical Physics*, 23(31), pp. 16469–16487. doi: 10.1039/D1CP02067F.
-

Zhang, F. *et al.* (2021) 'The analysis of parameter uncertainty on performance and reliability of photovoltaic cells', *Journal of Power Sources*, 507. doi: 10.1016/j.jpowsour.2021.230265.

Appendices

Appendix A – Standalone output data

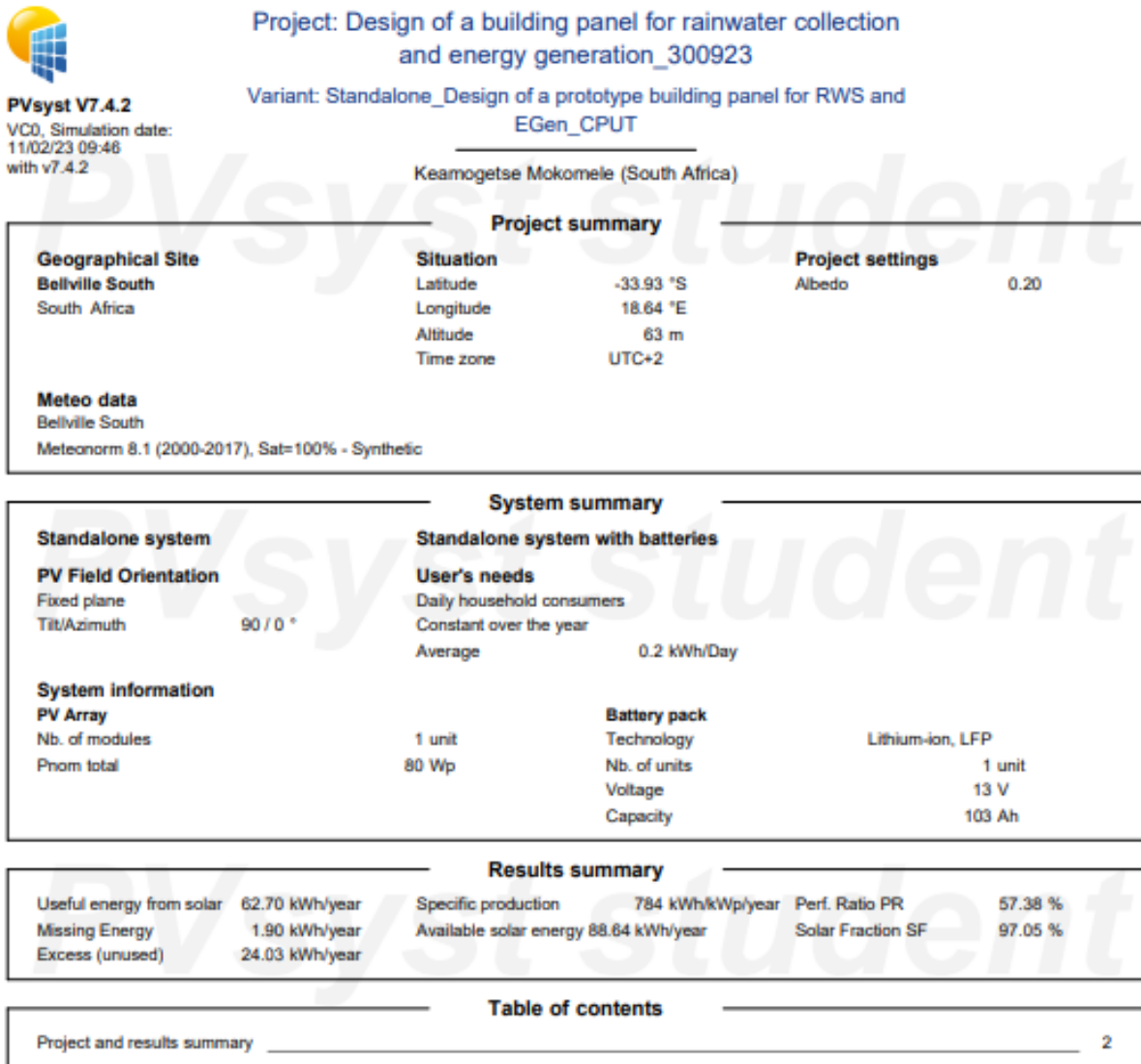


Figure 0.1 Standalone: Project summary

Appendix B – Grid-tied system output data



PVsyst V7.4.2

VC0, Simulation date:
11/01/23 21:35
with v7.4.2

Project: Design of a prototype building panel for RWS and EGeneration_GTied_CPOT

Variant: Design_CPOT_Desing of a prototype building panel for RWS and EGen

Keamogetse Mokomele (South Africa)

Project summary

Geographical Site Bellville South South Africa	Situation Latitude -33.93 °S Longitude 18.64 °E Altitude 63 m Time zone UTC+2	Project settings Albedo 0.20
Meteo data Bellville South Meteonorm 8.1 (2000-2017), Sat=100% - Synthetic		

System summary

Grid-Connected System Simulation for year no 10	No 3D scene defined, no shadings		
PV Field Orientation Fixed plane Tilt/Azimuth 90 / 0 °	Near Shadings No Shadings	User's needs Unlimited load (grid)	
System information			
PV Array		Inverters	
Nb. of modules 1 unit		Nb. of units 1 unit	
Pnom total 250 Wp		Pnom total 250 W	
		Pnom ratio 1.000	

Results summary

Produced Energy 273.8 kWh/year	Specific production 1095 kWh/kWp/year	Perf. Ratio PR 80.20 %
Apparent energy 273.8 kVAh/year		

Table of contents

Project and results summary	2
-----------------------------	---

Figure B.1 Grid-tied: Project summary

Appendix B – Grid-tied system output data

<p>Module type</p> <p><input checked="" type="radio"/> Standard</p> <p><input type="radio"/> Translucide Custom</p> <p><input type="radio"/> Not defined</p>	<p>Technology</p> <p><input type="radio"/> Monocrystalline cells</p> <p><input checked="" type="radio"/> Polycrystalline cells</p> <p><input type="radio"/> Thin film</p>
<p>Mounting disposition</p> <p><input type="radio"/> Flat roof</p> <p><input checked="" type="radio"/> Facade or tilted roof</p> <p><input type="radio"/> Ground based</p>	<p>Ventilation property</p> <p><input type="radio"/> Free air circulation</p> <p><input type="radio"/> Semi-integration</p> <p><input checked="" type="radio"/> Fully insulated</p>

Figure 0.2 Grid-tied: Preliminary System specifications

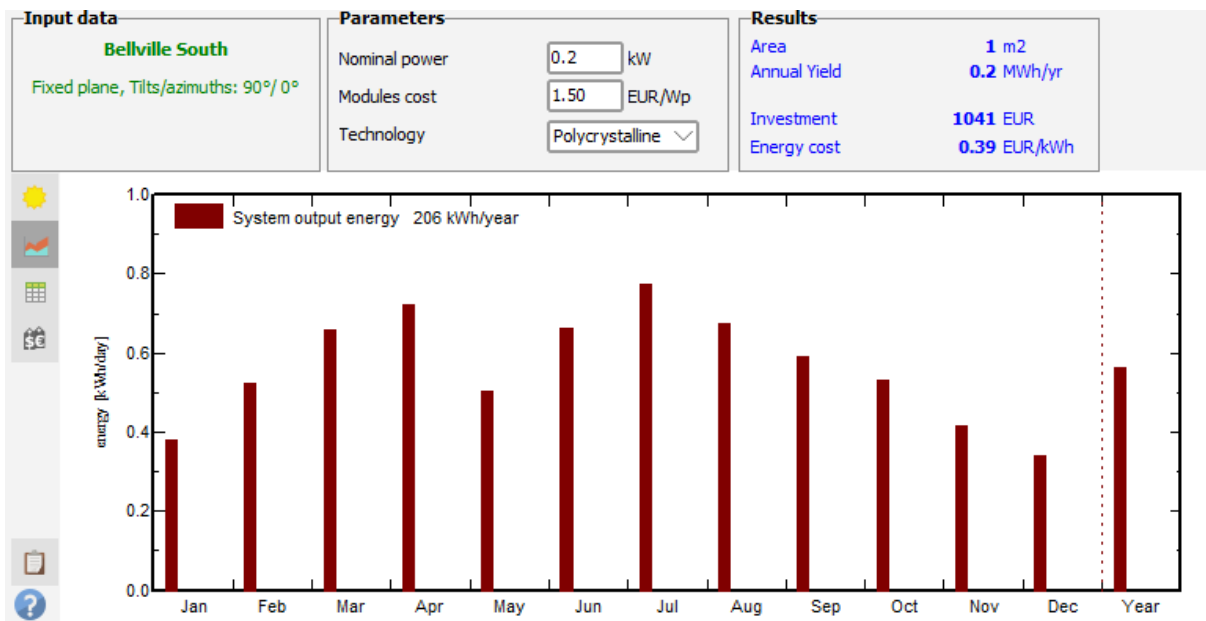


Figure 0.3 Grid-tied: Preliminary output energy

Appendix C – System Validation

Table C.1 Combined data for Rainwater collection, energy generation, and when the storage is 0% & 100%, respectively, with cumulative data at hourly intervals

Time(hrs)	RW collected D1	Hourly total RWC_D1	Energy Generated (W)_D1	Hourly Energy generation (W)_D1	RW collected D2	Hourly total RWC_D2	Energy Generated (W)_D2	Hourly Energy generation (W)_D2	RW collected D3	Hourly total RWC_D3	Energy Generated (W)_D3	Hourly Energy generation (W)_D3	RW collected D4	Hourly total RWC_D4	Energy (W) Generated _D4	Hourly Energy generation (W)_D4	RW collected D5	Hourly total RWC_D5	Energy Generated (W)_D5	Hourly Energy generation (W)_D5	
	27		0		25		0		26		0		29		0		26		0		
	28		0		24		0		24		0		30		0		27		0		
	27		0		25		0		26		0		30		0		26		0		
8:00-9:00	26	108	0		23	97	0		25	101	0		31	120	0		27	106	0		
	26		0		27		0		24		0		29		0		27		0		
	25		0		22		0		25		0		29		0		28		0		
	27		0		25		0		26		0		28		0		27		0		
9:00-10:00	28	106	0		26	100	0		26	101	0		30	116	0		26	108	0		
	27		0		26		0		26		0		31		0		27		0		
	28		0		27		0		27		0		30		0		26		0		
	25		0		25		0		26		0		31		0		26		0		
10:00-11:00	26	106	0		24	102	0		27	106	0		30	122	0		25	104	0		
	25		4,1		23		3,5		27		2,1		30		3,7		25		3,5		
	28		3,7		27		4,0		25		2,7		31		3,5		28		4,0		
	27		4,1		25		2,8		26		2,5		29		3,1		27		2,8		
11:00-12:00	25	105	4,2	16,1	25	100	3,9	14,2	26	104	2,5	9,8	30	120	4,2	14,5	25	105	3,9	14,2	
	29		4,2		26		5,0		26		2,9		31		4,2		29		5,0		
	27		3,5		27		1,5		25		3,5		31		3,5		27		1,5		
	27		3,6		27		4,0		27		3,6		32		3,6		27		4,0		
12:00-13:00	28	111	3,4	14,7	28	108	3,3	13,8	25	103	4,0	14	32	126	3,4	14,7	28	111	3,3	13,8	
	27		4,0		27		3,2		26		4,0		32		4,0		27		3,2		
	25		4,1		27		3,0		26		4,1		31		4,1		25		3,0		
	26		3,4		25		4,0		25		4,4		31		3,4		26		4,0		
13:00-14:00	26	104,0	3,7	15,2	26	105,0	4,0	14,2	25	102,0	4,7	17,2	30	124,0	3,7	15,2	26	104,0	4,0	14,2	
	23		4,1		28		4,0		27		4,5		20		3,9		19		3,9		
14:30-15:00	24	47,0	3,9	8,0	28	56,0	4,0	8,0	27	54,0	4,3	8,8	19	39,0	3,9	7,8	18	37,0	3,9	7,8	
	22		3,5		29		3,5		28		3,5		19		3,5		19		3,5		
	22		3,1		28		3,3		28		3,3		20		3,0		18		3,0		
	21		3,4		27		2,9		27		2,9		20		2,5		17		2,5		
15:00-16:00	20	85	3,1	13,1	28	112	2,5	12,2	27	110	2,5	12,2	19	78	2,5	11,5	16	70	2,5	11,5	
	20		0		27		0		27		0		19		0		17		0		
	21		0		27		0		27		0		20		0		17		0		
	20		0		27		0		26		0		20		0		16		0		
16:00-17:00	20	81	0		28	109	0		27	107	0		20	79	0		16	66	0		

Appendix C – System Validation

Table C.2 Continued

Time(hrs)	RW collected D6	Hourly total RWC_D6	Energy Generated W_D6	Hourly Energy generated (MWh) D6	RW collected D7	Hourly total RWC_D7	Energy Generated W_D7	Hourly Energy generated (MWh) D7	RW collected D8	Hourly total RWC_D8	Energy Generated W_D8	Hourly Energy generated (MWh) D8	RW collected D9	Hourly total RWC_D9	Energy Generated W_D9	Hourly Energy generated (MWh) D9	RW collected D10	Hourly total RWC_D10	Energy Generated W_D10	Hourly Energy generated (MWh) D10	
		26	0		27		0		26		0		29		0		29		0		
		25	0		26		0		26		0		28		0		29		0		
		26	0		27		0		25		0		29		0		27		0		
8:00-9:00		27	104	0	27	107	0		26	103	0		28	114	0		27	112	0		
		27	0		26		0		25		0		27		0		27		0		
		28	0		25		0		26		0		28		0		28		0		
		27	0		27		0		27		0		27		0		28		0		
9:00-10:00		28	110	0	26	104	0		27	105	0		29	111	0		29	112	0		
		27	0		25		0		26		0		28		0		29		0		
		27	0		26		0		27		0		28		0		28		0		
		26	0		27		0		26		0		27		0		27		0		
10:00-11:0		27	107	0	27	105	0		25	104	0		28	111	0		27	111	0		
		27		3,9	23		3,5		26		1,7		28		4,1		27		3,9		
		28		3,9	27		4,0		26		1,5		27		3,7		28		3,9		
	8			3,5	25		2,8		25		2,0		27		4,1		28		3,5		
11:00-12:0		27	90	3,0	14,3	25	100	3,9	14,2	26	103	3,3	8,5	26	108	4,2	16,1	29	112	3,0	14,3
		26		2,5	26		5,0		25		3,2		25		4,2		27		2,5		
		25		2,5	27		1,5		27		3,0		27		3,5		26		2,5		
		25		3,5	27		4,0		28		4,0		28		3,6		28		3,5		
12:00-13:0		26	102	4,0	12,5	28	108	3,3	13,8	27	107	4,0	14,2	29	109	3,4	14,7	26	107	4,0	12,5
		26		2,8	27		3,2		28		4,0		25		4,0		27		2,8		
		26		3,9	27		3,0		27		4,2		25		4,1		28		3,9		
		26		3,0	25		4,0		26		4,6		25		3,4		28		3,0		
13:00-14:0		27	105,0	4,0	13,7	26	105,0	4,0	14,2	25	106,0	4,6	17,4	26	101,0	3,7	15,2	29	112,0	4,0	13,7
		20		5,0	30		3,2		29		5,0		25		4,1		27		4,1		
14:30-15:0		19	39,0	1,5	6,5	31	61,0	3,0	6,2	28	57,0	3,3	8,3	24	49,0	3,7	7,8	27	54,0	4,0	8,1
		20		4,0	30		4,0		29		4,0		26		3,7		25		3,7		
		20		3,3	31		4,0		29		3,3		25		3,0		25		2,9		
		20		3,2	29		4,0		27		3,2		24		2,3		25		2,3		
15:00-16:0		21	81	2,9	13,4	30	120	4,2	16,2	28	113	2,7	13,2	25	100	2,1	11,1	25	100	2,1	11
		20		0	29		0		27		0		25		0		26		0		
		20		0	29		0		26		0		24		0		26		0		
		20		0	28		0		27		0		25		0		26		0		
16:00-17:0		21	81	0	29	115	0		26	106	0		26	100	0		26	104	0		

Table C.3 Continued

Time(hrs)	0-100% full tank	Energy (W) generated	Hourly Energy (W) generated
	0	0	
	0	0	
	0	0	
8:00-9:00	0	0	
	0	0	
	0	0	
9:00-10:00	0	0	
	0	0	
	0	0	
10:00-11:0	0	0	
	0	3,0	
	0	1,0	
	0	2,2	
11:00-12:0	0	1,5	7,7
	0	1,0	
	195	1,5	
	195	2,5	
12:00-13:0	195	3,6	8,6
	195	3,2	
	195	3,8	
	195	3,6	
13:00-14:0	195	4,0	14,6
	195	4,2	
14:30-15:0	195	3,8	8,0
	195	3,5	
	195	2,7	
	195	2,0	
15:00-16:0	195	1,8	10
	195	0	
	195	0	
	195	0	
16:00-17:0	195	0	

Appendix D – Model development

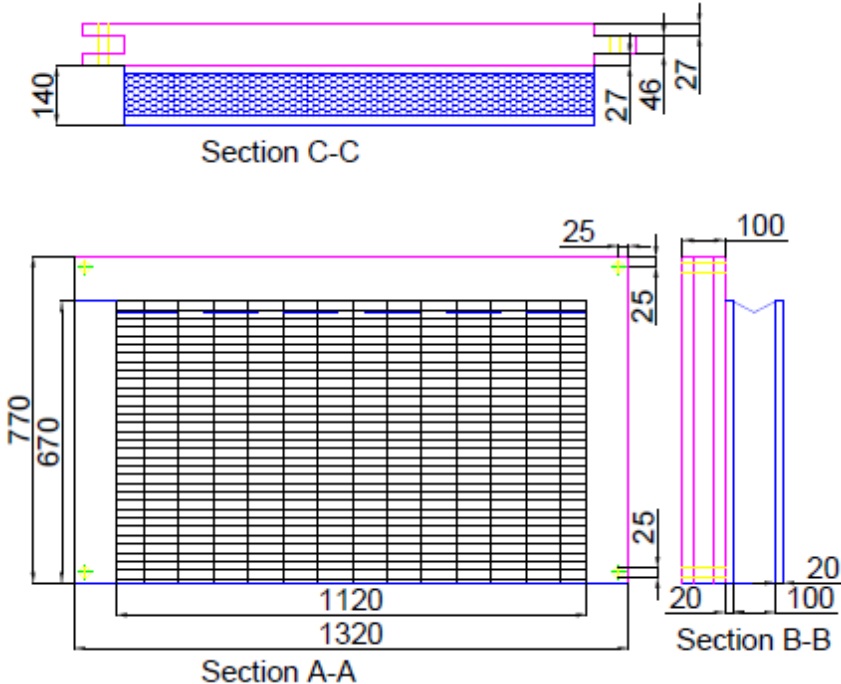


Figure D.1 Model: AutoCAD section on initial design

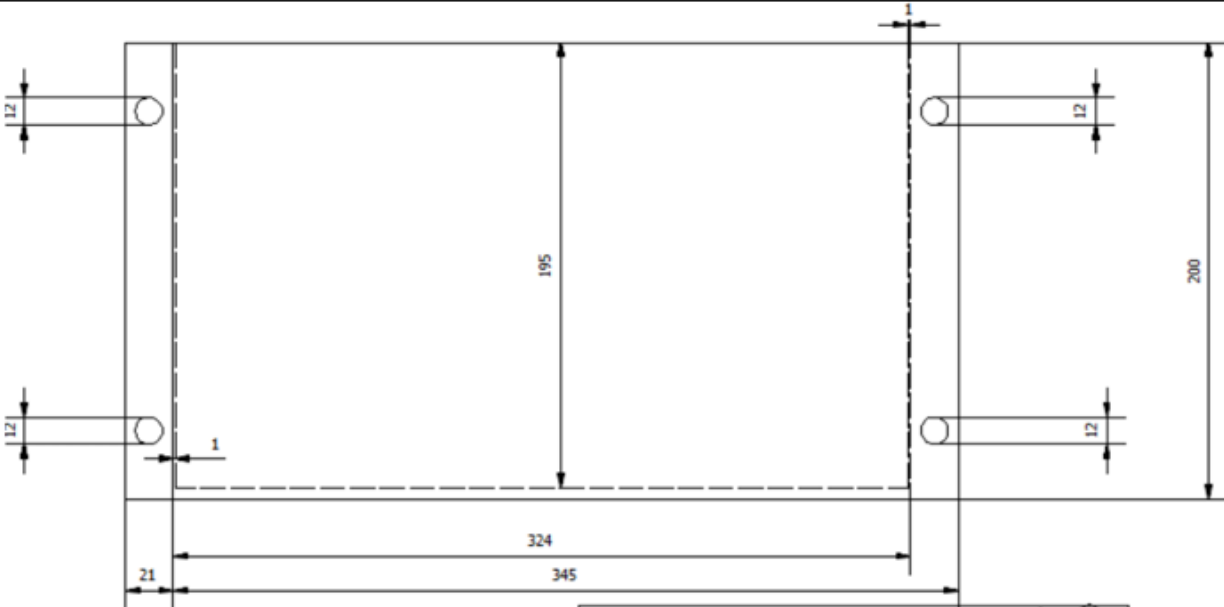


Figure D.2 Model: Revised section for model printing

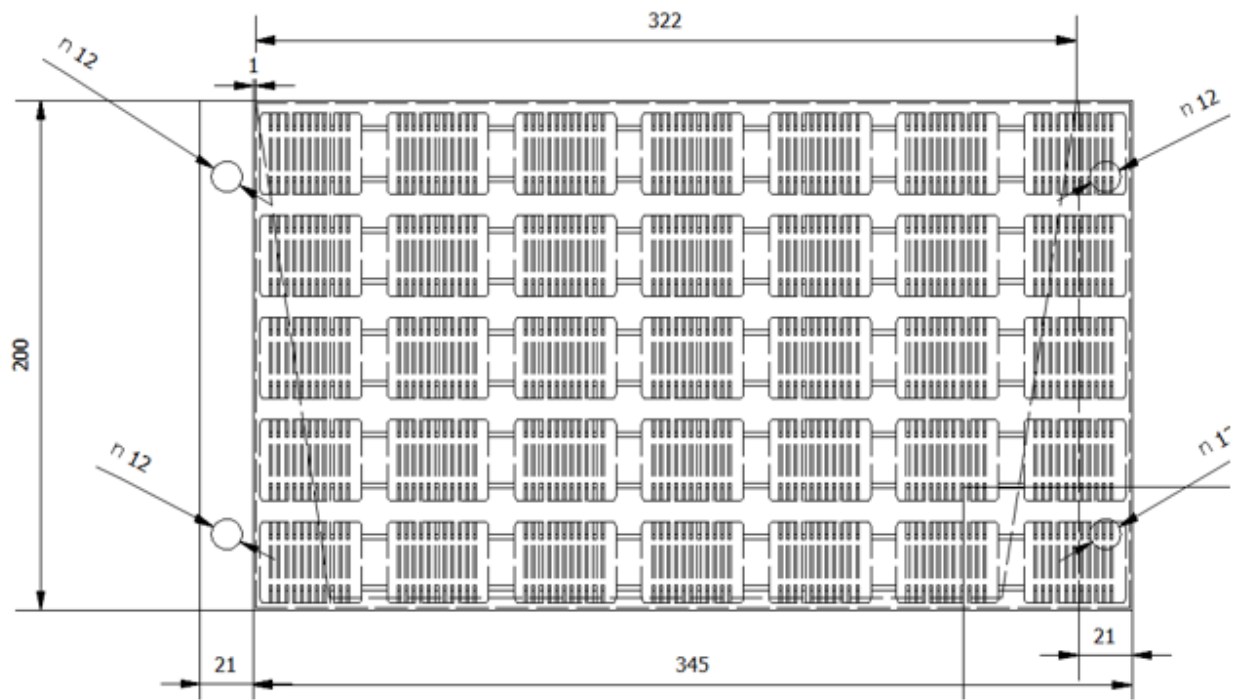


Figure D.3 Model: Revised section illustrating PV module



Figure D.4 Model: Image for the front and back view of a prototype building panel



Figure D.5 Model: An illustration of a top and side view of the prototype building panel



Figure D.6 Model: Prototype building panel showing rainwater tank, building panel and FSC



Figure D.7 Model: Prototype bottom view



Figure D.8 Model: Prototype side view

Appendix E – Graphs from system validation

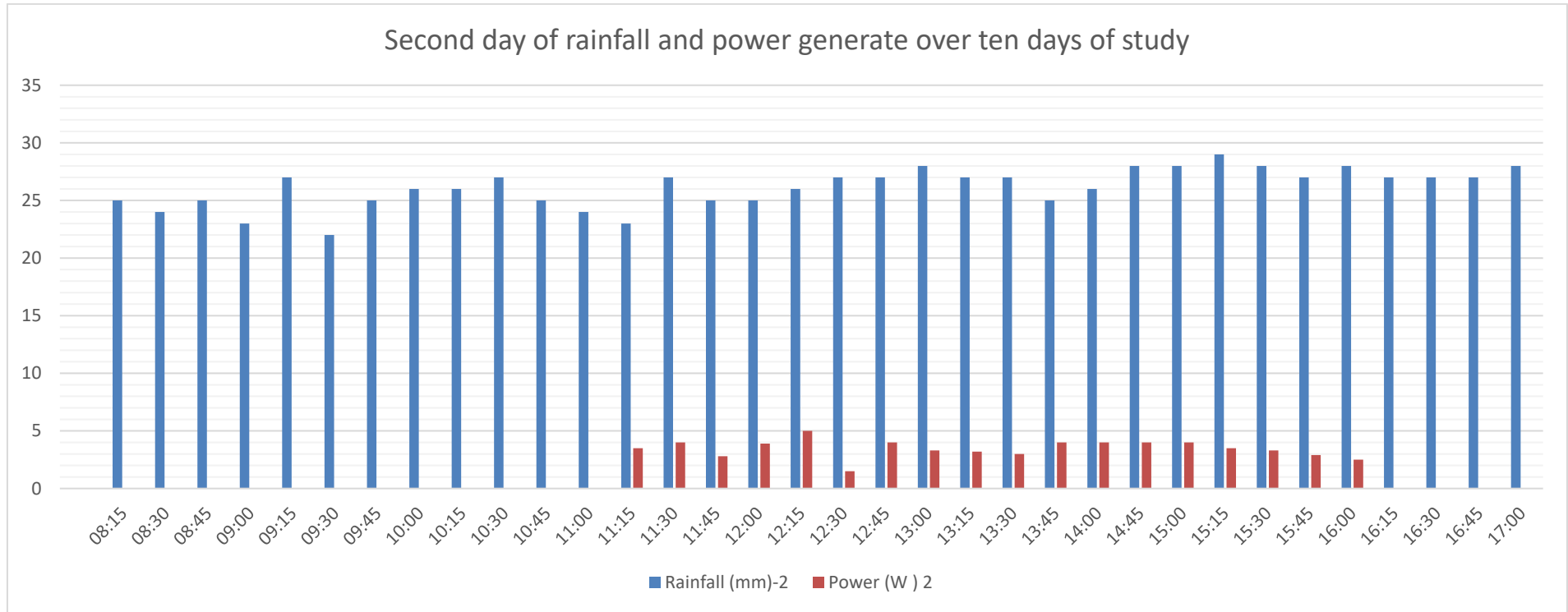


Figure E.1 Validation: Second day of rainfall and power generation

Appendix E – Graphs from system validation

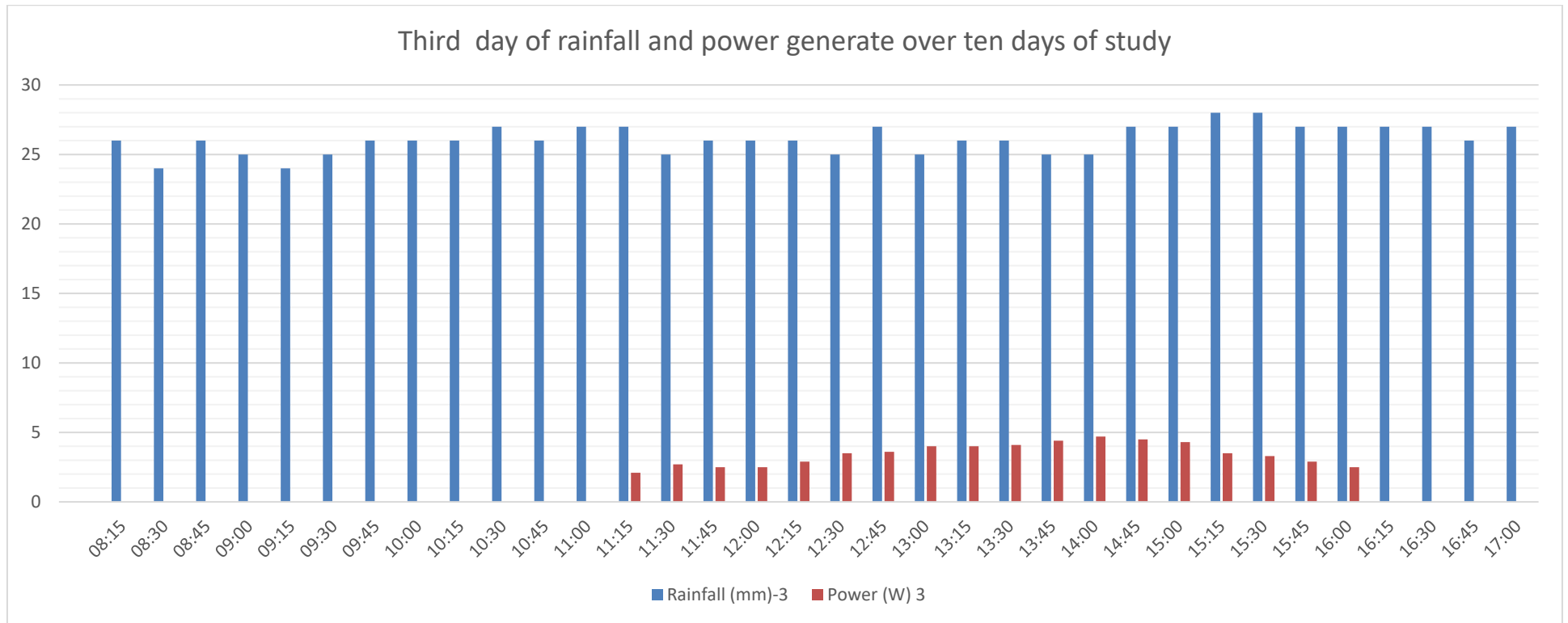


Figure E.2 Validation: Third day of rainfall and power generation

Appendix E – Graphs from system validation

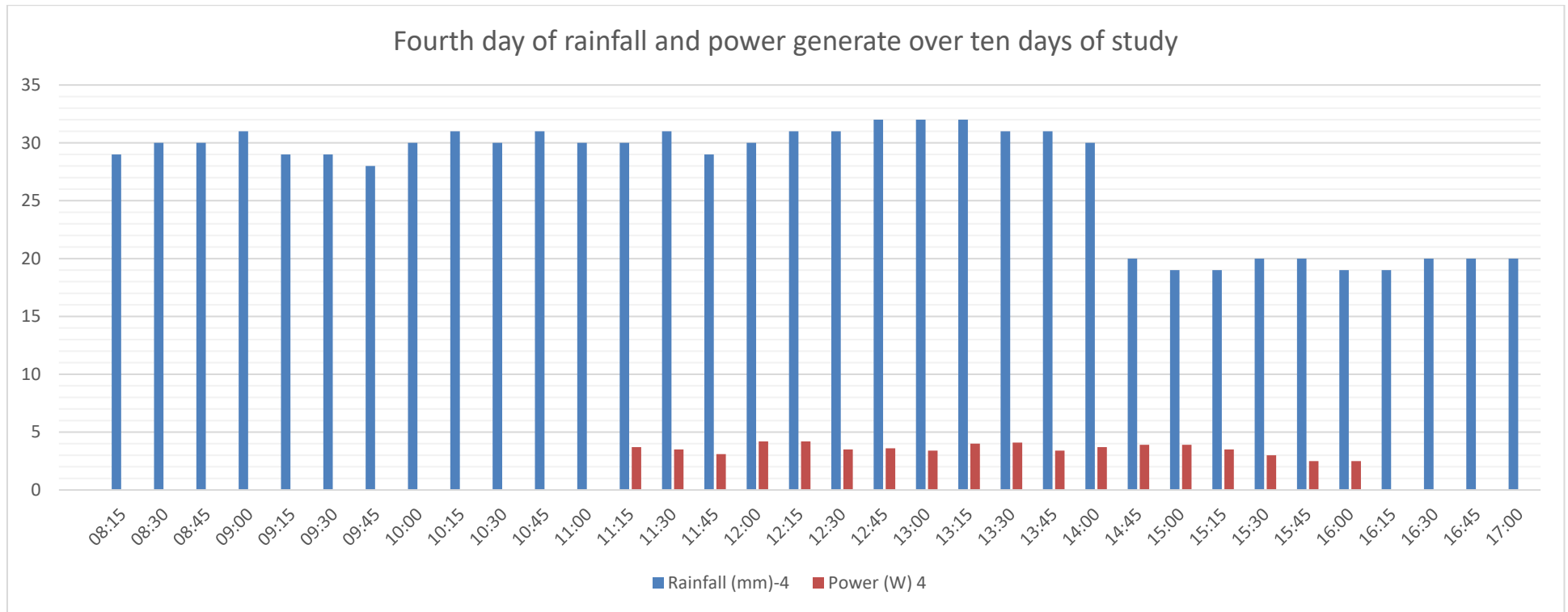


Figure E.3 Validation: Fourth day of rainfall and power generation

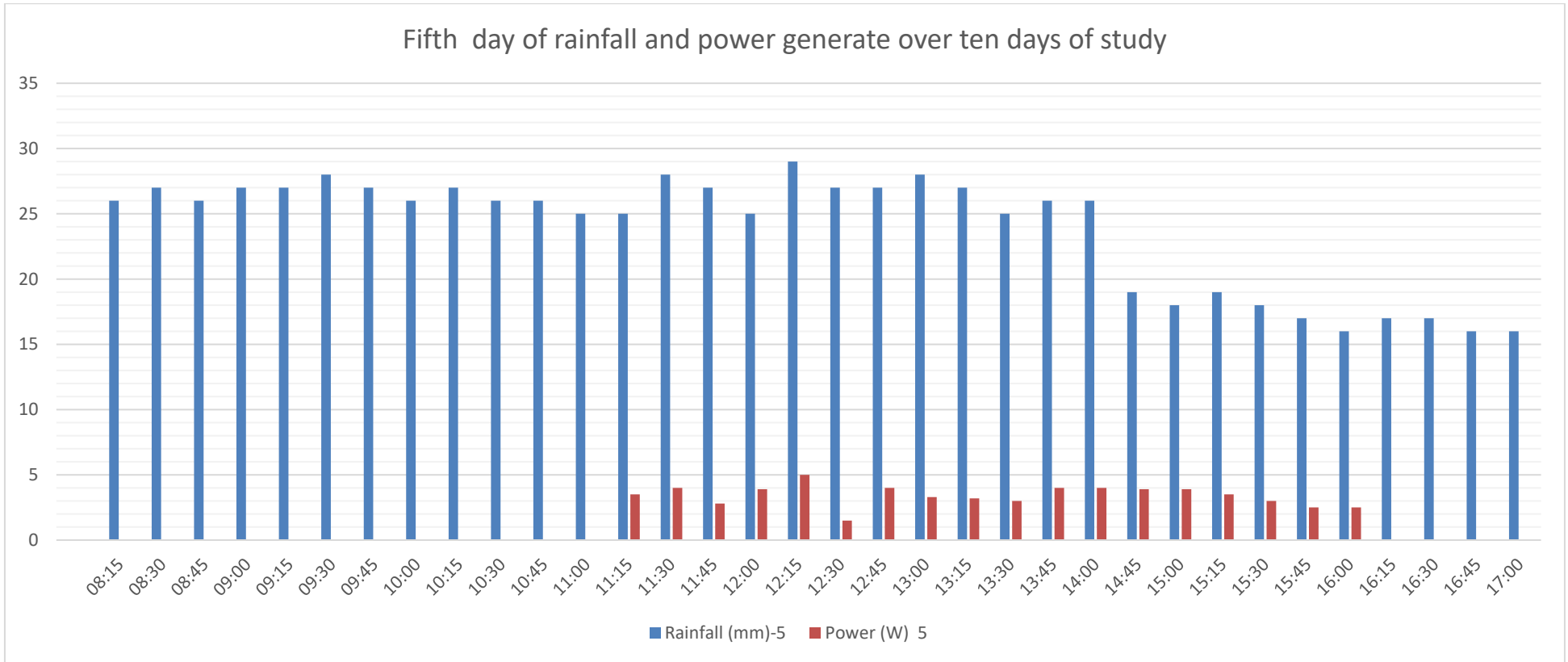


Figure E.4 Validation: Fifth day of rainfall and power generation

Appendix E – Graphs from system validation

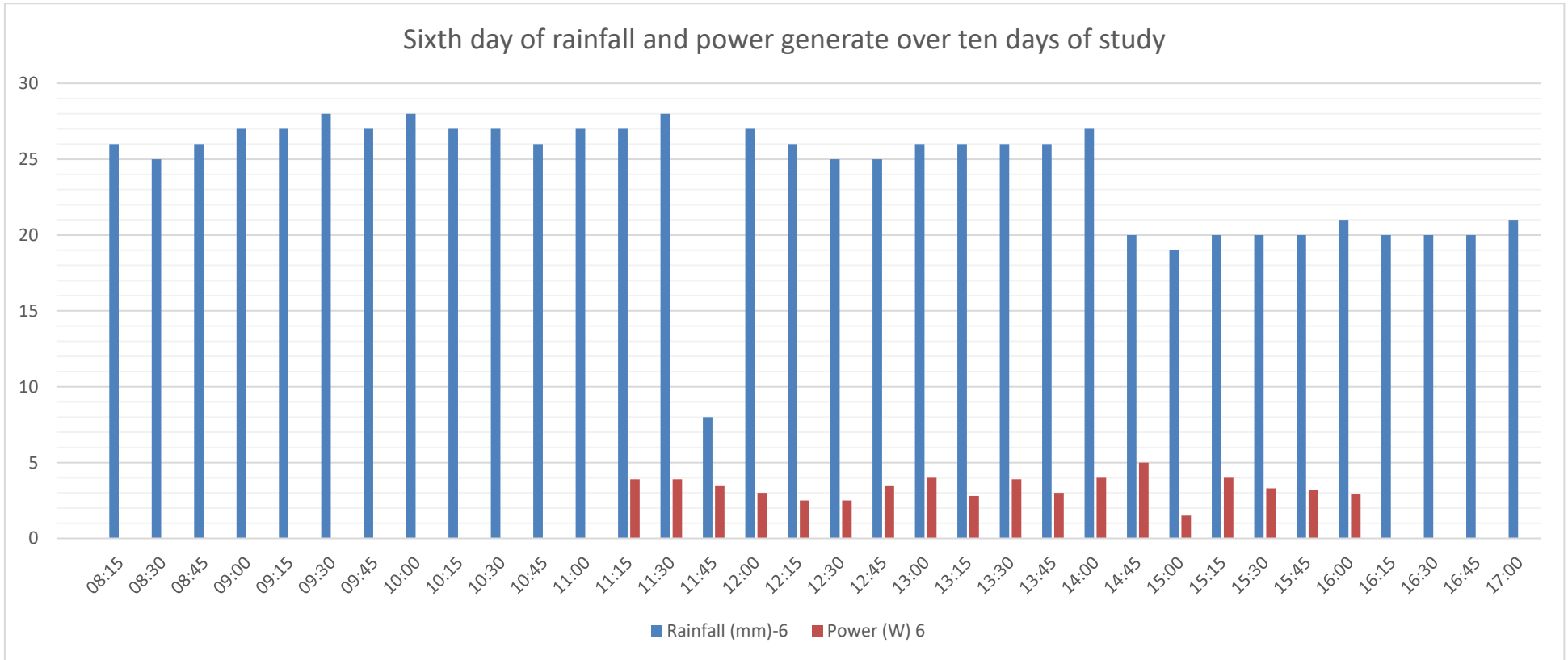


Figure E.5 Validation: Sixth day of rainfall and power generation

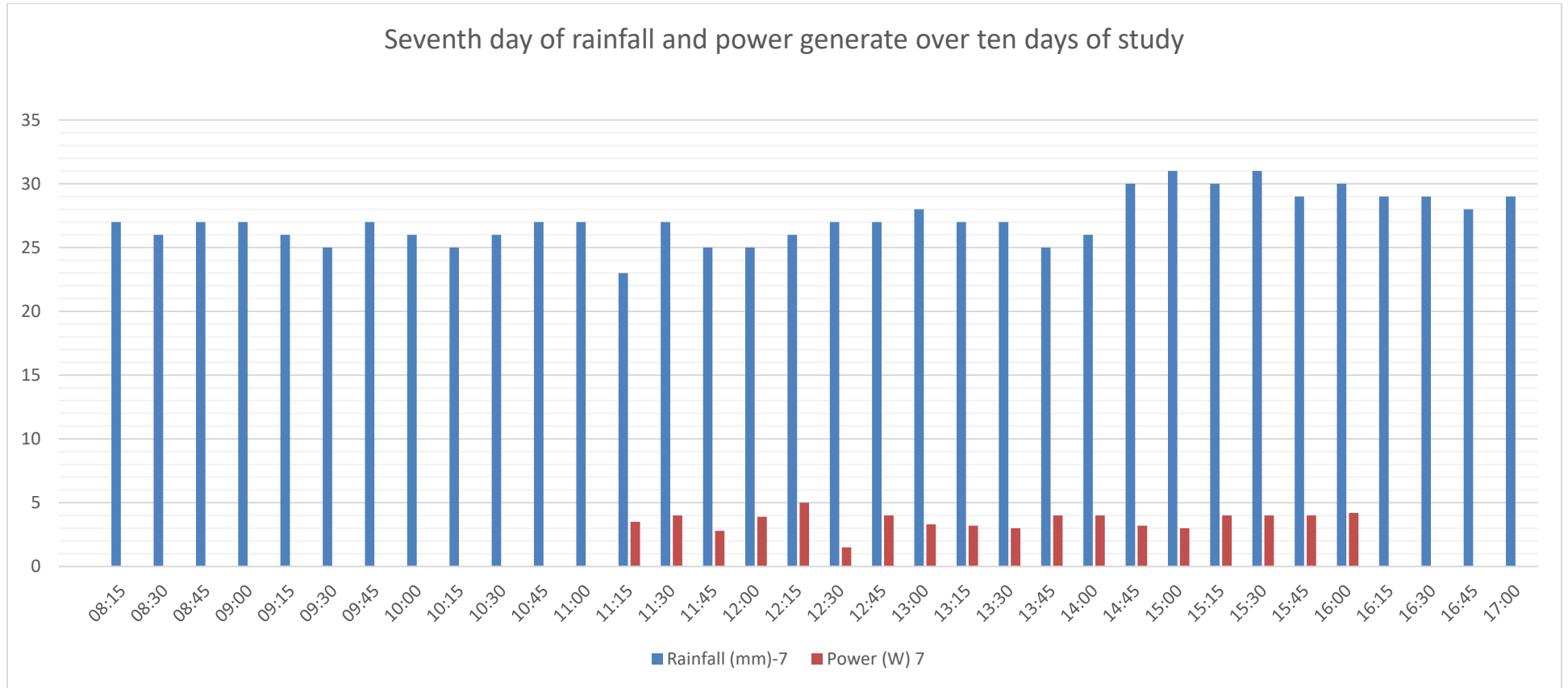


Figure E.6 Validation: Seventh day of rainfall and power generation

Appendix E – Graphs from system validation

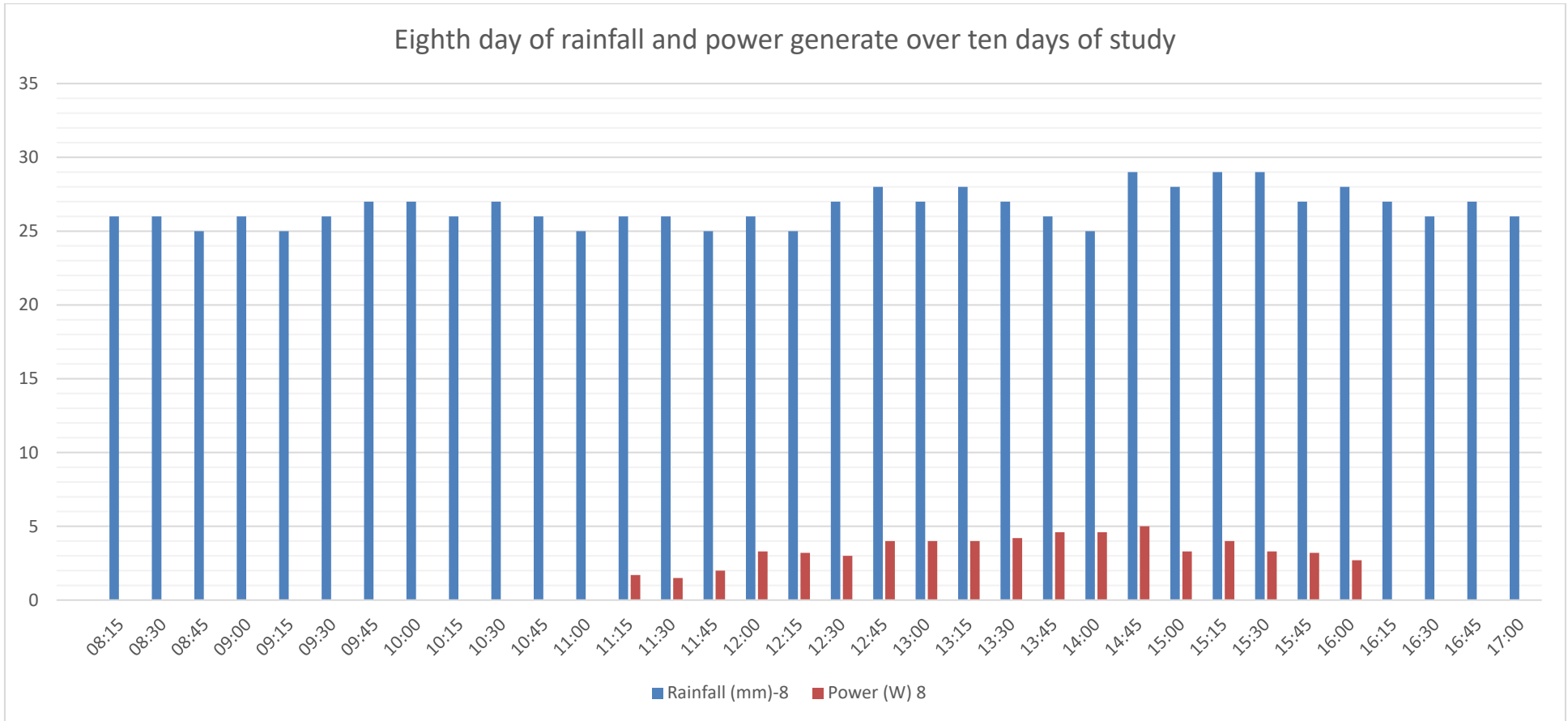


Figure E.7 Validation: Eighth day of rainfall and power generation

Appendix E – Graphs from system validation

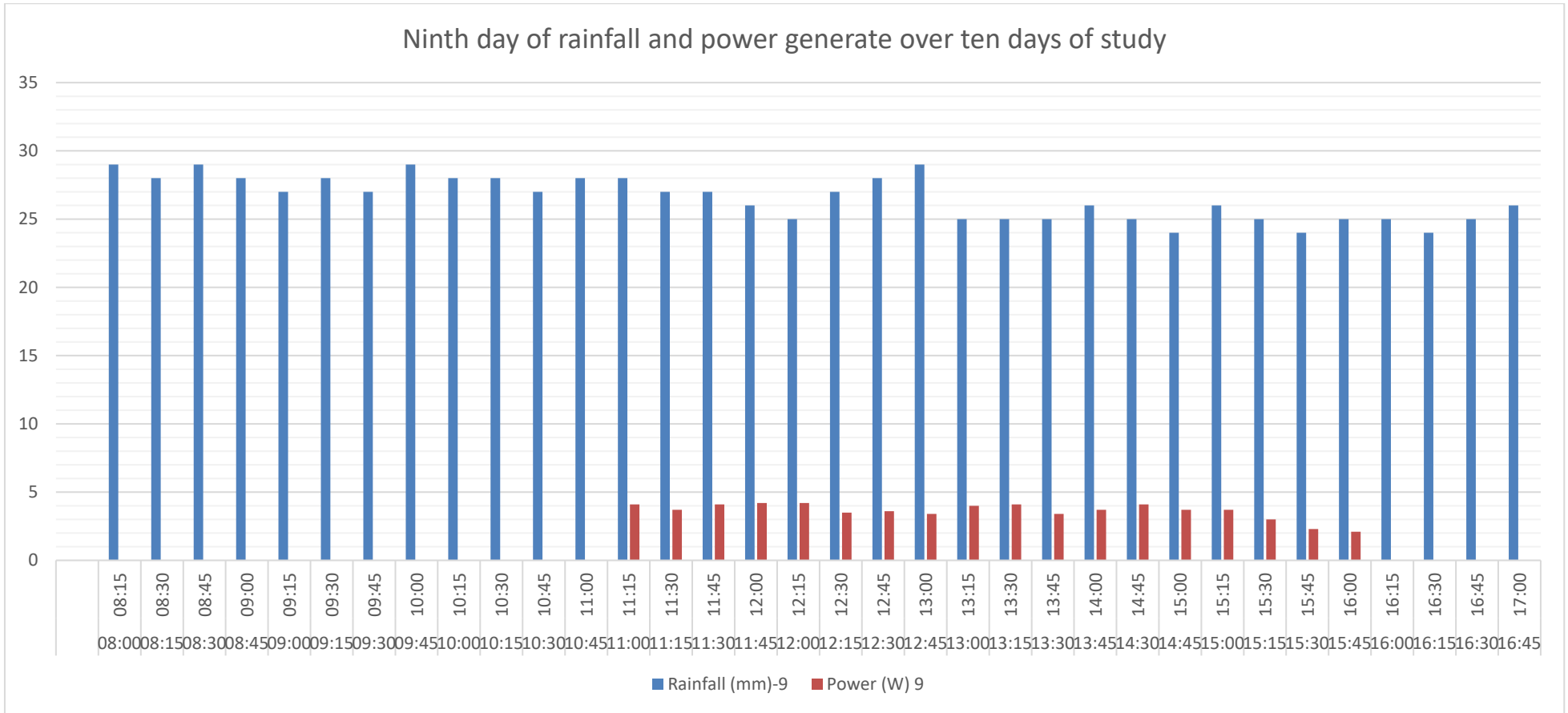


Figure E.8 Validation: Ninth day of rainfall and power generation

Appendix E – Graphs from system validation

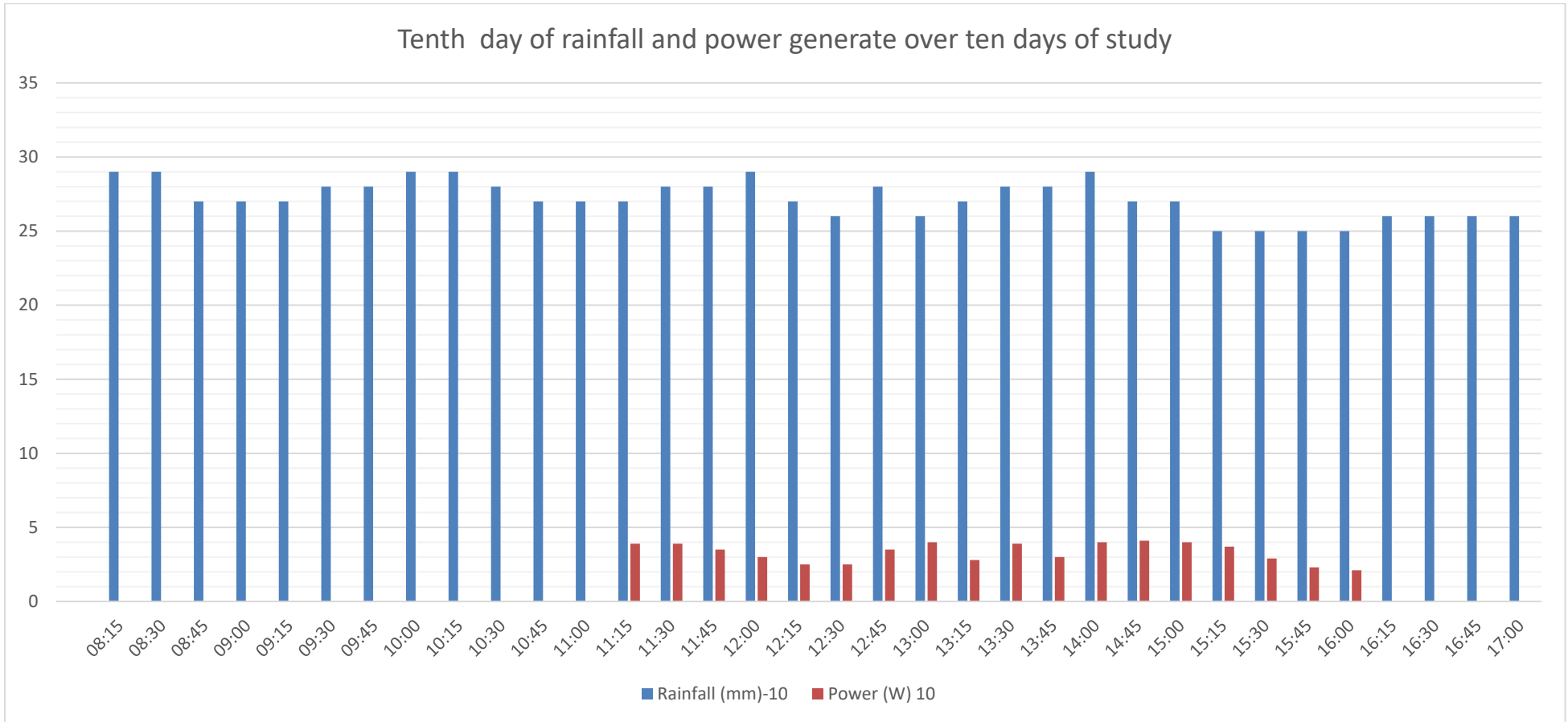


Figure E.9 Validation: Tenth day of rainfall and power generation

Appendix E – Graphs from system validation

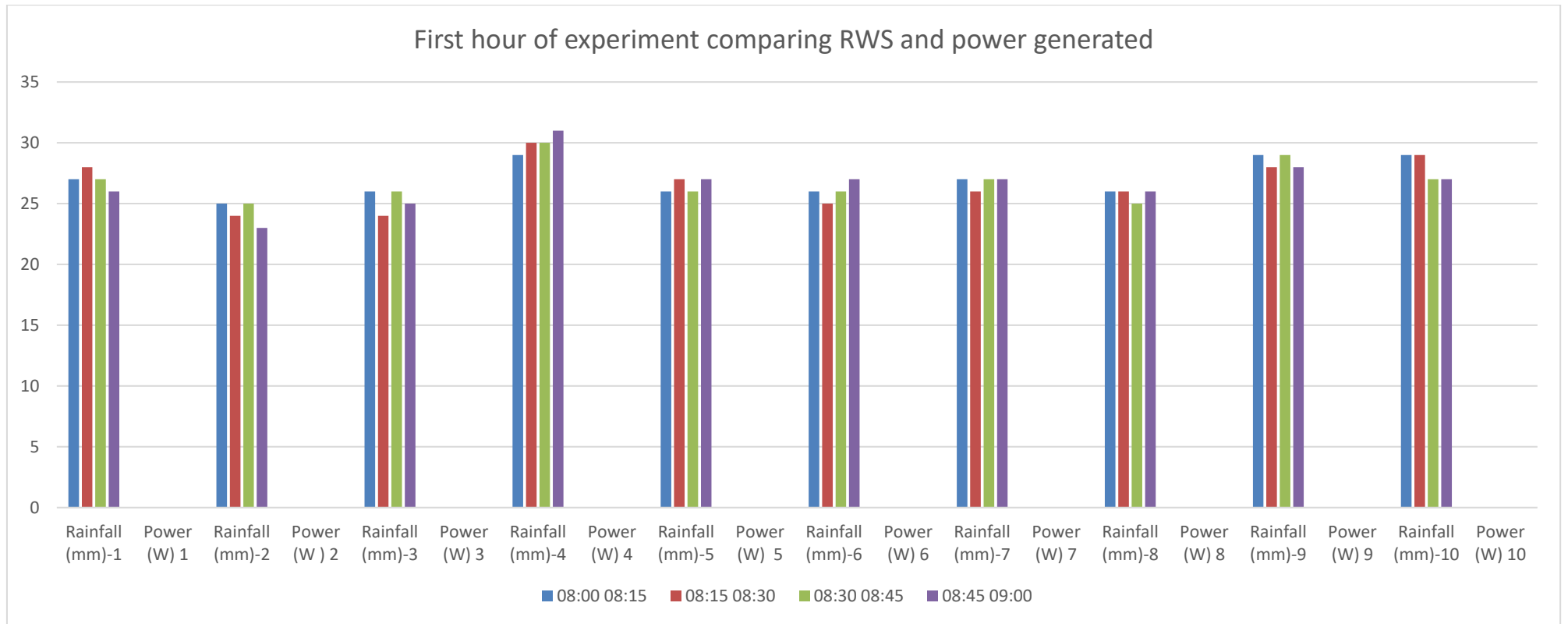


Figure E.10 Validation: Comparison of RWS and power generation during the first hour of the experiment

Appendix E – Graphs from system validation

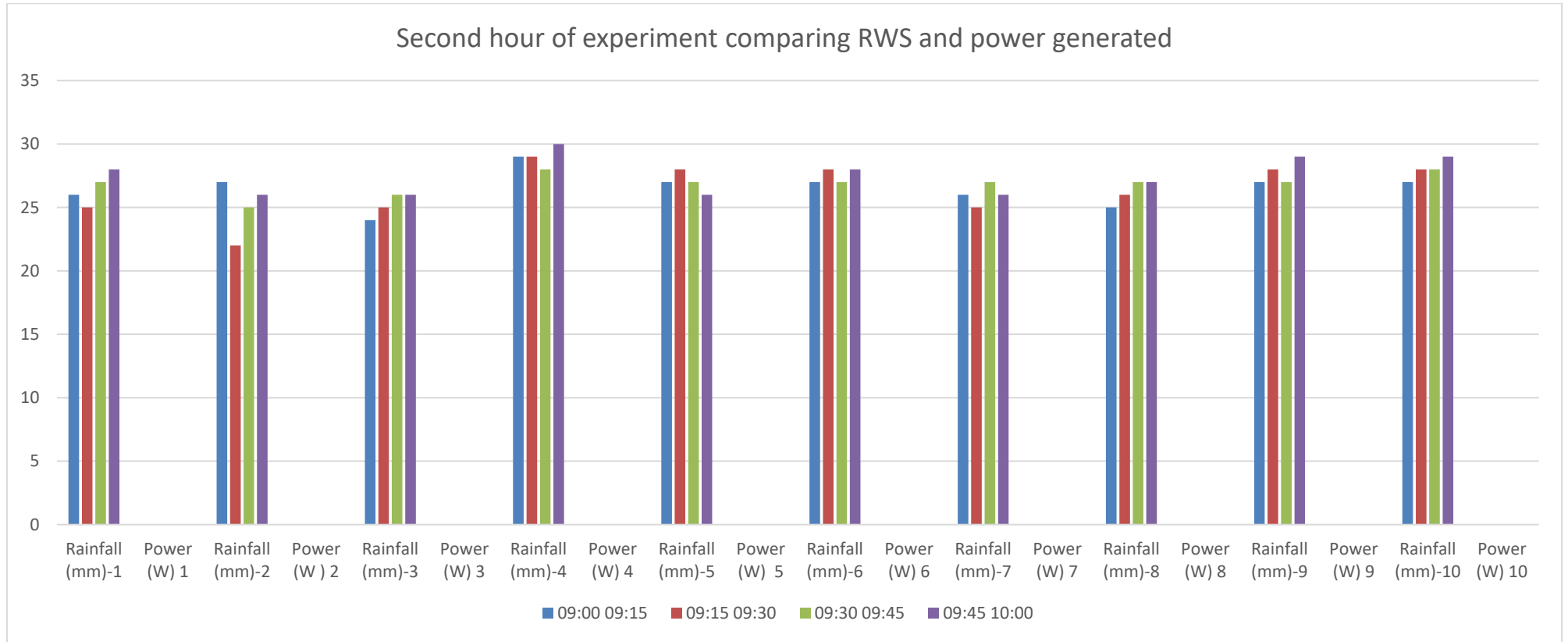


Figure E.11 Validation: Comparison of RWS and power generation during the second hour of the experiment

Appendix E – Graphs from system validation

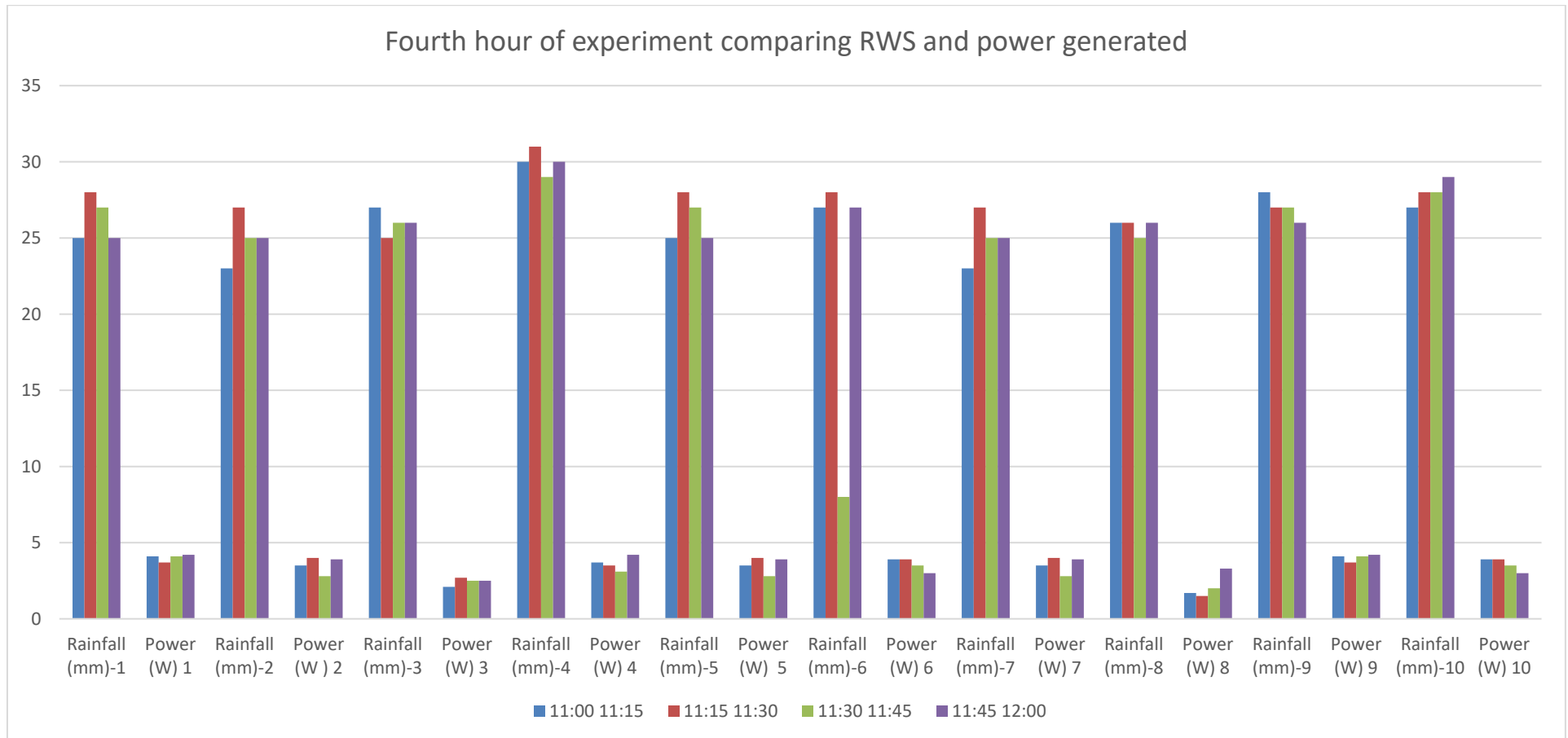


Figure E.12 Validation: Comparison of RWS and power generation during the fourth hour of the experiment

Appendix E – Graphs from system validation

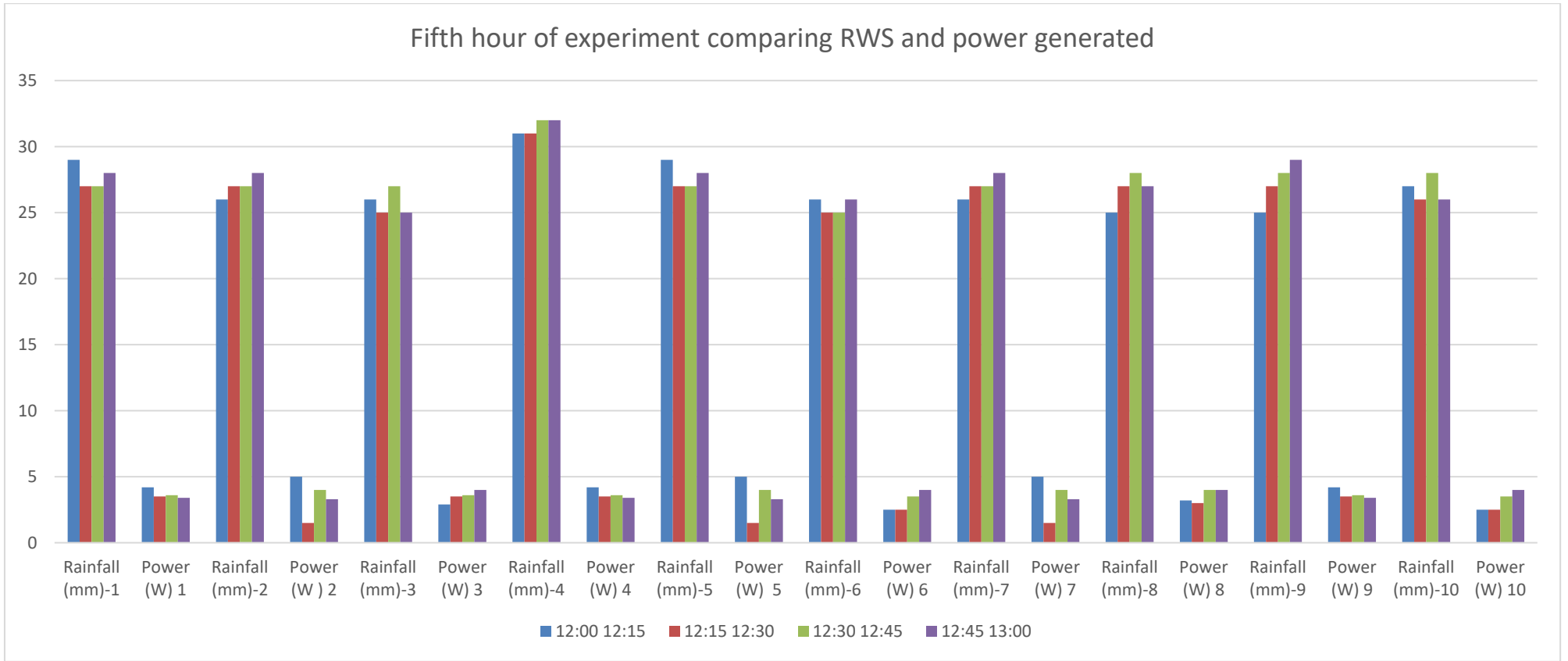


Figure E.13 Validation: Comparison of RWS and power generation during the fifth hour of the experiment

Appendix E – Graphs from system validation

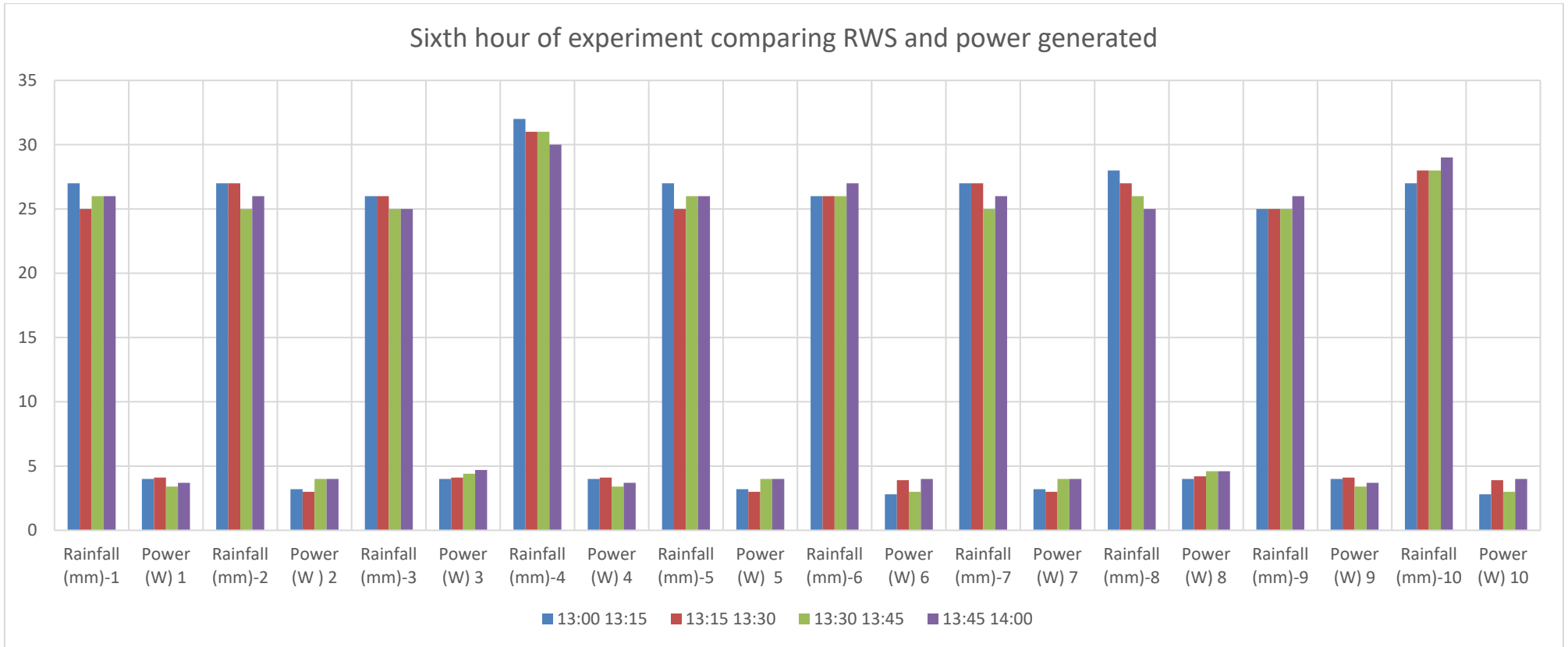


Figure E.14 Validation: Comparison of RWS and power generation during the sixth hour of the experiment

Appendix E – Graphs from system validation

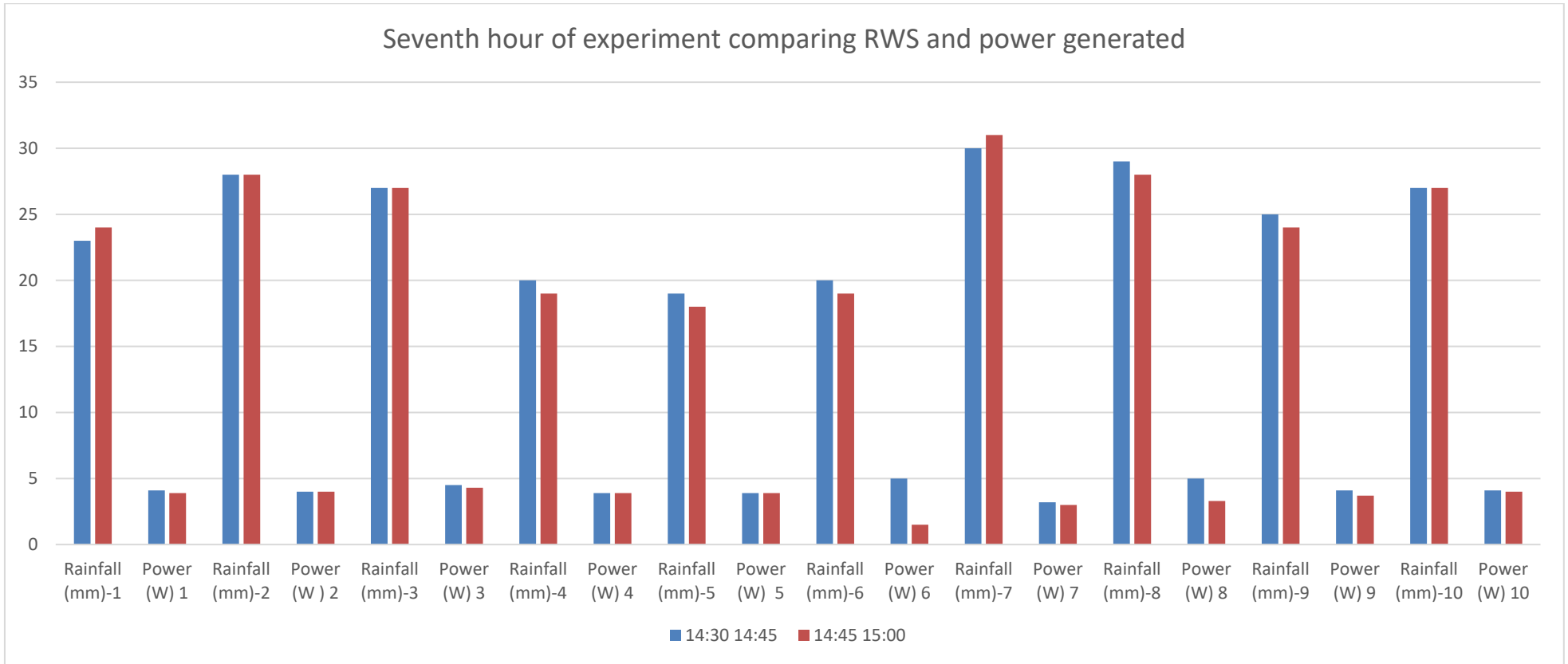


Figure E.15 Validation: Comparison of RWS and power generation during the seventh hour of the experiment

Appendix E – Graphs from system validation

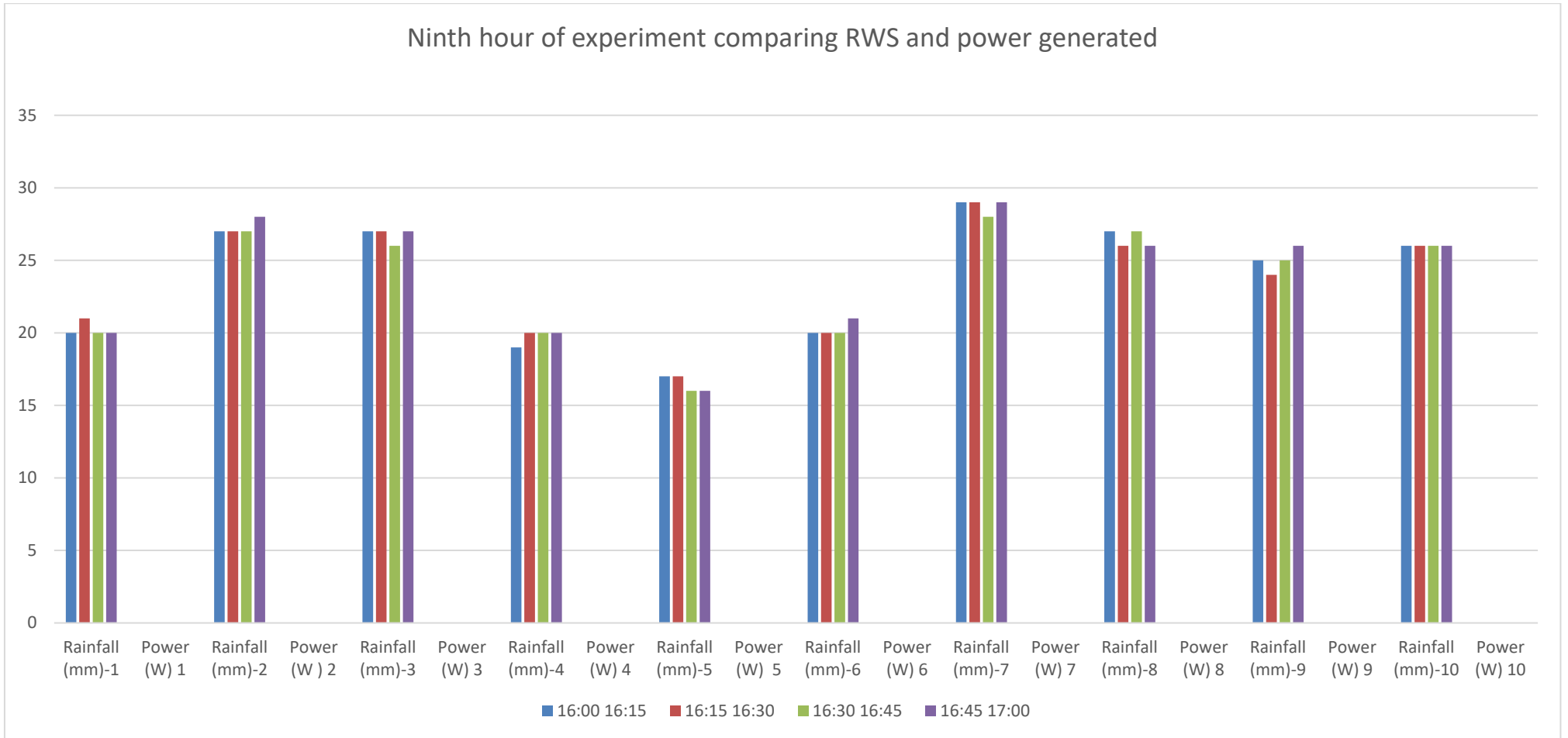


Figure E.16 Validation: Comparison of RWS and power generation during the ninth hour of the experiment

Appendix E – Graphs from system validation

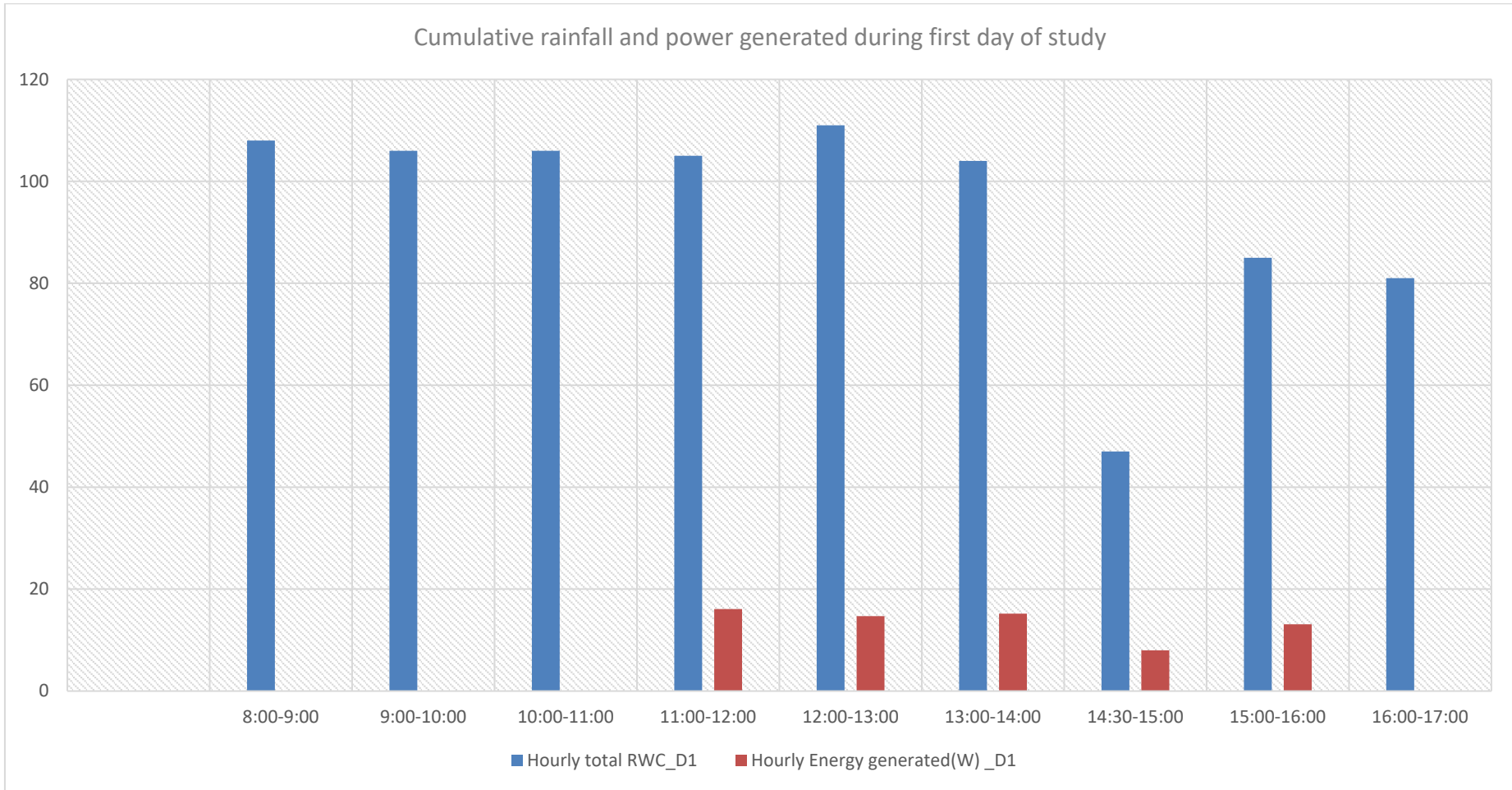


Figure E.17 Validation: Cumulative rainfall and power generated during the first day of study

Appendix E – Graphs from system validation

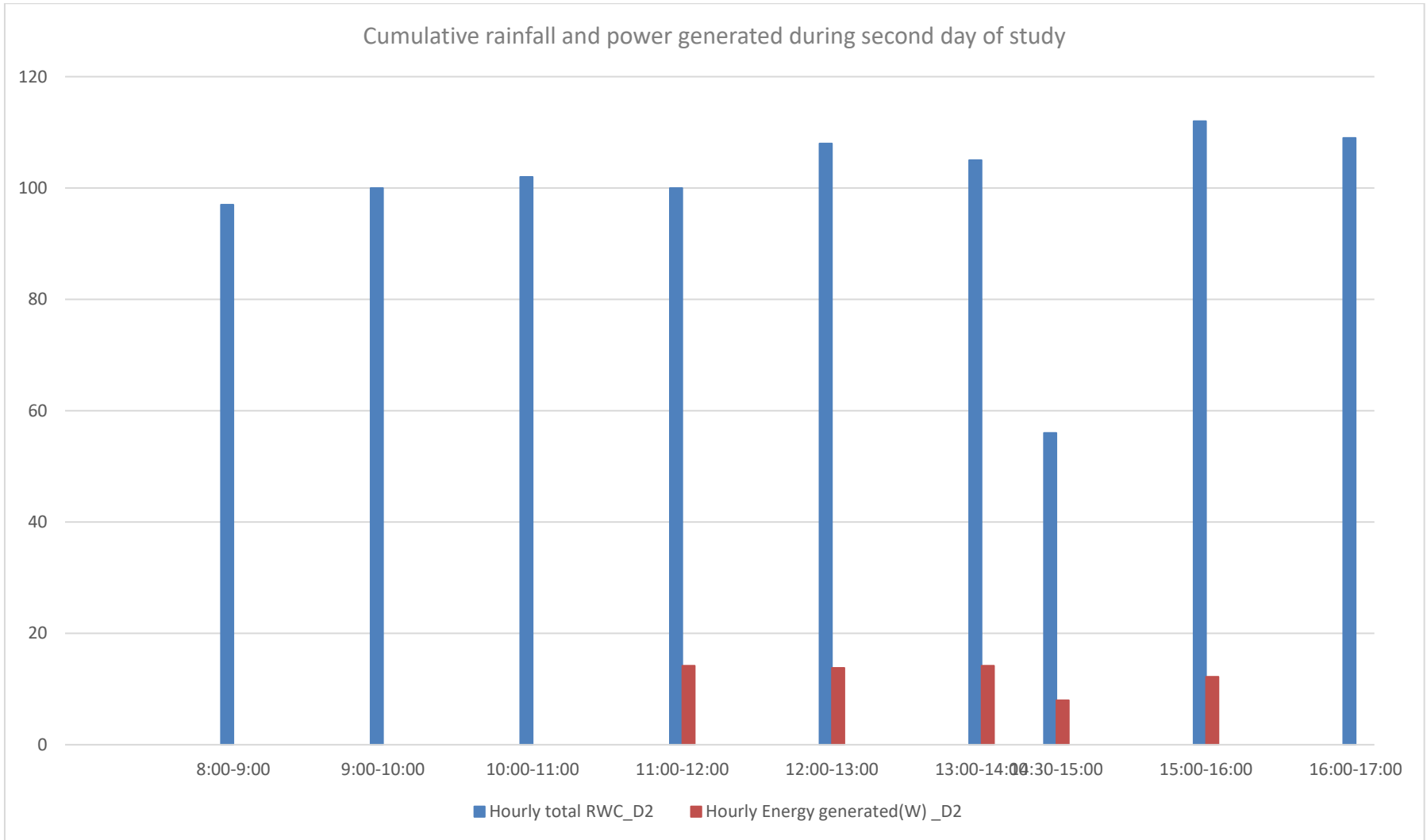


Figure E.18 Validation: Cumulative rainfall and power generated during the second day of study

Appendix E – Graphs from system validation

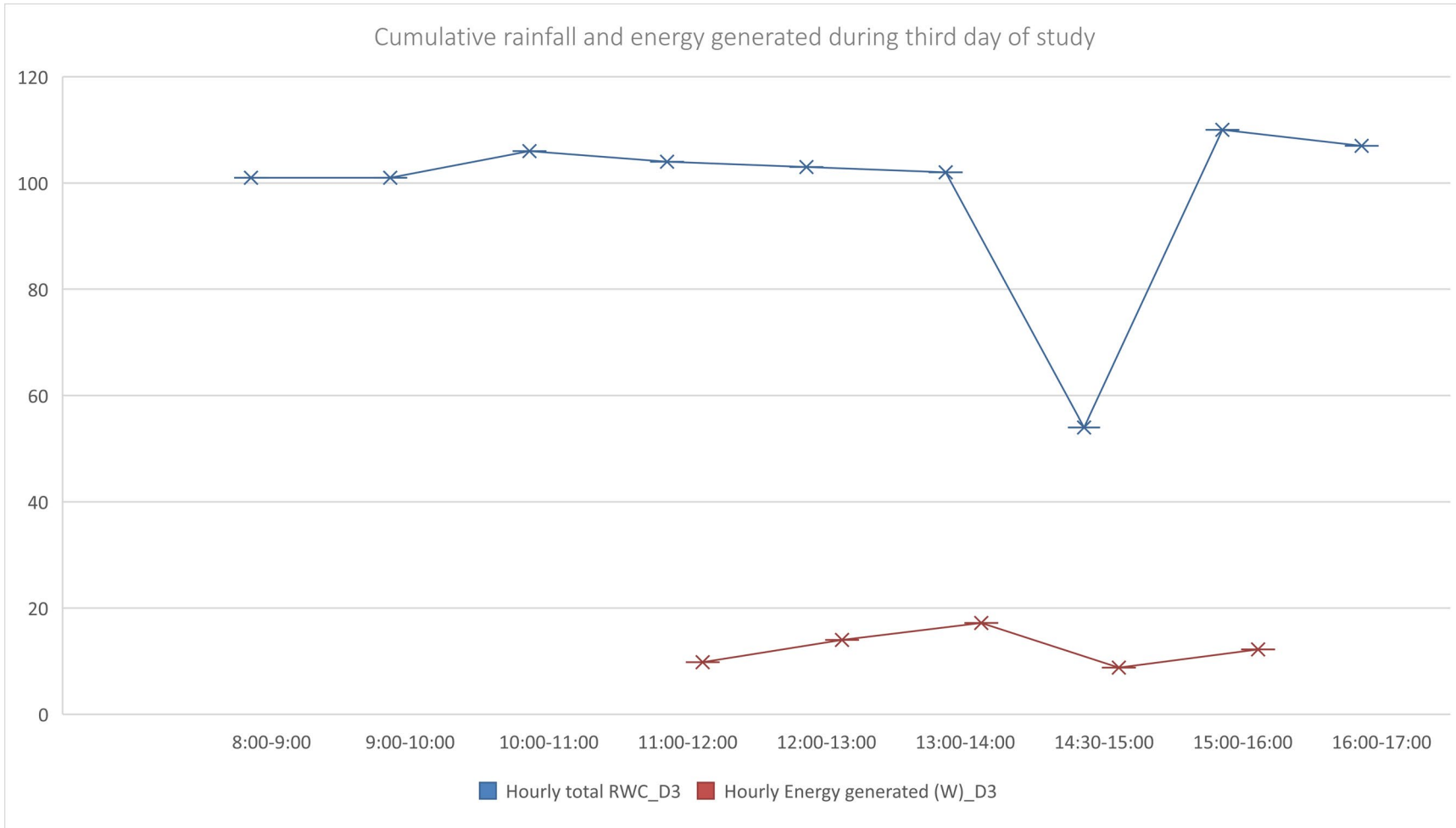


Figure E.19 Validation: Cumulative rainfall and power generated during the third day of study

Appendix E – Graphs from system validation

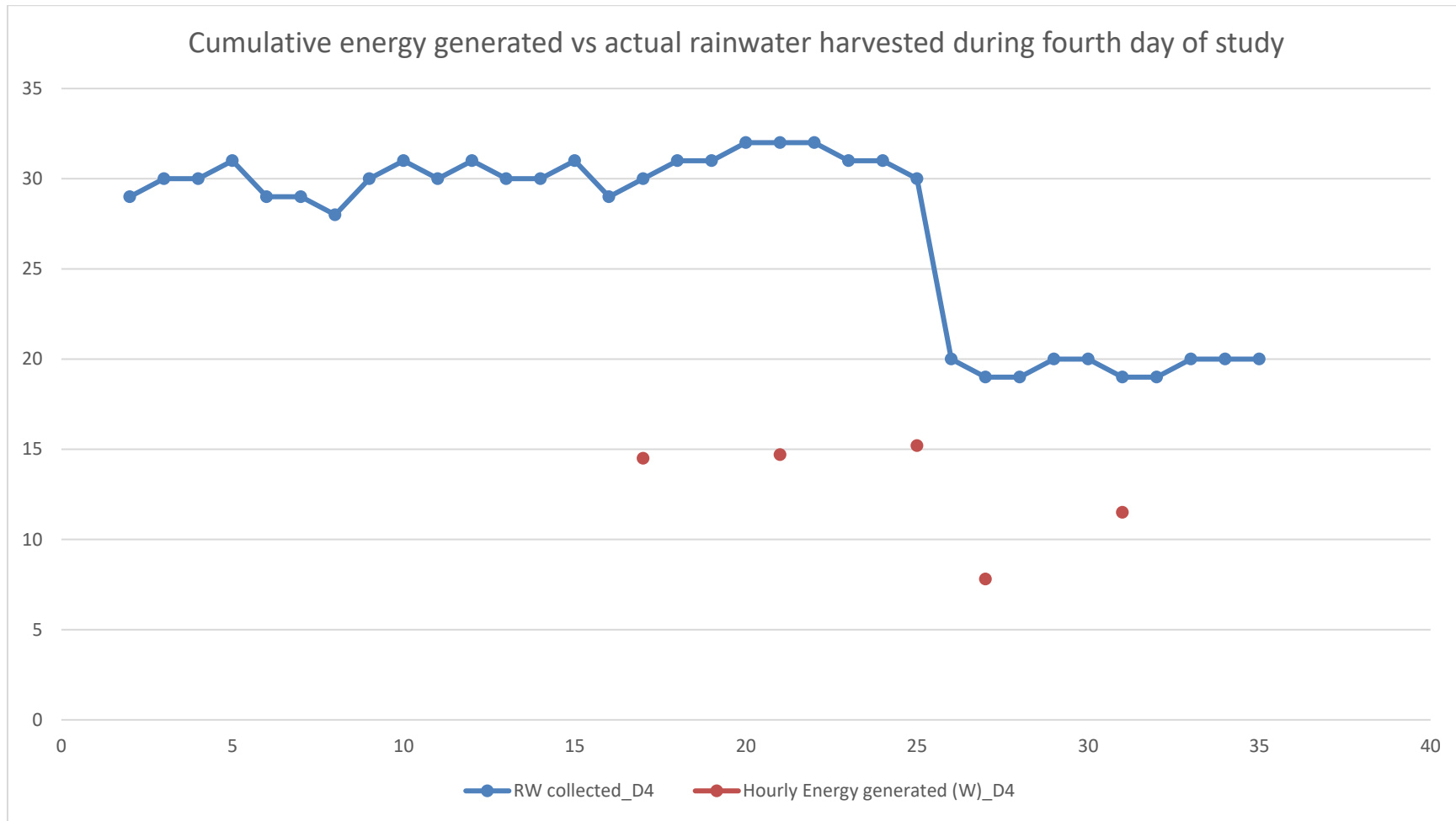


Figure E.20 Validation: Cumulative generated energy vs actual rainfall harvested during fourth day of study

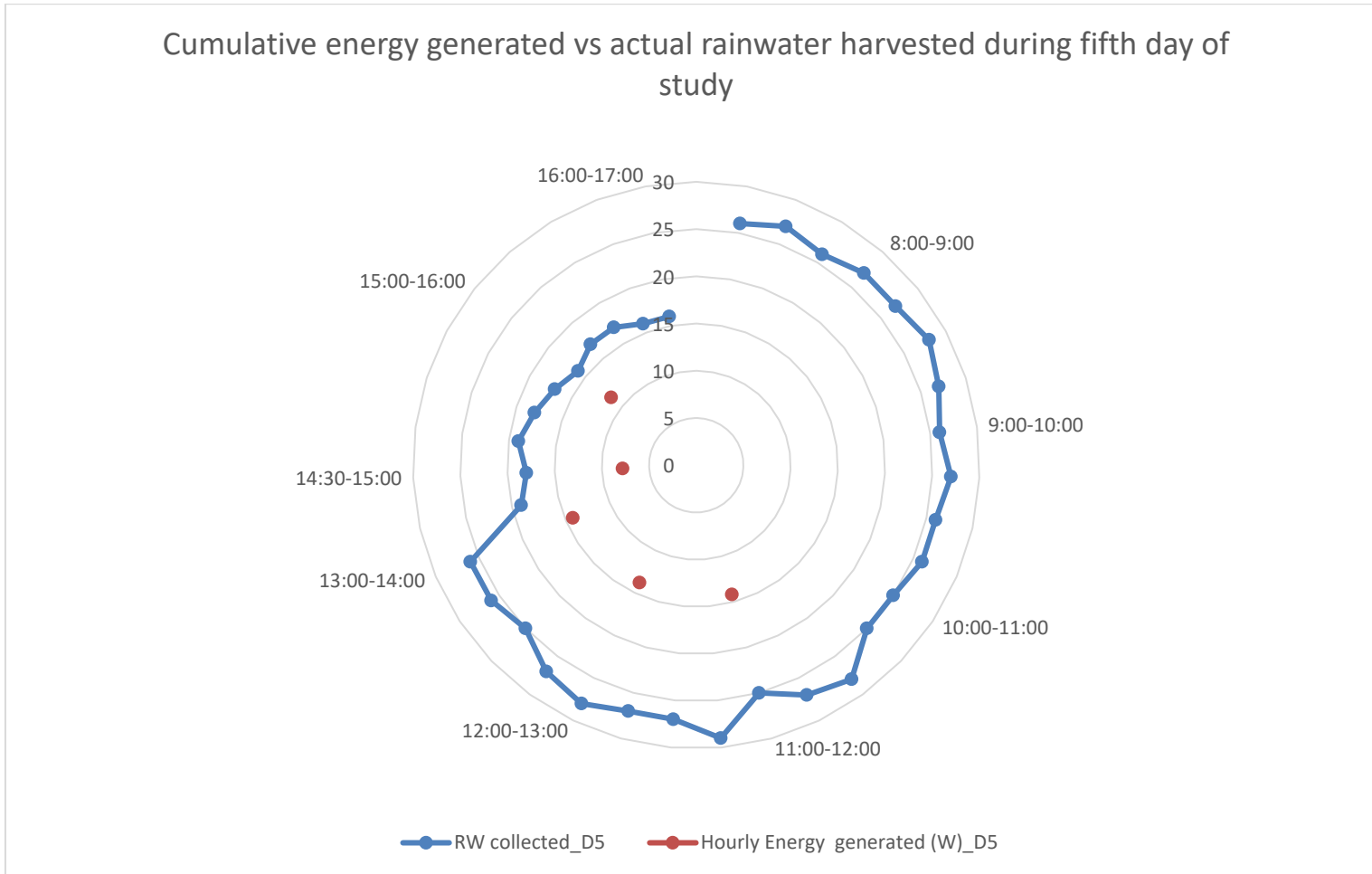


Figure E.21 Validation: Cumulative generated energy vs actual rainfall harvested during fifth day of study

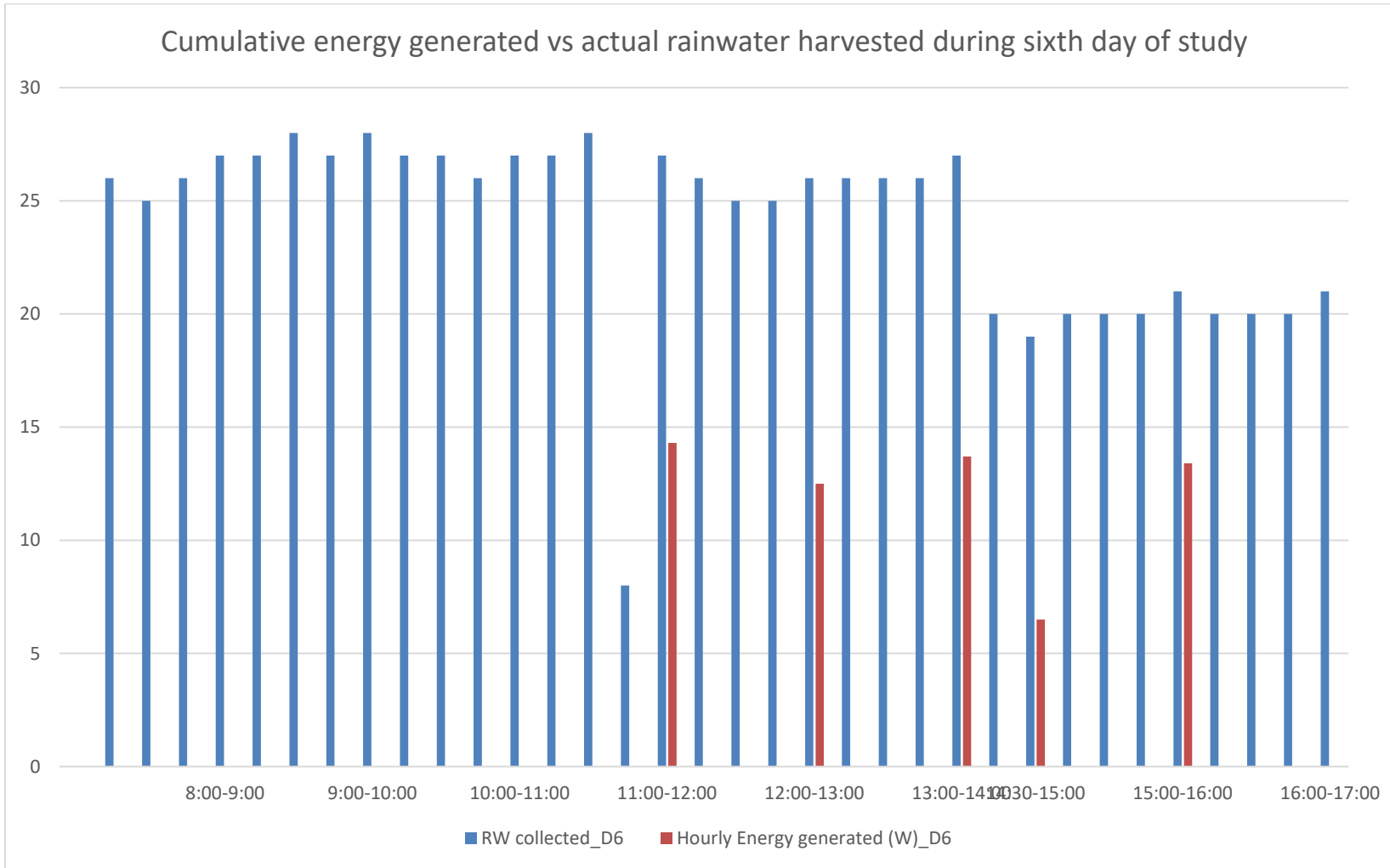


Figure E.22 Validation: Cumulative generated energy vs actual rainfall harvested during sixth day of study

Appendix E – Graphs from system validation

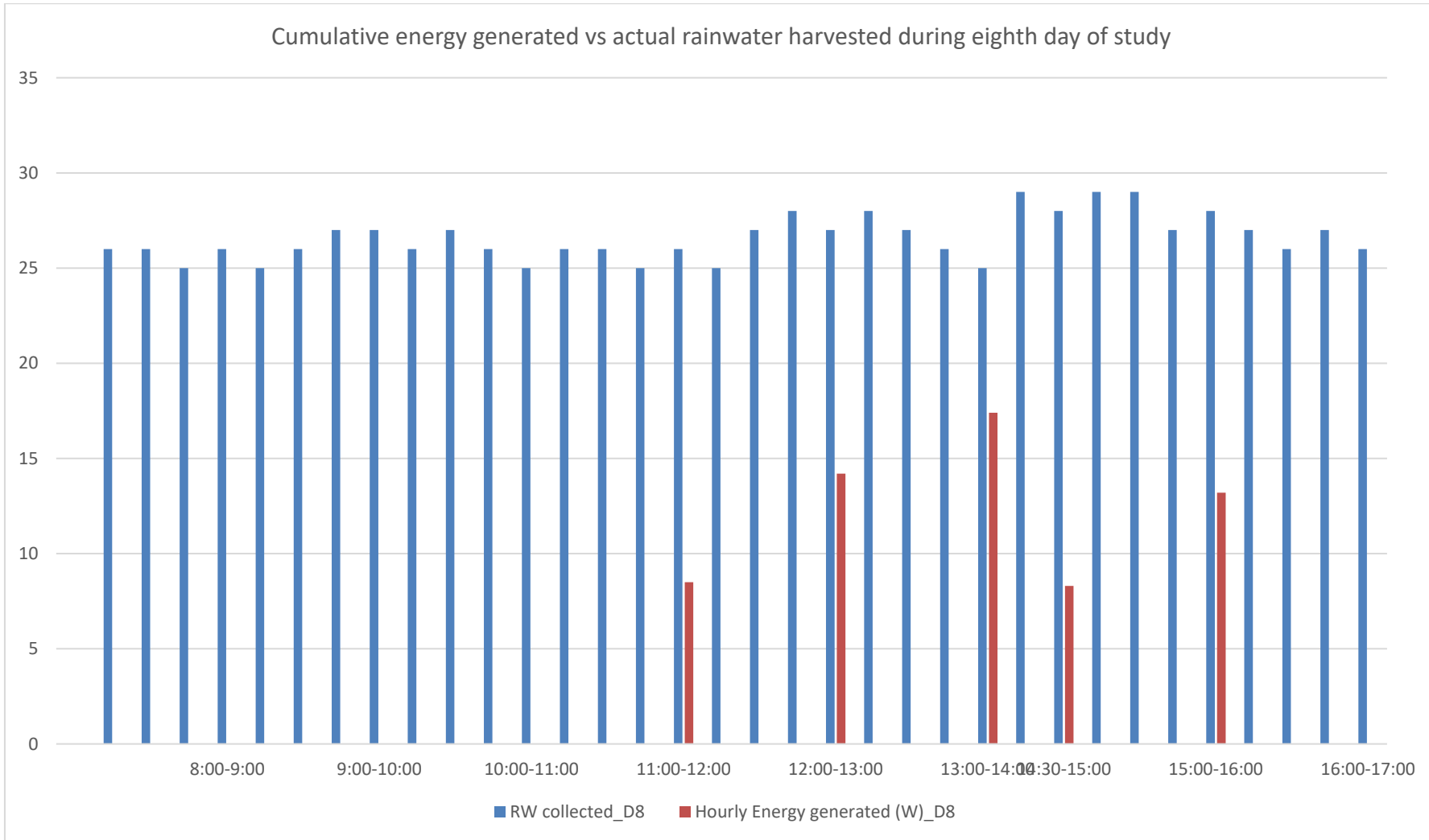


Figure E.23 Validation: Cumulative generated energy vs actual rainfall harvested during eighth day of study

Appendix E – Graphs from system validation

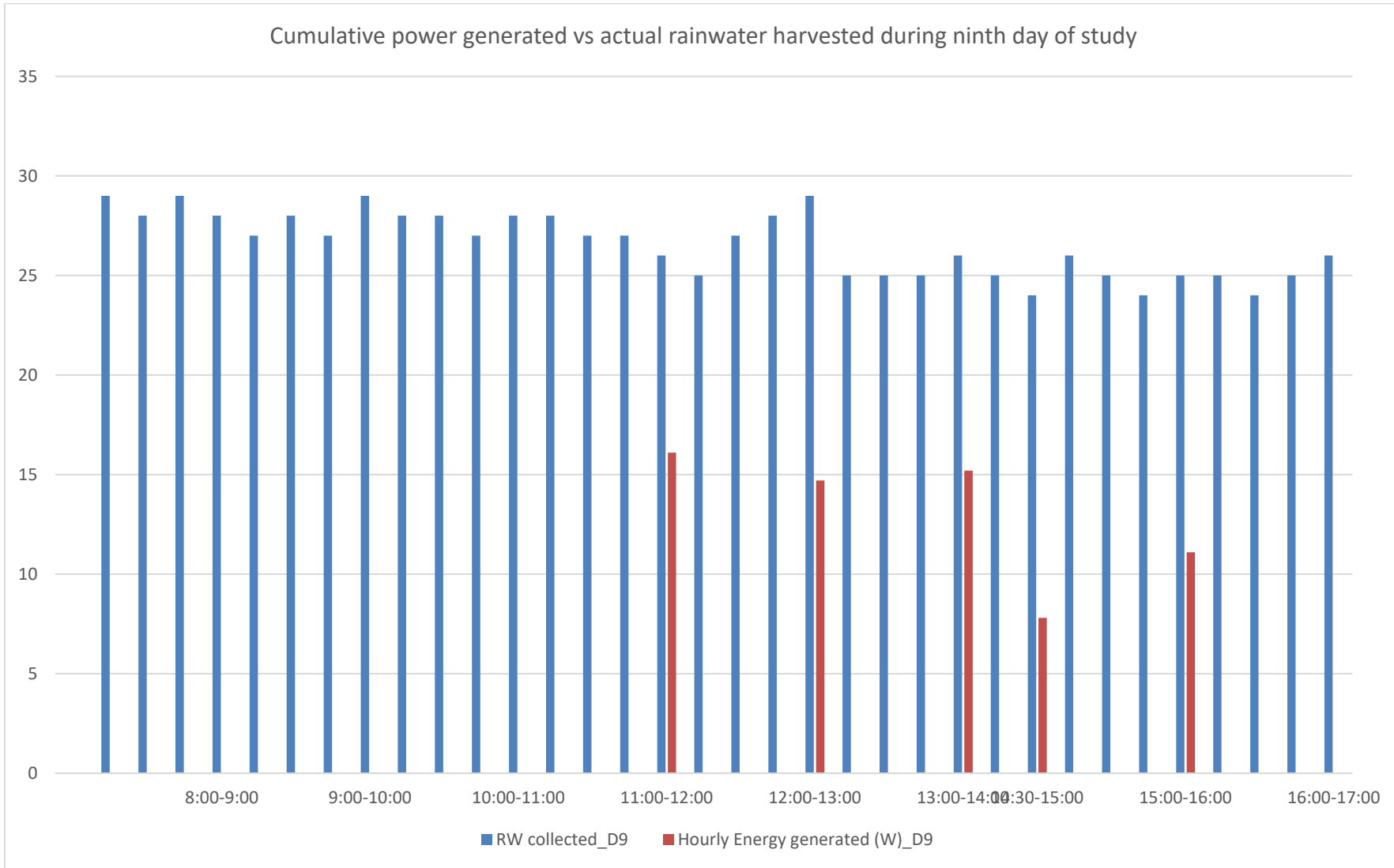


Figure E.24 Validation: Cumulative generated energy vs actual rainfall harvested during ninth day of study

Appendix E – Graphs from system validation

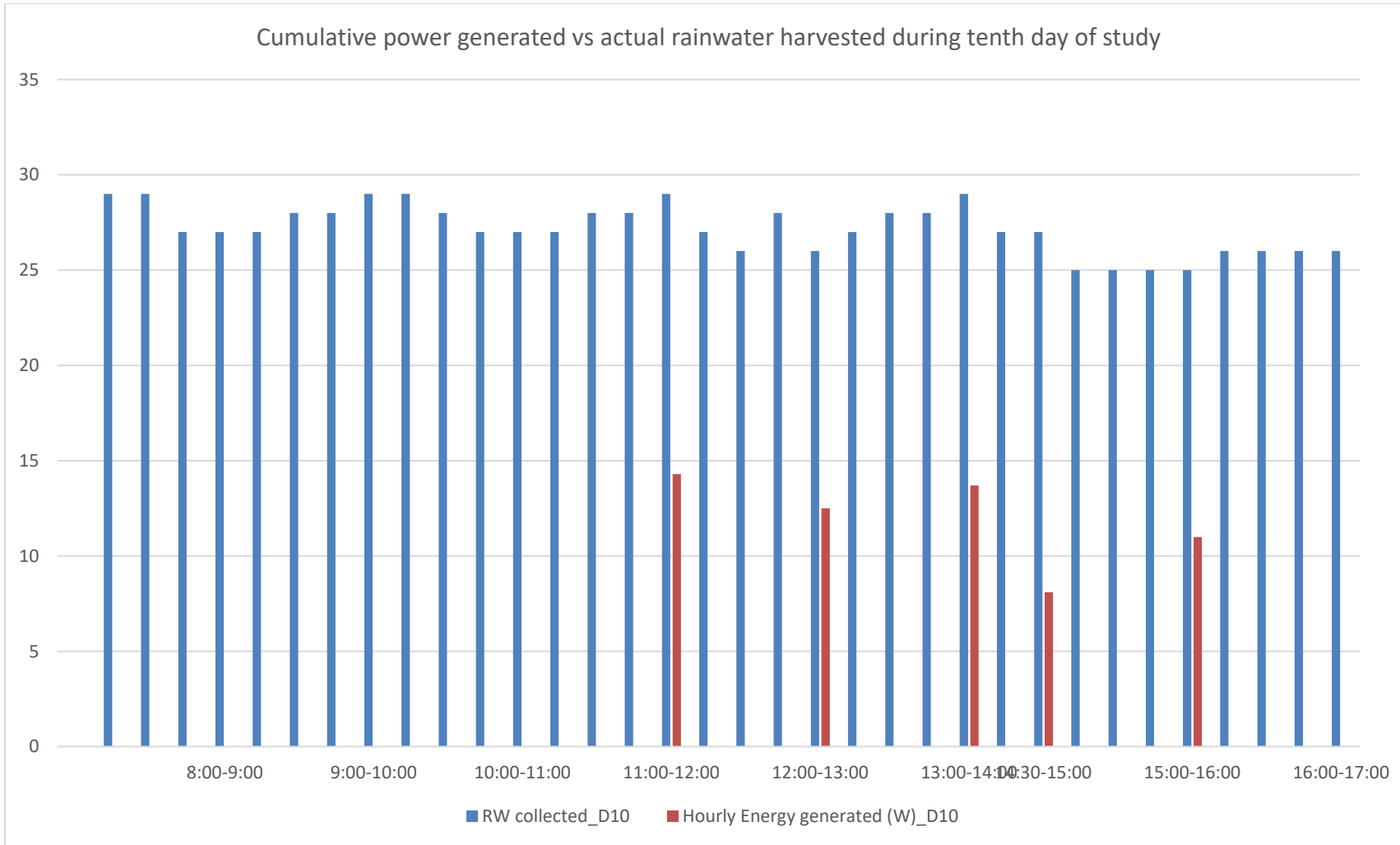


Figure E.25 Validation: Cumulative generated energy vs actual rainfall harvested during tenth day of study

Appendix E – Graphs from system validation

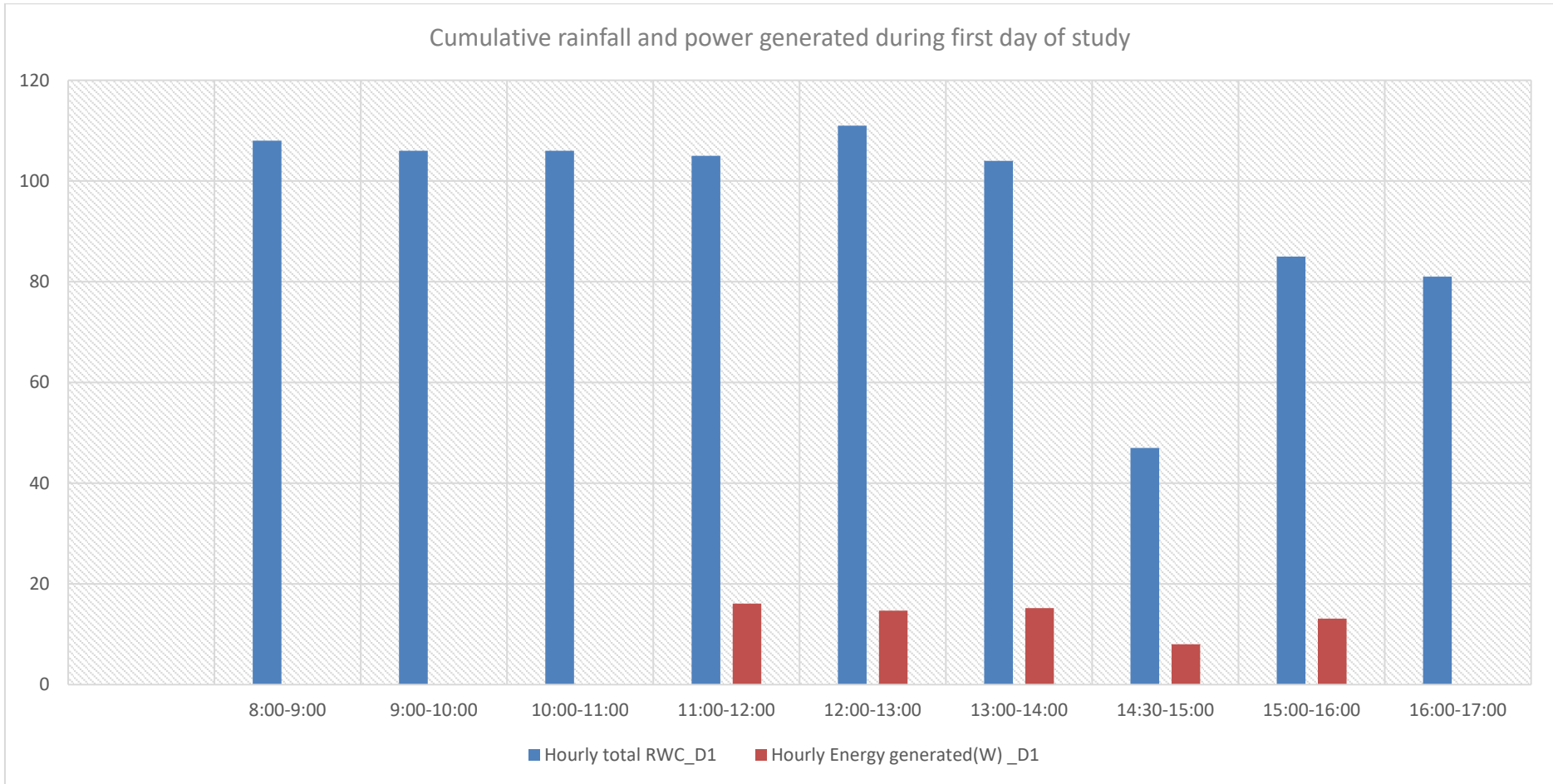


Figure E.26 Validation: Cumulative rainfall and power generated during first day of study

Appendix E – Graphs from system validation

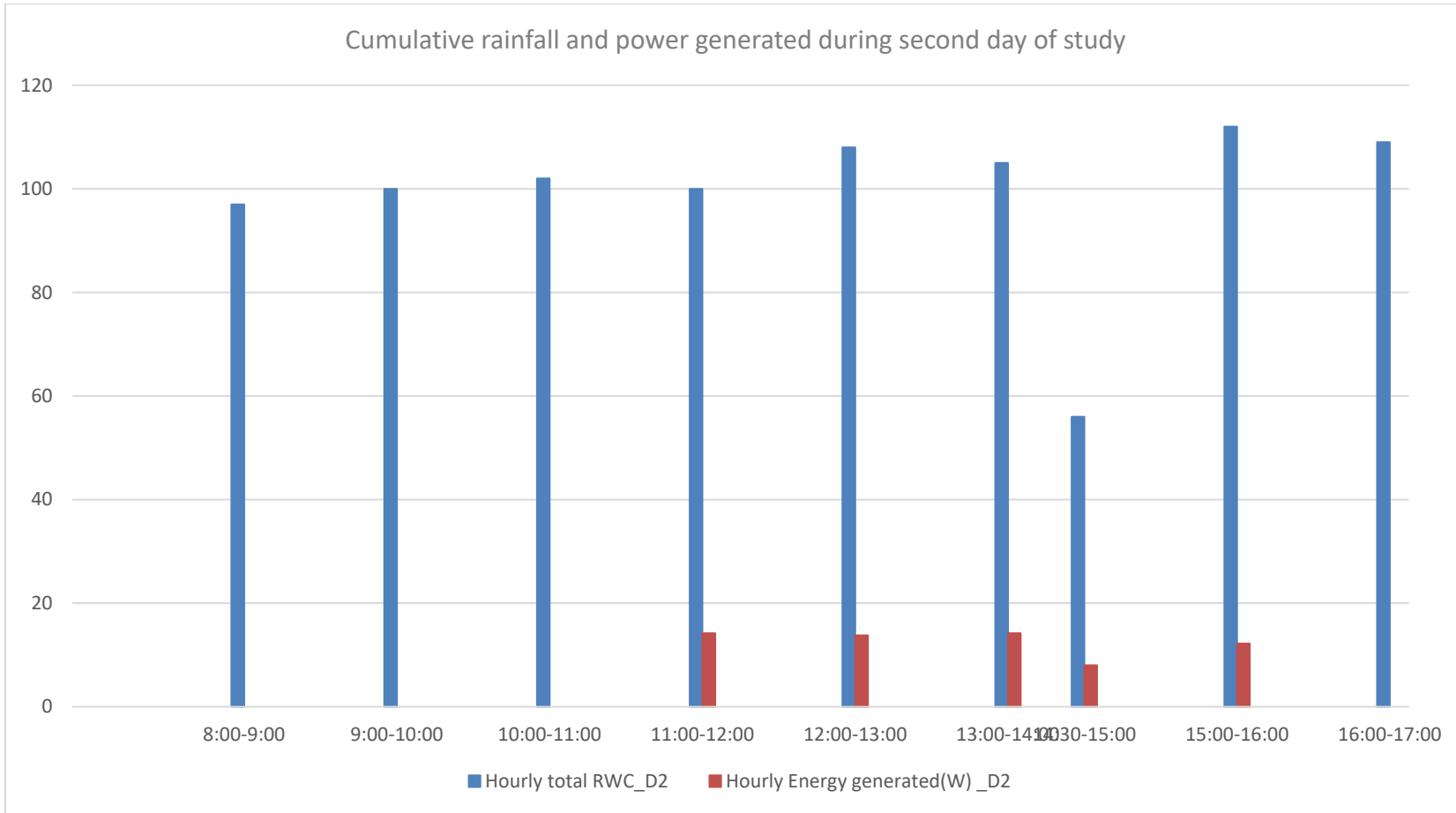


Figure E.27 Validation: Cumulative rainfall and power generated during second day of study

Appendix E – Graphs from system validation

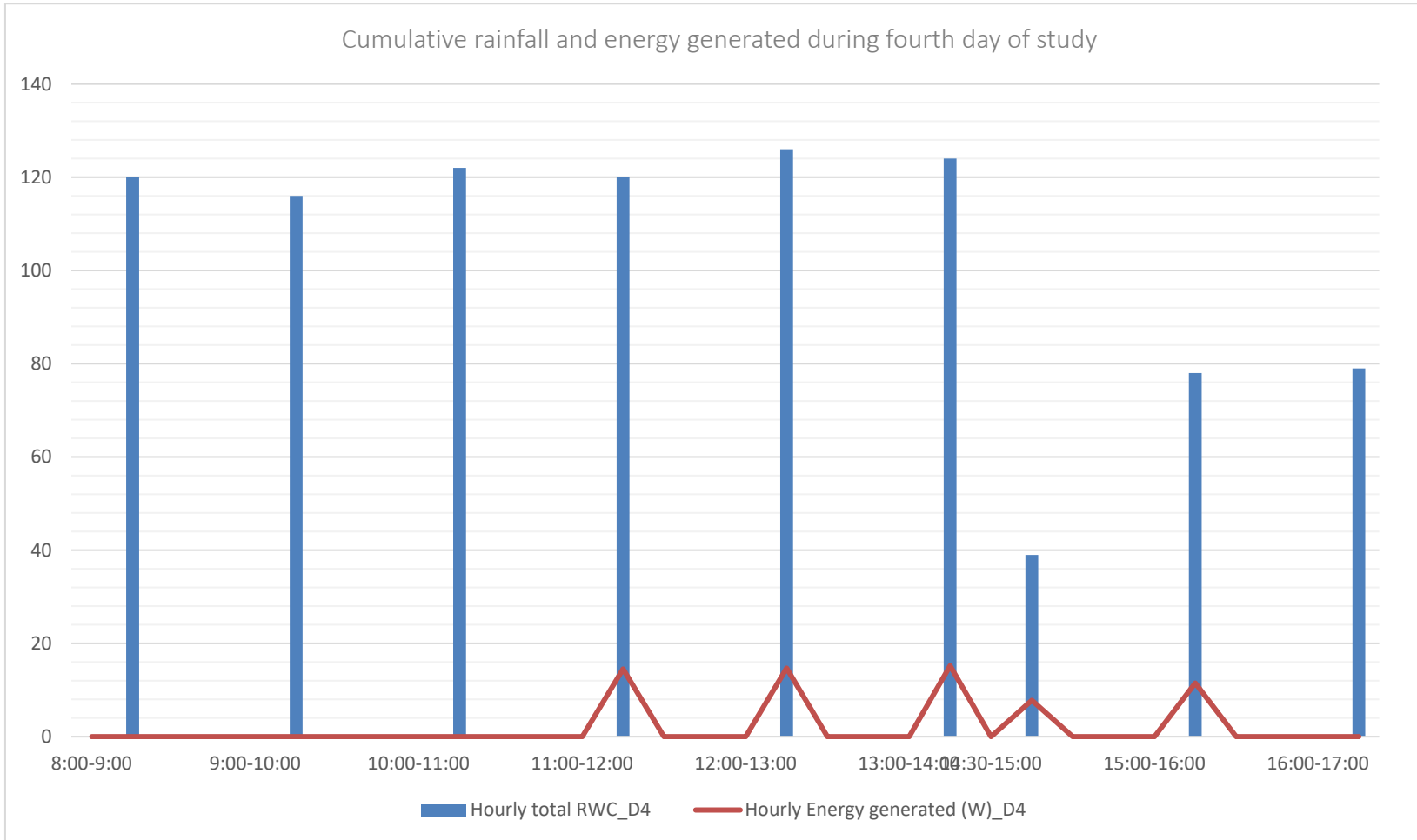


Figure E.28 Validation: Cumulative rainfall and power generated during fourth day of study

Appendix E – Graphs from system validation

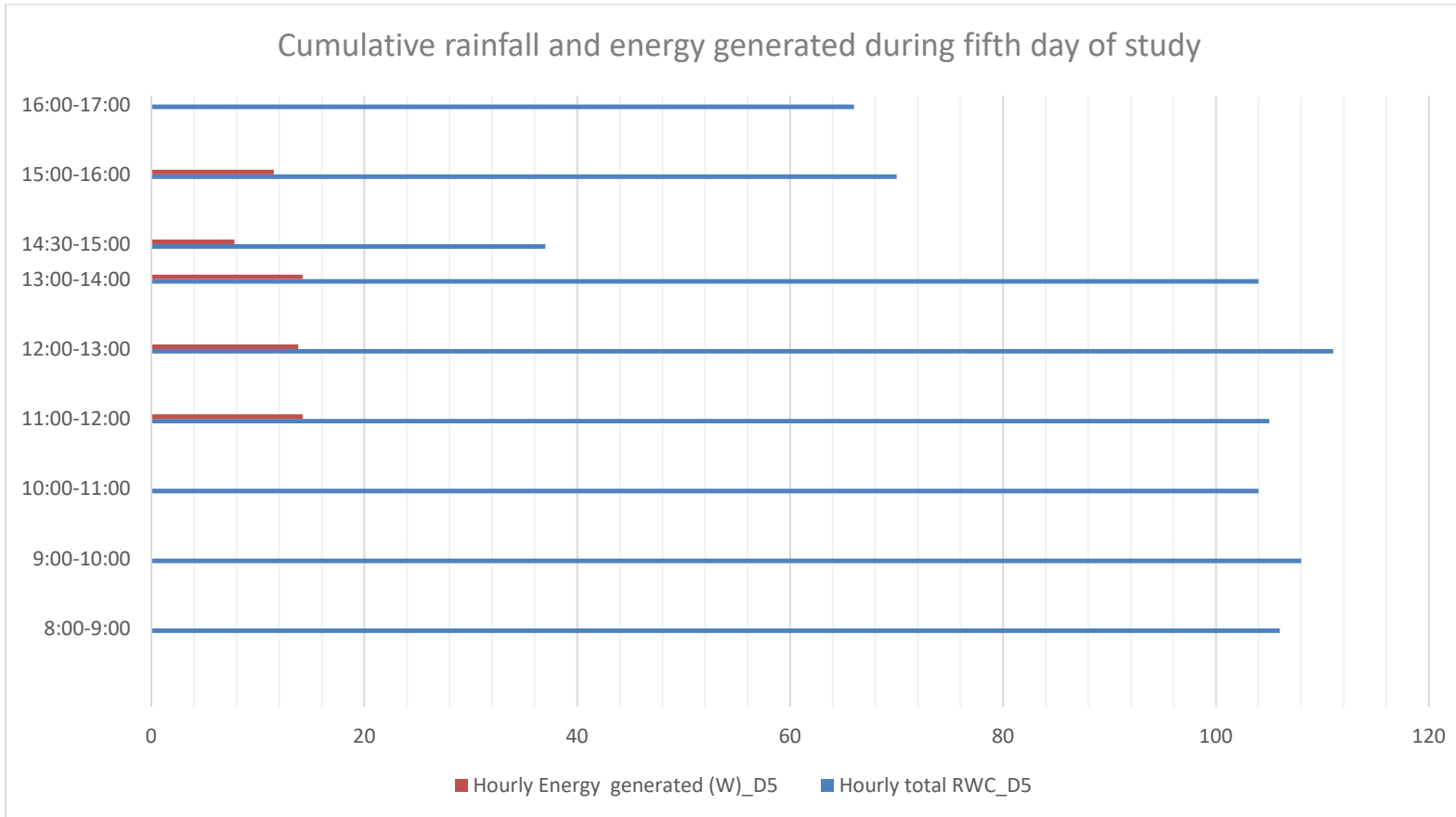


Figure E.29 Validation: Cumulative rainfall and power generated during fifth day of study

Appendix E – Graphs from system validation

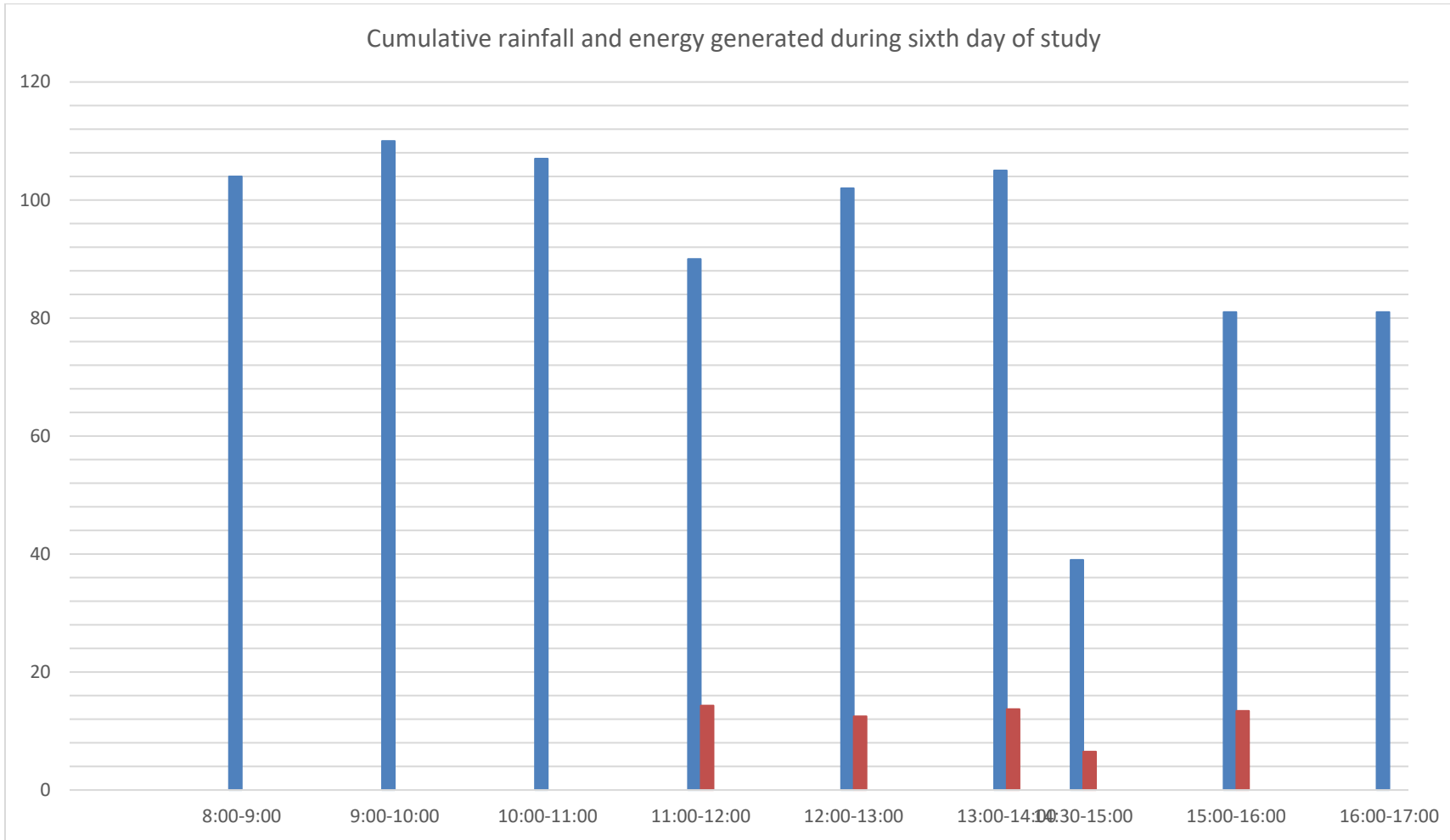


Figure E.30 Validation: Cumulative rainfall and power generated during the Sixth day of study

Appendix E – Graphs from system validation

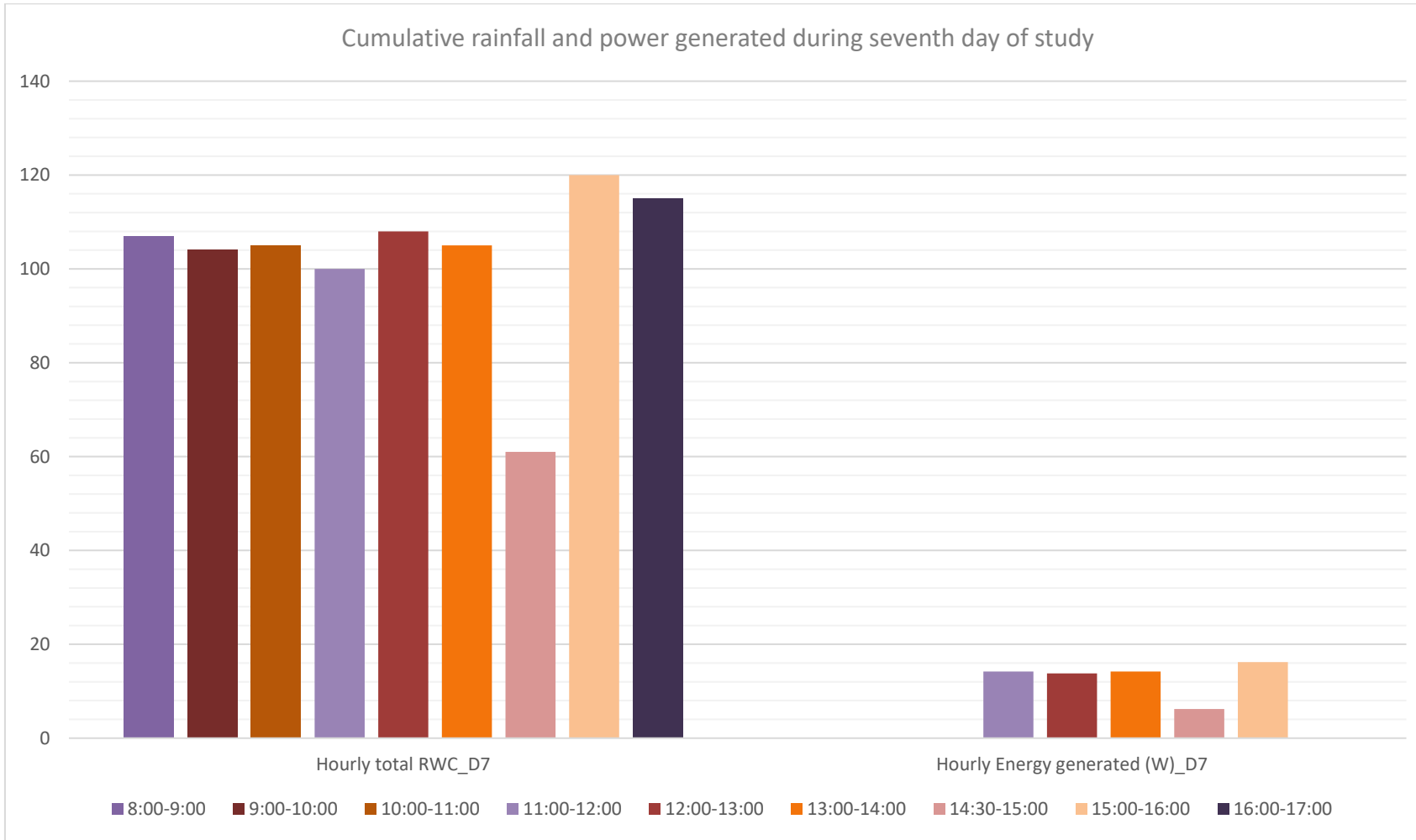


Figure E.31 Validation: Cumulative rainfall and power generated during the seventh day of study

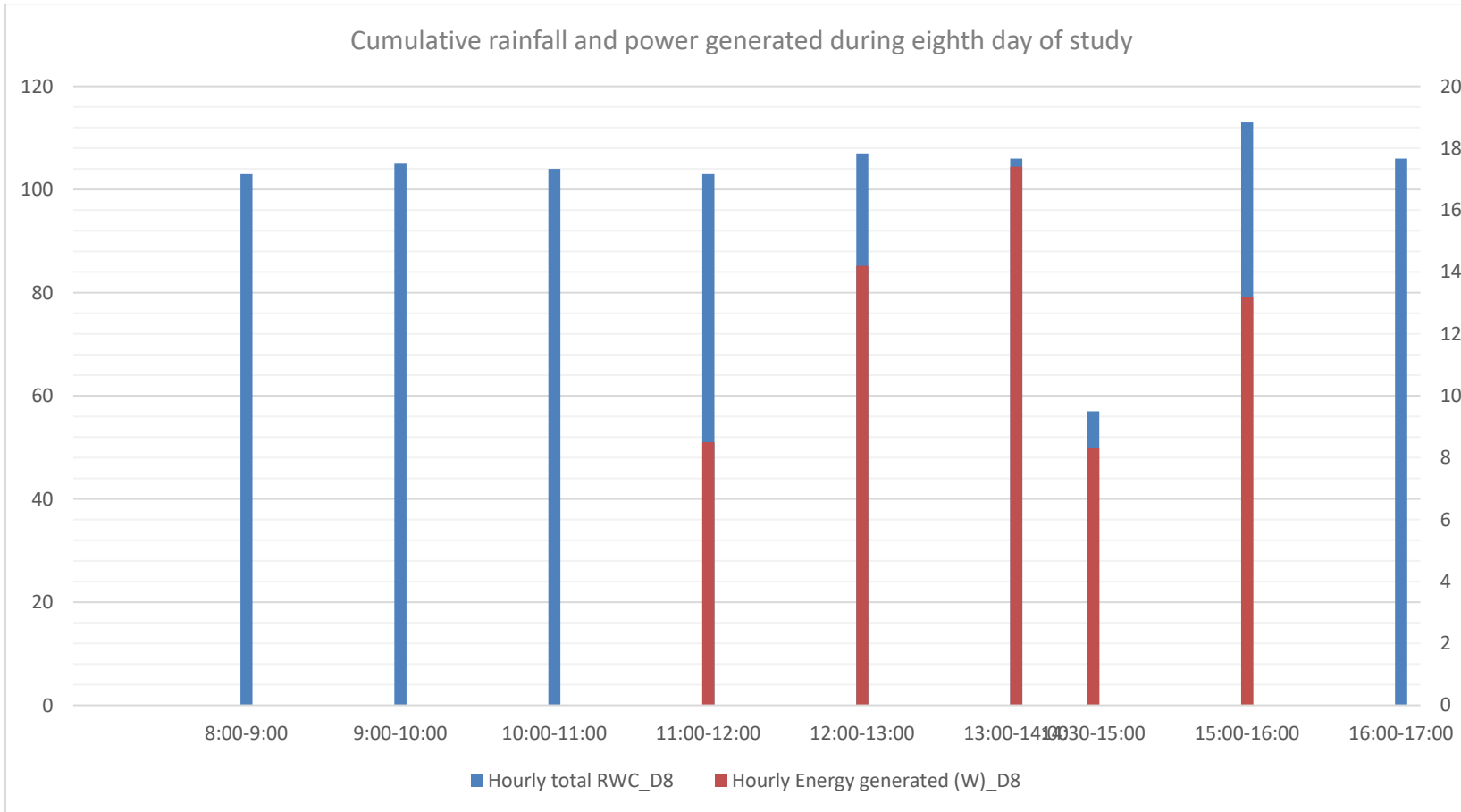


Figure E.32 Validation: Cumulative rainfall and power generated during the eighth day of study

Appendix E – Graphs from system validation

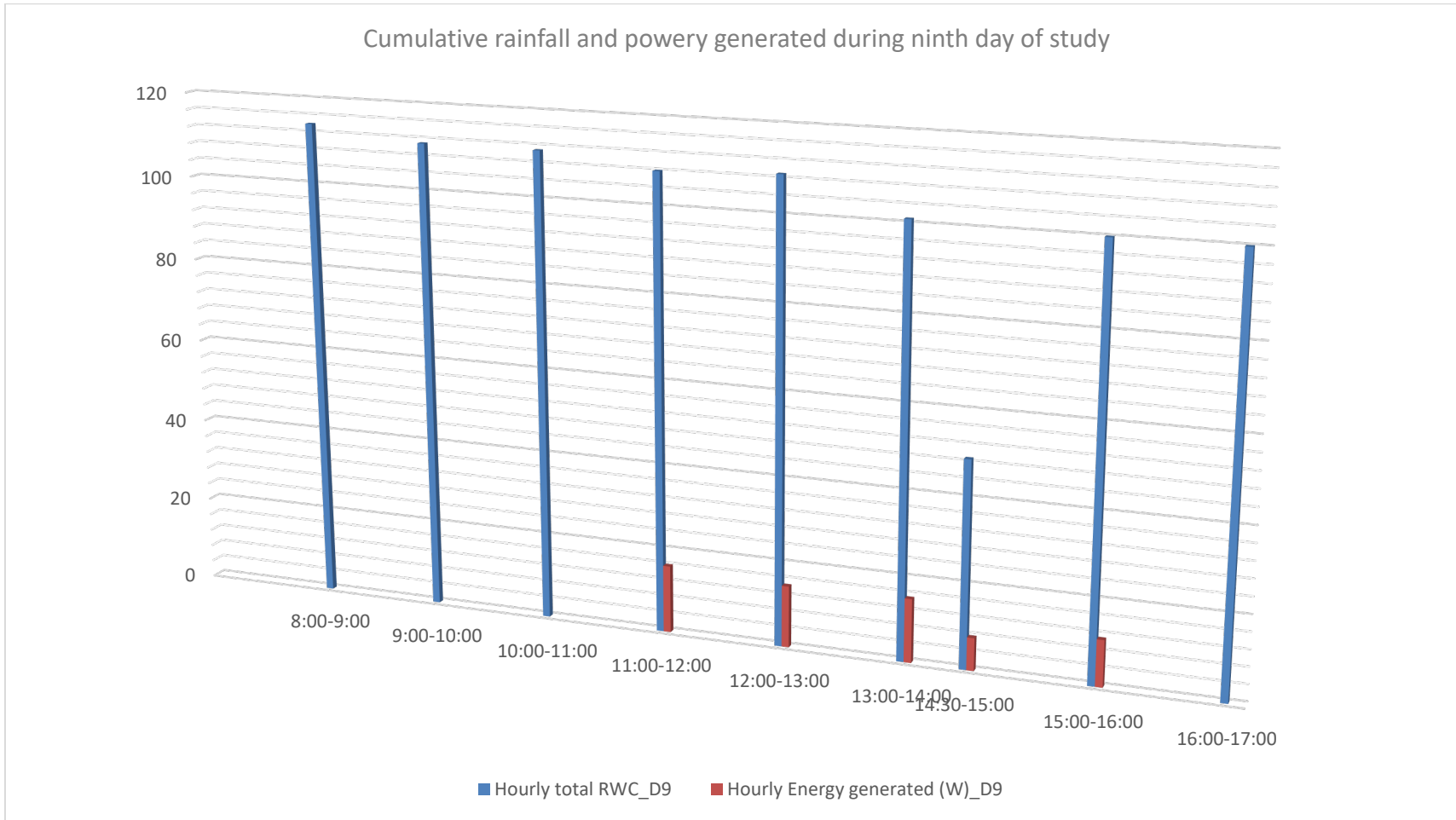


Figure E.33 Validation: Cumulative rainfall and power generated during the ninth day of study

Appendix E – Graphs from system validation

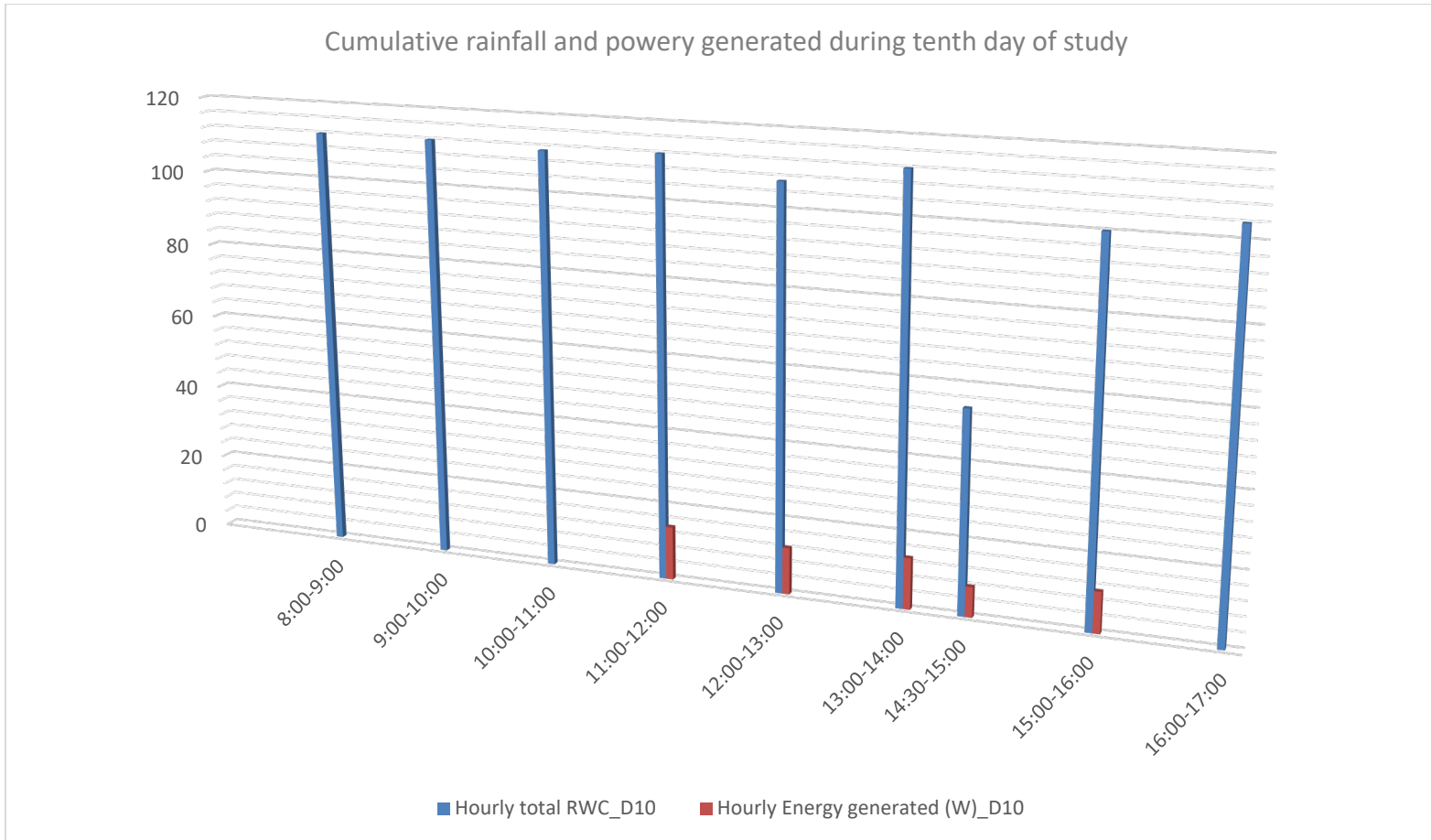


Figure E.34 Validation: Cumulative rainfall and power generated during the tenth day of study